

https://dspace.org/

Development of activated carbons from South African coal waste for application in natural gas storage

Abdulsalam, Jibril

2019

https://hdl.handle.net/10539/29078

Abdulsalam, Jibril. (2019). Development of activated carbons from South African coal waste for application in natural gas storage. University of the Witwatersrand, https://hdl.handle.net/10539/29078

Downloaded from a DSpace repository. https://dspace.org/



UNIVERSITY OF THE
WITWATERSRAND,
JOHANNESBURG

DEVELOPMENT OF ACTIVATED CARBONS FROM SOUTH AFRICAN COAL WASTE FOR APPLICATION IN NATURAL GAS STORAGE

JIBRIL ABDULSALAM (1571551)

UNIVERSITY OF THE WITWATERSRAND

2019



UNIVERSITY OF THE
WITWATERSRAND,
JOHANNESBURG

DEVELOPMENT OF ACTIVATED CARBONS FROM SOUTH AFRICAN COAL WASTE FOR APPLICATION IN NATURAL GAS STORAGE

Jibril Abdulsalam (1571551)

A thesis submitted to the Faculty of Engineering and the Built Environment, University of the Witwatersrand, Johannesburg, in fulfilment of the requirements for the degree of Doctor of Philosophy.

2019

DECLARATION

I declare this thesis to be my own work. The information derived from the literature has been duly acknowledged in the text and a list of references provided. It is being submitted for the degree of Doctor of Philosophy in the University of the Witwatersrand, Johannesburg. No portion of this thesis had earlier been submitted at any other university for any degree.

Signed:

_____

Jibril Abdulsalam

This _____ day of _____ 2019

ABSTRACT

Every year, South African coal sector generates over 60 million tons of coal waste, which are landfilled in discard dump and slurry ponds. The stockpile of this waste "resource" poses a severe danger to public health, the environment and the socio-economic development of the coal mining region. Therefore, there is an urgent need for an innovative strategy to coal waste reuse and recovery.

In this study, the potential of three South African coal waste samples (run-of-mine fines, discard and flotation slurry) were examined in synthesizing an activated carbon for application in natural gas storage. Activated carbons were prepared by KOH activation, and the impacts of KOH/sample weight ratio and temperature on the activated carbon adsorptive characteristics were examined and optimized using Response Surface Methodology (RSM). The results obtained indicated that with an increased temperature and KOH/sample weight ratio, the surface area and pore volume of the resulting activated carbon increased. The activated carbon with the highest surface area and pore volume from each of the samples were obtained at a temperature of 800 ^{o}C and KOH/sample weight ratio of 4:1.

The morphology, textural characteristics and elemental composition of the activated carbons produced were compared. The synthesized activated carbons were characterized by nitrogen at 77 K adsorption – desorption isotherms and SEM/EDS characterization. Surface area of 1925.34 m^2/g, 1826.41 m^2/g, 1484.96 m^2/g, pore volume of 1.26 cm^3/g, 1.21 cm^3/g, 1.03 cm^3/g and pore size of 2.90 nm, 2.66 nm and 2.51 nm were obtained for activated carbon from run-of-mine fines, discard and slurry, respectively. The SEM/EDS analysis showed pore development and high carbon content. The XRD evaluation confirms the activated carbons as amorphous. The presence of a hysteresis loop in the nitrogen isotherms and the pore size distribution (PSD) confirms highly porous activated carbons consisting of micropores and mesopores.

The characteristics of methane (the major constituent of natural gas) adsorption onto the activated carbons produced are measured for temperatures ranging from 0 to 50 ^{o}C, and pressures up to 40 bar. For this measurement, activated carbon with the highest surface area and pore volume from each of the coal waste samples was used. The activated carbon produced from the run-of-mine fines (ACR) offers a greater adsorption capacity due to its higher surface area and pore volume.

Three adsorption isotherm models (Langmuir, Toth, and Dubinin-Astakhov) were used to validate the measured adsorption data and the Dubinin-Astakhov isotherm model was found to be the most appropriate. The model described the measured data with an average regression error of less than 1% for all the three activated carbon samples. The impact of diffusion on adsorption kinetics was determined in relation to the time taken to achieve equilibrium for the methane/activated carbon system using a mass balance equation that defines pore and surface diffusion. The findings indicate the relationship between the adsorption kinetics, diffusivity, and temperature. An increase in temperature for the methane/activated carbon system was noted to cause an increase in diffusivity, thus reducing the time taken to attain equilibrium. The study indicated that adsorption characteristics (isotherm and kinetics) are the key information in designing and analysing an adsorbed natural gas storage (ANG) system.

An adsorption system using the activated carbons produced as the adsorbent bed was simulated using Aspen Adsorption Software (Adsim). In this study, adsorption capacity was found to be significantly increased by a lower flowrate. This enhances thermal stability and maximizes the quantity of gas adsorbed on the bed. The simulation shows that an ANG storage system's efficiency depends on the suitable selection of adsorbent, inlet flow conditions, and bed geometry.

LIST OF PUBLICATIONS

Journal Papers

1. **Jibril Abdulsalam**, Jean Mulopo, Bilainu O. Oboirien, Samson Bada, Rosemary Falcon, 'Experimental Evaluation Of Activated Carbon Derived From South Africa Discard Coal For Natural Gas Storage', International Journal of Coal Science & Technology, 2019. https://doi.org/10.1007/s40789-019-0262-5

2. **Jibril Abdulsalam**, Jean Mulopo, Mutiu K. Amosa, Samson Bada, Rosemary Falcon, Bilainu O. Oboirien, 'Towards a Cleaner Natural Gas Production: Recent Developments on Purification Technologies', Journal of Separation Science and Technology, 2019, Vol. 54, No. 15, pp. 2461–2497, 2019. https://doi.org/10.1080/01496395.2018.1547761

3. Jean Mulopo, **Jibril Abdulsalam**, 'Energy Storage Properties of Graphene Nanofillers. Graphene-Based Nanotechnologies for Energy and Environmental Applications, Elsevier; 2019. p. 155-79. https://doi.org/10.1016/B978-0-12-815811-1.00009-0

4. **Jibril Abdulsalam**, Jean Mulopo, Samson Bada, Bilainu O. Oboirien, 'Natural Gas Storage Properties of Adsorbents Synthesized from three different Coal Waste in South Africa'. Fuel (Under Review).

Conference Proceedings

1. **Jibril Abdulsalam**, Jean Mulopo, Samson Bada, Bilainu Oboirien 'Porous Carbon Materials from South Africa Coal waste for Gas Storage Applications: synthesis, characterization and high-pressure methane adsorption', 9th International Conference on Clean Coal Technologies, Houston, Texas, USA, June 3 - 7, 2019.

2. **Jibril Abdulsalam**, Jean Mulopo, Samson Bada, Rosemary Falcon, Bilainu Oboirien 'Low-Cost Microporous Material for Natural Gas Storage: Preparation and Characterization', 12th European Conference on Fuel and Energy Research and its Applications (ECCRIA), University of Cardiff, Cardiff, United Kingdom, September 5 – 7, 2018.

The abstracts of the papers are presented in Appendix A.

ACKNOWLEDGEMENTS

First of all, my gratitude to Almighty God, the Most Beneficent, the Most Merciful for His protection and for giving me good health to complete this study.

I recognize with pleasure the immeasurable contribution of my principal supervisor, Professor Jean Mulopo, whose valuable suggestions, encouragement, relevant and constructive criticisms have made this work a success.

I would also want to thank my Co-Supervisors, Dr. Samson Bada and Prof Bilainu Oboirien for their invaluable contribution to the success of this study.

I would like to express my special thanks and gratitude to Prof Rosemary Falcon and the Clean Coal Research Group for funding this research.

I wish to extend my appreciation to Prof Bilal Patel and Mr. Kabelo Ledwaba of the University of South Africa (UNISA) for granting me access to the HPVA equipment for adsorption experiments. My gratitude to Charles, Louis, and Timothy of Poretech, South Africa for the technical support provided during the use of the HPVA equipment.

My profound gratitude to the following people for their immeasurable contribution to the successful completion of this study; Prof Nikki Wagner, Dr Moshood Onifade, Dr Michael Bodunrin, Dr Yolanda Davids, Mr. Warren Carlson, Mr. Michael Van Rooyen of Anglo American Goedehoop Colliery, Dr Mutiu Amosa, Mr. Thomas Aniokete, Mr. Victor Mashindi, Mr. Tshepo Molefe, Mrs. Janet Smith, Mr. Motlatsi Phali, Mr. Bruce Mothibedi, Miss Ntokozo Dube, Mrs. Reghana Burns, Miss Sibongile Maswanganye and Mr. Phathutshedzo Sikhwari

I would like to thank the National Research Foundation of South Africa's SARChI Clean Coal Technology Grant (Grant Number: 86421) for their financial support for this project.

Last but not least, my heartfelt gratitude to my parents, my beloved wife, and my children for their understanding, kindness, and encouragement during my study.

Lastly, the opinions, findings, and conclusions stated in this thesis are those of the author and are not necessarily to be attributed to the National Research Foundation (NRF) and other institutions mentioned in this thesis.

TABLE OF CONTENTS

DECLARATION ..... **i**

ABSTRACT ..... **ii**

LIST OF PUBLICATIONS ..... **iv**

ACKNOWLEDGEMENTS ..... **v**

LIST OF FIGURES ..... **x**

LIST OF TABLES ..... **xii**

NOMENCLATURE ..... **xv**

CHAPTER 1 INTRODUCTION **1**

1.1 Overview 1

1.2 Research Motivation 2

1.3 Research Questions 5

1.4 Research Aim and Objectives 5

1.5 Thesis Structure 6

1.6 Summary 7

CHAPTER 2 LITERATURE REVIEW **8**

2.1 Introduction 8

2.2 Coal waste 8

2.2.1 Mining Waste 9

2.2.2 Washery Waste 10

2.3 The Need for Coal waste Beneficiation 11

2.3.1 Environmental Concerns 12

2.3.2 Economic Factors 14

2.4 Global and National Research Position on Coal waste 15

2.5 Natural Gas as an Energy Source 18

2.5.1 Natural Gas Storage and Transportation Technologies 20

2.6 Adsorbed Natural Gas (ANG) 25
2.6.1 Basic Principles of Adsorption 25
2.6.2 Overview of Adsorbents for ANG Storage System 28
2.6.3 Activated Carbon 30
2.6.4 Overview of ANG Storage System 39
2.7 Summary 44

CHAPTER 3 MATERIALS AND METHODS 45
3.1 Introduction 45
3.2 Materials 45
3.3 Methods 46
3.3.1 Sample collection 46
3.3.2 Sample Preparation 46
3.3.3 Sample Characterization 46
3.4 Synthesis of Activated Carbon 50
3.4.1 Chemical Activation 50
3.4.1.1 Experiment Design 51
3.5 Characterization of Synthesized Activated Carbon 52
3.5.1 Density Measurement 52
3.5.2 Measurement of Surface Area, Pore Volume and Size 53
3.5.3 SEM/EDS Technique 56
3.5.4 X-ray Diffraction (XRD) Technique 57
3.5.5 FT-IR Technique 59
3.6 Measurement of Methane Adsorption on Activated Carbons 59
3.6.1 Samples Preparation 60
3.6.2 Samples Degassing 62
3.6.3 Methane Adsorption/Desorption 63
3.7 Modeling and Simulation of Methane Adsorption onto Activated Carbon 64
3.8 Summary 64

CHAPTER 4 SYNTHESIS AND CHARACTERIZATION OF ACTIVATED CARBONS FROM COAL WASTE 65

4.1 Introduction 65

4.2 Samples Characterization 65

4.3 Experimental Design and Statistical Analysis 67

4.3.1 Response Analysis of synthesized activated carbon samples from Sample A 67

4.3.2 Response Analysis of synthesized activated carbon samples from Sample B 76

4.3.3 Response Analysis of synthesized activated carbon samples from Sample C 84

4.4 Selecting activated carbon samples for further studies 91

4.5 Nitrogen Adsorption Analysis 92

4.5.1 Pore Size Distribution (PSD) 94

4.6 SEM/EDS Analysis 96

4.7 XRD Analysis 98

4.8 FTIR Analysis 99

4.9 Summary 101

CHAPTER 5 ADSORPTION PROPERTIES OF METHANE ONTO THE ACTIVATED CARBONS 102

5.1 Introduction 102

5.2 Theoretical Background 102

5.3 Materials 109

5.3.1 Methane 109

5.3.2 Activated Carbon 110

5.4 Experiment 110

5.4.1 Measurement of Adsorbents Properties 110

5.4.2 Measurement of Adsorption Isotherms 110

5.5 Results and Discussion 110

5.5.1 High Pressure Methane Adsorption 110

5.5.2 Adsorption Isotherm Models 113

5.5.3 Heat of Adsorption 119
5.5.4 Adsorption Kinetics 120
5.6 Summary 123

CHAPTER 6 MODELLING AND SIMULATION OF METHANE ADSORPTION ONTO ACTIVATED CARBON 125
6.1 Introduction 125
6.2 Description of Storage System used for the Simulation 125
6.3 Model Development 126
6.3.1 Model Assumptions 126
6.3.2 Governing Equations 127
6.4 Results and Discussion 130
6.4.1 Pressure profile 130
6.4.2 Effect of Flowrate on Adsorbent Bed Temperature and Concentration 135
6.4.3 Effect of Adsorbent Bed Geometry on Temperature and Concentration 139
6.5 Summary 142

CHAPTER 7 CONCLUSIONS AND RECOMMENDATIONS 143
7.1 Introduction 143
7.2 Major Findings of this Research 143
7.3 Recommendations for Future Research 145

REFERENCES 147
APPENDICES 162
APPENDIX A: Abstract of Journal Publications and Conference Proceedings 162
APPENDIX B: MATLAB Programming Codes 168
APPENDIX C: SEM IMAGES Analysis in MATLAB 177
APPENDIX D: Adsim Specifications 182

LIST OF FIGURES

Figure 2.1 (a) Self-heating of run-of-mine fines (b) Aerial view of a stockpile of coal discard at Mpumalanga Highveld, South Africa (Rights, 2015) 9
Figure 2.2 Mechanized mining in operation (Mills, 2018) 9
Figure 2.3 Typical flow of run-of-mine coal from Mine to Washery 10
Figure 2.4 Slurry dump, adjacent to a coarse discard coal dump (Piechura, 2014) 11
Figure 2.5 Coal waste heap during spontaneous combustion (Onifade and Genc, 2018) 14
Figure 2.6 Share of Primary Energy Sources (Energy, 2018) 19
Figure 2.7 Schematic diagram of a typical adsorption process (Ruthven, 1984) 26
Figure 2. 8 Adsorption isotherm 27

Figure 3.1 Experimental Flowchart 45
Figure 3.2 Centrifugal Mill (Retsch ZM 200) 46
Figure 3.3 LECO TruSpec CHN Analyser 48
Figure 3.4 LECO C & S (CS23OSH) 49
Figure 3.5 Zeiss Axio M2M Reflected light Petrographic-microscope 50
Figure 3.6 Activated Carbon Preparation Setup 51
Figure 3.7 Image of Micromeritics Accupyc II 1340 Pycnometer 53
Figure 3.8 (a) Micromeritics Flow Prep 060 Unit and (b) Micromeritics TriStar 3000 instrument 54
Figure 3. 9 Start Analysis page of the SAIEUS software 56
Figure 3.10 Image of Carl Zeiss Sigma Field Emission Scanning Electron Microscope equipped with an Oxford X-act EDS detector 57
Figure 3.11 Image of Bruker D2 PXRD Phaser 58
Figure 3.12 Image of Perkin Elmer FTIR Spectrometer 59
Figure 3.13 Image of Particulate Systems High Pressure Volumetric Analyser (HPVA-200) 60
Figure 3.14 Cleaning HPVA II Sample Cylinder 61
Figure 3.15 Weighing the Empty Sample Cylinder 62
Figure 3.16 Connecting the furnace thermocouple cables to the Sample Compartment 62
Figure 3.17 Sample Analysis Compartment 63
Figure 3.18 HPVA II System Experiment Definition Window 63

Figure 4.1 Normal probability plot of residuals of (A) surface area and (B) pore volume 73
Figure 4.2 Residuals vs Predicted plot of (A) surface area and (B) pore volume 73
Figure 4.3 Predicted vs Actual plot of (A) surface area and (B) pore volume 74

Figure 4.4 3D surface plots showing the influence of temperature and weight ratio on (A) surface area and (B) pore volume 74
Figure 4.5 Contour plot of desirability and responses 76
Figure 4.6 Normal probability plot of residuals of (A) surface area and (B) pore volume 80
Figure 4.7 Residuals vs Predicted plot of (A) surface area and (B) pore volume 81
Figure 4.8 Predicted vs Actual plot of (A) surface area and (B) pore volume 81
Figure 4.9 3D surface plots of (A) surface area and (B) pore volume..... 82
Figure 4.10 Contour plot of desirability and responses 83
Figure 4.11 Normal probability plot of residuals of (A) surface area (B) pore volume 88
Figure 4.12 Residuals vs Predicted plot of (A) surface area and (B) pore volume 88
Figure 4.13 Predicted vs Actual plot of (A) surface area and (B) pore volume 89
Figure 4.14 3D surface plots showing the influence of temperature and weight ratio on (A) surface area and (B) pore volume 89
Figure 4.15 Contour plot of desirability and responses 91
Figure 4.16 Nitrogen adsorption-desorption isotherms of synthesized activated carbons 93
Figure 4.17 BET surface area plots of the synthesized activated carbons. 94
Figure 4.18 Pore size distribution of the activated carbon samples calculated by the NLDFT method..... 96
Figure 4.19 SEM images of (A) Sample A (B) Sample B (C) Sample C (D) ACR (E) ACD (F) ACS 97
Figure 4.20 XRD Profile of (A) Sample A; (B) ACR; (C) Sample B; (D) ACD and (E) Sample C (F) ACS 99
Figure 4.21 FTIR Images of (A) Sample A (B) Sample B (C) Sample C (D) ACR (E) ACD (F) ACS 100

Figure 5.1 Schematic diagram of Langmuir adsorption mechanism on a flat surface (Do, 1998) 103
Figure 5.2 Schematic of parallel pore and surface diffusion (Do, 1998)..... 107
Figure 5.3 Isotherms of methane adsorption onto the activated carbon samples 111
Figure 5.4 Langmuir model fitting of methane adsorption data onto activated carbon samples 115
Figure 5.5 Toth model fitting of methane adsorption data onto activated carbon samples ... 116
Figure 5.6 D-A model fitting of methane adsorption data onto activated carbon samples ... 117
Figure 5.7 Comparison of methane adsorbed amount with coal-based activated carbons at 25 ^{o}C. .. 118
Figure 5.8 Comparison of methane adsorbed amount at 25 °C with CNG 119
Figure 5.9 Heat of Adsorption of the Activated Carbon Samples 120

Figure 5.10 Plots of the amount adsorbed per unit volume versus time.....122

Figure 6.1 Schematic of an ANG system.....125
Figure 6.2 Process flow diagram (PFD) illustrating the ANG system in Adsim.....126
Figure 6.3 Fitting of the experimental adsorption data with the Langmuir model for methane adsorption on activated carbons produced.....130
Figure 6.4 Simulated pressure profiles of the activated carbon samples as a function of time 131
Figure 6.5 Simulated pressure profiles inside the ACR adsorbent bed along the bed height 132
Figure 6.6 Simulated pressure profiles inside the ACS adsorbent bed along the bed height.....133
Figure 6.7 Simulated pressure profiles inside the ACD adsorbent bed along the bed height 134
Figure 6.8 Average temperature distribution as a function of time for different adsorbent bed.....136
Figure 6.9 Average bed concentration as a function of time (A) ACR adsorbent bed (B) ACD adsorbent bed (C) ACS adsorbent bed.....138
Figure 6.10 Average bed temperature and concentration as a function of time for different D/H ratio (A) ACR bed (B) ACD bed (C) ACS bed 141

LIST OF TABLES

Table 2.1 Natural Gas Trade in 2015 in Billion Cubic Meters (BP, 2016) 20

Table 3.1 Structure and CCD Design Matrix of Synthesis Experiments.....52

Table 4.1 Proximate, Ultimate, Total sulfur and Petrographic analysis of coal waste samples.....66
Table 4.2 Results from Synthesis of Activated Carbon Samples from Sample A.....68
Table 4.3 ANOVA Results for surface area and pore volume of the synthesized activated carbon samples from Sample A 71
Table 4.4 Experimental values vs Predicted values of the Surface area and Pore volume of Activated Carbon Samples from Sample A 72
Table 4.5 Optimum conditions setting for optimized response 75
Table 4.6 Optimized Solutions 75
Table 4.7 Results from Synthesis of Activated Carbon Samples from Sample B.....77
Table 4.8 ANOVA Results for surface area and pore volume of the synthesized activated carbon samples from Sample B 79
Table 4.9 Experimental values vs Predicted values of the Surface area and Pore volume of Activated Carbon Samples from Sample B 80
Table 4.10 Optimum conditions setting for optimized response 82
Table 4.11 Optimized Solutions 83
Table 4.12 Results from Synthesis of Activated Carbon Samples from Sample C.....84
Table 4.13 ANOVA Results for surface area and pore volume of the synthesized activated carbon samples from Sample C 86
Table 4.14 Experimental values vs Predicted values of the Surface area and Pore volume of Activated Carbon Samples from Sample C 87
Table 4. 15 Optimum conditions setting for optimized response 90
Table 4.16 Optimized Solutions 90
Table 4.17 Physical and structural properties of the activated carbon samples.....92
Table 4.18 EDS analysis of Coal waste samples and its derived Activated Carbons.....98

Table 5.1 Summary of isotherm models used in this study 105
Table 5.2 Experimental Data of Methane adsorption onto the activated carbon samples.....112
Table 5.3 Adsorption parameters for Langmuir model 113
Table 5.4 Adsorption parameters for Toth model.....115

Table 5.5 Adsorption parameters for D-A model 117
Table 5.6 Parameters used in MATLAB code ADSORB1A.M 121

Table 6.1 Thermophysical parameters used in Adsim simulation 129
Table 6.2 Physical dimension of the Adsorbent Bed for various D/H ratio 139

NOMENCLATURE

A%	Percentage of ash
ACD	Activated carbon from discard
ACF	Activated carbon fiber
ACR	Activated carbon from run-of-mine fines
ACS	Activated carbon from Slurry
ad	Air-dried
adb	Air-dried basis
ANG	Adsorbed natural gas
ANOVA	Analysis of variance
ASTM	American Society for Testing and Materials
ATR	Attenuated total reflectance
b	Affinity constant
BET	Brunauer, Emmett, and Teller
BJH	Barrett-Joyner-Halenda
BP	British Petroleum
C(t)	volumetric concentrations in the gas phase
C_{μ}	Amount of adsorbed
$C_{\mu}(t)$	Volumetric concentrations in the adsorbed phase
$C_{\mu s}$	Saturated amount of adsorbate adsorbed
C_b	Bulk concentration
CCD	Central composite design
CEC	Cation exchange capacity
C_{eff}	Effective heat capacity
CFB	Circulating fluidized bed
CH_4	Methane
C_i	Initial concentration
cm^3/g	Cubic centimeter per gram
CMS	Carbon molecular sieves
CNG	Compressed natural gas
CO_2	Carbon dioxide
C_{pg}	Gas specific heat
C_{ps}	Adsorbent specific heat

CV	Calorific value
D/H	Diameter/Height
D-A	Dubinin-Astakhov
DME	Department of Mineral and Energy
DOE	Department of Energy
DOF	Degree of freedom;
Dp	Pore diameter
D_p	Pore diffusivity
D-R	Dubinin-Radushkevich
D_s	Surface diffusivity
D_{so}	Pre-exponential constant
E	Characteristic energy of adsorption
EDS	Energy Dispersive Spectroscopy
FC%	Percentage of fixed carbon
FCV	Flow controller
FMRF	Federal Mine Reclamation Fund
FTIR	Fourier Transform Infrared
GAC	Granular activated carbon
GHG	Greenhouse gases
GTL	Gas to liquids
GtS	Gas to solids
GTW	Gas to wire
GWe	Gigawatts of electricity
H_3PO_4	Phosphoric acid
ha	Hectare
H_{ads}	Heat of adsorption
HCl	Hydrochloric acid
HK	Horvath and Kawazoe
HPVA	High Pressure Volumetric Analyser
HS	Humic substance
HTC	Hydrothermal carbonization
ICCP	International Committee for Coal and Organic Petrology
in. mm	Including mineral matter

IRR	Internal rate of return
ISO	International Standard Organisation
k	Kelvin
K	Permeability
kg	kilogram
KJ	kilojoule
km^2	square kilometer
K_o	Knudsen diffusion parameter
KOH	Potassium hydroxide
LNG	Liquefied natural gas
M%	Percentage of moisture
m^2/g	square meter per gram
Mg	Molecular weight of gas
mg/g	Milligram per gram
min	Minute
MJ	Megajoule
M(t)	The amount adsorbed per unit volume as a function of time
MMscf	Million standard cubic feet
mmf	Mineral matter free basis
MOF	Metal-organic framework
mol	Mole
MPa	Mega Pascal
MPSD	Micropore size distribution
Mt	Million tons
MW	Megawatt
n	Dubinin-Astakhov parameter
N_2	Nitrogen
NaOH	Sodium hydroxide
NGH	Natural Gas Hydrates
NIST	National Institute of Standards and Technology
NLDFT	Nonlocal density functional theory
NOx	Nitrogen oxides
NPVs	Net present values

O%	Percentage of fixed oxygen
^{o}F	Degree Fahrenheit
OHC	Other hydrocarbons
P	Pressure
P/P_o	Relative pressure
PAC	Powdered activated carbon
P_c	critical pressure
PCV	Pressure gauge
PFD	Process flow diagram
Plc	Public limited company
P_o	saturation pressure
POAE	Percentage of absolute error
ppm	Part per million
PV	Pore volume;
q	The concentration of gas adsorbed on the bed
R	Gas constant
ROM	Run-of-mine
Rp	Particle radius
RSM	Response Surface Methodology
SA	Surface area;
SAIEUS	Solution of Adsorption Integral Equation Using Splines
SANS	South African National Standard
SEM	Scanning Electron Microscopy
SO_2	Sulfur dioxide
T	Temperature
t	Heterogeneity parameter
T_c	Critical temperature
TDE	ThermoData Engine
T_o	Reference Temperature
u_g	Gas velocity
USA	United States of America
v/v	Volume per volume
VLV	Valve

VM%	Percentage of volatile matter
V_p	Volume of the adsorbent
W	Gas uptake
W_o	Saturated volume uptake of the gas
wt. %	Weight percentage
XRD	X-ray diffraction
$Zncl_2$	Zinc chloride
ΔH	Change in enthalpy

Symbols

%	Percentage
<	Less than
>	Greater than
Å	Angstrom
ε	porosity
^oC	Degree Celsius
δ	Thermal expansion coefficient
ε_b	Inter-particle porosity
ε_p	Intraparticle porosity
ε_t	Total porosity
θ	Fractional Loading
λ_{eff}	Effective thermal conductivity of the adsorbent bed
λ_g	Thermal conductivity of gas
λ_s	Thermal conductivity of adsorbent
μm	micrometer
ρ_b	adsorbent bed density
ρ_g	gas density
ρ_s	Solid bed density without porosity

Subscripts

μ	Adsorbed phase
ads	Adsorption
b	bed

c	critical
eff	Effective
g	Gas
i	initial
p	pore
s	Solid adsorbent
t	total

CHAPTER 1 INTRODUCTION

1.1 Overview

Coal mining and beneficiation processes produce substantial amounts of coal waste. Huge quantities of coal waste are generated in many coal-producing countries. Sixty (60) million tons of coal waste is generated annually in South Africa and about 1.2 billion tons are stockpiled according to the study reported by the South African Mineral and Energy Department (Belaid *et al.*, 2013).

Coal waste has been categorized into three classifications: fines from run-of-mine also referred to as duff coal, discard coal and slurry coal (Pupier *et al.*, 2005). Previously, the requirement for major coal users in South Africa was a particle size of +6 mm, hence coal mines had to screen the specification for coal and particles below - 6 mm were referred to as fines from run-of-mine (Piechura, 2014). Discard coal is produced from coal beneficiation. It is the percentage of coal that is reported as sink in a float-sink coal beneficiation process and is characterized by high ash content (Moyo et al., 2018). The slurry is also produced from the process of coal beneficiation, but is too wet to be used in conventional combustion equipment and cannot be mechanically dewatered to an appropriate level (North *et al.*, 2015). The problem of stockpiling coal waste on the environment includes leaching, acidification, spontaneous combustion, the release of toxic substances (sulfur, mercury) and occupation of useful land (Belaid et al., 2013, Onifade and Genc, 2018).

There is growing pressure to reduce the environmental impacts of coal waste. As part of the overall strategy to provide viable, cost-effective and accessible energy in the future, this study investigates the opportunity to use coal waste to produce activated carbon to store natural gas. As a result of this, low-cost energy storage material, diversification of the energy mix, enhanced energy security, and increased natural gas utilization will be some of the benefits of this research.

Over the years, interest in natural gas has increased significantly as a viable alternative energy source. Besides being cheaper and cleaner than other conventional fossil fuels, countries wishing to reduce their over-reliance on imported crude oil are looking towards natural gas to satisfy their ever-increasing demand for energy. To fulfil this requirement, a suitable storage system is needed to facilitate access to and improve the use of natural gas.

The existing natural gas storage systems are compressed natural gas (CNG), liquefied natural gas (LNG) (Choi *et al.*, 2009). In the CNG storage system, the gas is stored in a cylindrical vessel at about 200 to 250 bar (Policicchio *et al.*, 2013). Some of the problems with CNG are the huge capital investment, high storage pressure, and safety issues. In LNG, natural gas is condensed to a liquid by rapid temperature drop to about -162 ° C and then stored in storage vessels (Alhasan *et al.*, 2016). Some of its shortcomings are high energy requirements and high capital infrastructure.

Adsorbed natural gas (ANG) storage system is a promising alternative to the current storage systems. ANG's technology includes storing natural gas on porous materials packed in a vessel at reduced pressure. The ANG technology makes it possible to store the same amount of gas at a much lower pressure as the CNG system (Pupier *et al.*, 2005). Lower pressure storage offers two significant competitive advantages; reduces the demand for high energy compression and also allows flexibility in storage tank design and configuration. In addition, since ANG utilizes porous adsorbent materials packed in a vessel, this provides higher energy density and higher storage capability.

The most promising porous adsorbents for ANG are activated carbons with high surface area (Quinn and MacDonald, 1992, Menon and Komarneni, 1998, Alcañiz-Monge et al., 2009a). There has been considerable effort to develop appropriate activated carbons for ANG storage system (Lozano-Castello et al., 2002a, Molina-Sabio and Rodrıguez-Reinoso, 2004, Prauchner and Rodriguez-Reinoso, 2008) and it has been found that activated carbons with an average pore diameter of less than 20Å are best suited for ANG (Biloe *et al.*, 2001, Esteves *et al.*, 2008) Activated carbons are usually produced using raw materials such as coal, coconut shells, rice husks, etc. through physical or chemical activation process. However, the appropriate raw material and optimum synthesis process must be well identified to produce activated carbon with high adsorption ability.

1.2 Research Motivation

Coal waste stockpile often has significant effects on the local climate and landscape (Antoszczyszyn and Michalska, 2016, Moyo et al., 2018, Mills, 2018). However, it can be expensive and complicated to address the issues. For instance, establishing ownership and accountability may be hard. For many centuries, some heaps of coal waste have been deserted and the mining firms responsible for creating them no longer exist. In other instances, even

where a business or its successor continues to operate, some have been reluctant or unable to take accountability for historical waste repositories. In addition to the existing stockpile of coal waste, more is produced annually through the mining processes, and a breakthrough is needed to beneficiate the coal waste to sustain the supply of affordable and accessible energy (Stolboushkin *et al.*, 2016).

In South Africa, exploring the energy potential of South African's coal waste has been a challenge and a major concern to the mining companies and the Department of Mineral and Energy (DME). While there are available studies on the beneficiation of coal waste, the focus has been on improving the quality of coal waste for electricity production (Piechura, 2014, North *et al.*, 2015, Belaid *et al.*, 2013). Attempts were made to produce briquettes from coal waste (Papin *et al.*, 2015, Borowski and Hycnar, 2013). However, there has not been any study that reports on the synthesis of activated carbons from South African coal waste and its subsequent evaluation for natural gas storage both at atmospheric pressure and high-pressure conditions.

Increasing global demand for energy has made natural gas popular as a viable option to produce affordable energy. Natural gas is an important source of energy. Distribution of natural gas is complex and highly capital-intensive, making it difficult to deliver natural gas to secondary consumers such as small and medium-sized sectors, small and medium-sized independent power plants, housing clusters, cities, and villages. Huge capital is spent on pipeline construction, large-scale compressor equipment procurement, and energy for system maintenance (Hamedi *et al.*, 2009).

Significant use of natural gas as an alternative vehicle fuel can ease the stress on the production and control of petroleum emissions. The present CNG storage system has high-pressure requirements, high energy expenses, and investment costs as some of its problems (Alhasan et al., 2016). In addition, drivers may often be reluctant to carry a gas cylinder with high pressure in vehicles. Therefore, efforts have been made to improve natural gas storage technology. The primary objective of this research is to reduce the storage pressure, as reducing the pressure leads to lower expenses and enhanced safety (Wang *et al.*, 2011, Wang and Kaskel, 2012, Wang *et al.*, 2018).

ANG technology has been suggested as a viable option for natural gas storage and transport, but its deployment and commercialization has been restricted owing to some problems such as

adsorbent cost and low storage capability compared to CNG. However, the ANG system can be designed to store natural gas in a low-weight vessel filled with porous adsorbent at comparatively low pressure (20 to 40 bar), which allows for excellent design flexibility in vessel configuration, as well as filling the storage tank with a cheap single-stage compressor. Wegrzyn and Gurevich (1996) reported the comparative cost analysis related to each technology. The study showed that the advantage of ANG over CNG and LNG include its reduced gas refueling and tank manufacturing costs. These attractive features of the ANG storage system over other storage methods are the primary motivating considerations for the continuous development of this technology.

ANG is a promising natural gas storage technology for automotive, industrial and domestic applications (Alhasan *et al.*, 2016). However, some variables limit the commercial implementation of ANG technology. High storage density is the primary objective of ANG application in vehicles in order to manufacture cars with a longer driving range (Judd *et al.*, 1998). For ANG applications in bulk storage of natural gas, the viability depends heavily on adsorbent costs (Judd et al., 1998). Therefore, good adsorbent for an ANG system must have high storage capacity and low cost among other variables.

Several studies have been conducted to develop appropriate adsorbents to improve storage capacity and lower ANG system costs. Alhasan *et al.* (2016) reported an activated carbon from coal to have a storage volume of 54 v/v. Esteves *et al.* (2008) revealed that some commercially activated carbons were able to adsorb the same volume of natural gas as CNG at 35 bar, which is 6 times less the pressure required for CNG. Lozano-Castello *et al.* (2002b) reported a storage capacity of 165 v/v at 40 bar and 25 °C from activated carbon derived from anthracite coal using KOH activation.

In view of the problems of coal waste on the environment and the high cost of adsorbent for the ANG storage system, this research is motivated to explore the synthesis of activated carbons as adsorbents from three different South African coal waste and evaluate their ability to store natural gas. Since the adsorption characteristic of the adsorbent is highly important to this study, it is therefore necessary to measure the adsorption isotherms and kinetics for methane adsorption onto the synthesized activated carbons.

1.3 Research Questions

The adverse impact of coal waste on the environment include pollution of the environment and an increased threat to public health. There are at least two prospective uses for coal waste: firstly, coal waste to produce other products, and secondly coal waste to generate electricity. This thesis seeks to answer the following questions from the foregoing:

- Is the coal waste (Fines, Discard, and Slurry) in South Africa good enough to be used as raw material for activated carbon?
- What is the potential of activated carbon produced from coal waste in natural gas storage application?

1.4 Research Aim and Objectives

The aim of this study is to develop porous adsorbents (activated carbons) from South African coal waste for application in natural gas storage. This is to provide solutions to the environmental issues of coal waste and to provide the ANG storage system with a cost-effective adsorbent.

The specific objectives of this study are to:

- Evaluate the characteristics (moisture, ash, volatile matter, fixed carbon, carbon, sulfur, and petrographic composition) of South African coal waste. This is done to assess the utility of producing activated carbons from the samples and for a better understanding of the properties of these samples;
- Synthesis and characterize activated carbons from these samples using KOH activation at different temperatures and KOH weight ratio;
- Measure the adsorbed amount of methane onto the activated carbons at different pressures and temperatures; and
- Simulate an ANG system to evaluate the adsorbent bed's thermal behavior during methane adsorption onto the activated carbons.

1.5 Thesis Structure

There are seven chapters in this thesis.

Chapter 1: Introduction

This section introduces the research subject and brings together the context, motivation, objectives, the structure of the thesis and the information concisely presented by each chapter in the thesis.

Chapter 2: Literature Review

Chapter 2, which has seven sections, provides an extensive literature review of coal waste and its possible application for the storage of natural gas. The first section presents the reader with the chapter's content. A short description of the types and sources of coal waste is given in the second section. Section three highlights the need to beneficiate coal waste in terms of its environmental and economic advantages. Section four provides a review of past research on coal waste beneficiation. Natural gas as an energy source is discussed in section five, highlighting the benefits of natural gas over other fossil fuels. In section 6, fundamental adsorption principles, adsorbents for the ANG storage system are described followed by a review of activated carbons and developments in the ANG storage system. Section 7 summarizes the content of the chapter.

Chapter 3: Experimental methods

This chapter discusses the different experimental techniques performed on the samples and the activated carbons synthesized. The chapter provides comprehensive detail on the test procedures and equipment used. The experimental studies involved sample preparation, sample characterization tests (proximate analysis, ultimate analysis, total sulfur, and petrographic analysis) and the characterization of synthesized activated carbons. The experimental details also include the measurement of adsorption characteristics, such as isotherms and kinetics for methane adsorption onto activated carbons.

Chapter 4: Synthesis and Characterization of Activated Carbons from Coal waste

This chapter presents and discusses the results of the activated carbon synthesis from coal waste. Response Surface Methodology (RSM) was used to evaluate the effect and interactions of KOH weight ratio and temperature on the physical characteristics of the activated carbons produced. The chapter also provides the evaluation of nitrogen adsorption (BET), SEM/EDS,

XRD, FTIR and pore size distribution of selected activated carbon samples from each of the coal waste samples being studied**.**

Chapter 5: Adsorption Properties of Methane onto the Activated Carbons

This chapter presents the analysis of the adsorption equilibrium, the impact of surface diffusion on adsorption kinetics, and the heat of adsorption of methane onto the activated carbons produced. Also discussed are the results of the adsorption experiment validated with isotherm models of Langmuir, Toth, and Dubinin-Astakhov (D-A). The chapter also provides a comparative analysis of the adsorption capacity of the activated carbon produced in this study with activated carbons from coal-related materials in the literature.

Chapter 6: Modelling and Simulation of Methane Adsorption onto Activated Carbon

This chapter presents the simulation of an adsorption system using the developed activated carbons. A gas model is simulated to study the impact of charging rate and bed geometry on temperature distribution in the adsorbent bed as a function of time.

Chapter 7: Conclusions and Recommendations

This chapter provides an overview of the research and outcomes based on the findings of experimental and model studies. The primary findings of this research as well as further recommendations are presented.

1.6 Summary

Chapter one introduces the reader to the research focus, motivation, research objectives, and the thesis structure. It also outlined the need for South African coal waste beneficiation and the significance of storing natural gas for cheap and accessible energy. The next chapter outlines the literature review on subjects related to this study.

CHAPTER 2 LITERATURE REVIEW

2.1 Introduction

In this chapter, an in-depth review of literature on the potential of waste derived from coal mining and processing and adsorbed natural gas (ANG) as an attractive storage system for natural gas is presented. The storage of natural gas is crucial in the use of natural gas as an energy source and as a feedstock in the production of other useful products. Several studies on the ANG storage system have been conducted and focus has been on developing an appropriate and cost-effective adsorbent. In addition, there are ongoing studies into the optimization of the system to enhance storage capacity and the development of an effective thermal management system. In presenting the review, the types of coal waste found in South Africa, the need to beneficiate the coal waste, national and global research position on coal waste beneficiation, global natural gas demand, the need for natural gas storage, an overview of various natural gas storage methods and adsorption fundamentals are presented.

2.2 Coal waste

Coal mining through mechanization and processing generates an enormous quantity of fines, which ends up in the dump or slurry pond. A significant quantities of coal waste have been produced in many coal-producing countries over the past decades (Mills, 2018). In South Africa alone, about 1.2 billion tons are said to have been generated and about 60 million tonnes generated annually (Belaid *et al.*, 2013). Since not much attention was placed in finding ways of beneficiating these wastes, coal waste has continued to accumulate over the years, occupying potentially useful land and polluting the environment with problems such as spontaneous combustion and groundwater contamination. A stockpile of run-of-mine fines undergoing spontaneous combustion and an aerial view of a stockpile of coal discard at Mpumalanga Highveld, South Africa is presented in Fig. 2.1(a and b). This coal dump contains significant amounts of usable carbon, some of which can be recovered and used as an inexpensive source of energy, thus reducing its impact on the environment and helping diversify the energy mix. With increasing strict regulations and government policies to reduce the impact of this waste on the environment, finding an alternative use for the waste has become highly imperative. Some coal waste can be used in some combustion system, sometimes the residual carbon can be recovered and used as fuel. While some coal waste might need slight pretreatment, others

may require an upgrade or blend with high quality coal before use (Ottiger *et al.*, 2006, Mills, 2018).



Figure 2.1 (a) Self-heating of run-of-mine fines (b) Aerial view of a stockpile of coal discard at Mpumalanga Highveld, South Africa (Rights, 2015)

2.2.1 Mining Waste

In the early days of mining, coal mining was done using methods highly dependent on manual labor. Originally, these labor dependent methods separate coal inorganic and undesirable associated minerals from the coal. With the advent of mechanized mining (Fig. 2.2) especially in underground mining, the proportion of unwanted materials has increased over time. The use of mechanized mining has resulted in the inclusion of more unwanted mineral matter and the generation more fine coal particles (Mills, 2018).



Figure 2.2 Mechanized mining in operation (Mills, 2018)

With the adoption of opencast mining method, most coal mined is often polluted with overburden, clays, and rocks (Mills, 2018). In addition, underground mining generates varying amounts of waste with coal. This waste includes coarse discard and fines and is often found together with the run-of-mine (ROM) coal. Waste generated from the current coal mining operations, often comprises of various types of coal organic, soil, clays, rocks, and other inorganic minerals. The constituents of the coal waste can vary widely and often dependent on factors such as coal type, the geology of the location, mining method, and the processing technique.

2.2.2 Washery Waste

Run-of-mine (ROM) coal is known as freshly mined and unprocessed coal. ROM coal often contains minerals that is extracted with the coal during mining. It is usually washed to remove the ash forming minerals and sulfur content in the coal as illustrated in Fig. 2.3. In addition, the washing process usually produces a stream of discard which includes coarse-grained material and fine-grained (less than 1 mm) waste often referred to as tailings (Chung and others, 2014).

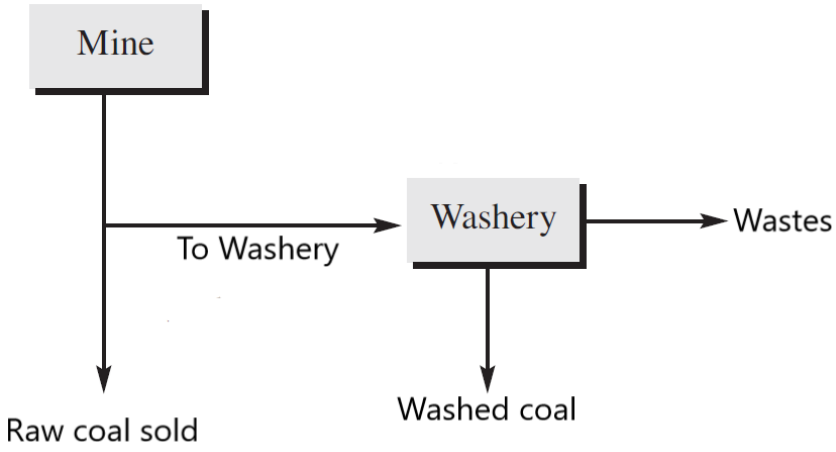


Figure 2.3 Typical flow of run-of-mine coal from Mine to Washery

As a result of declining coal quality in most coal producing countries especially in South Africa, the washing process has become a necessity to meet the market requirement and specification (Reid, 2017). The washing process which involves solid-solid and solid-liquid techniques often carried out after mining and prior to the transportation of the washed coal. The washing is done to reduce the concentration of ash, sulfur, and improve on the quality of

the ROM coal. Most of the washing process involves crushing the ROM and then grouping them into coarse, fine and ultrafine portions. A dense medium, i.e. sink/float process is used to separate coal from its associated gangues components/minerals, while froth flotation is used to recover the ultrafine particles (Mills, 2018). Screens or centrifuges are often used in removing water from coarse coal, while belt or vacuum filter and in some cases, thermal drying is used in removing water from coal fines. Removal of water from coal fines are usually difficult and expensive, thus the coal are often discarded as a slurry which contains water, coal fines, silt, clay, and other fine mineral particles into a settlement pond as shown in Fig. 2.4.



Figure 2.4 Slurry dump, adjacent to a coarse discard coal dump (Piechura, 2014)

2.3 The Need for Coal Waste Beneficiation

While the contribution of coal to global energy generation cannot be overemphasized, the effect of waste generated from coal-related operations cannot be overlooked either. The effects of coal waste on the environment include acidic run-off, water pollution and spontaneous combustion which pollutes the environment (Maiti, 2012, Le Roux, 2014, Gupta and Paul, 2015, Mills, 2018). The need to find solutions to huge stockpiles of coal waste and rehabilitate the sites they occupy has become of utmost importance. This in addition to increasing public health and safety awareness among the populace and increasing strict regulations. The need to beneficiate coal waste can be classified under two broad reasons; environmental, economic or a combination of both. Aside from the standpoint of providing a sustainable and safe

environment, mining industries are often required by law and legislation to provide adequate waste treatment and disposal processes to mitigate against the adverse effect of coal waste on the environment.

2.3.1 Environmental Concerns

Coal waste from coal processes has been a constant occurring feature in the mining industry. This waste has the potential as a huge energy resource, but its high sulfur, ash and moisture content limits its usage. The lack of technology, equipment costs have also been reported as some of the challenges in the beneficiation of coal waste (Swanepoel, 2008).

The areas of land occupied by coal waste are one of the impacts of coal waste on the environment. There is growing pressure around the world on the need to reclaim lands occupied by coal waste. This pressure comes in the form of legislation, penalties, and incentives (Mills, 2018). For example, in the United States, the government provided funding such as Federal Mine Reclamation Fund (FMRF), to rehabilitate waste dumps for the overall improvement of the environment. This effort has led to the restoration of about 2800 ha of land previously unusable (Mills, 2018). In India, increasing population and urbanization make land rehabilitation and recovery of coal waste of utmost importance. Land requirement for coal operations including land available for coal waste has been estimated to increase from 1470 km^2 in 2007, to 2925 km^2 by 2025 (Maiti, 2012). In South Africa, a guideline backed by legislation is the key driver in the restoration of coal waste dumps to its former useful state. This guideline is driven by three key objectives which are; restoration of a waste dump to the satisfaction of the host community not necessarily to its previously usable state, restoring the land to its previous usable state (in particular, land with high agricultural potential) and restoring the land to its previous state with no loss of its biodiversity (Tanner, 2007).

Continuous leaching of waste dumps can cause the discharge of several metals such as iron, chromium, lead, manganese, and aluminum. This leads to acid drainage, which pollutes available streams and rivers. Another toxic element found in coal waste dumps is mercury. The composition of toxic elements found in coal waste dumps varies (Chen *et al.*, 2014). For example, a coal waste dump in West Virginia, USA, is said to contain 10 ppm of arsenic, 0.3 ppm of mercury and 16- 20 ppm of lead, while another dump located at Pennsylvania contains about 50 ppm of arsenic, 0.7 ppm of mercury and 34 ppm of lead (Skinner and Brown, 2011).

In Poland, studies established that about 55 – 249 ppm of mercury is contained in coal waste and this is considerably higher than mercury content of the parent coal (Antoszczyszyn and Michalska, 2016). High sulfur level and high acidity has been reported in some coal waste dumps in China while waste dumps in Russia have been confirmed to contain high sulfur level and heavy metals (Mills, 2018, Chen *et al.*, 2014). A higher concentration of trace metals is obtained from the coal washing process in India (Gupta and Paul, 2015). In South Africa, iron, sulfur, lead, antimony, arsenic, manganese, and mercury have been identified as some of the major and trace elements contained in some of the coal dumps with a potentially harmful effect on the environment (Moyo *et al.*, 2018).

Spontaneous combustion is another consequence of coal waste dump on the environment. This occurs by the self-heating of coal in the presence of adequate oxygen to trigger the low-temperature reaction of coal with oxygen. Once spontaneous combustion occurs, the coal waste dump can burn for a long period of time, discharging toxic substances into the atmosphere. Fire occurrence due to spontaneous combustion is a recurring problem in most coal producing nations. For example, about forty coal waste stockpiles are said to be burning at any point in time in Pennsylvania, United State (Mills, 2018). In China, about one-third of the country's 3000 coal waste dumps undergoes spontaneous combustion causing substantial air pollution. In Ukraine, an estimated 500,000 tons of SO_2, NOx, and CO_2 are emitted yearly from spontaneous combustion of coal dumps (Mills, 2018).

In South Africa, there have been reports of the frequent occurrence of spontaneous combustion in coal waste dumps as shown in Fig. 2.5. (Onifade and Genc, 2018). The emission of greenhouse gases (GHG) such as CO_2 and CH_4 from the self-heating of these dumps has been a huge concern to the industry and the government of South Africa. Overall, the global impact of spontaneous combustion on the environment is of great concern, long term sustainable measures are therefore required to curtail the problem in addition to the existing solutions of minimizing the impact of spontaneous combustion.



Figure 2.5 Coal waste heap during spontaneous combustion (Onifade and Genc, 2018)

2.3.2 Economic Factors

The prospect of economic benefits is another significant factor in the need to beneficiate coal waste. In beneficiating coal waste and rehabilitation of waste dumps, a number of applicable options are available, some leading to the recovery of usable coal, while other options include the conversion of coal waste to valuable products. The beneficiation of coal waste for power generation in power plants can significantly improve fuel savings (North *et al.*, 2015). This, in turn, will lead to the availability of energy feedstock, a sustained supply of low-cost power and generally improve the cost and standard of living. For example, Severstal, the biggest steel company in Russia uses coal waste slurry in its power plant. This has resulted in savings of over 25 million rubles for the steel company (Group, 2014).

The benefits of coal waste beneficiation to South Africa, in particular, are enormous. The recovery of high quality coal waste from slurry pond or coal dump for power generation might lower the price of electricity, diversify the national energy mix and enhance energy security. The production of briquettes is another commercial use of coal waste in South Africa, but challenged by the high cost of binders (Borowski and Hycnar, 2013). The beneficiation of coal waste, therefore, offers a unique opportunity of providing a sustainable and affordable energy supply.

2.4 Global and National Research Position on Coal Waste

Several studies are available on the beneficiation of coal waste in the literature (Skinner and Brown, 2011, Borowski and Hycnar, 2013, Papin et al., 2015, Stolboushkin et al., 2016, Moyo et al., 2018). Most of these studies are conducted on coal fly ash while there are limited studies on coal discards, fines, and slurry. Within the limited studies available on coal discard, fines, and slurry, the main focus was on improving their quality for power generation.

Falcon and Falcon (1985) investigated the beneficiation potentials of some coal fines in South Africa. The potential was observed to vary substantially on the degree of weathering and oxidation, rank and composition of the parent coal as well as the separation method used. The study also investigated the organic and inorganic composition of three distinct coal fines typically found in the Witbank/Highveld coalfields. In addition, the beneficiation potential for upgrading coal fines through gravity separation unit and froth flotation unit was compared. The result showed that coal fines from a froth flotation unit have a higher beneficiation potential. The study also revealed that the coal microlithotype has a greater influence on the beneficiation potential of the coal than the individual maceral or mineral constituents.

Henmi (1987) synthesized hydroxyl sodalite from thermal plant coal waste ash as a waste utilization option to minimize the effect of the waste and also a means of recycling the waste material. The coal waste ash was made into a slurry using NaOH water solution. The slurry was heated to 90 ^{o}C for 3-24 hours. At the completion of the reaction, the mixture was washed and separated by centrifugation. The product derived from the coal waste ash was found to be of high cation exchange capacity (CEC). CEC is a measure of how much cations can be retained on the surface of the soil particle. The prepared hydroxyl sodalite was recommended as a soil amendment material.

Lloyd (2000) created a database providing a good estimate of and composition of the coal waste from each South African mine. The database included a list of 97 mines working as of 1990, their geological description and method(s) of mining. In addition to the quantity of coal waste from each of the listed mines, the total coal capacity of each mine was also listed. The study revealed that 43 million tonnes (Mt) of waste was generated out of 214 Mt of coal mined in 1990, representing 20% of the total coal mined. The data acquired also included the composition of the coal waste such as ash, volatile matter and fixed carbon content. The coal waste was found to contain >40% ash, 15 – 25% volatile matter and <35% fixed carbon. The sulfur content of coal waste was found to be above 2% which is higher than the South Africa

standard, but lower than the 3% commonly found in North America and European coal. Although the study classified these wastes as poor materials, the study concluded that, with the right equipment and the development of appropriate technology, coal waste could become a good source of energy.

Belaid *et al.* (2013) investigated the production and reserve estimate of South African coal discard and its potential (technical and economic) in power generation using circulating fluidized bed (CFB) combustion. The study was conducted by collating data from site visits, interviews, use of previously collated data, sampling, samples testing and combusting coal discard in a CFB pilot plant with Russian coal serving as reference material. As of 2011, the study revealed an accumulation of 1.2 billion tons of coal discard in South Africa, ranging from 2 MJ / kg to 14 MJ / kg in calorific value. This is in line with the study reported by Lloyd (2000), which showed that coal discard is of lower quality. While the study reported that coal discard beneficiation would have challenges such as initial capital cost, it reiterated that it is also an opportunity to harness new technologies that would lead to the creation of jobs. Belaid *et al.* (2013) concluded that coal discard beneficiation for power generation is one of the most sustainable options available for the use of coal discard. In addition, CFB has been shown to be the preferred technology to use beneficiated coal discard for electricity generation. The benefit includes cheaper energy and 3200 MW of prospective power production.

Borowski and Hycnar (2013) assessed the potential of coal fines from a processing plant in Poland for the production of briquette, as alternative fuel source. The homogenization of the coal fines and the impact of certain additives (molasses, starch and wood biomass) on the quality of briquettes produced were investigated. The findings indicated that the molasses briquette was not an excellent binder for coal briquetting. The briquette produced from a blend of 8% starch and 20% wood biomass met the minimum energy requirement with a calorific value (CV) of 23.7 MJ/kg and 21.5 MJ/kg, respectively. While the CV content of the starch briquette was found to be greater, the ash content of the wood biomass briquette was found to be lower at 8.6% compared to the 12.2% from the starch briquette. The addition of wood biomass was found to increase combustion efficiency with reduced ash content and sulfur emission. The briquettes produced with the addition of starch and wood biomass were found to be suitable as fuel for combustion in industrial and domestic boilers.

Piechura (2014) studied the application of Doosan Lentjes' advanced modularized circulating fluidized bed (*CFB*) technology and its application to South Africa coal discard. The study also

looked at the effect of varying coal discard properties on the CFB process. The study revealed that the coal discard utilized has varying low CV and high ash content. As the coal discard from the anthracite mines was found with a lower volatile matter compared to coal discard from the bituminous coal mines. The author concluded that it is important to analyze and understand the characteristics of coal discard in order to design a suitable CFB boiler. In addition, the South African coal discard was found to offer a tremendous opportunity for energy and heat production using CFB technology from Doosan Lentjes.

The economic feasibility of power generation using coal discard was assessed by North *et al.* (2015). The prospective value of coal discard in terms of how much electricity could be produced from it was assessed as the first phase of evaluation by the author. This assessment was carried out on pre-existing coal discard stockpiles and present deposits. The assessment outcome showed that approximately 6.5 gigawatts of electrical energy (GWe) could be produced from the current stockpiles – an amount equivalent to 16 percent of the current generating capacity in the country. Coal discard generated annually from coal mining at a rate of 60 million tons is capable of generating about 11.6 GWe. This study also noted that CFB combustion boilers are most suitable to use discard coal as fuel with high efficiency. Using discounted cash flow, the study found that the use of coal discard to generate electricity showed positive net present values (NPVs) and 21.4 percent internal rate of return (IRR).

Stolboushkin *et al.* (2016) examined the production of brick from coal waste from a coal processing plant in Abashevskaya, Russia. This was done using a semi-dry pressing method and the brick obtained was found to have a compressibility strength of 9-11 MPa, 15-17% water adsorption capacity and frost resistance of fewer than 25 cycles. In order to achieve a higher quality brick, a clay loam was added as an additive leading to a compressibility strength of 18.5 MPa for the brick. The results from the study confirmed that coal waste from the Abashevskaya coal processing plant could be used as the base raw material at 80% to produce a good quality ceramic brick.

Sekhohola and Cowan (2017) investigated the transformation of coal discard into an enriched humus soil-like material, used as a bioremediation strategy for coal discard dump rehabilitation. The study was carried out in pot trial experiments to evaluate the effect of the growth of Cynodon dactylon grass in the presence of arbuscular mycorrhizal (a coal degrading fungi). Coal discard used for the experiments has a CV of 8-10 MJ/kg, this was mixed with topsoil from a mine located in Mpumalanga province of South Africa. The topsoil and coal

discard were mixed in a 3:1 ratio to form a homogeneous mix. The study was carried out by cultivating Cynodon dactylon grass on coal discard and coal discard/topsoil in the presence of coal degrading fungi for a period of 23 and 47 days, respectively. The concentration of a humic acid-like substance (HS) was found to have increased by 8.6% in the coal discard pot after 23 weeks, while HS concentration increased by 25.6% in the coal discard/topsoil pot within the same period. After 47 weeks, an increase in HS concentration of 77.8% and 59.5% were reported for coal discard pot and coal discard/topsoil pot respectively. The result of the study confirmed that Cynodon dactylon grass in the presence of arbuscular mycorrhizal fungi aids the bioremediation of coal discard into enriched soil humic substance which aid plant growth. The results of the study show the potential of using coal discard as a carbon-based substrate to substitute topsoil as a bioremediation strategy in the rehabilitation of coal discard dumps.

Tudor (2019) described a novel technology that produces micro-fine hydrocarbon from coal discard that can serve as a blending feedstock for liquid fuel. This study was initiated due to the recovering of coal fines from dumps and slurry ponds. A sizing method is performed to ease the separation of hydrocarbons from the mineral content resulting in about 10-micron particle size. A ball mill or high shear grinding is used to reduce the particle size. The separation was conducted using froth flotation and the resulting coal product was found with an ash content less than 1 percent, and moisture content of less than 2 percent. In order to create a product called Arq fuel, a suitable mixing component for liquid fuels, the micro-fine hydrocarbon undergoes further conditioning processes. This new energy source, according to the author will lower the blended fuel oil cost per unit mass, and also provides a sustainable blend of energy from coal, and oil thus has the potential of being the most cost-effective fuel.

2.5 Natural Gas as an Energy Source

Global energy demand is expected to grow as the world's population increases. The demand for energy continues to increase, as prospects of emerging economies continue to soar. The energy sector is on the verge of a complete evolution as the energy mix is changing, largely propelled by improvements in technologies and environmental concerns. The changing energy dynamics present a significant challenge on how to meet the world's increasing demand for energy while protecting the environment from pollution by reducing carbon emissions. As a result, stakeholders in the energy sector are moving away from traditional fossil fuels to fuel with minimal carbon emissions such as natural gas.

Natural gas is a naturally occurring hydrocarbon gas mixture found under the earth. Natural gas is a major energy source in the provision of electricity, domestic heating, as fuel in vehicular transportation and as a feedstock in the production of chemicals and clean fuels. Natural gas as fossil energy is economically viable, with a competitive price and very effective as a fuel and in addition "cleaner" than other primary energy sources like coal or oil. For example, the use of natural gas to generate electricity in place of coal decreases CO_2 emissions up to about 60% (Deppe *et al.*, 2006).

The importance of natural gas as a major source of energy and feedstock for the petrochemical industries cannot be overemphasized. With the increasing demand for energy, natural gas will play a huge role in meeting global energy demand. Natural gas is expected to grow faster than oil or coal as shown in Fig. 2.6. With the increasing growth of liquefied natural gas (LNG) and other natural gas storage and transportation methods, access to natural gas is expected to grow significantly worldwide.

British Petroleum (BP) Plc in its 2017 energy outlook report stated that natural gas is the fastest-growing fuel, growing at 1.6% per annum; with its increasing share in primary energy, displacing coal to be the second-largest fuel source by 2035 (BP, 2017).

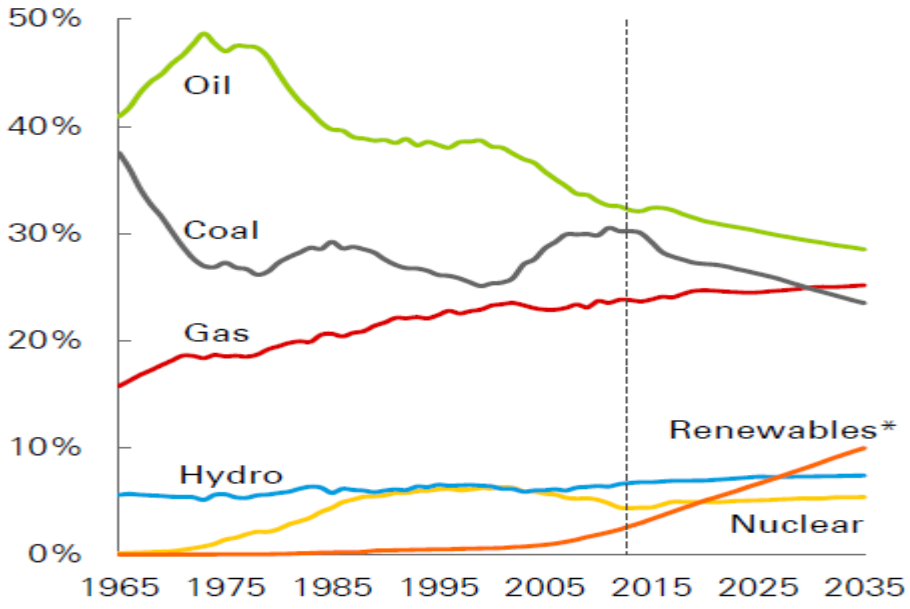


Figure 2.6 Share of Primary Energy Sources (Energy, 2018)

BP Plc in its report for 2016, reported an increase of 1.7% for 2015 in global natural gas consumption while global production of natural gas increased by about 2.3% in 2015 (BP, 2016). The information from the BP report has further shown the huge demand for natural gas. In addition, the BP report stated that global natural gas trade also increased by about 3.3%. The import and export trade via pipeline and LNG are presented in Table 2.1. Pipeline transactions grew by 4% while the LNG trade grew by 1.8% (BP, 2016).

Table 2.1 Natural Gas Trade in 2015 in Billion Cubic Meters (BP, 2016)

	Import		**Export**	
	Pipeline	LNG	Pipeline	LNG
North America	124.1	10.3	124	0.8
South & Central America	18.5	20.0	18.5	22
Europe	464.3	55.1	466	25.4
Middle East	27.3	10.5	28.2	126.2
Africa	8.9	3.8	36.1	48.7
Asia	61.2	238.6	31.5	115.2
Total World	704.3	338.3	704.3	338.3

Natural gas storage is emerging to be the most crucial technology option that will enable the widespread adoption and use of natural gas. The impact of natural gas storage is far-reaching, as it enables natural gas's penetration, addresses the increasing energy demand of rural areas and strengthen the value chain proposition of natural gas. The storage serves as a channel to the gas industry from production to pipelines to consumers. The storage of natural gas is a catalyst for the outstanding development in the energy industry.

2.5.1 Natural Gas Storage and Transportation Technologies

The increasing demand for natural gas across the globe and the need to deliver natural gas at lower costs drives the development of natural gas storage and transportation technologies. One of the main challenges in the storage and transportation of natural gas is its physical nature which requires high pressure and/or very low temperature to increase its bulk density for storage or transport purposes. This makes the cost of storage and transportation quite expensive, especially when compared with that of oil. While oil can be stored in low-cost tanks and subsequently transported in big tankers, such cannot be done for natural gas. Per unit energy cost in the transportation of oil is about ten times higher than that of natural gas, largely

due to its volume-pressure behavior (Dawe and Lucas, 2000, Princewill and Ikiensikimama, 2016).

The most common transportation method for natural gas is via pipeline and as LNG. Huge capital investment and energy cost for LNG has limited its vast deployment in natural gas storage and transportation. It cost about US$ 15/bbl oil equivalent for LNG production and small scale LNG production is not yet economically viable (BP, 2019). Therefore, for remote and smaller markets, there is a need for a more flexible and cost-effective alternative for storing and transporting natural gas.

In addition to pipelines and LNG, natural gas can be stored and transported as CNG, ANG, gas to liquids (GTL), gas to wire (GTW) and gas to solids i.e. natural gas hydrates (GtS) (Thomas and Dawe, 2003, Choi et al., 2009, Wood et al., 2012, Khan et al., 2016). Globally, research and development are ongoing with each of these methods. The commercial success of each of the methods will largely be dependent on the global price of natural gas and the market competitiveness of such a method.

2.5.1.1 Liquefied Natural Gas (LNG)

In LNG, natural gas is condensed into liquid form by a rapid temperature drop to approximately -162 ° C and then stored in storage tanks (Alhasan *et al.*, 2016). These tanks are a double-wall vacuum-insulated pressurized tank to keep the gas in liquid form (Clarke and DeBruyn, 2012). LNG is estimated to have a volume of about 1/600 of gas at room temperature (Thomas and Dawe, 2003). LNG has seen the increase in the supply of natural gas worldwide from production fields to distant markets largely due to the huge improvement in the technology and the efficiency of the LNG facilities. The LNG storage system's high energy requirement and high capital infrastructure cost are some of its shortcomings (Dawe and Lucas, 2000, Atoyebi, 2010, Alhasan et al., 2016). It should be noted, however, the capital cost of the LNG plant has decreased mainly owing to the improved thermodynamic efficiencies of the system (Thomas and Dawe, 2003). This has made LNG a major export method of natural gas worldwide, trading around 338.3 billion cubic meters as in 2015, with global supplies of LNG estimated to double in years to come (BP, 2016). Continuous growth in LNG has significantly increased access to natural gas worldwide, with LNG volumes expected to exceed interregional supplies of pipelines by the beginning of 2020 (BP, 2019).

2.5.1.2 Compressed Natural Gas (CNG)

Natural gas is stored under high pressure in the CNG system (Clarke and DeBruyn, 2012). The gas is usually compressed by a multi-stage compression that is expensive and then stored in a highly fortified storage tank (Mahboub *et al.*, 2012). The CNG system is used in natural gas vehicles (Clarke and DeBruyn, 2012). CNG offers a cheaper alternative energy source, which is one of its main advantages. With the price increase and unpredictable crude oil market, low-cost CNG as a fuel for transport offers a glimmer of hope. Apart from the cost, reducing emissions with the use of CNG made it a choice fuel. However, the high cost of the required infrastructure needed to deploy CNG as refueling points for CNG vehicles, compression stations has become the greatest threat to CNG's widespread deployment as a transport fuel. Due to its high pressure, safety is also a major concern for CNG (Khan *et al.*, 2016, Alhasan *et al.*, 2016).

The pressure vessels often used in CNG are heavily walled and very weighty. New lighter vessel designs are being developed to address the weight problem and reduce the associated costs as well. The Coselle is one of those new designs, which minimizes connections with the use of large outer diameter coils of about 158.75 mm. The Coselle is designed and structured to protect the pipe against damage and allow stacking up to 6 – 8 units. The Coselle also has several vertical supports around the outside, making it a large safe pressurized gas vessel (Stenning and Cran, 2000). Another design is the VOTRANS, a CNG transport system on ships with large diameter pipes capable of delivering about 25 to 1,000 million standard cubic feet (MMscf) per ship at considerably lesser costs. This is achieved by optimizing the storage pressure, temperature and the structural capabilities of used carbon steel pipes. (EnerSea, 2017).

CNG provides a cost-effective alternative to transport natural gas to places where it is not economically feasible for LNG or pipeline, despite the stated limitations (Alhasan et al., 2016). Besides, with increasing demand, improvement in technology and government incentives, the challenges facing the CNG technology can be overcome.

2.5.1.3 Natural Gas Hydrates (NGH)

Natural gas can be transported in solid form, as gas hydrate (Yamamoto, 2015). Gas hydrate can be described as crystalline solids that appear in a cage-like structure like ice surrounded by water molecules. The interaction of water molecules with gas stabilizes the structure of the gas hydrate. The gas hydrate is formed when gas molecules such as methane, ethane, and propane,

firm up the hydrogen bonds inside the water form a three-dimensional cage-like structure with the gas molecule enclosed within the cages (Radich *et al.*, 2009, Kim *et al.*, 2010, Yamamoto, 2015).

The high gas-to-solid ratio properties of hydrates t~~hat~~ makes them very attractive for use in natural gas storage and transport. The technology for natural gas hydrate is a safer option and much more suitable for transporting natural gas from small-scale natural gas fields (Taylor et al., 2003, Taheri et al., 2014, Chong et al., 2016). In comparison with LNG or pipeline for natural gas transport, NGH's capital investment and operating costs are lower (Chong et al., 2016). The natural gas hydrate technology involves three stages: manufacturing, transport, and re-gasification. NGH transport of natural gas includes combining water with natural gas at a pressure of approximately 80 – 100 bar and a temperature of approximately 2-10 ^{o}C. The mixture is further cooled to -15 ^{o}C to facilitate shipping in simple isolated bulk tanks that are cheap compared to LNG carriers (Badakhshan and Pooladi, 2000, Taylor et al., 2003). A regulated hydrate heating method is used to recover the gas, followed by an appropriate drying method depending on its final use. Subject to the manufacturing process, 1 m^3 of hydrate produces about 160 m^3 of natural gas (Gudmundsson et al., 1998, Thomas and Dawe, 2003).

The commercial attraction for NGH is that it can easily be carried out on a mobile platform onshore and can be used offshore on a floating production platform. There are challenges such as environmental concerns, the need for a deeper understanding of the interactions, structure, and stability of water and guest molecules, in-depth understanding of heat and mass transfer during the exchange process (Koh and Sloan, 2007, Chong et al., 2016). However, the simplicity, low cost and the flexibility of the NGH technology make it an attractive option for storage and transportation of natural gas.

2.5.1.4 Gas to Liquids (GTL)

GTL has emerged as a commercially viable technology option in which natural gas is converted to liquid fuels and other valuable liquid products which are more easily transported than natural gas. This has opened up the market to remote natural gas fields (Wood *et al.*, 2012).

The conversion process of natural gas to liquid hydrocarbons is achieved in three stages: conversion of the natural gas to syngas, conversion of the syngas to liquid hydrocarbons and separation and upgrading of the liquid product to its final specification. The production of syngas is carried out via steam reforming or partial oxidation, in which the natural gas feedstock

is mixed with steam or oxygen to produce a mixture of hydrogen and carbon monoxide. The second stage is the conversion of the syngas into liquid hydrocarbons by means of the Fischer Tropsch process with the aid of a catalyst. The Fischer Tropsch process generally produces hydrocarbons with a wide range of fractional composition. The temperature of synthesis is a key factor that normally determines the extent of the produced hydrocarbon composition. A low-temperature synthesis will produce hydrocarbons consisting of about 50% paraffin wax, while a high-temperature synthesis will produce mostly gasoline hydrocarbons, consisting of about 70% olefins (Eliseev, 2009). The third stage involves cracking and isomerization, in which, the produced hydrocarbon is tailored to meet the specification of the desired product.

GTL provides the opportunity to reduce worldwide dependency on crude oil-derived fuels. In addition, it also provides an opportunity for natural gas resource owners especially stranded natural gas and remote fields to diversify and reach target markets. However, the complex nature of the GTL technologies in addition to its high capital investment cost presents a considerable limitation to its widespread adoption and deployment. For GTL to dislodge the conventional refineries for the production of liquid fuels, a technology breakthrough especially the development of efficient, cost-effective novel catalysts is required (Wood et al., 2012). Furthermore, the GTL sector is subjected to fluctuations in petroleum and gas prices on the global market, as GTL needs a huge price difference to be economically and competitively viable (Alhasan et al., 2016). Solutions and breakthroughs to these limitations will see the rapid expansion of the GTL sector.

2.5.1.5 Gas to Wire (GTW)

GTW is the transportation of natural gas as an energy source for power generation (Atoyebi, 2010). Presently, most natural gases transported end up as fuel for power generation. GTW is a technology deployed in a close proximity to power plant, gas reservoirs or in remote fields where the gas from such fields is used to generate power and then evacuated via wires or cables to its destination (Marston and Gray, 2018). For example, stranded gas or gas at remote locations such as offshore could be used to generate power and sold to consumers onshore or other offshore consumers. In the United States, for example, GTW is been considered as an option in getting energy from the Alaskan gas and oil fields to densely populated locations such as California (Alhasan et al., 2016). However, the cost of installing power lines to transmit the electricity produced could be equal to the cost of pipelines, thus defeating the objective of finding a cheaper solution to transporting gas. Significant energy loss along the transmission

lines is another limitation to the GTW method, particularly over a long distance (Marston and Gray, 2018).

2.6 Adsorbed Natural Gas (ANG)

ANG technology has emerged as a viable alternative to both the CNG and LNG storage systems (Alhasan et al., 2016). The ANG system involves natural gas been stored on porous materials packed into a vessel at a lower pressure. The ANG storage system has become popular in the field of developing efficient gas storage and transportation technologies. The ANG technology enables the same capacity of gas to be stored as CNG tanks, but at a much lower pressure (Pupier *et al.*, 2005). ANG uses porous materials packed inside a vessel, this results in a much higher energy density and volumetric storage capacity compared to CNG, making ANG more cost-effective (Alhasan et al., 2016). The use of ANG will ease the delivery of natural gas to secondary consumers such as small and medium scale industries, small and medium independent power plants, residential clusters, towns, and villages, thereby ensuring the security of supply at a reduced cost. These attractive features of the ANG storage system over the conventional storage methods are the prime motivating factors for the ongoing developments of this technology, and this research.

2.6.1 Basic Principles of Adsorption

2.6.1.1 Adsorption Process

In the ANG storage system, the gas is stored under pressure in a vessel containing appropriate porous solid (adsorbent). The process of adsorption involves the transportation of molecules from a phase onto a solid surface, and the molecules then diffuse into the pores of the solid. This process is highly dependent on the intermolecular forces between the gas and the surface of the adsorbent such as activated carbon (Meisen and Shuai, 1997).

The adsorption process is often classified as a physical and chemical process based on the nature and the strength of the surface forces. Chemical adsorption involves the formation of a chemical bond between the surface of the adsorbent and the adsorbate molecule while physical adsorption involves weak intermolecular forces (Karger and Ruthven, 1992). The adsorption process in an ANG storage system is physical adsorption (physisorption) in which the intermolecular forces between the adsorbent and the surface of the adsorbent is known as van

der walls forces (Do, 1998). An illustration is presented in Fig. 2.7 to better understand the adsorption process.

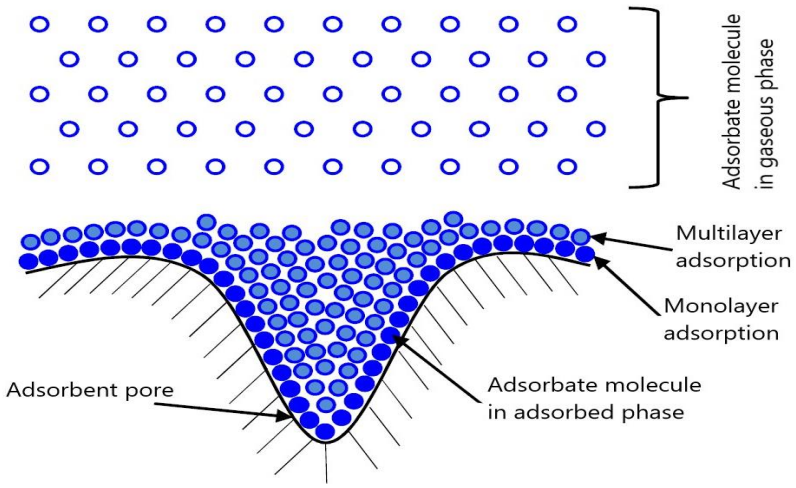


Figure 2.7 Schematic diagram of a typical adsorption process (Ruthven, 1984)

The adsorption of the gas molecules is fully reversible and is largely dependent on variables such as temperature, pressure, surface force, and adsorbent pore sizes (Mondal *et al.*, 2012). Increasing temperature significantly impedes the adsorption process; as a result, adsorption equilibrium is usually investigated at a fixed temperature as a function of pressure. Equilibrium data from such a study is referred to as adsorption isotherms. The larger the adsorbent surface available, the more volume of gas adsorbed at a particular pressure and temperature. Hence, efficient materials for gas storage are those that have large surface areas and pore volume (Suzuki, 1990).

2.6.1.2 Adsorption Equilibrium

Information on the equilibrium of an adsorption process is very important for a better understanding of the process. The equilibrium information gives a clear understanding of how much the adsorbent can adsorb the gas (adsorbate). The information is also useful in studying the kinetics of the adsorption process (Do, 1998). During the adsorption process, as the component to be adsorbed begins to adhere to the surface of the adsorbent, the amount being adsorbed increases linearly with an increase in pressure to a time when the amount adsorbed reaches saturation capacity. This is the equilibrium state and the amount adsorbed at this state is known as the equilibrium adsorbate uptake which is a function of pressure and temperature

(Do, 1998). At a constant temperature, the change in the amount adsorbed as the pressure changes is known as the adsorption isotherm (El Qada *et al.*, 2006) as shown in Fig. 2.8.

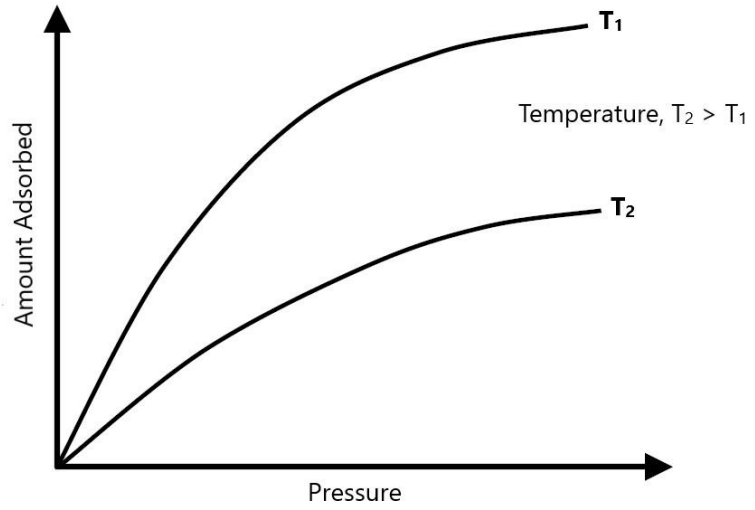


Figure 2. 8 Adsorption isotherm

The adsorption isotherm can also be described as an equation used to describe the relationship between the amount of adsorbate adsorbed by the adsorbent at a given temperature (El Qada *et al.*, 2006). In the design of any adsorption system such as the ANG storage system, the adsorption isotherm of the adsorbate and adsorbent is one of the important information required (Do, 1998). Several adsorption isotherm models were developed to describe the amount of gas adsorbed on the adsorbent as a function of pressure at a constant temperature. Some of the widely used isotherm models include Langmuir, BET (Brunauer, Emmett and Teller), Freundlich, Sips, Toth, Dubinin-Radushkevich (D-R), and Dubinin-Astakhov (D-A) isotherm models amongst others.

2.6.1.3 Adsorption Kinetics

The mass transfer of the adsorbate to the surface of the adsorbent followed by adsorbate diffusion into the pores of the adsorbent is governed by the kinetics of adsorption (Largitte and Pasquier, 2016). The study of the kinetics of an adsorption process is required to examine the effectiveness of the process. From the kinetic study, it will be possible to determine the rate-limiting step of the process and to also understand the adsorption mechanism (Sohn and Kim, 2005). The performance of an ANG storage system is also dependent on the adsorption capacity and rate of adsorption, so it is necessary to estimate the kinetics of adsorption based on these

two parameters. In order to estimate adsorption kinetics, the role of diffusion in the adsorption process is very important.

Diffusion is the rate-limiting step in an adsorption process given that the inherent adsorption rate is considerably faster than the diffusion rate (Ruthven, 1984). The diffusion process is typically described using a parameter known as the apparent diffusivity. The apparent diffusivity describes the process of flow within a solid particle (Do, 1998) and it provides a physical insight about the kinetics of an adsorption process. The understanding of the diffusion process will provide information about adsorption kinetics as a function of the adsorption system parameters such as particle size, bulk concentration, pressure, temperature, pore size, and adsorption affinity (Ruthven, 1984, Do, 1998).

2.6.1.4 Thermodynamics of Adsorption

In an adsorption process, the adsorbed molecules are more stable on the adsorbent surface than in the gaseous phase. This is due to a reduction in the energy level of the adsorbed molecules within the adsorbent pores (Chakraborty *et al.*, 2009). The measure of the strength of the interaction between the adsorbent surface and the gas molecules is the heat of adsorption which is also an indication of the change in enthalpy prior to and after the adsorption process (Delavar *et al.*, 2012). This heat of adsorption can be evaluated using the Clausius–Clapeyron equation (Zhou *et al.*, 2004):

$$H_{ads} = RT^2 \left[\left(\frac{\partial(\ln P)}{\partial T}\right)_c\right] \tag{2.1}$$

where P is the pressure at constant equilibrium uptake; R is the gas constant and T is the temperature. The heat of adsorption can be evaluated from the slope of a plot of ln P against $\frac{1}{T}$ from Eq. 2.1. As a rule of thumb, Rodrigues and da Silva (2010) reported that the heat of adsorption above 80 kJ/mol is an indication of chemical adsorption (chemisorption) and values below an indication of physical adsorption (physisorption).

2.6.2 Overview of Adsorbents for ANG Storage System

Adsorption capacity and rate properties are the main criteria for the selection of adsorbents for the ANG storage system (Rahman *et al.*, 2012b). Therefore, the success of an ANG system is dependent on the behavior of the adsorbents and its adsorption equilibrium and kinetics.

According to Rahman *et al.* (2012a), a good adsorbent for ANG storage system must have a high surface area with high micropore volume. In the design and performance assessment of the ANG system, the adsorption equilibrium and kinetics are important data that are required and these data are determined based on the surface area characteristics and pore structure of the adsorbent. Adsorption capacity is controlled by the surface area of the adsorbent, while the selectivity of the adsorbent is determined by pore size distribution (Rahman *et al.*, 2012b). Therefore, the primary goal in designing an ANG storage system is to identify adsorbents with higher surface area, smaller pore sizes, and adequate porosity.

In general, any material that is porous in nature can be used as an adsorbent in the purification, separation, and storage of gas (Yang, 2013). On the basis of the porous structure, examples of adsorbents are silica gel, molecular sieves, zeolites, activated carbons and metal-organic framework (MOF) (Ruthven, 1984, Policicchio *et al.*, 2017). Silica gel is a hard, unbroken network of spherical particles of colloidal silica (Yang, 2013). It is commercially produced from the mixture of sodium silicate solution with sulfuric acid or hydrochloric acid. Silica gel is a good sorbent for drying due to its high surface area and its distinctive surface properties (Yang, 2013). Zeolites occur naturally and can also be produced through chemical synthesis followed by pelletization and calcination (Yang, 2013). Zeolites are widely used in separation processes and in crude oil refining as catalysts (Ruthven, 1984). The potentials of zeolites as an adsorbent for ANG storage have been investigated prior to the widespread discovery of activated carbon (Karger and Ruthven, 1992). However, zeolites are not commonly used as activated carbons due to certain constraints that may affect their ability to adsorb methane. Its smaller micropore volume and hydrophilic nature are some of its constraints (Arami-Niya *et al.*, 2011).

Another adsorbent is carbon molecular sieves (CMS), it has not gained much attention, especially in ANG storage application, possibly due to its slow kinetics (Rahman *et al.*, 2010). It is however used to separate gases on the basis of differential diffusion rates (Suzuki, 1990).

Metal-organic frameworks (MOFs) are gaining enormous attention as porous adsorbents for adsorbed natural gas storage due to their exceptional high surface area (Policicchio et al., 2017). MOFs can be described as hybrid solids which is a combination of inorganic matters such as metal ions and organic matters resulting in a three-dimensional structure (Li *et al.*, 1999). MOFs have been used in catalysis, in gas separation processes, and for gas storage. This is as a result of its high surface area, its high thermal stability and porosity (Mueller *et al.*, 2006).

Several researches have been conducted on the evaluation of MOFs as an adsorbent for methane storage. A pyrazine based MOF was evaluated for the adsorption of methane and the adsorbed value obtained was found to be similar with some zeolites (Kondo *et al.*, 1999). The adsorption mechanism for methane storage on MOF was described by Wu *et al*. (2010), and the author reported a higher adsorbed methane from this study. Although MOFs may have outstanding prospects for natural gas's high storage capacity, it is not cost-competitive (Policicchio et al., 2017). In reducing the cost implications, cheaper materials and low-energy reaction pathways will go a long way.

2.6.3 Activated Carbon

Activated carbon can be described as carbonaceous material with high adsorption capacity (Sun *et al.*, 1997). The high adsorption capacity of activated carbons results from some of the material's inherent properties such as high surface area, large pore volume and favourable pore size distribution (Teng and Lin, 1998). Activated carbons contain micropores, mesopores and macropores that are vital for the easy access of the adsorbed molecules to the carbon particle interior (Ahmadpour and Do, 1996). These features make activated carbon suitable for the ANG storage system (Parkyns *et al.*, 1995). Over the years, studies have been carried out in the preparation, characterization and adsorption properties of activated carbon with particular emphasis on how to achieve optimum adsorption storage capacity, and its application in different field.

Ahmadpour and Do (1996) investigated the characteristics of activated carbons prepared from bituminous coal using chemical and physical activation methods. A coal with a particle size of 212 – 250 μm was used in both activation methods. To optimize the process, the influence of factors such as activation time, temperature, particle size, chemical reagents, method of mixing and impregnation ratio was studied. In comparison to the physical activation method, the study reported the chemical activation method was more flexible and produces activated carbons with superior surface properties and porosity. The study also found the impregnation ratio to be the most important factor in the chemical activation of coal using KOH and $ZnCl_2$. The author also found temperature having a significant impact on the development of the pores. The optimum conditions for KOH activation were found to be at a temperature of 700 ^oC and activation time of 2 hours, while the optimum conditions for $Zncl_2$ activation were found to be 500 ^oC and 1 hour.

Sun *et al.* (1997) also produces activated carbons using bituminous coal from an Illinois basin, from the United of America. The method used involved the oxidation of coal in air at approximately 150 - 250 °C, followed by volatile removal at approximately 500 - 730 °C in a nitrogen atmosphere and finally gasified at approximately 730 - 880 °C. The resulting activated carbons from this process were characterized to determine their surface area and porosity. The results showed that 80% of the activated carbons produced from this process had surface areas above 1000 m^2/g. The activated carbons were also tested for toluene adsorption, and their performance was found to have the better adsorption capacity than Darco coconut charcoal, a commercial activated carbon. A cost analysis was also conducted, and the author reported that the most economical product is not the one with the highest surface area, but the product with the lowest cost per square meter of surface area.

The influence of different chemical reagents on activated carbons derived from bituminous coal was investigated by Hsu and Teng (2000). The chemical reagents utilized are $ZnCl_2$, H_3PO_4, and KOH. The chemical activation process involved impregnating the reagent with the coal sample, followed by activation at varying temperatures in a nitrogen flow. Compared to activated carbons from the $ZnCl_2$ and H_3PO_4 process, carbon yield was found to be lower from KOH activated carbons. For all reagents, a general trend was observed in which porosity of the activated carbons from each of the reagents increases with an increase in temperature to a peak and then decreases as temperature rises further. Activated carbons produce from KOH were reported to have the highest surface area followed by $ZnCl_2$ and H_3PO_4 with the values of 3300, 960 and 770 m^2/g, respectively. The result revealed that acid reagents like $ZnCl_2$ and H_3PO_4 are not suitable for producing high porous activated carbons, compared to a base reagent (KOH). In addition, the author also observed that a larger particle size of coal produces an activated carbon with a lower yield and low porosity. This result was attributed to the low external surface area possess by larger particles, which resulted into a low contact between the coal and the reagents, and higher resistance for the reagent's intraparticle diffusion.

A study on the utilization of different porous materials for methane adsorption was conducted by Lozano-Castello et al. (2002a). The materials used include activated carbon fibers prepared using physical activation, activated carbon from the chemical activation process and activated carbon monoliths. These activated carbons were prepared using different coals (anthracite and bituminous coal). Using KOH as a reagent, the coal materials were activated using chemical activation method. KOH was mixed with coal in varying weight ratios and then subjected to

pyrolysis in nitrogen flow until the activation temperature was attained. The resulting product was washed with a solution of HCl and distilled water and then dried. Results from BET analysis of the produced activated carbons revealed that the samples have surface area ranging from 700 to 3290 m^2/g. Activated carbon synthesized from anthracite coal at 700 ^oC, KOH/coal weight ratio of 4:1 and activation time of 1 hour was found with the highest surface area. The methane adsorption was carried out at a pressure of up to 4 MPa and a temperature of 298 K using the prepared activated carbons. The result showed that samples with higher micropore volume had a higher adsorption capacity. The study concluded that the chemical activation process has many more advantages over the physical activation method.

The use of central composite design to examine the effect of activation temperature, activation time and the ratio of steam to char by weight on the physical activation of Luscar char was investigated by Azargohar and Dalai (2005). The models developed for surface area and yield were used to evaluate the optimum test conditions. It was found that the best-activated carbon produced had a surface area of 502 m^2/g and a yield of 54.1% at 708 ^oC, and steam to char ratio of 0.93 and 1-hour activation time. This result showed that the surface area and yield produced under the optimum conditions achieved were consistent with the results from the models developed.

Another investigation conducted by Dai *et al.* (2006) resulted in the development of a super activated carbon for ANG application by combining chemical and physical activation process. This was done to enhance the micropore size and volume of the activated carbon, key features responsible for enhanced gas storage. The results from the adsorption analysis of the activated carbon produced showed a higher adsorption capacity compared to activated carbons prepared from either chemical or physical activation methods.

An investigation into the synthesizing of activated carbons from bituminous coal using KOH and NaOH as reagents was reported by Cuhadaroglu and Uygun (2008). The influence of the chemical reagent weight ratio was investigated. The results showed that increasing the weight ratio of the chemical reagent from 1 to 4 increased the BET surface area from 785 to 1295 m^2/g for KOH and from 657 to 1566 m^2/g for NaOH.

Gong *et al.* (2009) studied and suggested a method for modifying the pore size distribution of activated carbons prepared from coal. The modification focused on enhancing the formation of mesopores in the prepared activated carbon. The modification was done with the background

knowledge that, the best way to increase the mesopore volume of activated carbon is by catalyzing the steam activation process with metals that have been found to promote the formation of mesopores. In preparing and modifying the activated carbons, pulverized bituminous coal was mixed with varying mass fraction of KOH. The mixture was heated under nitrogen flow until it reaches temperature of 600 °C and held at this temperature For 45 min. The char from the carbonization process was washed with a 5% mass fraction of HCl and distilled water until a pH of 6 was attained. After the washing process, steam activation was carried out on the sample at 900 °C. Results from the characterization of the prepared activated carbons revealed that the amount of K-containing compounds present in the char can be regulated by varying the quantity of KOH mixed with the coal sample. The adsorption test revealed that an increase in KOH increases the adsorption capacity of the resulting activated carbon. The pore size was reported to have increased from 2.379 to 2.636 nm, while an increase in mesoporosity was reported from 30.9 to 46.1%. In conclusion, the study was able to modify the pore size distribution of activated carbons from coal by varying the quantity of KOH added to the coal.

Arami-Niya *et al.* (2011) examined the textural and surface properties of activated carbons prepared from oil palm shell in relation to their capacity for methane adsorption. Chemical activation method using H_3PO_4 and $ZnCl_2$ was used, followed by physical activation with CO_2. The results from the study revealed that combining chemical and physical activation in preparing activated carbon from palm oil shell provided an improved and consistent pore size distribution. The study concluded that, while high surface area and pore development is crucial to improved methane adsorption, another equally important factor is the homogeneity of the pore sizes of the activated carbon.

Martin *et al.* (2011) evaluated the methane adsorption capacity of activated carbon prepared from Indonesian low-grade coal. The physiochemical analysis revealed that the coal sample contains moisture, ash, carbon and total sulfur content of 13.56, 4.80, 56.47 and 2.41% respectively. The coal sample was pulverized to a particle size of 0.10 mm and subjected to physical activation using CO_2 up to a temperature of 950 ^oC for 6 hours. The BET surface area, pore volume and density of the produced activated carbon was reported to be 668 m^2/g, 4.7 cm^3/g and 2200 kg/m^3, respectively. The activated carbon was evaluated for methane adsorption in comparison with a commercial activated carbon (Carbotech) having a surface area of 885 m^2/g and a pore volume of 5.14 cm^3/g. Methane adsorption was carried out at a

pressure of 3.5 MPa and temperature range of 300 to 318 K. The results showed that the activated carbon from low-grade coal adsorbed less volume of methane than activated carbon from Carbotech. This was reported to be as a result of its lower surface area and pore volume, compared to the Carbotech activated carbon.

An investigation into the correlation between microporosity and methane adsorption capacity of activated carbons prepared from anthracite coal was reported by Luo *et al.* (2011). The activated carbons were prepared by chemical activation using KOH at 750 ^{o}C, 1-hour activation time and varying KOH/coal weight ratio of 1:1, 2:1, 3:1, 4:1, and 5:1. The methane adsorption data from the prepared activated carbons were obtained at 25 °C and pressures up to 35 bar. The measured data were fitted to the Dubinin-Astakhov (D-A) model. The activated carbon produced with KOH/coal ratio of 4:1 was reported to have the largest methane adsorption capacity, with surface area, micropore volume and pore diameter of 2071 m^2/g, 0.833 cm^3/g and 1.40 nm, respectively. The author reported that the higher the micropore volume and surface area, the higher the adsorbed amount of methane. The methane adsorption kinetics followed the pseudo-second order kinetic model. It was also found that the activated carbon with the highest adsorbed amount of methane has a faster adsorption rate. In addition, the calculated parameters of the D-A model showed that the most heterogeneous is the activated carbon with the highest adsorbed amount and that heterogeneity is partly responsible for its higher adsorption capacity.

An overview of the use of porous materials for methane storage was provided by Makal *et al.* (2012), and activated carbon was one of the materials reviewed. The survey disclosed that the most suitable adsorbent for methane adsorption and storage application are activated carbons with narrow pore size distribution. It also disclosed that activated carbons with slit-shaped pores have the highest methane storage capacity. In addition, the study revealed that 0.8 – 1.5 nm pore diameter activated carbons were most effective in adsorbing large volumes of methane. Furthermore, the study found that mesopores and macropores make a significant contribution to methane delivery capacity in activated carbons.

Okhovat *et al.* (2012) investigated the influence of different chemical reagents and weight ratios on the pore structure of activated carbons derived from bituminous coal. In preparing the activated carbons, 10g of the coal sample of particle size 212–250 μm was mixed with KOH or $ZnCl_2$ solution in a weight ratio of 50 to 200%. After drying, the resulting mixture was

heated to a final temperature of 500 ^{o}C for $ZnCl_2$ and 700 ^{o}C for KOH in a nitrogen flow and held for 1 hour at this temperature. The products were washed with acid and distilled water after the activation process and then dried. Four models (Dubinin-Stoeckli, Stoeckli, Horvath-Kawazoe, and enhanced Horvath-Kawazoe) were used to characterize the adsorption isotherms of the prepared activated carbons. Overall, the results from the various models were similar. In all the activated carbons prepared with KOH and $ZnCl_2$, the pore volume increased as the impregnation ratio increased from 50% to 200%. The activated carbons produced showed a microporous structure at a lower ratio of $ZnCl_2$, while those produced with higher $ZnCl_2$ ratios were mesoporous in nature. The activated carbons prepared with various KOH ratios displayed a microporous structure with an increase in the KOH ratio. Moreover, it was observed that the increase in micropores had no effect on pore sizes.

The adsorption characteristics of activated carbons from microcrystal cellulose powder prepared by CO_2 physical activation was examined for methane adsorption by Policicchio *et al.* (2013). The methane adsorption was carried out at a temperature of 25 °C and pressure up to 35 bar in a high-pressure volumetric equipment. The results from the study revealed a correlation between the surface area of the activated carbons and methane adsorption capacity. As the surface area increased from 346.86 to 1784.36 m^2/g, there was a corresponding increase in methane adsorption from 77.1 to 146.4 v/v. The amount of methane adsorbed was close to the United State of America Department of Energy (DOE) specification for methane storage in porous material for vehicular application, which is set at 150 v/v at 35 bar and 25 °C. The study also found that one of the activated carbons with a surface area of 1465.67 m^2/g had methane storage capacity of 147.2 v/v. The study then concluded that while a linear correlation exists between surface area and storage capacity, the ability of some porous materials to adsorb depends not only on the surface area but also on pore sizes and the interaction between the gas and the pore walls.

The application of sugarcane molasses as a source for producing activated carbon was examined by Sreńscek-Nazzal *et al.* (2013), using KOH as a reagent in a chemical activation process. The activated carbon was prepared under a temperature range of 400 – 800 ^{o}C, 1 hour activation time and different KOH weight ratio. The methane storage capacity of the produced activated carbon with the highest surface area was examined. The result from the BET analysis showed that, activated carbon produced at 780 ^{o}C with KOH/molasses weight ratio of 2.8:1 has the highest surface area and micropore volume of 2202 m^2/g and 1.30 cm^3/g, respectively. It

was also observed from the isotherms of methane adsorption that there was a corresponding increase in the volume of adsorbed methane for an increase in pressure. An increase in temperature, however, reduces the volume of the adsorbed methane. The methane adsorbed at 40 bar has an adsorption capacity of 134.12 mg/g at 40 ^{o}C and 181.61 mg/g at 20 ^{o}C. The largest volume of methane adsorbed with the activated carbon produced from sugar molasses was 197.23 mg/g at 50 bar and 20 ^{o}C.

Shamsuddin *et al.* (2016) synthesized activated carbons from kenaf core fiber, agricultural biomass using phosphoric acid reagent (H_3PO_4). The porous structure and surface properties of the produced activated carbons were evaluated before and after activation. The preliminary proximate analysis of the kenaf core fiber revealed high fixed carbon content and low ash content, a good indication of its potential for activated carbon production. In synthesizing the activated carbons, kenaf core fiber was washed in hot distilled water and subsequently dried in an oven at 105 °C. The dried sample was cut and sieved to a particle size of 500-600 μm. The sample was then carbonized from room temperature up to 400 °C for 1 hour under a nitrogen atmosphere. The char from the carbonization process was impregnated with H_3PO4 at a weight ratio of 1:4. The impregnated sample was heated to a temperature of 500 °C and held for 1 hour. The activated sample was subsequently washed and dried. The result of the BET analysis revealed that the activated carbon obtained from H_3PO_4 activation has an improved surface area and pore development when compared to the carbonized sample. This confirms the efficiency of H_3PO_4 as an activating agent in activated carbon production. The activated carbon produced had a surface area of 299.02 m^2/g and a micropore volume of 0.12 cm^3/g. On the other hand, the carbonized sample was reported to have a surface area of 13.68 m^2/g and a micropore volume of 0.004 cm^3/g. The morphology of the sample before and after activation revealed a clear increase in pore development as a result of H_3PO_4 activation. It is worth noting that while the study confirmed that activated carbon can be produced from kenaf core fiber using H_3PO_4, the surface area and pore volume of the produced activated carbon is not sufficiently significant to make it suitable for gas storage application. Process improvement and/or change of activating agents were suggested to improve the properties of the produced activated carbon.

The use of petroleum pitch mixed with coal powder as a source for preparing activated carbon was investigated by Gao *et al.* (2017) using the KOH activation method. The study also evaluated the influence of coal particle sizes on the structure and adsorption capacity of the

produced activated carbon. The pulverized pre-treated pitch was mixed with coal powder and KOH in a weight ratio of 1:1:1. The mixed sample was heated in a horizontal tube furnace under argon flow to a temperature of 800 ^{o}C and held for 1 hour. The resulting product was washed with 0.2 M HCl and rinsed with distilled water then dried overnight. The capacity of the prepared activated carbon to adsorb gases such as CO_2, N_2, and CH_4 were tested using the gravimetric sorption method at a pressure of 3.5 MPa and temperature of 298 K. The result from the characterization and gas adsorption test showed that, activated carbon produced from coal of particle size 0 – 53 µm had the highest surface area of 1401 m^2/g with CO_2 adsorption capacity of 8.87 mol/kg, 5.43 mol/kg of CH_4 and 3.09 mol/kg of N_2 at 3.5 MPa and 298 K. The study also investigated the influence of the coal particles on the stability of the activated carbon produced. This was accomplished by activating pre-treated pitch and KOH in the furnace without coal particles. The result showed that pitch without coal particles caused the furnace crucible to overflow and produced no stable activated carbon. Furthermore, the study observed that the high selectivity of CO_2 over N_2 and CH_4 reveals that the produced activated carbon has good potential for pressure swing adsorption.

Policicchio *et al.* (2017) provided an overview of different materials that can be used for methane storage, particularly activated carbon. The study analyzed the correlation between structural characteristics such as bulk density, surface area and porosity of activated carbon and their impact on methane adsorption capacity. The study was carried out using data from previous studies and data from laboratory tests. The study reiterated the benefits of using activated carbons; raw materials are widely available, cost-effective production on an industrial scale and available characterization techniques. Analysis of the collated data revealed there exists a relationship between the structural characteristics of a material and its methane adsorption capacity. This study revealed that surface area, apparent density, and micropore volume are factors that influence methane adsorption capacity. The study concluded that the understanding of this relationship and its influence on adsorption capacity is crucial for efficient methane storage and the development of ANG storage systems for vehicular and bulk storage applications.

A recent investigation into the hydrothermal carbonization (HTC) of camphor and camellia leaves, along with KOH activation in preparing activated carbon was conducted by Yang *et al.* (2019). The influence of HTC temperature on pore structure and adsorption capacity of the prepared activated carbons were evaluated and compared for the two leaves. First of all, the

activated carbons were prepared by immersing a certain amount of treated leaves in deionized water of 60 ml and placing them in a hydrothermal reactor and heating them to varying temperatures (180 – 300 ^{o}C). The hydrochar obtained was subsequently mixed with KOH at a weight ratio of 1:3. The mixture was then heated to 800 ^{o}C under nitrogen flow and held for 1 hour. The activated product was finally washed and dried. The results from the characterization and adsorption test revealed that HTC temperature had a significant influence on the structure of the activated carbons and its adsorption capacity. The results also revealed that activated carbon prepared from camellia leaves at HTC temperature of 240 ^{o}C was the most microporous in nature with the highest surface of 1823.77 m^2/g. Analysis of the adsorption isotherms of all prepared activated carbons revealed that the Langmuir isotherm model described the adsorption equilibrium data better than the Freundlich isotherm model. The experimental data of activated carbons prepared from camphor leaves fits well with a pseudo-first-order kinetic model. While activated carbons prepared from camellia leaves exhibited both pseudo-first and pseudo-second-order kinetic model features. The study concluded that the prepared activated carbons have gas storage potential for low cost and sustainability.

2.6.3.1 Types and Characteristics of a Good Activated Carbon for Natural Gas Storage

Several raw materials such as coal char, bituminous coals, petroleum coke, palm solid waste, empty fruit bunch, wood, bean husk, coconut shell have been used in the production of activated carbon (Azargohar and Dalai, 2005, Cuhadaroglu and Uygun, 2008, Zhang *et al.*, 2008, Nasri *et al.*, 2014, Amosa *et al.*, 2015, Yorgun and Yıldız, 2015, Mondal *et al.*, 2015, Isah *et al.*, 2015). Of all these raw materials available for the activated carbon production, coal has often been used as a result of its inherent microstructure and surface chemical properties (Teng and Lin, 1998). Studies have also shown the successful production of high grade activated carbon from coal (Sun *et al.*, 1997).

Suzuki (1990) classified activated carbon into powdered activated carbon (PAC), granular activated carbon (GAC), carbon molecular sieve (CMS) and activated carbon fiber (ACF) based on the precursor used and the production process. Out of these four, the potential of PAC, ACF, and GAC in the ANG storage system has been investigated (Lozano-Castello *et al.*, 2002b, Prauchner and Rodriguez-Reinoso, 2008). A comparative analysis was conducted by Lozano-Castello *et al.* (2002b) on the performance of PAC and ACF in the storage of methane. The result showed that ACF has higher packing density than PAC, but PAC exhibits a higher methane storage capacity than ACF as a result of PAC having better micropore size

distribution. The storage capacity of 95 v/v at 35 bar and ambient temperature was reported for GAC samples produced by the chemical activation of coconut shell with zinc chloride and physical activation with carbon dioxide at a higher temperature (Prauchner and Rodriguez-Reinoso, 2008).

The adsorption storage capacity of natural gas is highly dependent on the textural characteristics of the activated carbons (Alcañiz-Monge et al., 2009b). Therefore, a good activated carbon for storage of natural gas should have the following characteristics;

- A surface area greater than 1000 m^2/g (Blanco *et al.*, 2010)
- Large microporosity leading to a high capacity for adsorption (Marsh and Reinoso, 2006)
- Narrow pore size distribution (Matranga *et al.*, 1992)
- Low mesoporosity to facilitate the kinetics of the process of adsorption and desorption (Marsh and Reinoso, 2006).

2.6.4 Overview of ANG Storage System

In an ANG storage system, natural gas is stored in porous materials packed into a vessel at low pressure. Two major benefits are derived from using low pressure: it allows good design flexibility in storage tanks and reduces the cost required to compress natural gas to high pressure (Vasiliev *et al.*, 2000). Other benefits include low capital and operating cost of compression and refueling equipment (Vasiliev *et al.*, 2000). In addition to low cost, the reduction in pressure also leads to enhanced safety (Zhou *et al.*, 2010).

In an ANG storage system, the volume of adsorbed gas is highly dependent on the porous material used, temperature and pressure (Alhasan *et al.*, 2016, Zhou *et al.*, 2010). An increase in pressure and reduction in temperature will enhance the efficiency of the adsorption process (Alhasan *et al.*, 2016). Apart from the adsorbent storage capacity, there are two other factors that can affect the performance of an ANG system, namely the adsorbent characteristics and the management of heat effects on the system (Alhasan *et al.*, 2016). Adsorbent characteristics such as bulk density, high surface area, and pore volume are factors that determine the quality of a good adsorbent for gas storage (Alhasan *et al.*, 2016). An ANG system's performance and efficiency are assessed on volumetric storage capacity, so the development of porous materials with excellent characteristics is vital to the success of the ANG storage system.

Managing the thermal effects on the system is another factor contributing to the ANG storage system performance. It is necessary to remove the heat released during the charging process from the system to ensure that a high volume of natural gas is stored. If the heat is not removed, it heats up the system and less gas is adsorbed, thus reducing the capacity of the system to store natural gas. Similarly, a drop in temperature occurs during the discharge process, resulting in less natural gas being delivered (Mota *et al.*, 1997). To ensure large storage capacity and delivery, an effective system is required to manage the heat effects.

2.6.4.1 Global Research Position on ANG Storage System

Several studies have been conducted over the years in order to improve the performance of the ANG storage system since its emergence as a viable alternative to existing CNG and LNG systems. The recurring study point in most of the studies to date has been the improvement of storage capacity by developing high-capacity adsorbents and managing the thermal effects of the system to improve storage and delivery capacity.

Wegrzyn and Gurevich (1996) presented a review addressing the technologies available for storing natural gas. Furthermore, ANG, CNG, and LNG were technically compared and the associated refueling costs were examined. While the review reiterated that extending the driving range is a key challenge in applying ANG in natural gas vehicles, the study suggested that designing a conformable storage tank with carbon adsorbents will increase gas storage and extend the driving range of natural gas vehicles. The review concluded with the following suggestions on how to address some of ANG's technical challenges;

- Volumetric storage efficiency can be improved from 150 to 200 v/v by enhancing the adsorbent packing density.
- The life cycle of the adsorbents can be improved by controlling the number of gas impurities onto the adsorbent bed.
- A complete fill up can be achieved by managing efficiently the thermal effects during refueling.

A model to study the effect of heat on an ANG system was developed by Mota *et al.* (1997). The model showed that there is a drop in temperature during the discharge process, and this drop in temperature can be minimized or completely eliminated by heat transfer from the environment.

Judd *et al*. (1998) studied the use of ANG technology in natural gas vehicles (NGVs) and in bulk storage. The study reiterated that maximum gas storage density is the crucial prerequisite for NGVs with an acceptable mileage range. Conformation of storage vessels and adsorbent characteristics are key for ANG use in bulk storage. Moreover, the study stated that the economic viability of the ANG system depends largely on the choice of an adsorbent. While a low cost and highly effective adsorbents are desired, the intricate compromise between cost and performance will determine the success of the ANG technology.

The effects of natural gas composition on the efficiency of the ANG storage system was also investigated by Mota (1999). The author developed a mathematical model, in which the results from the simulation run showed a significant reduction in the system's delivery capacity due to the heavier hydrocarbons in the natural gas. The study recommended a specific carbon-based filter to be used during the loading and discharge process to improve storage capacity.

Vasiliev *et al.* (2000) examined the storage performance of two carbon adsorbents (monolithic carbon and carbon fiber) in an ANG system. A theoretical model of a cylindrical gas storage tank with an internal heat exchange system was developed to study the thermal effects and also acquire temperature and gas concentrations during the discharge process. The study found that the carbon fiber material called "Busofit", developed from the pyrolysis of cellulose was found to be the most capable of delivering about 150 v/v of methane at 35 bar. The study recommended a multi-cell vessel with a thermal control heat pipe as suitable for efficient storage and transportation of natural gas through ANG technology.

Yang et al. (2005) examined the heat effects during the discharge process of an ANG storage system. It was found that maximum temperature fluctuation occurred in the middle of the adsorbent bed during the discharge process. The study recommended a novel heating/cooling system involving the design of a U-shaped heat exchange pipe at the center of the storage vessel using hot or cold water to manage the temperature fluctuations of the system. This will reduce the discharge time by about 60%.

From the investigation conducted by Basumatary *et al.* (2005) on the heat and gas flow in an ANG system, a portable steel cylinder with porous activated carbon as the adsorbent bed was developed from the modelling of the ANG system. The study examined the effects of gas inlet stream temperature and its charging rate on the temperature of the adsorbent bed and the amount of time needed to fill the cylinder. The study found that the charging rate has a minimal

effect on the adsorbent bed temperature. It was recommended that the time required for charging can be significantly reduced by increasing the charging rate with minimal effect on the adsorbent bed. However, in order to keep the adsorbent bed temperature to about 365K, the study suggested the cooling of the gas prior to filling.

The investigation on the thermal effect of the heat of adsorption on the adsorption and desorption process in an ANG system was conducted by Sáez and Toledo (2009). Dual storage tanks with thermal control systems and different activated carbons as the adsorbent bed were used for the experiment. It was observed that temperature fluctuations were most severe at the center of the adsorbent bed during the adsorption and desorption process. It was also observed that the maximum volume of gas was discharged at 4 MPa. The study suggested improving the activated carbon characteristics as one way of mitigating the temperature fluctuations.

Sahoo *et al.* (2011) investigated the charging efficiency of an activated carbon adsorption bed by carrying out both experimental and simulation studies. The simulation was carried out using COMSOL Multiphysics software. Data from the experiment were collected at varying flow rates for different pressure and temperature and compared with the simulated values. The model accurately predicts filling times as well as temperature rise in the center of the bed. The study reported that, for effective use of ANG technology in vehicles, and for a given adsorbent, the amount of gas stored as reflected in the storage efficiency will be dependent on the discharge amount required to meet desired driving range. Furthermore, the study reported that the charge rate is controlled by the rate at which heat is removed from the system and that the introduction of an external convective cooling system will provide the maximum storage volume.

A study on the influence of natural gas composition on activated carbon adsorption capacity in an ANG system was also reported by Rios *et al*. (2011). This study was conducted in an activated carbon filled prototype storage tank. The study revealed that adsorption of heavier components and CO_2 helped partially deactivate the activated carbon bed, thereby reducing the system's storage capacity.

Rahman *et al*. (2011) introduced a fin tube type heat exchanger placed in a pressurized cylinder in an effort to improve the thermal efficiency of the ANG system during charge and discharge cycle. A distributed parameter model was developed and simulations carried out at different charging and discharging conditions. The result of the simulations showed that both the

charging and discharging process were improved as a result of the introduction of the fins and tubes in the adsorbent bed. This led to a shorter charge period and an increase in the quantity of methane adsorbed.

Another study on the influence of temperature on the filling and discharge process of the ANG system was reported by Zakaria and George (2011). A commercial activated carbon was used in a 0.5-liter pressurized vessel to store methane at a pressure of 3.5 MPa. The study concluded that the rate of charging and discharging of gas in and out of the system affects the storage and delivery capacity. According to the study, a faster charging rate will lead to a rise in temperature, while a faster discharge rate will cause a higher temperature drop leading to reduced storage capacity and delivery efficiency.

Beckner and Dailly (2015) studied the methane storage capacity for five different porous materials (activated carbon, copper-based MOF, aluminum-based MOF, zinc-based MOF, porous polymer) at ambient temperature and different pressures up to 250 bar. The study was conducted using a 110-liter pressurized storage vessel. The outcome of the study showed that at 50 bar, all the five adsorbents exceeded the storage capacity of the existing CNG system. The result revealed that two of the five adsorbents activated carbon and copper-based metal-organic framework surpass the storage capacity of CNG at 250 bar pressure.

Alhasan *et al.* (2016) provided an overview of the ANG storage technology and highlighted five key factors crucial to the success of the system. The highlighted factors are adsorbent characteristics, thermal effects, desorption, and delivery rate. In the author's summation, different adsorbent materials present different challenges to the storage system in terms of the rate of absorption/desorption and the cost of the overall system. The following are a summary of the study;

- Activated carbons with large surface area, micropore volume, narrow micropore size distribution, and higher packing density will be required for an efficient and sustainable ANG storage system
- An internal thermal management control system that utilizes a cooling/heating arrangement is required to minimize the adverse thermal effects on the charging and discharging process.

2.7 Summary

This chapter reviewed the issues associated with waste, also known as discard/tailings from coal mining and processing plants to the environment, and its potential and benefit through beneficiation to the social economic development of the society. Increasing demand for natural gas as an energy source, the need to store natural gas, available natural storage and transportation technologies were also presented. The application of ANG as a viable technology of choice for natural gas storage was discussed. Also addressed was the principle of adsorption, choice of adsorbent and the thermal management of the ANG system to improve its adsorption capacity. The research positions on coal waste beneficiation, activated carbons for natural gas storage and the ANG storage system were presented.

Some of the highlights from this chapter are as follows:

- The huge stockpiles of coal waste in South Africa and there are challenges associated with safe disposal;
- Previous studies have concentrated primarily on how coal waste can be used for power generation;
- No study yet on the use of South African coal waste as a porous material for natural gas storage is available in the literature
- Low cost activated carbon is the adsorbent of choice for natural gas storage.

In lieu of the aforementioned, developing activated carbons from South African coal waste for natural gas storage will result in coal waste beneficiation and low-cost material for natural gas storage, side-stepping a major obstacle associated with the use of ANG system. The materials and experimental methods used in this study are discussed in the next chapter.

CHAPTER 3 MATERIALS AND METHODS

3.1 Introduction

This chapter describes the raw materials used for the synthesis of activated carbons from coal waste, experimental procedures and various characterization tests carried out. A description of the preliminary analysis carried out on the coal waste samples and the types of analyses conducted on the activated carbons derived from these materials are discussed. Noteworthy, synthesis of all the activated carbons used in this study was achieved by the chemical activation process using potassium hydroxide (KOH), with the aim of improving the surface properties and storage capacity of the activated carbons produced. The first section of this chapter discusses sample preparation and activation methods while the second section discusses the various equipment used during the course of this study.

3.2 Materials

Figure 3.1 shows the flowchart of the experimental methods adopted at various stages in this study.

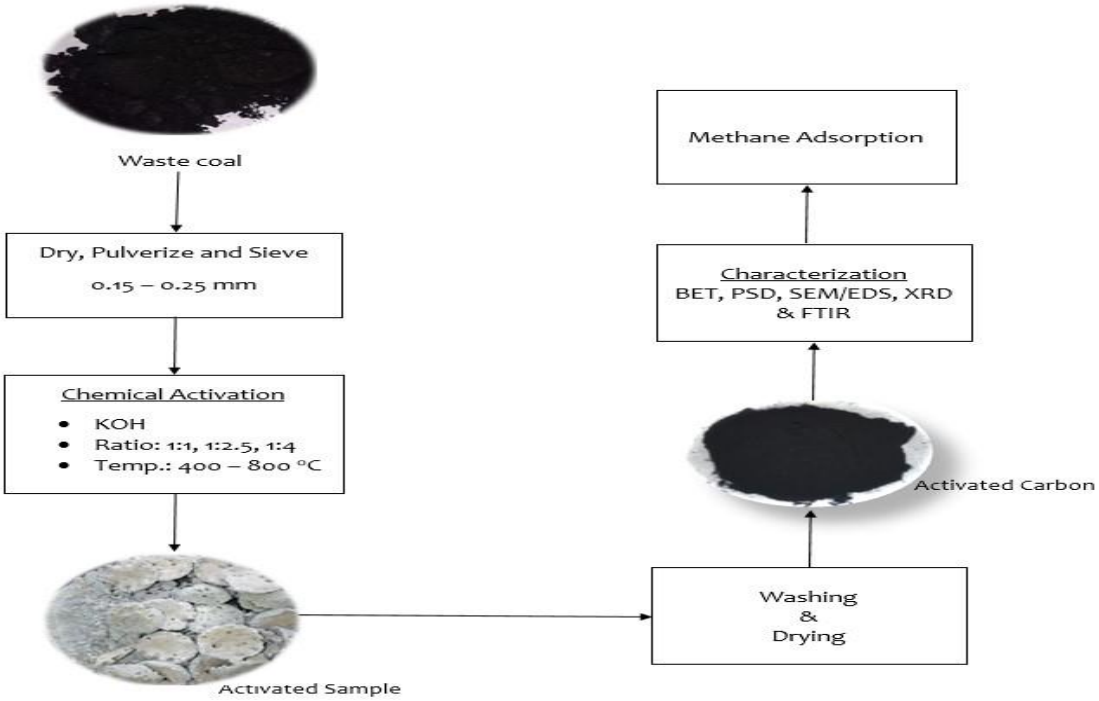


Figure 3.1 Experimental Flowchart

3.3 Methods

3.3.1 Sample collection

Samples of coal discard, run-of-mine (ROM) fines and slurry from floatation process were collected (using the ply sampling method) from a Mine situated 15 km south-west of Witbank in Mpumalanga, South Africa. The samples were collected in airtight sample bags and each sample bag was clearly labeled for proper identification. The samples were stored and prepared under laboratory conditions (room temperature).

3.3.2 Sample Preparation

The samples were dried under laboratory conditions for 48 hours. After drying, the samples were milled using a centrifugal mill (Retsch ZM 200) as shown in Figure 3.2 and sieved to obtain different particle sizes for each test, 0.15 – 0.25 mm particle size for proximate, ultimate, total sulfur analysis and activated carbon preparation. For the petrographic analysis, the coal samples were milled to - 1 mm analysis.



Figure 3.2 Centrifugal Mill (Retsch ZM 200)

3.3.3 Sample Characterization

3.3.3.1 Proximate Analysis

Proximate analysis was carried out to determine the moisture, ash, volatile matter and fixed carbon content of these samples in accordance with ISO 13909-4: 2001, ISO 11722: 1999, ISO

1171: 2010, ISO 562: 2010. One gram (1g) of each of these samples was used for the analysis. The moisture content, ash content and volatile matter are determined analytically, while the fixed carbon was determined by difference and the analysis was carried in an air-dried (ad) basis. Each of the analytical technique is further described below:

(i) Moisture Content (ISO 11722)

In determining the moisture content, the weight loss of each pulverized sample was measured and expressed as a percentage (%). One gram (1g) of the sample was weighed into a dish and heated in an oven at 110 ^{o}C for one hour. The sample was then allowed to cool to room temperature and weighed to determine the loss in mass. The loss in weight, expressed as a percentage of the sample used, is the moisture content as expressed by equation (3.1).

$$M\% = \frac{w_1 - w_2}{w_1} \quad (3.1)$$

where M% is the percent moisture; w_1 is the initial weight, and w_2 is the final weight.

(ii) Ash Content (ISO 1171)

About 1g of coal waste sample was weighed into a dish and placed in a furnace ventilated by air. The sample was slowly heated until temperature reaches 800 ^{o}C. The temperature was maintained until a constant weight was achieved. The dish was removed from the furnace, cooled and weighed. The mass of ash, expressed as a percentage of the weight of the sample used, is the ash content as expressed by equation (3.2)

$$A\% = \frac{w_{ad} - w_d}{w_s} - M\% \quad (3.2)$$

where A% is the Ash content in percentage; w_{ad} is the weight of ash and dish; w_d is the weight of the dish and w_s is the weight of the sample.

(iii) Volatile Matter Content (ISO 562)

In determining the volatile matter, one gram (1g) of the sample was weighed into an already weighed crucible with a close-fitting lid. The crucible was placed in a furnace at 900 ^{o}C under nitrogen flow, the furnace was closed and allowed to heat for seven minutes. The crucible was removed after the heating period, then allowed to cool and then weighed. The loss in weight, expressed as a percentage of the sample, less the moisture content, is the volatile matter content of the sample expressed by equation (3.3):

$$VM\% = \frac{w_1 - w_2}{w_1} - M\% \quad (3.3)$$

where VM% is the percent volatile matter, M% is the percent moisture; w_1 is the initial weight, and w_2 is the final weight.

(iv) Fixed Carbon

Fixed carbon is not determined, but obtained by subtracting the sum of the moisture, ash and volatile matter contents expressed as percentages, from 100% as expressed by equation (3.4).

$$\%FC = 100 - (\%M + \%A + \%VM) \quad (3.4)$$

where; %FC is the percentage of fixed carbon.

3.3.3.2 Ultimate and Total Sulfur Analysis

These analyses were carried out to determine the elemental composition of the coal waste samples (total carbon, hydrogen, nitrogen) in accordance with ISO 12902, instrumental method, while the total sulfur was determined according to ISO 19579. The percentage of oxygen content was calculated by difference. LECO TruSpec CHN equipment was used for the ultimate analysis, while LECO C & S Analyser was used for the total sulfur as shown in Figure 3.3 and Figure 3.4, respectively.



Figure 3.3 LECO TruSpec CHN Analyser

(i) Analysis of Carbon, Hydrogen, and Nitrogen (ISO 12902)

One gram (1g) of the coal sample was placed in a carousel and inserted into the furnace to heat to 950 ^{o}C in the presence of oxygen for combustion. An infrared detector was used to determine the emitted gases of carbon and hydrogen, while a thermal conductivity detector was used to detect the nitrogen within the coal.

(ii) Analysis of Oxygen content

The oxygen content (%) of the samples on air-dried basis were determined as by the difference of the sum of the percentage of moisture, ash, carbon, hydrogen, nitrogen, and sulfur from 100% as expressed by equation (3.5)

$$O\% = 100 - (M+A+C+H+N+S)\ \% \quad (3.5)$$

Where, O% is the percentage of oxygen by difference present in the analysed sample; M is the percentage of moisture; A is the percentage ash content; C is the percentage total carbon; H is the percentage of hydrogen; N is the percentage of nitrogen and S is percentage of total sulfur.

(iii) Total sulfur (ISO 19579)

A measured quantity of the samples was completely burned in oxygen. Sulfur inherent in the samples reacted during the combustion to form sulfur dioxide (SO_2). The combustion gases were purified after passing through a dust filter and moisture absorber. Infrared scanning of the evolved gas was used to measure the sulfur content.



Figure 3.4 LECO C & S (CS23OSH)

3.3.3.3 Petrographic Analysis

The petrographic analysis was carried out to determine the maceral composition and mineral matter content of the coal waste samples. In carrying the petrographic analysis, the samples were block mounted following SANS ISO 7404 part 1-5 standard method and prepared to a

final 0.05-micron polish using a Struers Tegraforce polisher. The polished blocks were analysed using a Zeiss Axio Imager M2M reflected light petrographic microscope fitted with a Hilgers Fossil system for vitrinite reflectance and maceral determination at a magnification of x500 under reflected white light, with oil immersion. In addition, the vitrinite reflectance of the coal samples was examined. The results of the analysis are reported as inclusive of mineral matter (vol %) and mineral matter free basis (vol %, mmf).

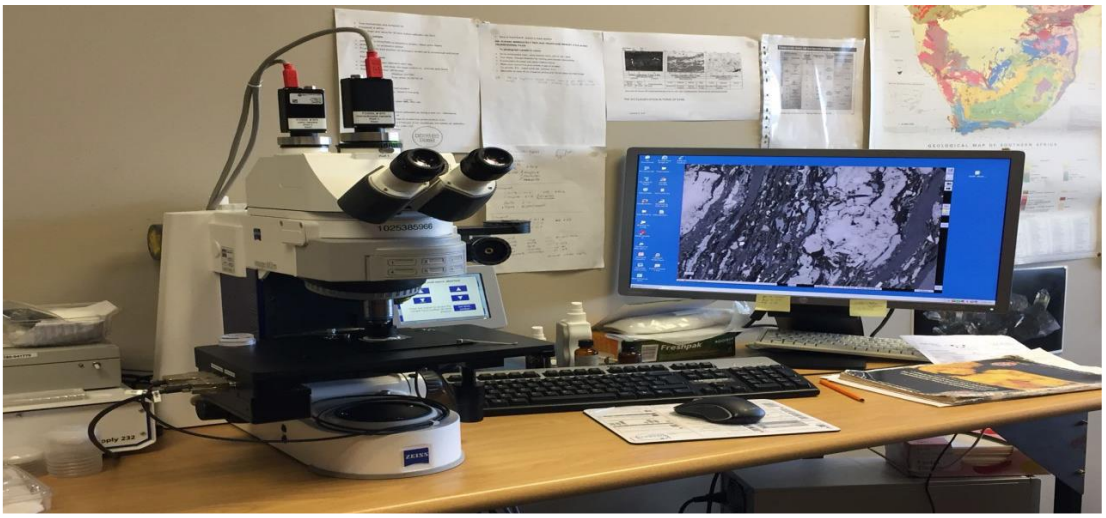


Figure 3.5 Zeiss Axio M2M Reflected light Petrographic-microscope

3.4 Synthesis of Activated Carbon

3.4.1 Chemical Activation

For this study, potassium hydroxide (KOH) activation was carried out at a temperature range of 400 to 800 ^{o}C and KOH weight ratio of 1 to 4. In synthesizing the activated carbon samples, the dried coal waste samples were physically mixed with KOH at a predetermined (coal waste/KOH) weight ratio (1 – 4). The mixed samples were placed in a furnace and heated at 10 ^{o}C/min under nitrogen at a flow rate of 100 ml/min from room temperature to a final temperature within the range of (400 - 800 ^{o}C). The procedure was utilized in accordance with the test procedure outlined by (Aaron and Tsouris, 2005) in preparing activated carbon. At the final temperature, the activated carbon produced/samples were held for 2 hours, then cooled under nitrogen flow. The samples were washed using 0.5N HCl to remove residual alkali (Wu *et al.*, 2005), and subsequently washed with distilled water, centrifuged until the pH of the samples/distilled water solution was 6 (Hu and Srinivasan, 1999). The washed sample was then

kept in an oven at 110°C overnight to dry, and thereafter stored in a bottle for subsequent analysis and characterization. The setup for the preparation of the activated carbon samples is as shown in Fig. 3.6. This is consistent with previous studies reported by Dai *et al.* (2006), and Omri and Benzina (2012). The nitrogen gas (UHP 99.99 %) used was supplied by AFROX (African oxygen Ltd) and was accompanied by a certificate of analysis. The Potassium Hydroxide (A.R grade with concentration of >=85%) was supplied by Sigma Aldrich.

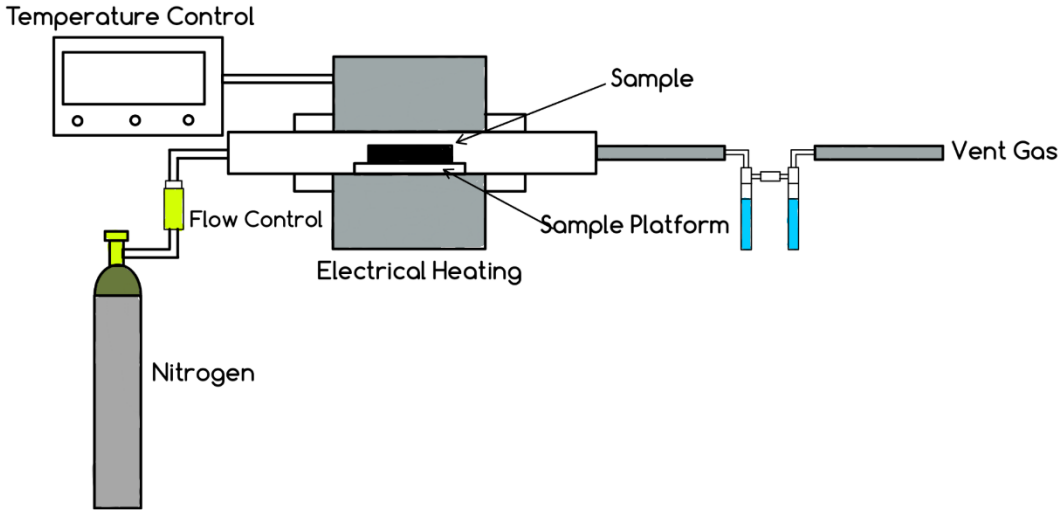


Figure 3.6 Activated Carbon Preparation Setup

3.4.1.1 Experiment Design

The activated carbon synthesis experiment was designed using Design-Expert software (version 7.0.0) by Stat-Ease, Inc. The central composite design (CCD) component of the software was used to apply to the Response Surface Methodology (RSM) (Zhao *et al.*, 2011). The central composite design consists of three design points; two-level factorial design points; axial points and center points. Two factors were varied in this study; KOH/coal waste sample ratio (W) and activation temperature (T). The structure and design matrix of the synthesis experiments are as shown in Table 3.1. There are four factorial points, four axial points, and five center points which were repeated five times to obtain an accurate estimate of experimental error.

Table 3.1 Structure and CCD Design Matrix of Synthesis Experiments

# Run	Coded Factors		Actual Factors	
	T	W	T (^{o}C)	W
1	-1	-1	400	1
2	0	-1	600	1
3	0	0	600	2,5
4	1	0	800	2,5
5	0	0	600	2,5
6	0	1	600	4
7	-1	0	400	2,5
8	1	1	800	4
9	1	-1	800	1
10	0	0	600	2,5
11	-1	1	400	4
12	0	0	600	2,5
13	0	0	600	2,5

3.5 Characterization of Synthesized Activated Carbon

3.5.1 Density Measurement

The density of the synthesized activated carbons was determined by the Helium Pycnometer using Micromeritics Accupyc II 1340 device (Fig. 3.7). This system uses a gas displacement method to measure volume accurately. Helium is used as the analysis gas due to the extent of helium penetration into surfaces, hence ensuring accurate volume measurement. The activated carbon sample is loaded into a calibrated chamber of known volume, then the analysis gas (helium) is introduced. The gas molecules rapidly fill the void volume of the chamber including the pores of the sample. The pressure obtained upon filling the sample chamber is discharged into another empty chamber which allows for the computation of the sample solid phase volume. The Accupyc repeats the analysis by automatically purging water and volatiles from the sample under analysis. The analysis is done severally until successive measurement converges upon consistent results. The density is obtained by dividing the measured volume by the weight of the sample.



Figure 3.7 Image of Micromeritics Accupyc II 1340 Pycnometer

3.5.2 Measurement of Surface Area, Pore Volume and Size

The gas adsorption techniques have been adjudged to be successful in characterizing porous materials such as the nitrogen (N_2) adsorption test. The N_2 adsorption test measures the surface area, total pore volume and pore size of a material.

3.5.2.1 Nitrogen Gas Adsorption Technique

In carrying out the nitrogen adsorption test at 77 K, 0.2g of each sample was measured and degassed at 150 °C for 6 hours in a nitrogen flow using a Micromeritics Flow Prep 060 unit (Fig. 3.8a). The samples were then transferred to a Micromeritics Trista 3000 instrument (Fig. 3.8b) for analysis. The nitrogen adsorption data was used to calculate (i) Surface area, S_{BET}, using BET method (Brunauer *et al.*, 1938); (ii) total pore volume, V_T, determined at a relative pressure of $P/P_o = 0.99$ (Gregg *et al.*, 1967); (iii) pore size was obtained from the desorption data of the N_2 isotherms using the Barrett-Joyner-Halenda (BJH) method (Barrett *et al.*, 1951).

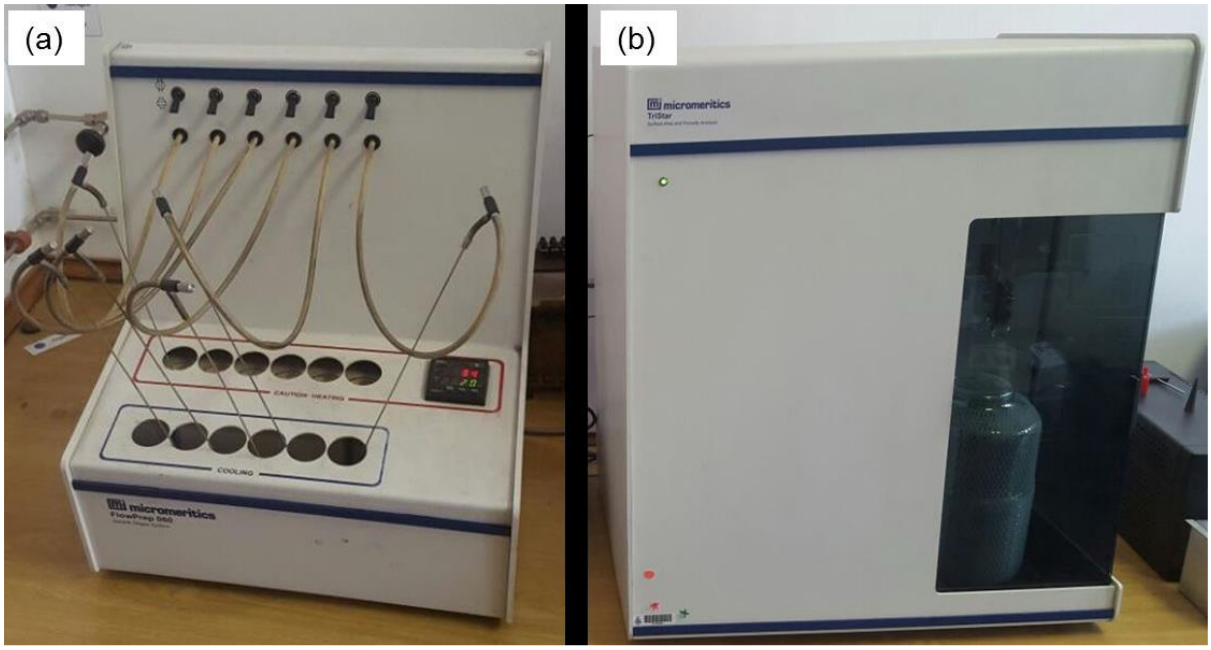


Figure 3.8 (a) Micromeritics Flow Prep 060 Unit and (b) Micromeritics TriStar 3000 instrument

3.5.2.2 Brunnet Emmett Teller (BET) Technique

The adsorption isotherms obtained from the N_2 adsorption test are conventionally analysed using the BET model to obtain surface area and pore volume. Two key physical properties of porous materials with significant influence on its storage performance are the surface area and porosity. The Brunauer–Emmett–Teller method has been widely used to measure the surface area, total pore volume and pore diameter of porous materials (Rouquerol *et al.*, 2013, Cohen, 2007, Lowell *et al.*, 2012). In the application of the BET method, there are two steps. The first step is the transformation of the physical adsorption (physisorption) isotherm into the BET plot from which a value known as BET monolayer capacity (n_m) is derived. The second step is to calculate the BET surface area (a_{BET}) from n_m by choosing an appropriate value for the molecular cross-sectional area, σ (Thommes *et al.*, 2015). The linearized form of the BET equation is as shown in equation 3.6 (Rouquerol *et al.*, 2013)

$$\frac{{}^{P}/_{P_o}}{n(1-{}^{P}/_{P_o})} = \frac{1}{n_m C} + \frac{C-1}{n_m C}({}^{P}/_{P_o}) \tag{3.6}$$

where; n is the amount adsorbed at relative pressure P/P_o and n_m is the specific monolayer capacity.

To calculate the BET monolayer capacity n_m from the BET equation, the BET plot is used which defines the linear relationship between $\frac{{}^{P}/_{P_o}}{n(1-{}^{P}/_{P_o})}$ and P/P_o. The monolayer capacity n_m

is then used to calculate the BET area. This will require information about the average area, σ_m (molecular cross-sectional area), occupied by the adsorbate molecule in the complete monolayer (Rouquerol *et al.*, 2013). Thus, the relationship is as expressed by equation (3.7)

$$a_s(BET) = n_m . \frac{L.\sigma_m}{m} \quad (3.7)$$

where; a_s (BET) is the BET specific area of the adsorbent (of mass m).

3.5.2.3 Pore Size Distribution (PSD)

Pore size distribution (PSD) is widely issued in characterizing and describing the internal structure of activated carbons and other porous materials (Davies *et al.*, 1999, Zhao *et al.*, 2011, Okhovat *et al.*, 2012, Wang *et al.*, 2018). PSD provides a representation of the internal structure of the material using a simplified model. PSD is defined as:

$$f(w) = \frac{dV}{dw} \quad (3.8)$$

where w is pore width and V is the corresponding pore volume.

The PSD of a material is obtained by solving the adsorption integral equation (AIE) (Eq. 3.9) which provides a definite correlation between the PSD function (Eq. 3.8) and the adsorption isotherm of the material (Wang *et al.*, 2018).

$$N(P_i) = \int_0^\infty f(w)\, \rho(w, P) dw \quad i = 1.....n \quad (3.9)$$

where $N(P_i)$ is the experimentally measured adsorption isotherm of the material, $\rho(w, P)$ is the adsorption density in a model pore of width w and $f(w)$ is the PSD and n is a number of adsorption measurements used in the analysis.

Nitrogen at 77 K adsorption isotherm is widely used in characterizing the PSD of activated carbons (Davies and Seaton, 1998, Wang *et al.*, 2018). The nitrogen adsorption isotherm is most often analysed using the nonlocal density functional theory (NLDFT) method along with a mathematical model for PSD characterization. While, there are other methods aside NLDFT such as Barret, Joyner, and Halenda (BJH), Horvath and Kawazoe (HK), NLDFT provides a much more significant accuracy in characterizing the pore structure of the material (Okhovat *et al.*, 2012, Wang *et al.*, 2018).

In this study, "Solution of Adsorption Integral Equation Using Splines" (SAIEUS) software (Version 3.0) from Micromeritics is used to analyse the nitrogen adsorption isotherm of the synthesized activated carbon samples for PSD characterization. NLDFT is integrated into the SAIEUS software for the PSD characterization using the conventional slit pore model. The

procedure of using the software is to save the adsorption data as a text file and import it into the software for PSD characterization. Carbon-N_2 –NLDFT, Standard slit was selected as the model to be used as shown in Fig. 3.9.

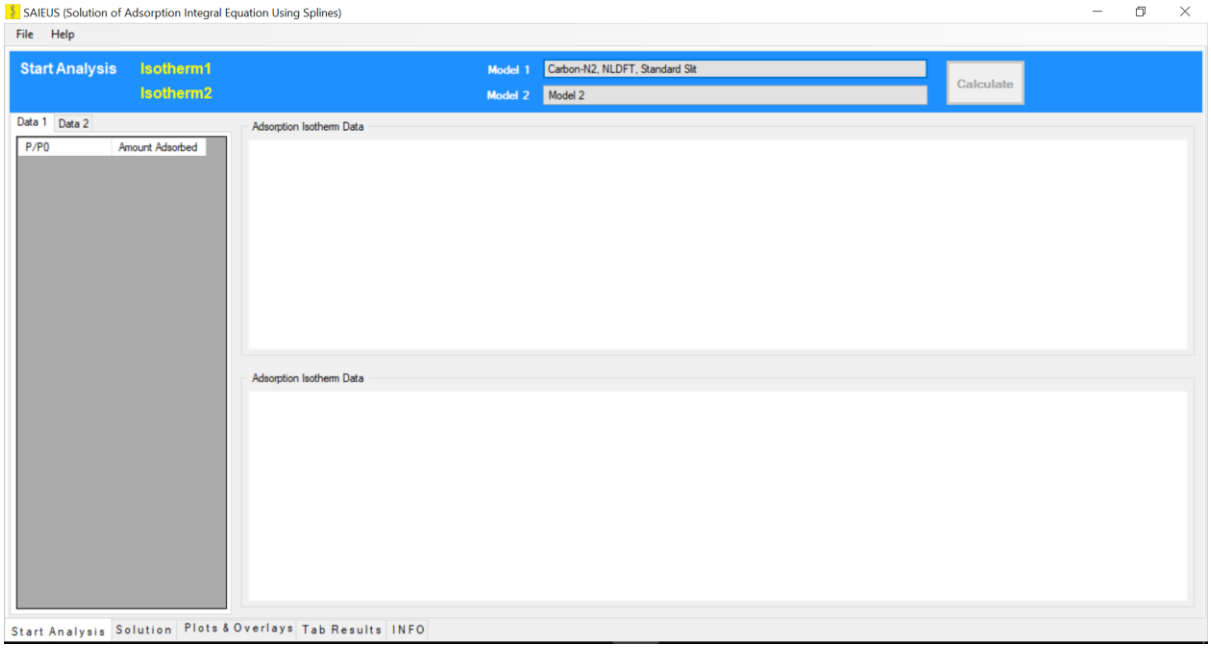


Figure 3. 9 Start Analysis page of the SAIEUS software

3.5.3 SEM/EDS Technique

The surface morphology and elemental analysis of the synthesized activated carbons and their precursors were studied using scanning electron microscopy (SEM) technique using Carl Zeiss Sigma Field Emission Scanning Electron Microscope equipped with Oxford X-act EDS detector (Fig. 3.10). In preparing the samples for SEM/EDS analysis, the samples were first mounted on a stub with the use of carbon tape. Thereafter, thin coatings of carbon (graphite) and gold/palladium alloy were applied to each sample. The coatings ensure the samples are electrically conductive, thereby minimizing charging and other related imaging artifacts during analysis. Once the coating is completed, the stubs containing the coated samples are labeled and introduced into the specimen chamber of the equipment. In carrying the analysis, the electron beam strikes the surface of the sample at an angle, triggering secondary electrons discharge from the surface atoms. These electrons strike a detector which is also placed at an angle to the surface. The signal is enhanced by a photomultiplier and this is followed by the generation of an image. This form of microscopy yields information about the surface structure of a sample (Lin *et al.*, 2003)

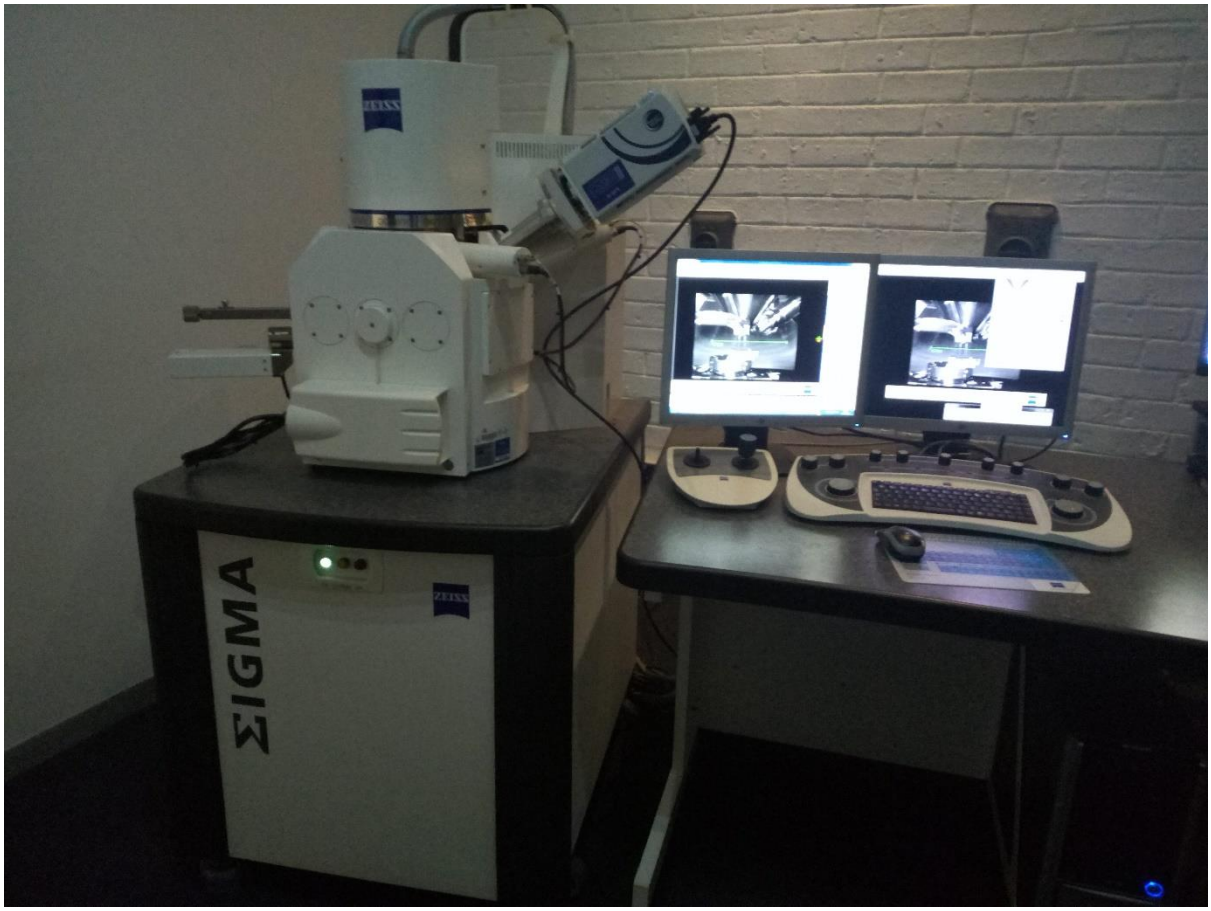


Figure 3.10 Image of Carl Zeiss Sigma Field Emission Scanning Electron Microscope equipped with an Oxford X-act EDS detector

3.5.4 X-ray Diffraction (XRD) Technique

XRD analysis is a distinctive technique used to determine the crystallinity of a compound and can also be used to differentiate amorphous and crystalline materials. The working principle of XRD analysis is centered on the interference of monochromatic X-rays and crystalline material. An XRD equipment (diffractometer) comprises an X-ray tube, a sample holder, and an X-ray detector. The cathode ray tube produces the X-rays, which is filtered to generate monochromatic radiation, and directed toward the material to be analysed. The interaction of the incident rays with the material creates a diffracted ray when conditions satisfy Bragg's Law as expressed by equation (3.10)

$$n\lambda = 2d \sin \theta \quad (3.10)$$

where, n is an integer depicting the order of the diffraction peak; λ is the wavelength; d is the lattice spacing and θ is the scattering angle (Birkholz, 2006).

Bragg's law correlates the wavelength of electromagnetic radiation to the scattering angle and the lattice spacing in a crystalline material. The typical x-ray diffraction pattern produced in a typical XRD analysis generates a distinctive "pattern" of the crystals present in the material. An accurate interpretation of such a pattern requires comparing the pattern with available reference patterns, thus allowing accurate classification.

The X-ray powder diffraction analysis of the activated carbons and its precursors was conducted using D2 PHASER Bruker Meas Srv D2-208365 with SSD 160 operated at 30 kV and 10 mA (Fig. 3.11) for the response patterns, purity, and crystallography of the powdered activated carbon samples. The diffraction peaks were then compared with reference patterns using DIFFRAC.SUITE Eva software suite which allows for peak search and creation of peak data for phase identification.

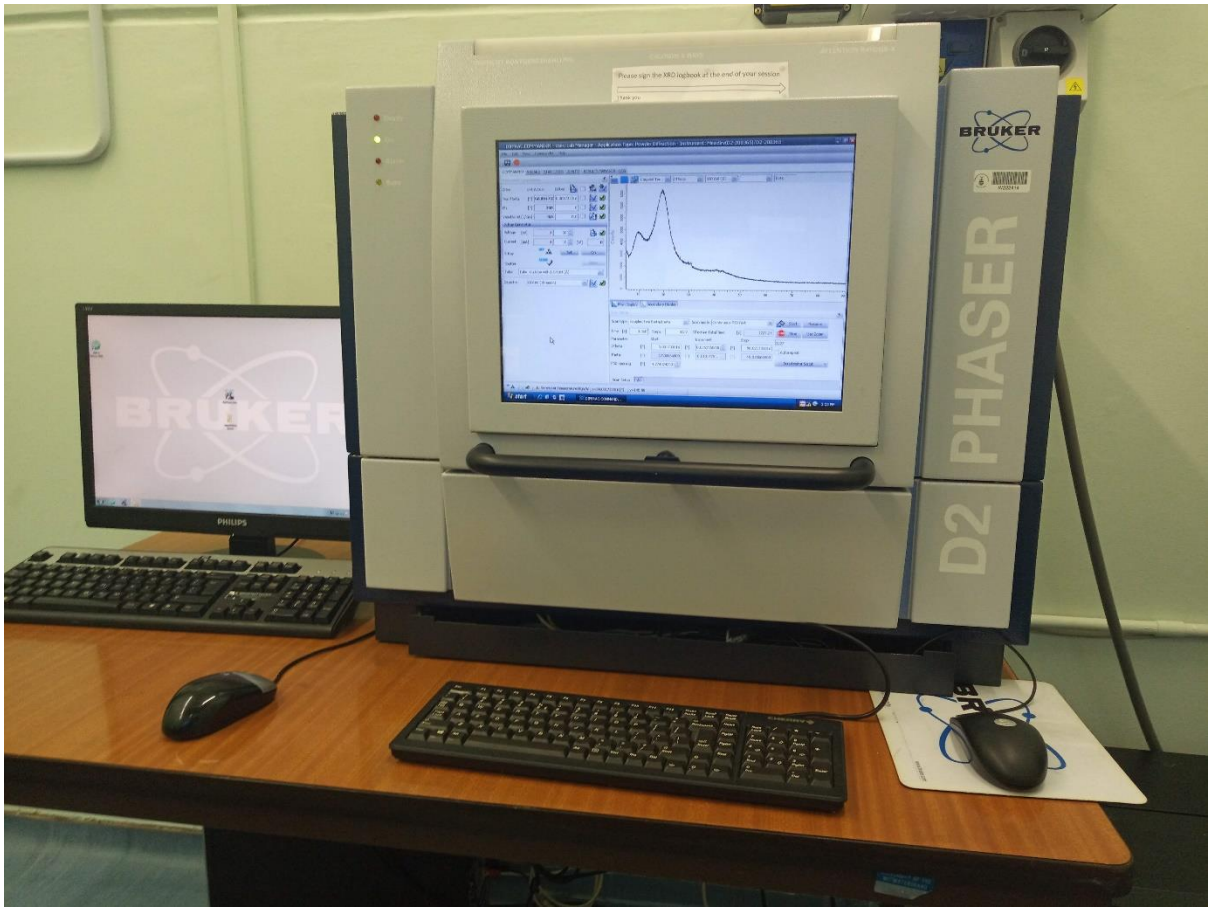


Figure 3.11 Image of Bruker D2 PXRD Phaser

3.5.5 FT-IR Technique

The Fourier transform infrared (FT-IR) analysis of the samples and the activated carbons produced were carried out using Perkin Elmer FTIR Spectrometer - Spectrum Two (Fig. 3.12), to ascertain the chemical functionality of the samples and the synthesized activated carbons. The analysis was carried out in the wavelength range 4000-450 cm^{-1} in transmittance mode. For the analysis, about 0.2g of the samples were placed on the instrument diamond attenuated total reflectance (ATR) accessory. The sample was positioned on the instrument holder. The knob was used to exert pressure on the sample in order to produce the spectrum. Each sample produced vibrational spectra and signals characteristics of the material.

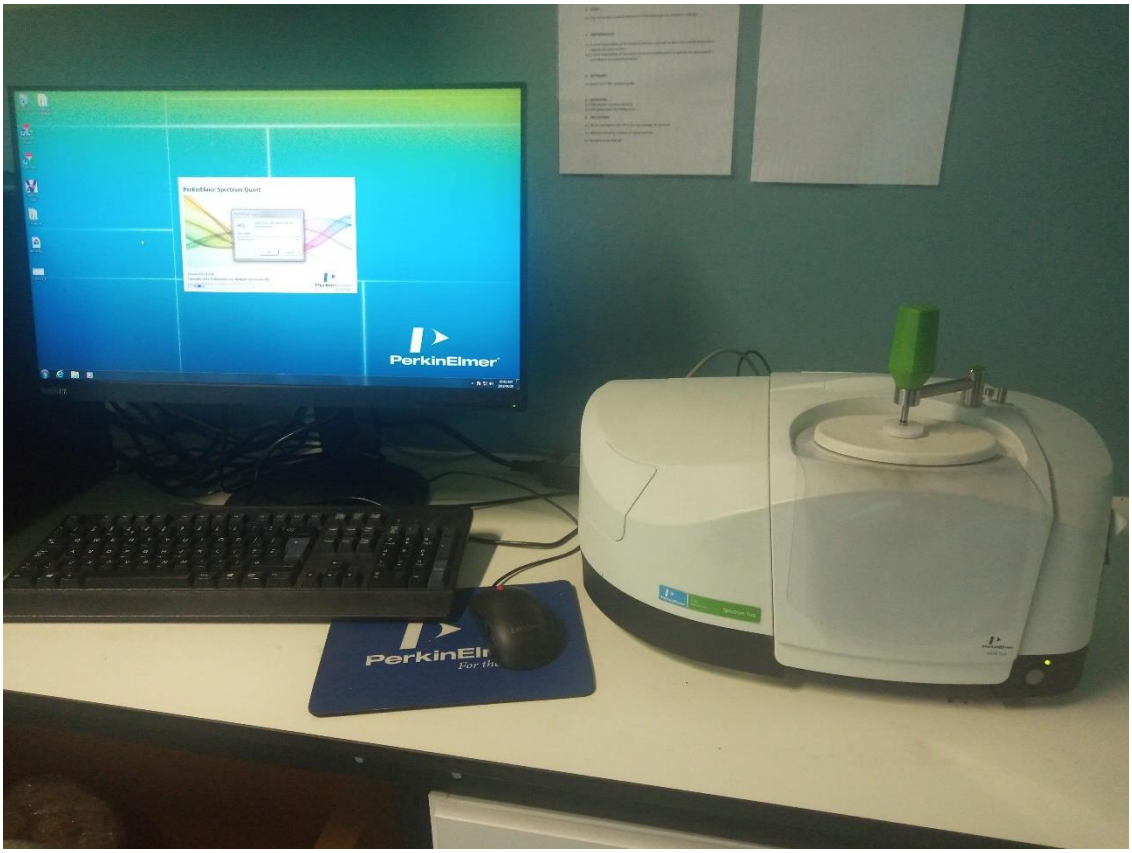


Figure 3.12 Image of Perkin Elmer FTIR Spectrometer

3.6 Measurement of Methane Adsorption on Activated Carbons

The capacity of the synthesized activated carbons for storing methane at different temperatures and pressures up to 40 bars was carried out using Particulate Systems High Pressure Volumetric Analyser (HPVA II) (Fig. 3.13). The equipment (HPVA II) utilizes the volumetric method in

its analysis to produce high pressure adsorption and desorption isotherms using different gases such as CH_4, CO_2, and H_2 (Particulate and Systems, 2011).

In the volumetric method, a known volume of gas is introduced into the sample chamber for analysis. On attaining equilibrium between the sample and the gas, the final equilibrium pressure is noted. Calculating the amount of gas adsorbed by the sample is done using the equilibrium pressure data. The adsorption analysis is carried out repeatedly at specified pressure intervals until it reaches the maximum set pressure. To obtain the adsorption isotherm, data of the quantity of gas adsorbed is plotted against the equilibrium pressure. In carrying the desorption analysis, the pressure is reduced steadily to obtain the desorption isotherms.

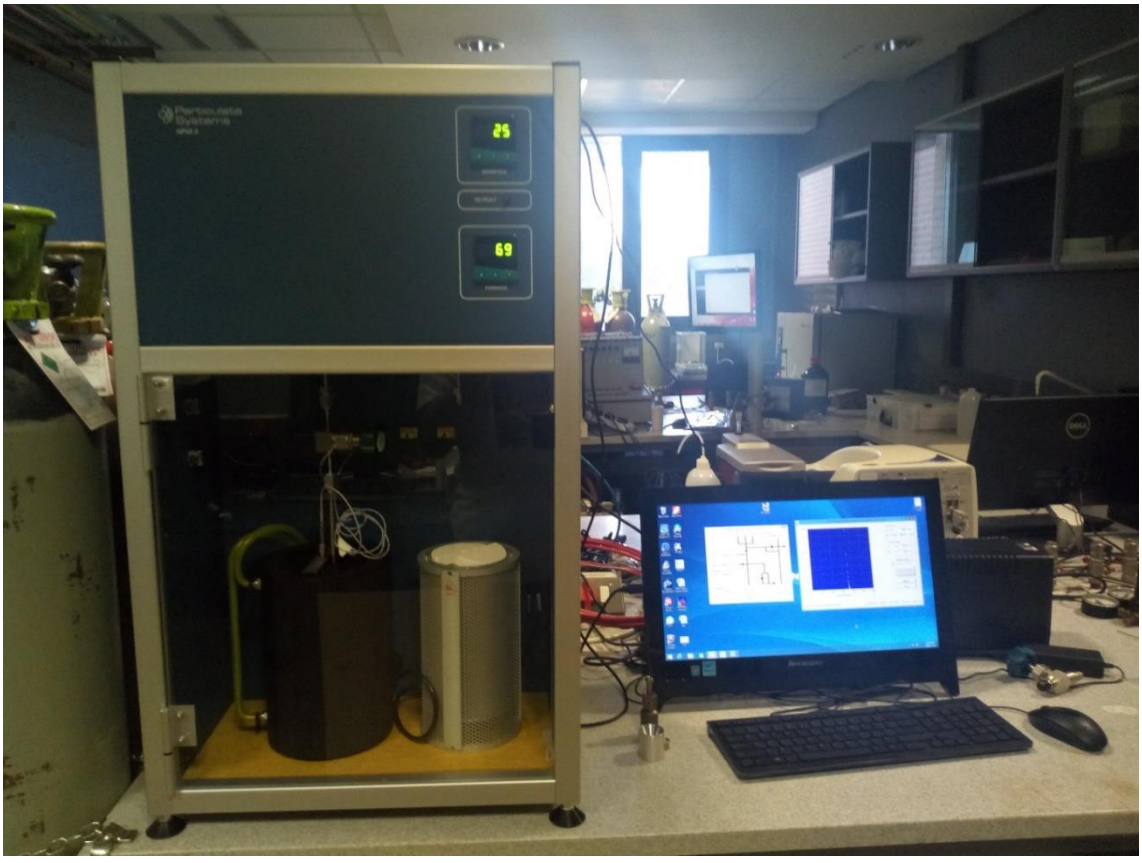


Figure 3.13 Image of Particulate Systems High Pressure Volumetric Analyser (HPVA-200)

3.6.1 Samples Preparation

In preparing the samples for analysis, the sample cylinder is first cleaned using alcohol and subsequently rinsed severally with warm water as shown in Fig. 3.14. The rinsed sample cylinder is then placed in an oven and preheated to 110 ^oC and then held at this temperature for two hours. After two hours, the sample cylinder was taken out of the oven and allowed to cool.



Figure 3.14 Cleaning HPVA II Sample Cylinder

Thereafter, the sample cylinder is weighed by first ensuring the weighing balance is tared and allowed to stabilize to zero. The sample cylinder was placed on the balance (Fig. 3.15) and the weight was recorded as the weight of the empty sample cylinder, W_1. Afterward, the sample cylinder was removed from the balance and a funnel was placed on top of the cylinder to add the sample to be analysed. The weighing was repeated and the new weight was recorded as the weight of sample cylinder plus sample, W_2. The weight of the sample was then calculated as the difference between W_1 and W_2 as expressed by equation (3.11).

$$W_s = W_2 - W_1 \tag{3.11}$$

The weight of the sample is represented as W_s; W_2 is the weight of the sample cylinder + sample; and W_1 is the weight of the empty sample cylinder. Once the weight of the sample was taken and recorded, a 20M VCR metal gasket seal from Swagelok was placed on top of the cylinder tightly screwed to the sample holder to avoid leaks.

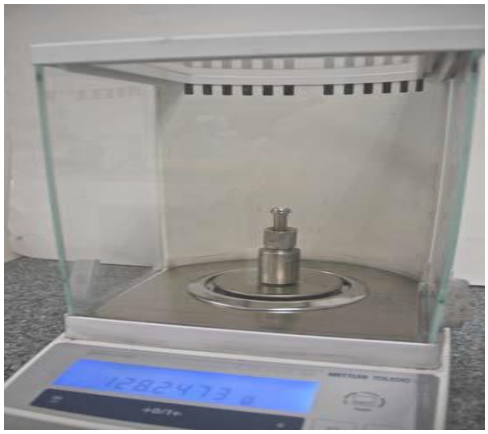


Figure 3.15 Weighing the Empty Sample Cylinder

3.6.2 Samples Degassing

To degas the samples, the sample holder was placed inside the sample compartment of the HPVA equipment with the furnace thermocouple cables inserted into the thermocouple connectors of the sample compartment (Fig. 3.16). The sample holder was afterward connected to the degassing port by hand tightening the connector in place. Once the sample holder was properly placed, sample evacuation was carried out to ensure a vacuum is in place. Thereafter, furnace temperature was set, first at 90 ^{o}C, and was gradually increased until it reaches 200 ^{o}C. The sample was allowed to degas as required to allow for proper analysis of the activated carbon sample. At the end of the degassing process, the furnace temperature was set to 0 ^{o}C and the sample was allowed to cool to room temperature. Afterward, the sample holder was removed from the degassing port.



Figure 3.16 Connecting the furnace thermocouple cables to the Sample Compartment

3.6.3 Methane Adsorption/Desorption

To carry out methane adsorption/desorption analysis, the sample holder after removing from the degassing port was inserted inside the sample analysis compartment and then connected to the analysis port of the HPVA equipment. Prior to the connection, water was added to the sample analysis compartment (Fig. 3.17). Thereafter, the temperature probe was immersed in the sample compartment to monitor temperature variation during the analysis.

To run the adsorption/desorption experiment, the pressure, temperature and gas port (methane) parameters were defined on the system experiment definition window (Fig. 3.18). Once the parameters were well-defined, the "Run Experiment" button on the window was clicked and the experiment was allowed to run.



Figure 3.17 Sample Analysis Compartment

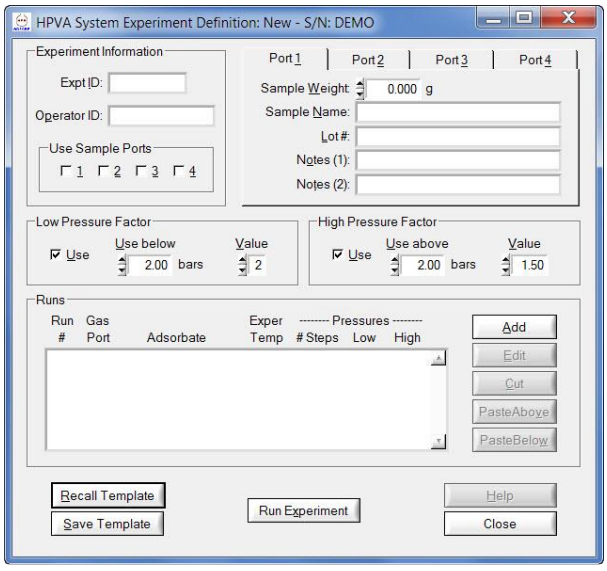


Figure 3.18 HPVA II System Experiment Definition Window

3.7 Modeling and Simulation of Methane Adsorption onto Activated Carbon

The model utilized in this study was developed for methane adsorption onto the synthesized activated carbons produced and simulated using Aspen Adsorption (Adsim Version 10). This provide a better understanding of the filling and discharge characteristics of the adsorbent bed and also the thermal effects associated with adsorption and desorption process. The simulation utilizes a dynamic gas model in which hydrodynamics, heat transfer and adsorption principle are studied.

The Adsim software provides a great interactive platform for modeling and solving ~~a lot~~ of scientific and engineering problems. The software offers an integrated desktop environment with a Model Builder that provides a complete overview of the model and access to all functionality. With the in-built physics interface and several material properties, models can be built easily by outlining the appropriate physical quantities such as material properties, constraints, etc. By applying these variables, Adsim systematically then internally assembles a group of equations describing the model. In solving the models, Adsim uses the finite element method (Aspen, 2012).

3.8 Summary

In this chapter, the methodology and experimental techniques used in analysing and characterizing the coal waste samples (ROM fines, discards/tailings and flotation slurry), and the synthesized activated carbon samples were presented. In addition, characterization methods that included, proximate, ultimate, total sulfur and petrographic analysis of the samples used in this study were presented. The analytical procedures used for the characterization and determining the capability of the activated carbon produced for methane storage were also presented. The combination of the analytical procedures for the coal waste samples and the activated carbons produced provided an in-depth understanding of activated carbons from coal waste samples for gas storage applications. The results of the experimental investigations conducted on all the coal samples utilized and the activated carbon produced are discussed in the next chapter.

CHAPTER 4 SYNTHESIS AND CHARACTERIZATION OF ACTIVATED CARBONS FROM COAL WASTE

4.1 Introduction

The results of the synthesis of activated carbons from coal waste samples are presented and discussed in this chapter. The chemical activation route with the use of KOH reagent was applied in the development of the activated carbons. The effects of KOH/sample weight ratio (1 to 4) and temperature (400 to 800 ^{o}C) on the physical properties of the activated carbons were methodically evaluated and optimized using Response Surface Methodology (RSM). The results of BET, SEM/EDS, XRD, and FTIR characterization were also discussed. The chapter also highlighted the improvement made on the quality of the synthesized activated carbons over activated carbons produced from coal-related materials from previous studies.

4.2 Samples Characterization

To assess the potential of the activated carbon produced from the coal waste samples used in this study, it is important to understand the physicochemical properties of the samples. The purpose of these analyses such as proximate, ultimate and petrographic analysis is to determine the quality and the rank of the samples. The results obtained from the proximate, ultimate, total sulfur content and petrographic analyses carried out on these samples are presented in Table 4.1.

Table 4.1 Proximate, Ultimate, Total sulfur and Petrographic analysis of coal waste samples

Analysis	Standards Used	Sample A (ROM Fines)	Sample B (Discard)	Sample C (Slurry)
Proximate Analysis (wt.%, adb)				
Moisture Content	ISO 11722: 1999	2.2	2.1	2.6
Ash	ISO 1171: 2010	25.2	35.4	36.3
Volatile Matter	ISO 562: 2010	23.2	20	20.8
Fixed Carbon	By difference	49.4	42.5	40.3
Ultimate Analysis (wt. %, adb)				
Carbon	ISO 12902	58.30	48.90	48.90
Hydrogen	ISO 12902	3.19	2.67	2.84
Nitrogen	ISO 12902	1.43	1.15	1.21
Oxygen	By Difference	36.23	45,94	45.84
Total Sulfur (wt.%, adb)	ISO 19579: 2006	0.85	1.34	1.21
Petrographic Analysis (vol.%, in. mm)				
Vitrinite	ISO 7404-3: 2009	23	7.2	13.6
Inertinite	ISO 7404-3: 2009	40	49.3	42.9
Liptinite	ISO 7404-3: 2009	1.0	3.9	2.8
Mineral Matter	ISO 7404-3: 2009	36	39.7	40,7

ROM: run-of-mine; in. mm: including mineral matter; adb: air-dried basis and O [100-(M+Ash+H+C+N+S)

From the proximate analysis test, the moisture, volatile matter, fixed carbon, and ash content of all the samples are determined. The inherent moisture content, as shown for sample C has the highest moisture of 2.6%, while sample B has the lowest at 2.1%, as seen in Table 4.1. The fixed carbon from the three samples contain a high percentage of fixed carbon at over 40%, an indication of their suitability for use as material for activated carbon (Azargohar and Dalai, 2005, Lillo-Ródenas *et al.*, 2007, Zhao *et al.*, 2011, Martin *et al.*, 2017). The samples contain high ash content ranging from 25 - 36%. Sample A, which was the discarded coal fines from the ROM, was found with the highest fixed carbon content (49.4%) and the lowest ash content (25.2%). This was expected, as both sample B and C are discard coals or tailings from the dense medium and flotation processes, respectively. Coal A can be categorized as a moderately high-ash coal according to ISO coal Classification (ISO, 2005).

The petrographic analysis presents the maceral composition of the samples and classified them as vitrinite, inertinite, liptinite, and mineral matter according to the International Committee

for Coal and Organic Petrology (ICCP, 2001). As shown in Table 4.1, the three samples are rich in inertinite maceral component ranging from 40 to 49%. This is consistent with the findings reported by Falcon and Ham (1988), and Hattingh *et al.* (2008) on South African high ash ROM coal. The three samples were found to possess low content of liptinite maceral at 1 to 3.9%. The ROM fine coal possesses the highest vitrinite composition compared to both tailing samples. The reason being that the majority of the vitrinite component of the coal has been recovered to the concentrate during the beneficiation of the coal. A good correlation was observed to exist between the ash content of the samples from the proximate analysis and the mineral matter of the samples from the petrographic analysis. It was observed that the higher the mineral matter of the sample, the higher the corresponding ash content as shown in Table 4.1. This is expected, as the mineral matters contained the ash forming minerals, in which after the coal combustion, the residue left is the coal ash content. Coal C was seen with a slightly higher mineral matter of 40.7% compared to coal B, and this correlates with the higher incombustible ash of 36.3% obtained compared to sample B with 35.4%.

4.3 Experimental Design and Statistical Analysis

In this section, the Response Surface Methodology (RSM) was used to analyze the influence of activation temperature (T) and KOH weight ratio (W) on the surface area and pore volume of synthesized activated carbons. The Analysis of variance (ANOVA) was carried out to determine the significance of each of the factors analyzed. The quadratic model developed to correlate T and W with the surface area and pore volume of the activated carbon samples is discussed below. The desirability function used to determine the optimal parameter for maximizing the responses (surface area and pore volume) is also discussed.

4.3.1 Response Analysis of synthesized activated carbon samples from Sample A

The surface area and pore volume of the activated carbon samples synthesized from Sample A are shown in Table 4.2.

Table 4.2 Results from Synthesis of Activated Carbon Samples from Sample A

Run Order	Factor 1	Factor 2	Response 1	Response 2
	T (^oC)	W	Surface Area (m^2/g)	Pore Volume (cm^3/g)
1	400	1	294	0.226
2	600	1	448	0.414
3	600	2.5	628	0.560
4	800	2.5	1535	1.103
5	600	2.5	588	0.512
6	600	4	880	0.785
7	400	2.5	471	0.295
8	800	4	1925	1.290
9	800	1	1359	0.958
10	600	2.5	662	0.582
11	400	4	626	0.482
12	600	2.5	667	0.586
13	600	2.5	665	0.586

T – Activation Temperature; W – KOH weight ratio

The effect of temperature and KOH weight ratio on the surface area and pore volume of the activated carbon produced in this study are illustrated in Table 4.2. It can be observed in Table 4.2 that as the temperature and KOH weight ratio increases, the surface area and pore volume of all the activated carbon synthesized from sample A increases. The increase in the sample pore volume and surface area is due to the increase in the reaction temperature and quantity of KOH utilized. In addition, the extent of reaction between the carbon in the coal and the KOH also lead to the opening of more pores and widening thus increasing the pore volume (Linares-Solano *et al.*, 2012).

The effect of KOH on pore formation can be attributed to micropore formation and pore widening mechanisms (Rodriguez-Reinoso and Molina-Sabio, 1992). At a low KOH weight ratio, micropore formation becomes the dominant mechanism, but as the KOH weight ratio increases, pore widening becomes increasingly dominant leading to the formation of mesopores. Therefore, the formation of mesopores, as well as total pore volume, increases as the KOH weight ratio increases. An increase in the KOH weight ratio from 1 to 4 increases the

surface area and pore volume of the synthesized activated carbon produced in this study at an average of 84% and 79%, respectively at the different temperatures. An increase in the KOH weight ratio also shows an increase in the surface area and pore volume simultaneously. This result is similar to that obatined by Lozano-Castello *et al.* (2001), Lillo-Ródenas *et al.* (2007), Linares-Solano *et al.* (2007) and Linares-Solano *et al.* (2008).

According to Table 4.2, it can be seen that as the temperature increases from 400 to 800 ^{o}C, a substantial increase in the surface area and pore volume of the activated carbon samples produced at different KOH weight ratios increases at an average of 265% and 255%, respectively. The highest surface area of 1925 m^2/g and pore volume of 1.290 cm^3/g was obtained at a temperature of 800 ^{o}C and KOH weight ratio of 4 for coal sample A

The result from the analysis of variance (ANOVA) for sample A based on the experimental variables applied in this study is depicted in Table 4.3. The F-value and P-value are key indicators of the significance and suitability of the selected quadratic model (Hou *et al.*, 2013, Abdalla *et al.*, 2019). The surface area and pore volume have an F-value of 390.03 and 248.42, respectively and P-value of less than 0.05. This demonstrates that the model is appropriate and fits the experimental data. The lack of fit values for surface area and pore volume, can be seen in Table 4.3, as 0.3338 and 0.5444, respectively. This lack-of-fit can be considered insignificant with a P-value > 0.10 (Stat-Ease, 2018).

The surface area and pore volume have a high R^2 value of 0.9964 and 0.9944, respectively, which is close to 1 and is desirable. The Adj. R^2 of 0.9939 and 0.9904 is in reasonable agreement with the Pred. R^2 of 0.9789 and 0.9732 for surface area and pore volume respectively. The difference between the Adj. R^2 and Pred. R^2 should be less than 0.20 for them to be in reasonable agreement (Kraber, 2013). From Table 4.3, the difference between the Adj. R^2 and Pred. R^2 is 0.015 and 0.017 for surface area and pore volume, respectively. Adequate precision compares the predicted values at the design point to the average prediction error and a value greater than 4 is expected for the model to be suitable and to have adequate precision (Kraber, 2013). The adequate precision for surface area and pore volume is 62.125 and 53.31, respectively. The P-value shows that the parameters, T and W are significant factors that influence the surface area and pore volume of the activated carbon samples. A quadratic equation as presented in Eq. 4.1 to 4.4 is the selected model used to evaluate the effect of T and W on the responses (surface area and pore volume). The model equation is expressed in terms of coded factors and actual factors.

Coded factor:

Surface area = $638.4 + 571.31T + 221.68W + 58.67TW + 373.66T^2 + 34.59W^2$ (4.1)

Pore volume = $0.56 + 0.39T + 0.16W + 0.14T^2 - 0.037W^2$ (4.2)

Actual factor:

Surface area = $2307.32 - 8.84T + 46.4W + 0.1956TW + (9.34\times10^{-3}\times T^2) + 15.4W^2$ (4.3)

Pore volume = $0.4559 – (2.14\times10^{-3}\times T) + 0.0242W + (3.41\times10^{-6}\times T^2) - 0.0165W^2$ (4.4)

Table 4.3 ANOVA Results for surface area and pore volume of the synthesized activated carbon samples from Sample A

Source	Sum of squares		DOF		Mean square		F-value		P-value		Remark
	SA	PV	SA	PV	SA	PV	SA	PV	SA	PV	
Model	2.754E+006	1.15	5	5	5.508E+005	0.23	390.03	248.42	< 0.0001	< 0.0001	Sig.
T	1.958E+006	0.92	1	1	1.958E+006	0.92	1386.88	991.84	< 0.0001	< 0.0001	
W	2.949E+005	0.15	1	1	2.949E+005	0.15	208.82	165.46	< 0.0001	< 0.0001	
T×W	13767.50	1.444E-003	1	1	13767.50	1.444E-003	9.75	1.56	0.0168	0.2520	
T^2	3.856E+005	0.051	1	1	3.856E+005	0.051	273.08	55.59	< 0.0001	0.0001	
W^2	3303.91	3.792E-003	1	1	3303.91	3.792E-003	2.34	4.09	0.1700	0.0828	
Residual	9884.52	6.485E-003	7	7	1412.07	9.264E-004					
Lack-of-fit	5218.52	2.480E-003	3	3	1739.51	8.267E-004	1.49	0.83	0.3448	0.5444	Not Sig.
Pure error	4666.00	4.005E-003	4	4	1166.50	1.001E-003					
Cor. Total	2.764E+006	1.16	12	12							
R^2	0.9964	0.9944									
Adj. R^2	0.9939	0.9904									
Pred. R^2	0.9789	0.9732									
Adeq. Prec.	62.125	53.310									

SA: surface area; PV: pore volume; DOF: degree of freedom; T: activation temperature; W: KOH/sample B weight ratio; Cor. Total: Total sum of squares corrected for the mean; R^2: correlation coefficient; Adj: adjusted; pred: predicted; sig: significant; and Adeq Prec: Adequate Precision.

Table 4.4 shows the predicted values as compared with the experimental values which are the actual measured response against the values predicted by the model. A good correlation is observed between the model's predictions and the actual values. The difference observed between the predicted and actual values is within the acceptable limit which confirms that the regression model for the two responses, surface area, and pore volume provides a good fit.

Table 4.4 Experimental values vs Predicted values of the Surface area and Pore volume of Activated Carbon Samples from Sample A

Run Order	**Actual Value**	**Predicted Value**	**Actual Value**	**Predicted Value**
	Surface Area (m^2/g)		Pore Volume (cm^3/g)	
1	294.28	312.32	0.23	0.19
2	448.00	451.31	0.41	0.44
3	628.00	638.40	0.56	0.56
4	1535.00	1583.37	1.10	1.09
5	588.00	638.40	0.51	0.56
6	880.00	894.68	0.79	0.76
7	471.14	440.75	0.29	0.31
8	1925.34	1898.31	1.29	1.29
9	1358.95	1337.61	0.96	0.97
10	662.00	638.40	0.58	0.56
11	626.00	638.35	0.48	0.51
12	667.00	638.40	0.59	0.56
13	665.00	638.40	0.59	0.56

Fig. 4.1 shows the normal probability plot of residuals of the two responses (surface area and pore volume). The normal probability plot establishes if the residuals follow a normal distribution. The residuals measure the deviations of the predictions from the actual values of the responses. The normal probability plot of residuals is used to confirm the normality assumption of the ANOVA analysis. The assumption is affirmed if the residuals follow a straight line and do not have a definite pattern like an S shape. According to Fig 4.1, the plot is normal and is in line with the plot reported by Kraber (2013). In addition, the model was observed to provide a good approximation of the actual values of the responses as shown in Fig. 4.1. The normal probability plot of the residuals is approximately linear, an indication that the error terms are normally distributed.

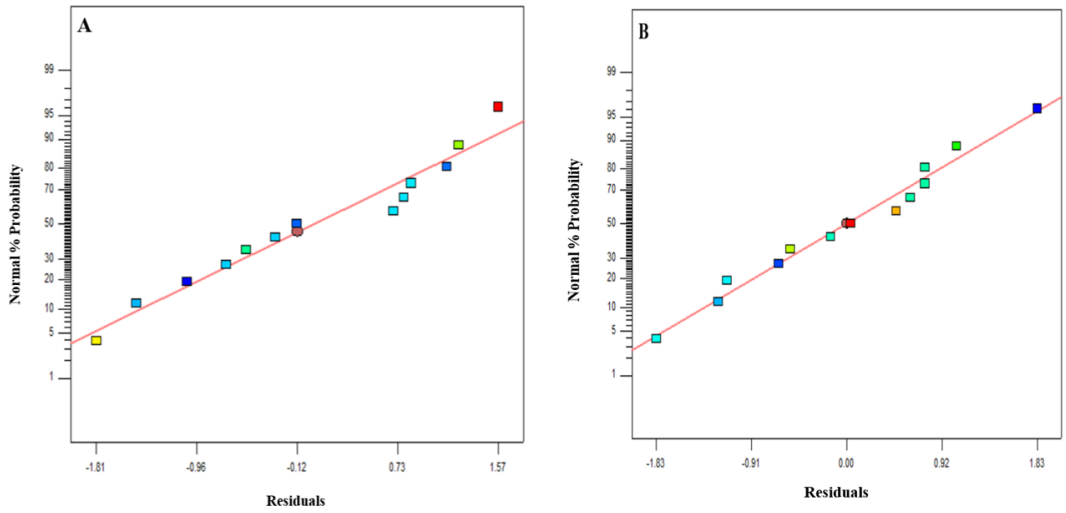


Figure 4.1 Normal probability plot of residuals of (A) surface area and (B) pore volume

Fig. 4.2 below shows the residuals vs. predicted plot of the responses. This plot is used to confirm the constant variance assumption of the ANOVA analysis (Kraber, 2013). For the assumption to be valid, all points are expected to be within the limits depicted with a red line in Fig. 4.2. It can be observed that all the data points are within the limits which validate the assumption of constant variance in the ANOVA analysis of the responses data.

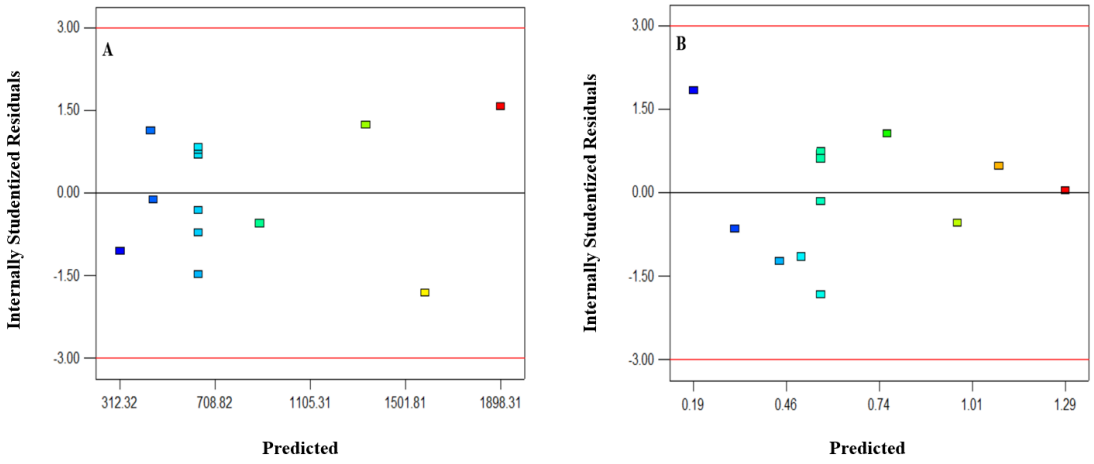


Figure 4.2 Residuals vs Predicted plot of (A) surface area and (B) pore volume

Fig. 4.3 shows the predicted vs. actual plot. The plot is used to check the model accuracy. The more data points close to the straight line indicates the precision of the model. Data points clustered above the straight line is an indication of the model over prediction, while the cluster of data points below the straight line is an indication of the model underprediction (Kraber,

2013). The data points as shown in Fig. 4.3 are close to the straight line, while other points are on the straight line. Fig. 4.3 shows a plot expected of a model that provides a good fit.

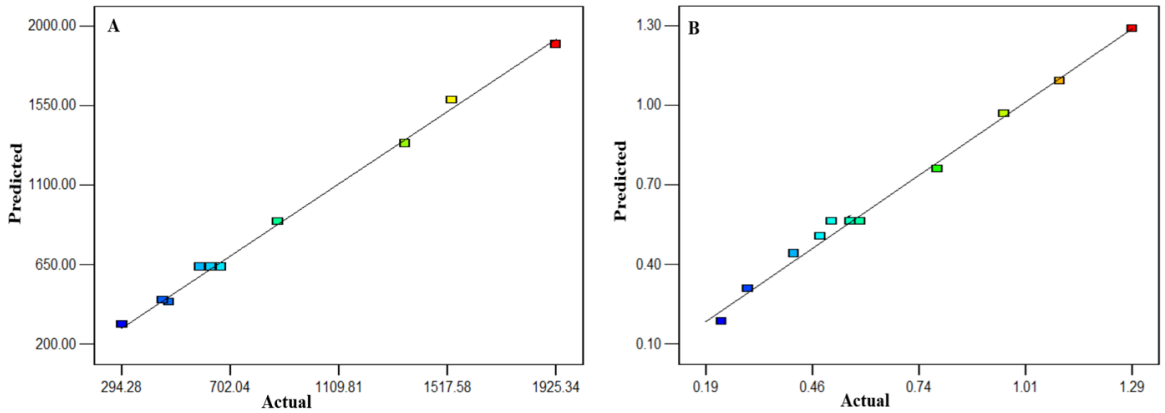


Figure 4.3 Predicted vs Actual plot of (A) surface area and (B) pore volume

The influence of changing levels of the two factors (T and W) on the surface area and pore volume of the activated carbon samples can be observed in the 3D surface plots (Fig. 4.4). This 3D plot, as reported by Bezener, (2015) is used in checking model accuracy. According to Fig. 4.4, the curve is seen to fit well with the design points which are the actual observed points. None of the design points is seen to be way above or below the curve, an indication of the accuracy of the model. The 3D plot also shows the effect of temperature and weight ratio on the surface area and pore volume of the activated carbons from sample A. An increase in temperature and weight ratio showed a corresponding increase in surface area and pore volume.

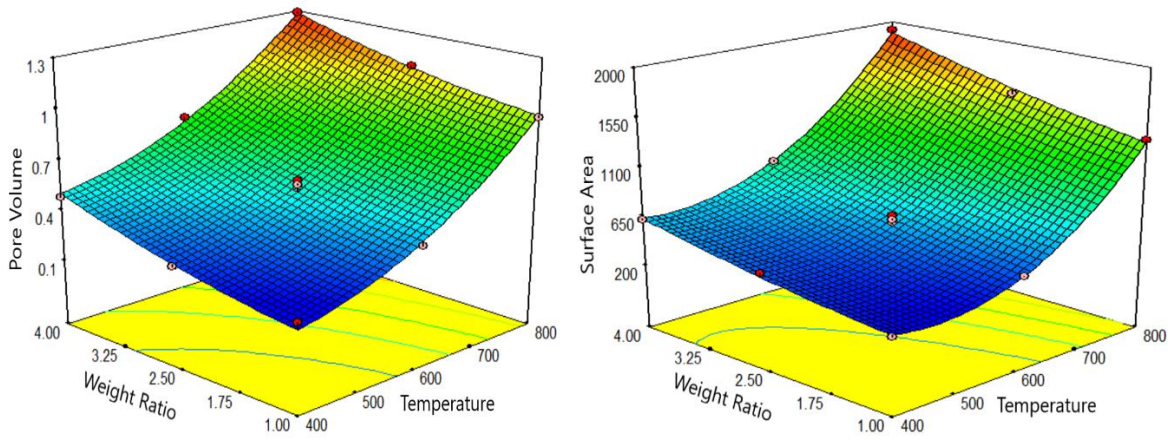


Figure 4.4 3D surface plots showing the influence of temperature and weight ratio on (A) surface area and (B) pore volume

To obtain the optimum conditions of the factors (T and W), a desirability function was used to maximize the surface area and pore volume. Table 4.5 lists the parameter setting for the desired target response.

Table 4.5 Optimum conditions setting for optimized response

Constraints	Goal	Lower Limit	Upper limit
Temperature (T)	Is in range	400	800
Weight Ratio (W)	Is in range	1	4
Surface area	Maximize	294.28	1925.34
Pore volume	Maximize	0.226	1.290

The objective criteria are maximized surface area and pore volume. In applying the desirability function, the condition that gave the maximum desirability factor was taken as the optimum condition (Gopalakannan and Senthilvelan, 2013). Table 4.6 presents the optimum solutions, with solution 1 selected, having the highest desirability value of 0.991. The highest possible surface area and pore volume were predicted in this region. The optimum condition for the factors or process conditions corresponds to a temperature of 800 ^{o}C and a KOH weight ratio of 4.

Table 4.6 Optimized Solutions

Solution	Temperature (^{o}C)	Weight ratio	Surface area (m^2/g)	Pore volume (cm^3/g)	Desirability	Remark
1	800	4	1898.31	1.289	0.991	selected
2	797.46	4	1880.9	1.281	0.982	
3	800	3.86	1865	1.267	0.971	
4	791.73	4	1841.97	1.262	0.961	

Fig. 4.5 shows the desirability plot and that of the responses. The plot shows the predicted values after optimization of 1898.31 m^2/g and 1.289 cm^3/g for surface area and pore volume respectively. The optimized results are in good agreement with the experimental measurement, with an error percentage of 1.4% and 0.08% for surface area and pore volume respectively as calculated using Eq. 4.5:

$$\text{Percentage of absolute error (POAE)} = \frac{\text{Experimental - Predicted}}{\text{Experimental}} \times 100 \quad (4.5)$$

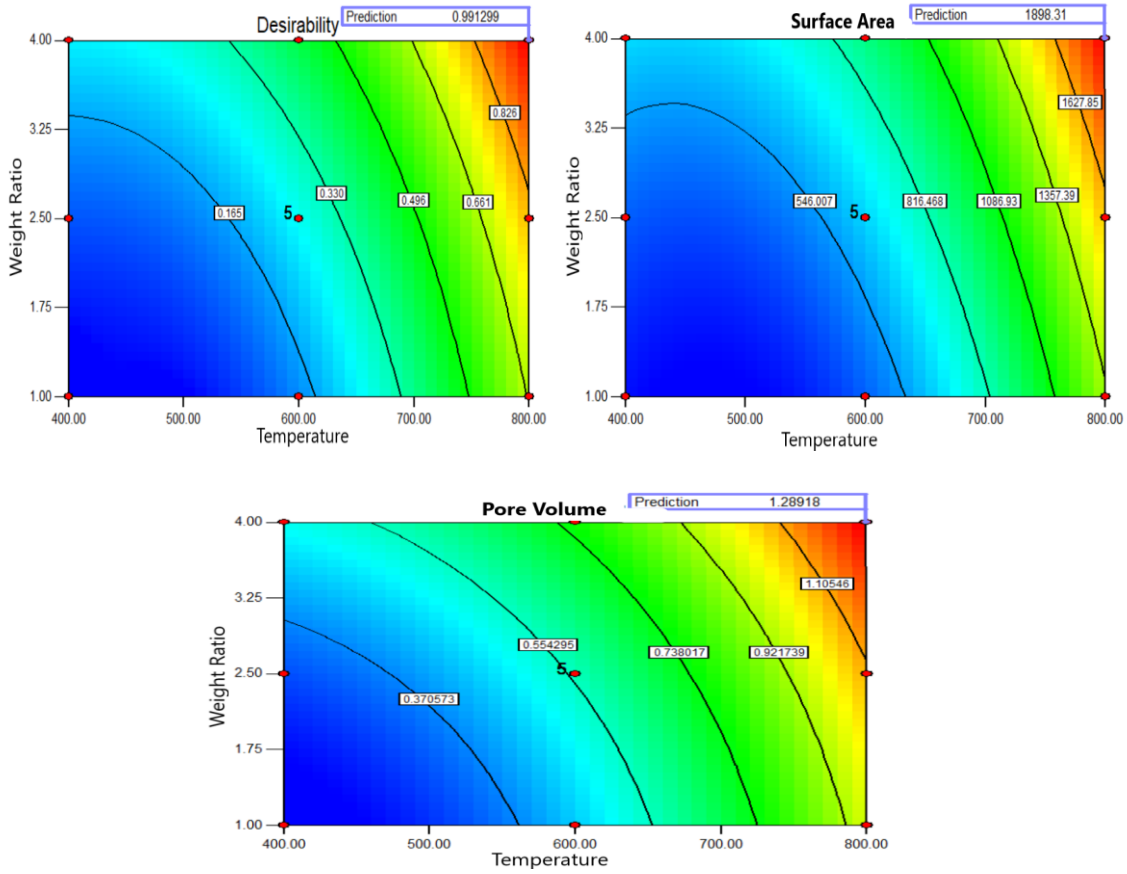


Figure 4.5 Contour plot of desirability and responses

4.3.2 Response Analysis of synthesized activated carbon samples from Sample B

The influence of two factors (T and W) on the responses (surface area and pore volume) of the synthesized activated carbon samples from sample B (coal discard) are analysed in this section. Table 4.7 shows the results from the synthesis of activated carbon samples from coal sample B.

Table 4.7 Results from Synthesis of Activated Carbon Samples from Sample B

Run Order	**Factor 1**	**Factor 2**	**Response 1**	**Response 2**
	T (^oC)	W	Surface Area (m^2/g)	Pore Volume (cm^3/g)
1	400	1	143.84	0.220
2	600	1	275.15	0.360
3	600	2.5	471.86	0.655
4	800	2.5	1374.20	1.037
5	600	2.5	356.31	0.586
6	600	4	671.68	0.698
7	400	2.5	161.54	0.280
8	800	4	1826.41	1.252
9	800	1	1216.36	0.765
10	600	2.5	463.67	0.612
11	400	4	258	0.440
12	600	2.5	366.54	0.632
13	600	2.5	453.14	0.568

As previously reported for Sample A, an increase in temperature and KOH weight ratio increases the surface area and pore volume of all activated carbon samples synthesized from sample B. This is also attributed to the extent of reaction between the carbon in sample B and KOH. An increase in the KOH weight ratio from 1 to 4 increases the surface area and pore volume by an average of 86% and 91%, respectively under different temperatures. Increasing the temperature from 400 to 800 ^oC also lead to the increase in the surface area and pore volume by an average of 702% and 234%, respectively for all the activated carbon samples at different KOH weight ratios. The highest surface area and pore volume of 1826.41 m^2/g and pore volume of 1.252 cm^3/g were obtained at a temperature of 800 ^oC and KOH weight ratio of 4:1.

The results from the analysis of variance ANOVA are presented in Table 4.8. The surface area and pore volume of the samples was seen with an F-value of 252.41 and 105.35, respectively and prob.>F-value less than 0.05. This shows that the model is suitable and provides a good fit for the experimental data. The lack-of-fit P-value obtained was 0.6574 and 0.2302 for the surface area and pore volume, respectively. These values are higher than the expected lack-of-fit P-value which should be insignificant at P-value > 0.10 (Stat-Ease, 2018). The surface area

and pore volume have an R^2 value of 0.9945 and 0.986, respectively. The Adj. R^2 of 0.9905 and 0.9775 is in reasonable agreement with the Pred. R^2 of 0.9786 and 0.9298 for surface area and pore volume, respectively. Adequate precision is 48.277 and 36.152 for surface area and pore volume, respectively. These values are greater than 4 that is expected for the model to be suitable and to have adequate precision (Kraber, 2013).

The selected model applied to assess the effect of the two factors (T and W) on the responses (surface area and pore volume) is a quadratic equation as presented in Eq. 4.6 – 4.9. The model equation is expressed in terms of coded factors and actual factors.

Coded factor:

$$\text{Surface area} = 416.49 + 642.27T + 186.79W + 123.97TW + 365.92T^2 + 71.47W^2 \quad (4.6)$$

$$\text{Pore volume} = 0.60 + 0.35T + 0.17W + 0.067TW + 0.092T^2 - 0.037W^2 \quad (4.7)$$

Actual factor:

$$\text{Surface area} = 2290.09 - 8.80T - 282W + 0.41TW + (9.2\times10^{-3}\times T^2) + 31.76W^2 \quad (4.8)$$

$$\text{Pore volume} = 0.3139 - (1.57\times10^{-3}\times T) + 0.07W + (2.23\times10^{-4}\times T\times W) + (2.31\times10^{-6}\times T^2) - 0.02W^2 \quad (4.9)$$

Table 4.8 ANOVA Results for surface area and pore volume of the synthesized activated carbon samples from Sample B

Source	Sum of squares		DOF		Mean square		F-value		P-value		Remark
	SA	PV	SA	PV	SA	PV	SA	PV	SA	PV	
Model	3.259E+006	0.97	5	5	6.519E+005	0.19	252.41	105.35	< 0.0001	< 0.0001	Sig.
T	2.475E+006	0.74	1	1	2.475E+006	0.74	958.35	405.21	< 0.0001	< 0.0001	
W	2.093E+005	0.18	1	1	2.093E+005	0.18	81.06	99.01	< 0.0001	< 0.0001	
T×W	61476.72	0.018	1	1	61476.72	0.018	23.8	9.70	0.0018	0.0170	
T^2	3.698E+005	0.024	1	1	3.698E+005	0.024	143.20	12.85	< 0.0001	0.0089	
W^2	14107.57	3.785E-003	1	1	14107.57	3.785E-003	5.46	2.06	0.0521	0.1945	
Residual	18078.14	0.013	7	7	2582.59	1.838E-003					
Lack-of-fit	5495.51	8.016E-003	3	3	1831.84	2.672E-003	0.58	2.20	0.6574	0.2302	Not Sig.
Pure error	12582.63	4.851E-003	4	4	3145.66	1.213E-003					
Cor. Total	3.277E+006	0.98	12	12							
R^2	0.9945	0.9869									
Adj. R^2	0.9905	0.9775									
Pred. R^2	0.9786	0.9298									
Adeq. Prec.	48.277	36.152									

Table 4.9 shows the predicted values of the model compared to the experimental values. As shown in Table 4.9, there is a satisfactory correlation between the predictions of the model and the actual values.

Table 4.9 Experimental values vs Predicted values of the Surface area and Pore volume of Activated Carbon Samples from Sample B

Run Order	Actual Value	Predicted Value	Actual Value	Predicted Value
	Surface Area (m^2/g)		Pore Volume (cm^3/g)	
1	143.84	148.80	0.22	0.19
2	275.15	301.17	0.36	0.39
3	471.86	416.49	0.66	0.60
4	1374.20	1424.68	1.04	1.04
5	356.31	416.49	0.59	0.60
6	671.68	674.75	0.70	0.74
7	161.54	140.15	0.28	0.34
8	1826.41	1806.91	1.25	1.25
9	1216.36	1185.38	0.77	0.76
10	463.67	416.49	0.61	0.60
11	258.00	274.43	0.44	0.41
12	366.54	416.49	0.63	0.60
13	453.14	416.49	0.57	0.60

Fig. 4.6 shows the normal probability plot of residuals of surface area and pore volume of activated carbon samples from sample B. The plot is almost a straight line, an indication that the error terms are normally distributed.

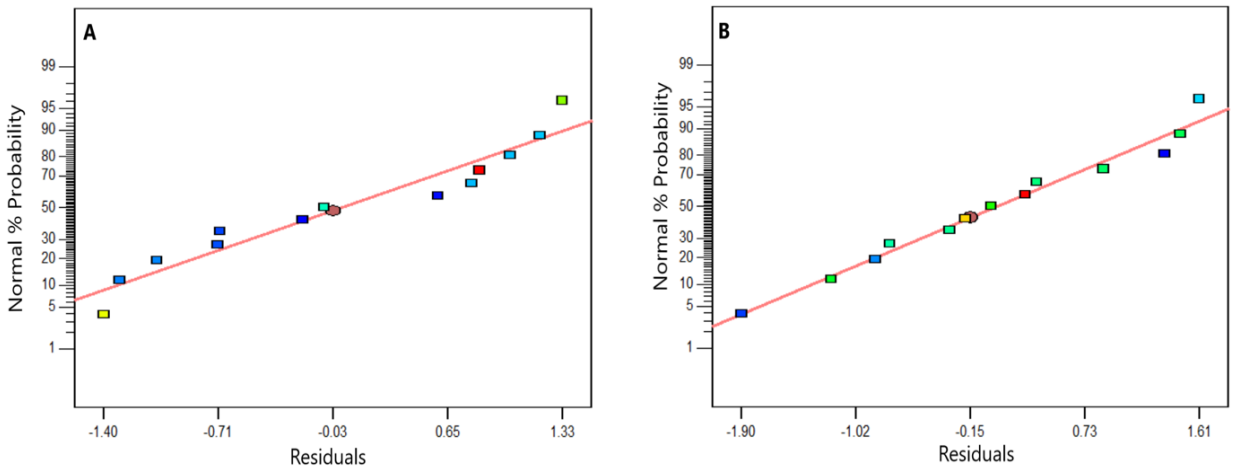


Figure 4.6 Normal probability plot of residuals of (A) surface area and (B) pore volume

Fig. 4.7 shows the residuals vs predicted plot of the responses for activated carbon samples from Sample B. This plot also confirms the validity of the assumption used in the ANOVA analysis, as all data points are within the expected limit.

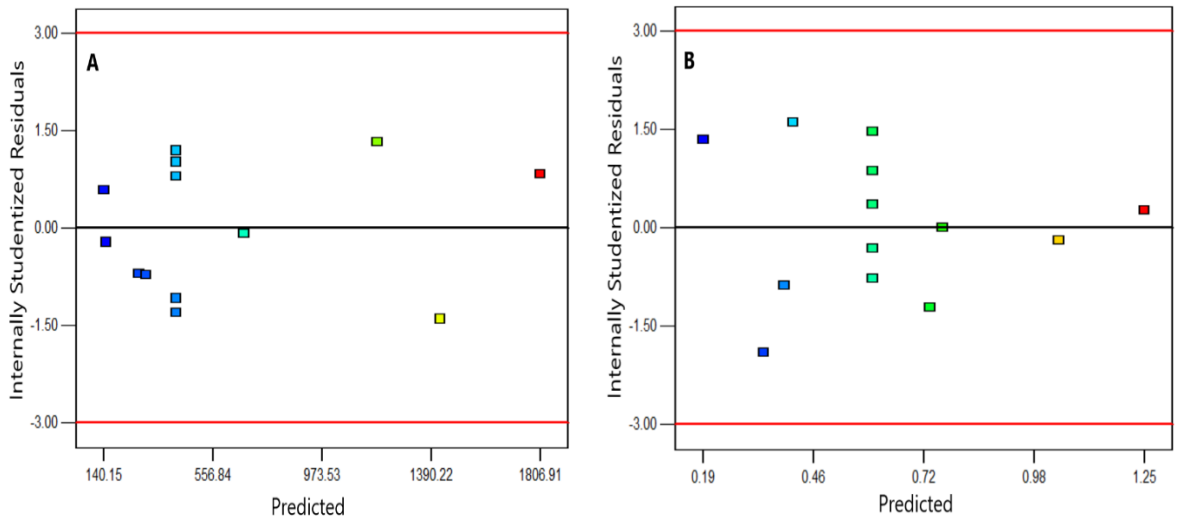


Figure 4.7 Residuals vs Predicted plot of (A) surface area and (B) pore volume

Fig. 4.8 shows the predicted vs actual plot of the responses of the activated carbon samples from sample B. The plot also confirms the model's validity as the data points are as close as expected to the straight line.

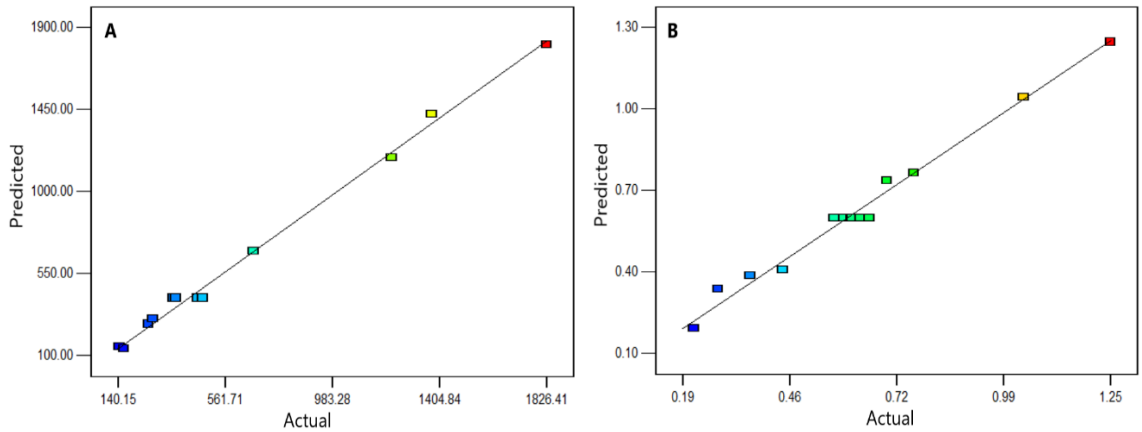


Figure 4.8 Predicted vs Actual plot of (A) surface area and (B) pore volume

Fig. 4.9 shows the 3D surface plots of the responses and how the data points fit with the curve. The curve is seen to fit well with the design points. None of the design points is seen to be way above or below the curve, an indication of the accuracy of the model. The 3D plot also shows the linear relationship between the two factors and the responses, similar to what was observed for activated carbons from sample A.

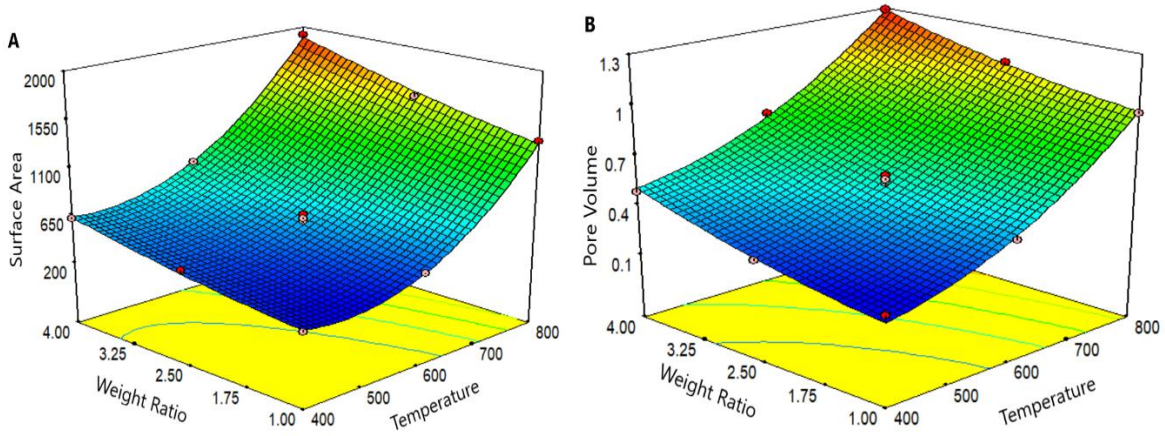


Figure 4.9 3D surface plots of (A) surface area and (B) pore volume

Table 4.10 shows the parameter settings used to obtain the optimum condition of the process parameters using the desirability function.

Table 4.10 Optimum conditions setting for optimized response

Constraints	Goal	Lower Limit	Upper limit
Temperature (T)	Is in range	400	800
Weight Ratio (W)	Is in range	1	4
Surface area	Maximize	143.84	1826.41
Pore volume	Maximize	0.22	1.252

The objective is to maximize the surface area and pore volume. Three solutions were obtained with solution 1 selected as the most desirable having desirability of 0.992 as shown in Table 4.11. The optimum process conditions are also equivalent to a temperature of 800 ^{o}C and a weight ratio of 4.

Table 4.11 Optimized Solutions

Solution	Temperature (°C)	Weight ratio	Surface area (m^2/g)	Pore volume (cm^3/g)	Desirability	Remark
1	800	4	1806.91	1.247	0.992	selected
2	795.57	4	1773.91	1.233	0.975	
3	800	3.81	1749.43	1.224	0.964	

Fig. 4.10 shows the contour plot of the desirability function and that of the responses. The plot shows the predicted values after optimization of 1806.91 m^2/g and 1.247 cm^3/g for surface area and pore volume respectively. The results are close to the experimental results, with an error percentage for surface area and pore volume of 1.07% and 0.4% respectively.

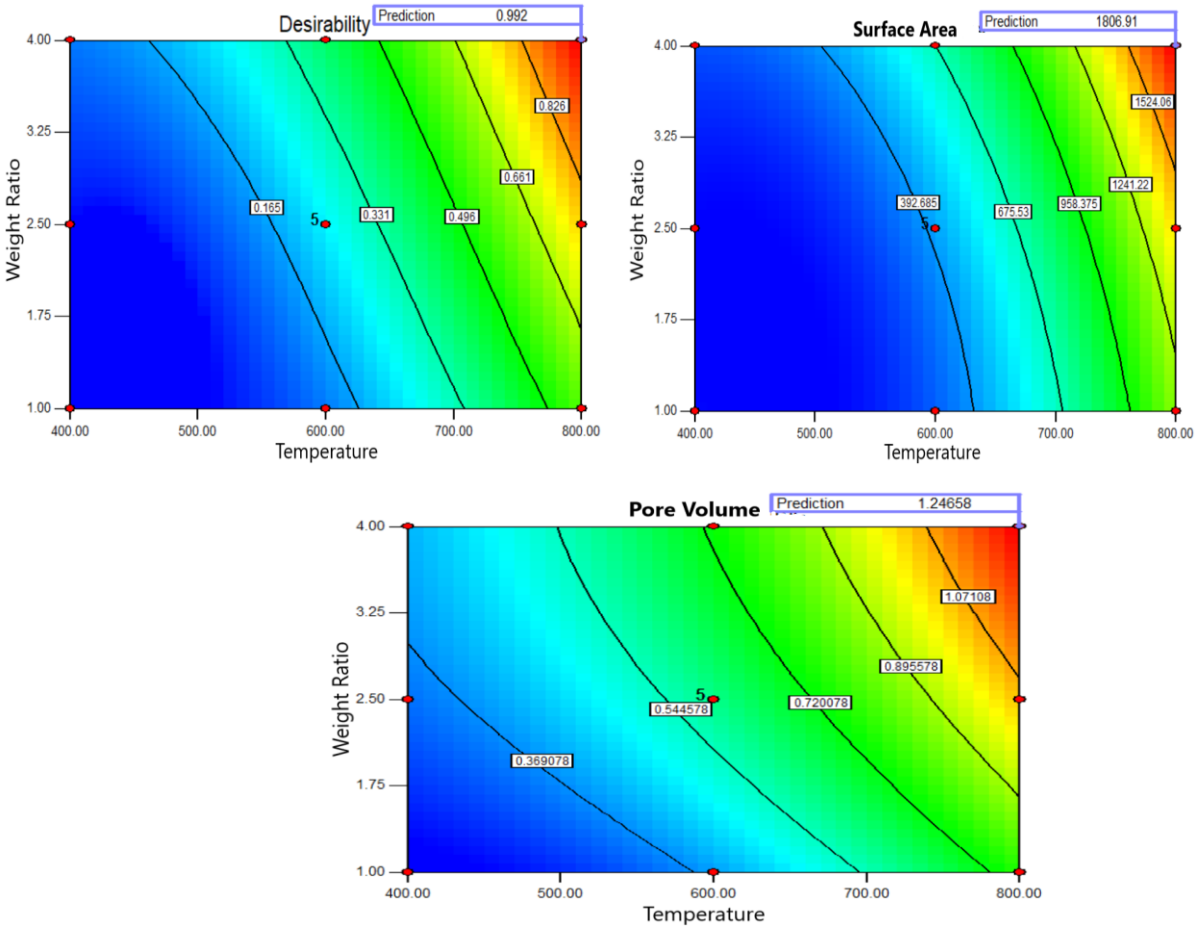


Figure 4.10 Contour plot of desirability and responses

4.3.3 Response Analysis of synthesized activated carbon samples from Sample C

Table 4.12 shows the results of the synthesis of activated carbon samples from sample C.

Table 4.12 Results from Synthesis of Activated Carbon Samples from Sample C

Run Order	Factor 1	Factor 2	Response 1	Response 2
	T (^oC)	W	Surface Area (m^2/g)	Pore Volume (cm^3/g)
1	400	1	115.72	0.105
2	600	1	298.9	0.268
3	600	2.5	415.63	0.288
4	800	2.5	1268.1	0.988
5	600	2.5	468.32	0.355
6	600	4	662.52	0.481
7	400	2.5	227.14	0.223
8	800	4	1484.96	1.042
9	800	1	1131.24	0.82
10	600	2.5	463	0.355
11	400	4	268	0.265
12	600	2.5	467.12	0.355
13	600	2.5	465.76	0.355

It is evident from the results that, with an increase in temperature and KOH weight ratio, surface area and pore volume increased as similarly reported for Sample A and Sample B activated carbon samples. An increase in the KOH weight ratio from 1 to 4 increases the surface area and pore volume at different temperatures by an average of 95% and 86%, respectively. Temperature increase from 400 to 800 ^oC increases the surface area and pore volume of the activated carbon samples by an average of 597% and 439%, respectively. The highest surface area and pore volume of 1484.96 m^2/g and 1.042 cm^3/g were obtained at a temperature of 800 ^oC and a KOH weight ratio of 4.

From the result of the ANOVA as presented in Table 4.13, the surface area and pore volume have an F-value of 366.15 and 179.73, and a P-value of less than 0.05. An indication that the model is a good fit for the experimental data. In addition, the R^2 value of 0.9962 and 0.9923 for surface area and pore volume respectively confirm a very good regression. The Adj. R^2

value of 0.9935 and 0.9867 is in reasonable agreement with the Pred. R^2 value of 0.9699 and 0.9643 for the surface area and pore volume. The difference between the Adj. R^2 and Pred. R^2 is 0.024 and 0.022 for surface area and pore volume. The adequate precision for surface area and pore volume is 58.812 and 40.563.

The equations as shown in Eq. 4.10 to 4.13 is the selected model equation used to evaluate the impact of the two factors (T and W) on the surface area and pore volume.
Coded factor:

$$\text{Surface area} = 459.05 + 545.57T + 144.94W + 50.36TW + 280.85T^2 + 13.94W^2 \quad (4.10)$$

$$\text{Pore volume} = 0.35 + 0.38T + 0.099W + 0.015TW + 0.23T^2 - (5.91\times10^{-3}\times W^2) \quad (4.11)$$

Actual factor:

$$\text{Surface area} = 1398.92 - 6.13T - 435.07W + 0.1679TW + (7.02\times10^{-3}\times T^2) + 6.2W^2 \quad (4.12)$$

$$\text{Pore volume} = 1.1458 - (5\times10^{-3}\times T) + 0.0483W + (5.17\times10^{-5}\times TW) + (5.63\times10^{-6}\times T^2) - (2.63\times10^{-3}\times W^2) \quad (4.13)$$

Table 4.13 ANOVA Results for surface area and pore volume of the synthesized activated carbon samples from Sample C

Source	Sum of squares		DOF		Mean square		F-value		P-value		Remark
	SA	PV	SA	PV	SA	PV	SA	PV	SA	PV	
Model	2.187E+006	1.07	5	5	4.374E+005	0.21	366.15	179.73	< 0.0001	< 0.0001	Sig.
T	1.786E+006	0.85	1	1	1.786E+006	0.85	1494.85	713.37	< 0.0001	< 0.0001	
W	1.260E+005	0.059	1	1	1.260E+005	0.059	105.50	49.58	< 0.0001	0.0002	
T×W	10144.52	9.610E-004	1	1	10144.52	9.610E-004	8.49	0.81	0.0225	0.3987	
T^2	2.178E+005	0.14	1	1	2.178E+005	0.14	182.34	117.57	< 0.0001	< 0.0001	
W^2	536.54	9.659E-005	1	1	536.54	9.659E-005	0.45	0.081	0.5242	0.7840	
Residual	8362.93	8.331E-003	7	7	1194.70	1.190E-003					
Lack-of-fit	6313.50	4.740E-003	3	3	2104.50	1.580E-003	4.11	1.76	0.1029	0.2934	Not Sig.
Pure error	2049.43	3.591E-003	4	4	512.36	8.978E-004					
Cor. Total	2.196E+006	1.08	12	12							
R^2	0.9962	0.9923									
Adj. R^2	0.9935	0.9867									
Pred. R^2	0.9699	0.9643									
Adeq. Prec.	58.812	40.563									

Table 4.14 shows the model predicted values and the experimental values. The closeness of the predicted and experimental values confirms the suitability of the model.

Table 4.14 Experimental values vs Predicted values of the Surface area and Pore volume of Activated Carbon Samples from Sample C

Run Order	**Actual Value**	**Predicted Value**	**Actual Value**	**Predicted Value**
	Surface Area (m^2/g)		Pore Volume (cm^3/g)	
1	115.72	113.69	0.11	0.11
2	298.90	328.05	0.27	0.25
3	415.63	459.05	0.29	0.35
4	1268.10	1285.47	0.99	0.95
5	468.32	459.05	0.35	0.35
6	662.52	617.93	0.48	0.45
7	227.14	194.33	0.22	0.20
8	1484.96	1494.71	1.04	1.06
9	1131.24	1104.12	0.82	0.83
10	463.00	459.05	0.35	0.35
11	268.00	302.84	0.27	0.28
12	467.12	459.05	0.35	0.35
13	465.76	459.05	0.35	0.35

Fig. 4.11 shows the normal probability plot of residuals of surface area and pore volume of activated carbon samples from sample C. Most of the data points are on the straight line, an indication that residuals (deviations of predicted values from the experimental values) follow a normal distribution, thus confirming the validity of the model.

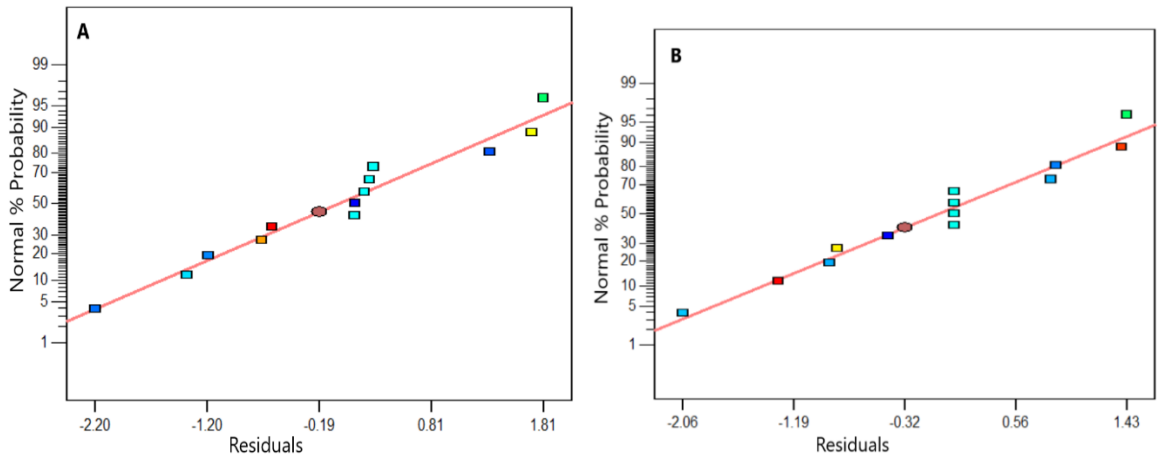


Figure 4.11 Normal probability plot of residuals of (A) surface area (B) pore volume

Fig. 4.12 shows the residuals vs predicted plot of the responses for activated carbon samples from Sample C. This plot also confirms the validity of the assumption used in the ANOVA analysis since all data points are within the expected limit.

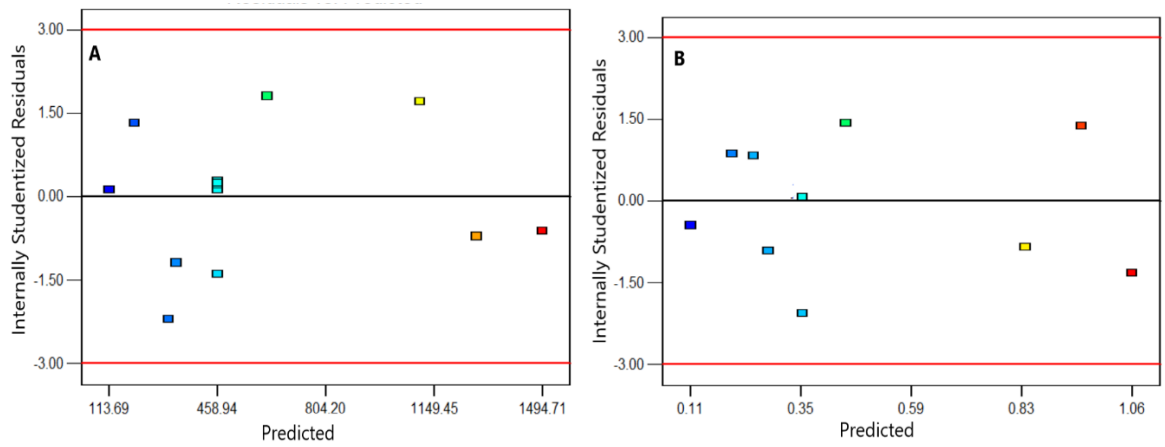


Figure 4.12 Residuals vs Predicted plot of (A) surface area and (B) pore volume

Fig. 4.13 shows predicted vs actual plot of activated carbon samples from sample C. The plot also proves the validity of the model as the data points are positioned as expected.

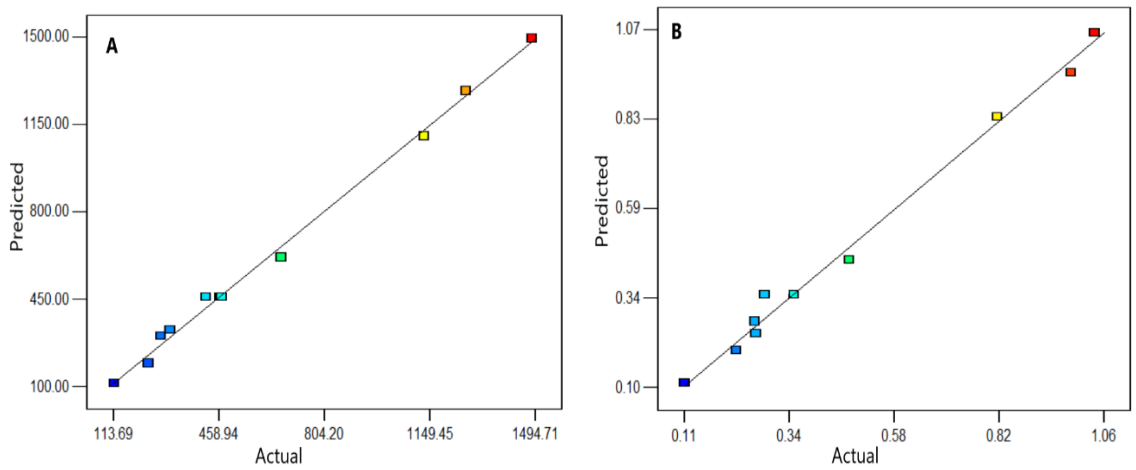


Figure 4.13 Predicted vs Actual plot of (A) surface area and (B) pore volume

The 3D surface plots are seen to fit well with the design points as shown in Fig. 4.14. The design points are seen to be well aligned with the curve, an indication of the accuracy of the model.

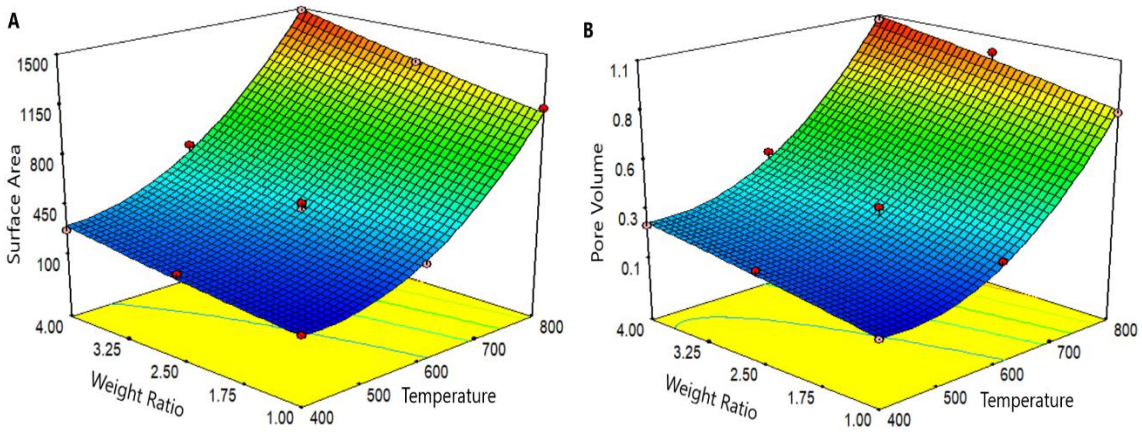


Figure 4.14 3D surface plots showing the influence of temperature and weight ratio on (A) surface area and (B) pore volume

Table 4.15 lists the parameter set used to obtain the optimum conditions of T and W.

Table 4. 15 Optimum conditions setting for optimized response

Constraints	Goal	Lower Limit	Upper limit
Temperature (T)	Is in range	400	800
Weight Ratio (W)	Is in range	1	4
Surface area	Maximize	115.72	1484.96
Pore volume	Maximize	0.105	1.042

The solutions of the optimization are presented in Table 4.16. The first solution with the highest surface area and pore volume is the most desirable. The optimum T and W were found to be 800 ^{o}C and 4 respectively.

Table 4.16 Optimized Solutions

Solution	Temperature (^{o}C)	Weight ratio	Surface area (m^2/g)	Pore volume (cm^3/g)	Desirability	Remark
1	800	4	1486.74	1.05833	1.000	selected
2	800	3.89	1478.41	1.05512	0.998	
3	800	3.81	1466.5	1.0495	0.993	
4	800	1.92	1211.78	0.908551	0.829	

Fig. 4.15 shows the desirability plot and that of the responses. The plot shows the predicted values after optimization to be 1486.74m^2/g and 1.058cm^3/g for surface area and pore volume respectively. This is close to the experimental values obtained at 800 ^{o}C and KOH weight ratio of 4. The percentage error is 0.12% and 1.5% for surface area and pore volume respectively.

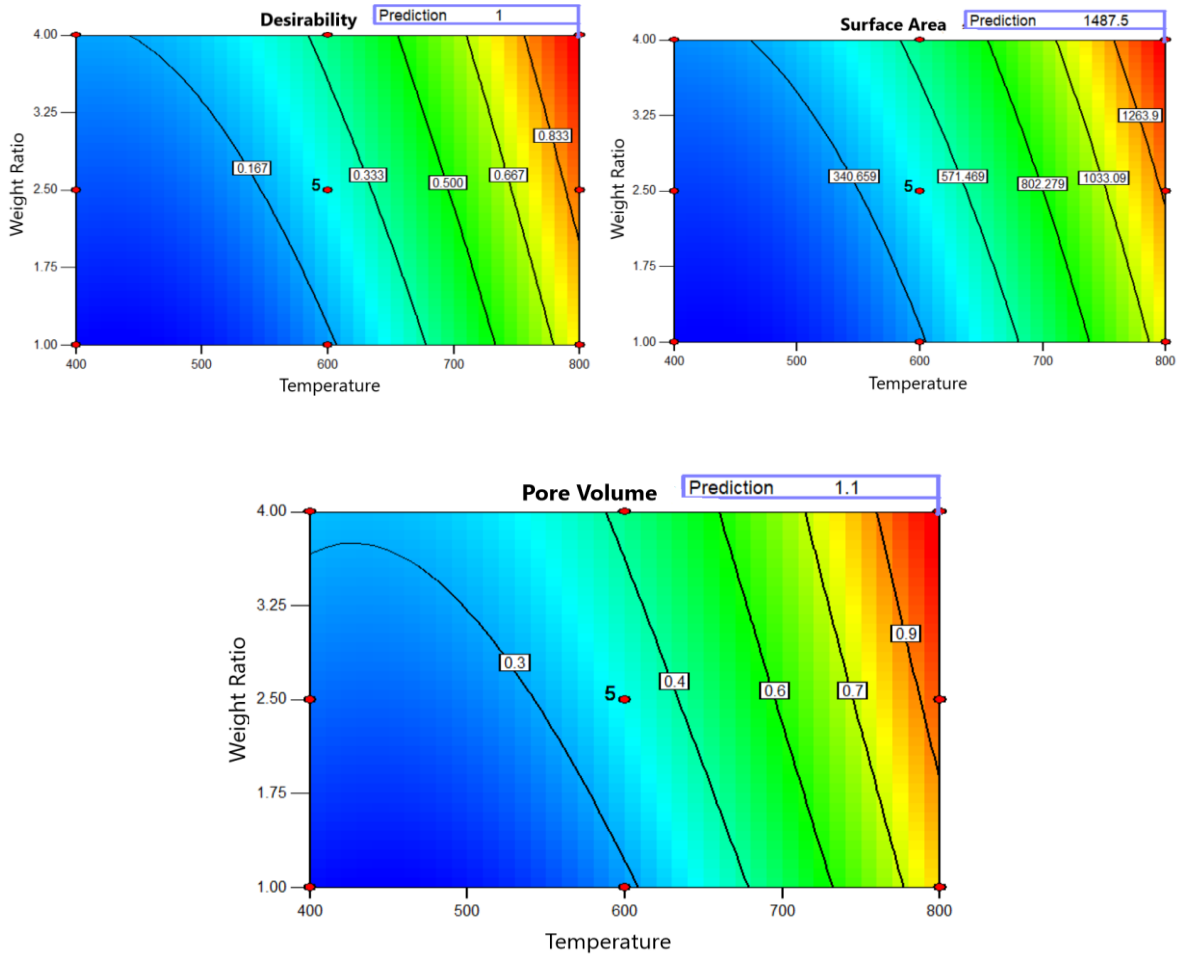


Figure 4.15 Contour plot of desirability and responses

4.4 Selecting activated carbon samples for further studies

Tables 4.2, 4.7 and 4.12 shows the surface area and pore volume of the activated carbon samples synthesized from the three coal waste samples examined in this study. It can be observed that activated carbon with the highest surface area and pore volume from each of these coal samples were obtained at a temperature of 800 ^{o}C and KOH weight ratio of 4. This is also in agreement with the predicted results from the RSM statistical analysis. The activated carbon samples obtained at these conditions are highly porous with a large surface area. A linear correlation has been reported to exist between the surface area and the adsorption capacity of activated carbon by Rodríguez-Reinoso *et al.* (2008), Alcañiz-Monge et al. (2009b), Sun *et al.* (2009) and Thu *et al.* (2014). The correlation states that the higher the surface area of an activated carbon sample, the higher its adsorption capacity.

4.5 Nitrogen Adsorption Analysis

The activated carbon samples with the highest surface area from each of the coal samples namely; activated carbon sample from coal sample A (ACR), coal sample B (ACD) and coal sample C (ACS) are used for the nitrogen adsorption analysis and subsequent tests. The results from nitrogen (N_2) adsorption at 77 K and density measurement of the activated carbon samples (ACR, ACD, ACS) are shown in Table 4.17. The surface areas, pore volumes and pore sizes of the activated carbon samples as determined by BET and BJH methods were observed to have an increasing order of ACR > ACD > ACS. The average pore diameter of the three samples was observed to be in the mesopore range (2 nm ≥ D_p ≤ 50 nm) (Sing *et al.*, 1985). The difference in the adsorption and desorption result from the BJH surface area values can be attributed to the fact that equilibrium may not have been attained during the adsorption process, but was attained during the desorption process. This is similar to the result reported by Şenel *et al.* (2001), and Thommes (2010). The densities of the activated carbons obtained in this study are ACR (2348.6 kg/m^3), ACD (2241.9 kg/m^3) and ACS (2491.4 kg/m^3). ACS with the lowest BET surface area has the largest density. ACD with the second-largest BET surface area has the lowest density, and ACR with the largest BET surface area has the second-largest density.

Table 4.17 Physical and structural properties of the activated carbon samples

Properties	**Method Used**	**ACR**	**ACD**	**ACS**
N_2 adsorption results				
BET surface area (m^2/g)	BET	1925.34	1826.41	1484.96
BET adsorption total pore volume (cm^3/g)	BET	1.290	1.252	1.042
BJH adsorption surface area (m^2/g)	BJH	1395.15	1265.24	924.48
BJH desorption surface area (m^2/g)	BJH	1605.46	1589.25	1013.50
BJH average pore diameter (4V/A) nm	BJH	2.90	2.66	2.51
Helium Pycnometer Measurement				
Skeletal (apparent) density (kg/m^3)	HP	2348.6	2241.9	2491.4

BET – Brunauer Emmet Teller; BJH - Barrett-Joyner-Halenda; HP – Helium Pycnometer

Nitrogen adsorption-desorption isotherms of the activated carbons are shown in Fig. 4.16 and were observed to be of type IV isotherm of the IUPAC classification (Thommes *et al.*, 2015). The isotherms are characterized by volumes adsorbed at lower P/P_o, followed by a knee

showing characteristic of micropore development of wide pore diameter, and a horizontal plateau. The knee is a result of steady pore filling, which is similar to the isotherm obtained by Zhao *et al.* (2011). Nitrogen uptake at low relative pressure and large uptake at higher relative pressure with a horizontal plateau provides a clear indication of a material with a combination of micro and mesopores (Hu *et al.*, 2000). The uptake at low relative pressure is on the account of increased adsorbent-adsorptive interactions in narrow micropores leading to the filling of micropores at a low relative pressure (Sing *et al.*, 1985). In addition, the hysteresis loop, which is an indication of the presence of mesopores was also observed. In a Type IV isotherm, such as shown in Fig. 4.16, hysteresis occurs just after capillary condensation. The occurrence of hysteresis is caused by the pore width exceeding a particular critical width. This critical width depends on the adsorption process and temperature (Blanco *et al.*, 2010, Sing *et al.*, 1985).

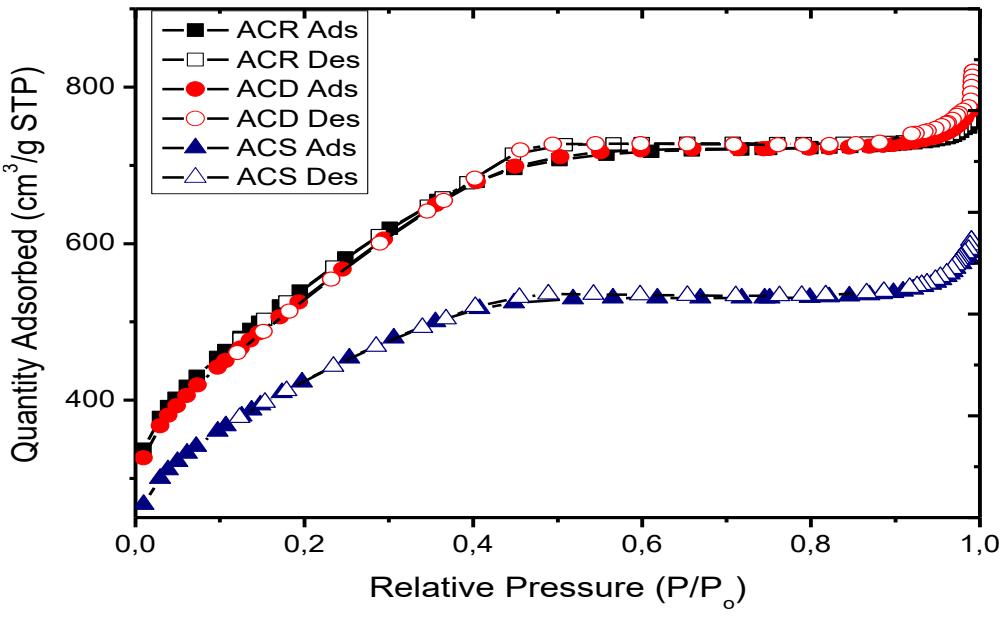


Figure 4.16 Nitrogen adsorption-desorption isotherms of synthesized activated carbons

The nitrogen adsorption capacity of activated carbons differs greatly. The BET surface area plots from which the activated carbons surface areas were evaluated are shown in Fig. 4.17.

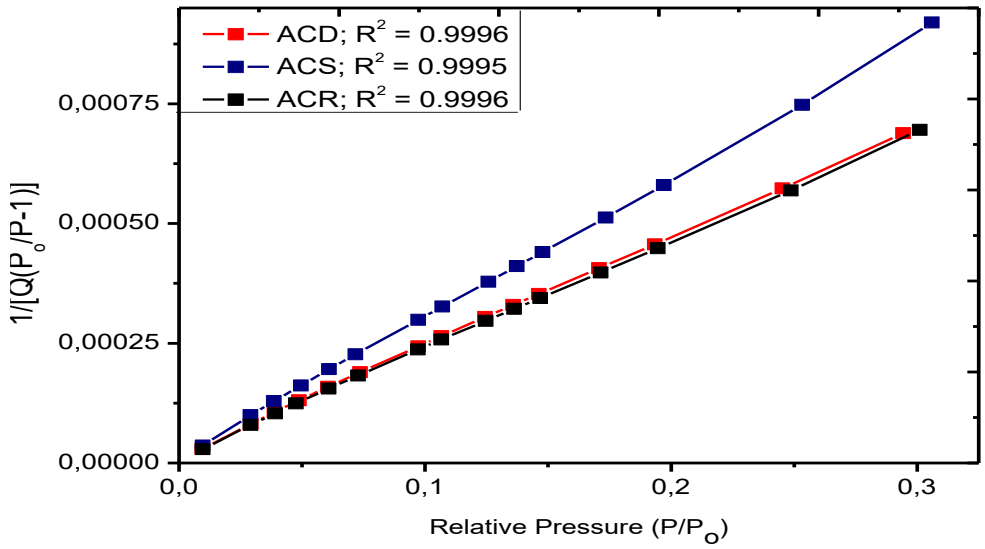


Figure 4.17 BET surface area plots of the synthesized activated carbons.

Nitrogen uptake data of the three activated carbons provide a correlation between surface area and the quantity of nitrogen adsorbed. It is observed that the nitrogen adsorption capacity of the activated carbons differs and corresponds to the surface area which seems to govern its adsorption capacity. The higher the surface area, the higher the adsorption capacity of the activated carbons. This is in agreement with the results reported by Panella *et al.* (2005) and Bénard and Chahine (2007). The studies revealed that, for several carbon materials, nitrogen adsorption capacity at 77 K corresponds with the surface area. Furthermore, Düren *et al.* (2004) applied computational methods to estimate adsorption capacity and surface areas of various carbon materials and found that the surface area is an important property of carbon materials that influences gas adsorption.

4.5.1 Pore Size Distribution (PSD)

The nitrogen isotherm of the selected activated carbon samples was used to obtain the PSDs of the activated carbon samples using the Non-Local Density Functional Theory (NLDFT) method as shown in Fig. 4.18. The NLDFT method was used to normalize the pore volume to the pore width interval (differential volume dV/dW, cm^3/Å/g) and using a standard slit-shaped pore model, the PSDs of the three activated carbons were obtained. The PSD analysis shows remarkable differences between the activated carbon samples. From Fig. 4.18, it can be observed that the activated carbon samples exhibit two peaks on the PSD curve presenting a bimodal distribution in the micropore region (≤ 2 nm) and mesopore (2 nm ≥ Pore radius ≤ 50

nm) region. The peak corresponds to pore width of 7.94 Å (0.794 nm), 7.76 Å (0.776 nm) and 7.92 Å (0.792 nm) for ACR, ACD and ACS respectively in the micropore region and 22.9 Å (2.29 nm), 23.1 Å (2.31 nm) and 20.6 Å (2.06 nm) for ACR, ACD and ACS, respectively in the mesopore region. The pore volume decreases evenly further past the micropore region and becomes negligible at pore width of 50 Å for ACR, 48 Å for ACD and 44.5 Å for ACS; points at which the pores have been fully filled with nitrogen.

For sample ACR, the peaks correspond to pore volume of 0.047 and 0.034 $cm^3/Å/g$ in micropore and mesopore region, respectively. In the case of Sample ACD, the peaks correspond to pore volume of 0.044 and 0.035 $cm^3/Å/g$ in micropore and mesopore region respectively. In the mesopore region, the pore volume is higher than sample ACR which indicates the presence of more mesopores in Sample ACD. However, the total pore volume of Sample ACD is lower than the sample ACR. For Sample ACS, the peaks correspond to pore volume of 0.039 $cm^3/Å/g$ within the micropore region and pore volume of 0.025 $cm^3/Å/g$ in the mesopore region.

The PSD profile confirms that the three samples are highly porous consisting of micropores and mesopores. This is consistent with the observation made from the nitrogen adsorption isotherm of the three samples. Sample ACR is observed to be highly microporous among the three samples having the highest pore volume within the micropore region. Sample ACD has a wider pore size distribution containing the most mesopores of the three samples. Sample ACS has the narrower pore size distribution among the three samples. By observing the physical and structural properties in Table 4.17, nitrogen adsorption isotherms of Fig. 4.16 and the PSD profiles of Fig. 4.18 for the three activated carbon samples, it is noted that nitrogen adsorption increases alongside an increase in microporosity and surface area. In addition, it can be inferred that sample ACR is the most porous with the largest surface area and highest pore volume.

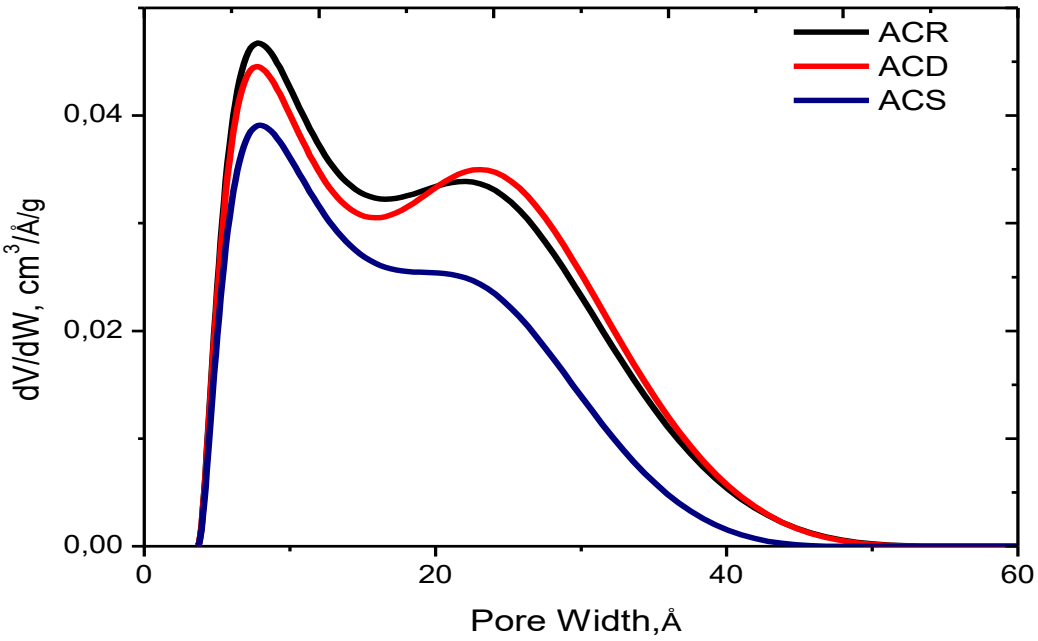


Figure 4.18 Pore size distribution of the activated carbon samples calculated by the NLDFT method.

4.6 SEM/EDS Analysis

SEM images of coal sample A, coal sample B, coal sample C and the activated carbon samples (ACR, ACD, and ACS) are shown in Fig. 4.19. A thick wall structure with no visible cavities or pores can be observed from the SEM images of the samples A to C (Fig. 4.19 A, B and C). After the activation of the samples with KOH, well-developed pores are seen clearly on the surface of the prepared activated carbon samples as shown in Fig. 4.19 D, E and F. Pore development is a result of the reaction of KOH with the samples during the activation process. This is in line with the results reported by Lua and Yang (2004) and Omri and Benzina (2012). The studies revealed that activation at 800 ^{o}C with KOH leads to significant pore development and volatiles removal. Furthermore, Lillo-Ródenas *et al.* (2003) and Linares-Solano *et al.* (2012) reported that, during the activation process, the diffusion of KOH molecules into the pores of the material improves the KOH-carbon interaction, thereby leading to the creation of more pores. The pore development is very important as it increases the surface area and pore volume of the activated carbon. The SEM analysis confirms the activated carbon samples to be highly porous with pore development of various sizes. This is consistent with observations from nitrogen adsorption isotherms and the PSD profiles.

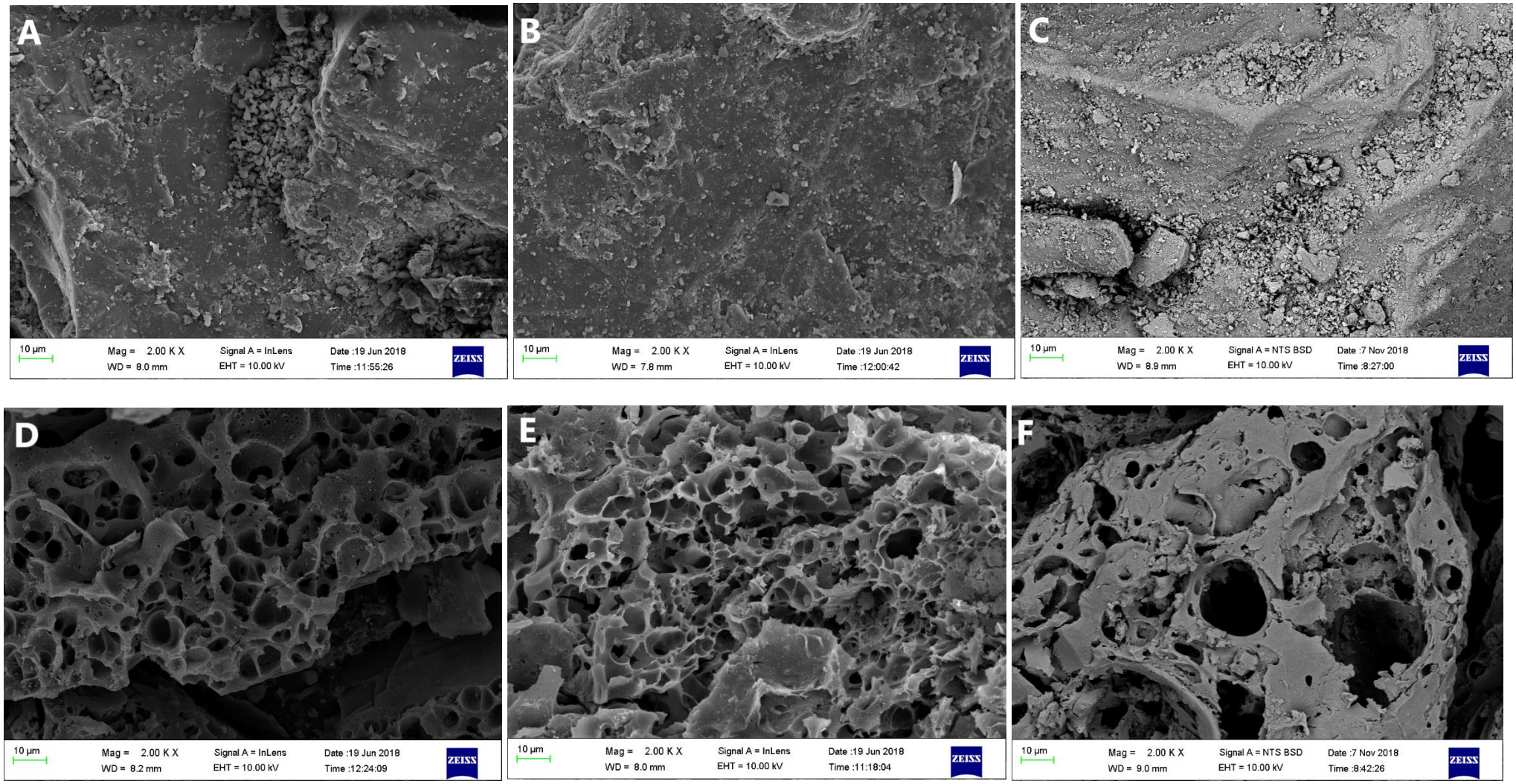


Figure 4.19 SEM images of (A) Sample A (B) Sample B (C) Sample C (D) ACR (E) ACD (F) ACS

The results of EDS analysis, which reveal the composition of the elements present in the samples and the synthesized activated carbons are provided in Table 4.18.

Table 4.18 EDS analysis of Coal waste samples and its derived Activated Carbons

Element	Sample A	ACR	Sample B	ACD	Sample C	ACS
	Weight (%)					
C	75.67	85.78	71.41	79.49	35.13	60.04
O	15.42	11.30	20.02	14.62	31.61	26.51
Al	2.42	-	1.36	2.67	11.87	-
Si	2.99	2.92	1.12	3.22	16.51	13.16
Ca	1.48	-	3.42	-	1.46	0.14
K	2.02	-	2.68	-	3.42	0.15

C – carbon; O – oxygen; Al – aluminum; Si – silicon; Ca – calcium; K – potassium

The EDS analysis reveals the presence of elements such as C, O, Al, Si, Ca and K in varying weight percentages. The presence of Si, Al and Ca in the activated carbons be attributed to the presence of mineral/ash content in the samples. The EDS analysis also shows no presence of potassium (K) in ACR and ACD and very little amount in ACS. This is an indication of the efficient washing process in which the synthesized activated carbons were washed with hydrochloric acid (HCl) to totally remove all traces of KOH used during the activation process.

4.7 XRD Analysis

Fig. 4.20 reveals the XRD profile of sample A, sample B, sample C and the activated carbon samples (ACR, ACD, and ACS). The profile in Fig. 4.20 (A, C and E) reveals the presence of inorganic contents with well-defined peaks observed at 2θ = 3, 13, 26, 27, 28, 39.3 and 68^{o}. Sample A, which was the ROM fines, was seen with a more organic hump, indicates lower mineral matter compared to both sample C and D, which are discards and slurry obtained from dense medium separation and flotation processes. This organic hump is also as a result of the organic vitrinite and total carbon composition of sample A. The intensity of minerals matter, which might be quartz in sample C was seen to be very strong compared to the other samples. When compared to the profile for the activated carbon samples in Fig. 4.20 (B, D, and F), ~~showed~~ a broad diffraction background with lack of a well-defined peak was observed. This is an indication of a predominantly amorphous structure as expected for carbon materials such as

activated carbon. A similar observation was reported by Wang and Lu (1997) and Köseoğlu and Akmil-Başar (2015).

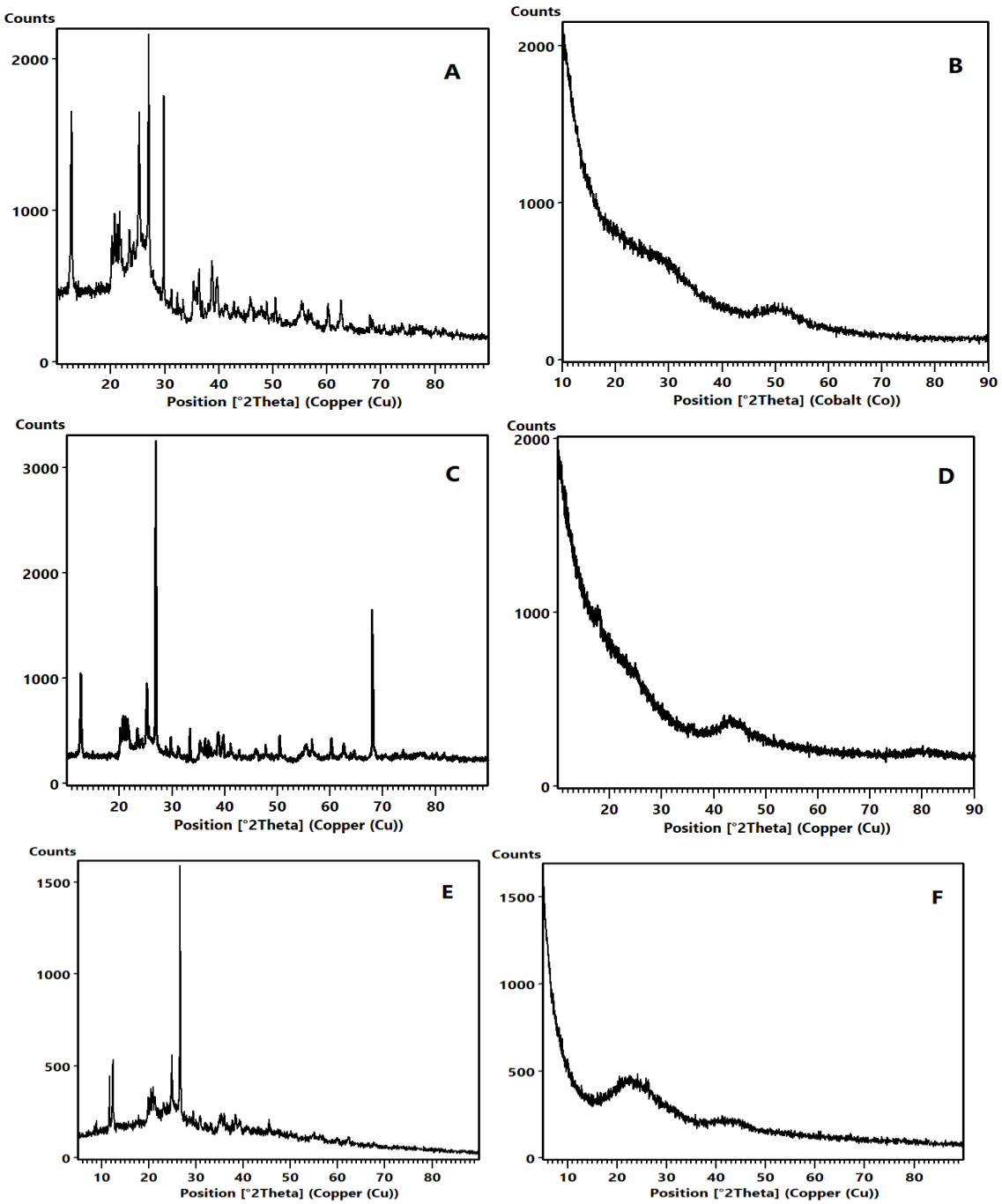


Figure 4.20 XRD Profile of (A) Sample A; (B) ACR; (C) Sample B; (D) ACD and (E) Sample C (F) ACS

4.8 FTIR Analysis

The FTIR spectra of sample A, sample B, sample C and the activated carbon samples (ACR, ACD, and ACS) are shown in Fig. 4.21. The spectra of the samples as shown in Fig. 4.21A, B

and C revealed a broad absorption band between 3000 and 3750 cm^{-1} which shows the presence of OH groups (Dağdelen *et al.*, 2014, Figueiredo *et al.*, 1999). The band at approximately 1080 cm^{-1} belongs to C-O stretching vibrations in alcohols, phenols, or ester groups (Hesas *et al.*, 2013, Martins *et al.*, 2015). The FTIR spectrum of the activated carbon samples in Fig. 4.21 (D, E, and F) have fewer adsorption bands than the samples under study. This is a confirmation that the functional groups present in these samples prior to activation were removed during the activation process. A similar band of 1080 cm^{-1} is also observed within the spectrum of the activated carbon samples. This band is attributed to C-O stretching in carboxyl acids, alcohols, phenols, and esters usually found in oxidized carbons (Üner *et al.*, 2015, Martins *et al.*, 2015). In addition, Chiang *et al.* (2002) also observed that alkali treatment of the carbon precursors increases the amount of oxygen functional groups, particularly, phenolic groups. Carbon skeleton vibrations were also observed in the activated carbon samples, the main characteristic of activated carbon samples (Omri and Benzina, 2012).

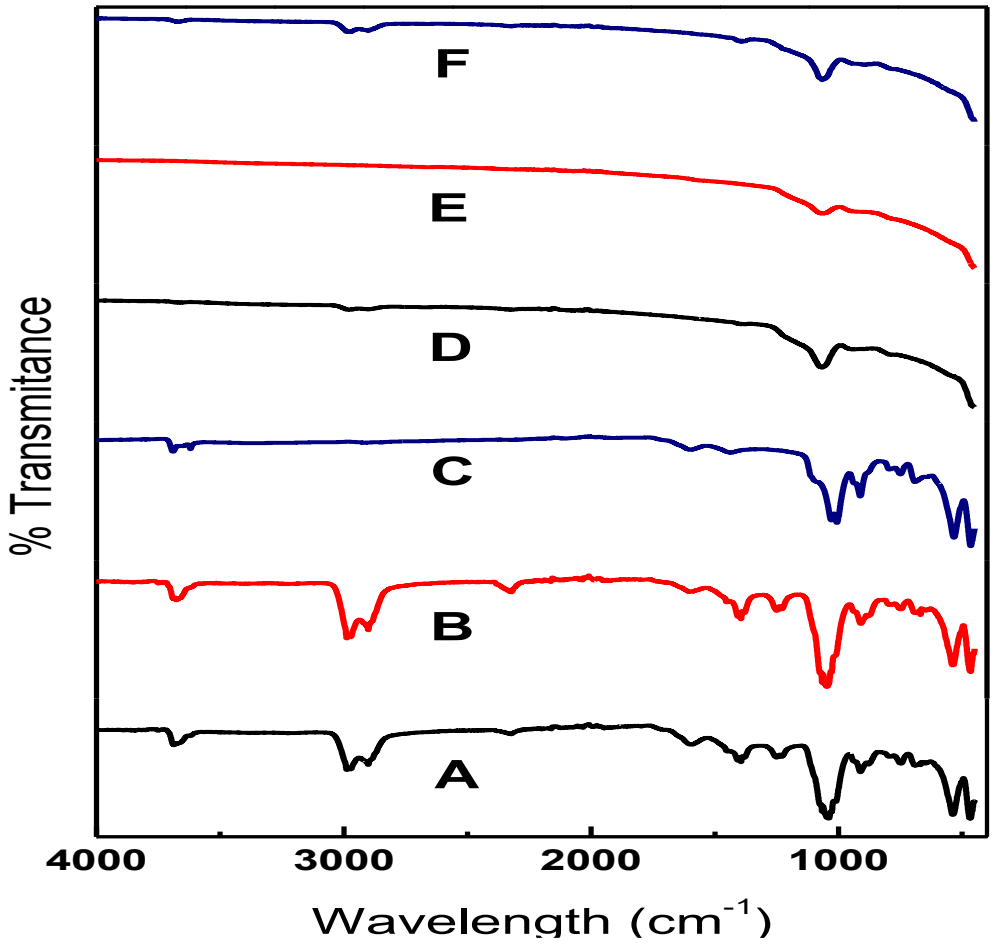


Figure 4.21 FTIR Images of (A) Sample A (B) Sample B (C) Sample C (D) ACR (E) ACD (F) ACS

4.9 Summary

In this chapter, the results from the characterization of the three coal samples, along with the synthesized activated carbon produced in this study were presented. Detailed experimental design using Response Surface Methodology to synthesize and evaluate the effect of temperature and KOH weight ratio on surface area and pore volume of the activated carbon samples were also presented. This includes the analysis of variance (ANOVA), checking the validity of ANOVA assumptions as it relates to the results obtained and the accuracy of the selected model.

The results from the analysis presented in this chapter established that South African coal waste samples are good raw materials to produce highly porous activated carbon, and a promising adsorbent for natural gas storage. The results also established a positive correlation between surface area and adsorption capacity of activated carbon samples. The influence of temperature and KOH weight ratio on the surface area and pore volume of the activated carbon samples was established.

Activated carbon prepared from sample A (run-of-mine fines) was found to have the largest surface area of 1925.34 m^2/g and pore volume of 1.290 cm^3/g, followed by activated carbon from sample B (discard), 1826.41 m^2/g and pore volume of 1,252 cm^3/g and then activated carbon from sample C (slurry) with surface area of 1484.96 m^2/g and pore volume of 1.042 cm^3/g. The morphology, textural properties, functional groups and elemental composition of the synthesized activated carbons with the largest surface areas from each of the three samples were compared. The presence of a hysteresis loop in the N_2 adsorption-desorption isotherms and result from the PSD analysis confirms the activated carbon samples to be highly porous consisting of micropores and mesopores. SEM/EDS analysis showed the development of pores and the presence of high carbon elements. XRD analysis reveals a broad diffraction background, an indication of largely amorphous carbon material. The combination of the characterizations discussed in the chapter provided an in-depth understanding of activated carbon samples from South African coal waste and their suitability for natural gas storage applications. The experimental evaluation of the three activated carbon samples for gas storage is discussed in the next chapter.

CHAPTER 5 ADSORPTION PROPERTIES OF METHANE ONTO THE ACTIVATED CARBONS

5.1 Introduction

This chapter presents the adsorption isotherms, kinetics and heat of adsorption of methane onto the three activated carbons synthesized from coal waste samples. The analysis of these activated carbon samples has shown that they are highly porous materials with large surface areas. Isotherms of methane adsorption on these samples were measured using the high pressure volumetric method at different temperatures (0, 15, 25, 35 and 50 ºC) and pressure up to 40 bar. The results from the adsorption experiment compared favorably with those reported in the literature (Frère and De Weireld, 2002, Martin *et al.*, 2011, Luo *et al.*, 2011). The adsorption results were validated with the Langmuir, Toth, and Dubinin-Astakhov (D-A) adsorption isotherm models. The adsorption isotherm of methane onto the activated carbon samples revealed that activated carbon derived from sample A (ACR) gives the highest adsorbed amount of methane. This can be attributed to its larger surface area and higher porosity compared to other samples.

The study of the adsorption equilibria, the influence of surface diffusion on adsorption kinetics and the heat of adsorption of methane onto the three activated carbon samples are presented in this chapter. The chapter also provides a comparative analysis to compare the adsorption capacity of the samples of the present work with activated carbons derived from coal-related materials in the literature.

5.2 Theoretical Background

5.2.1 Adsorption Isotherms

Three isotherm models were used to validate the experimental data on methane adsorption, namely Langmuir, Toth, and Dubinin-Astakhov models. The Langmuir model is a simple model that describes monolayer adsorption of a gas-solid phase adsorption such as methane onto activated carbon. The assumptions of the Langmuir model include: homogenous surface of the adsorbent; adsorption takes place within definite localized sites and the sites are all equal and each site can contain one molecule at a time. The Langmuir theory is based on a kinetic principle, which states that the rate of adsorption (i.e. the rate at which the gas molecules

(adsorbate) hits at the surface of the adsorbent) is equal to the rate of desorption from the surface and this is illustrated Fig. 5.1 (Do, 1998).

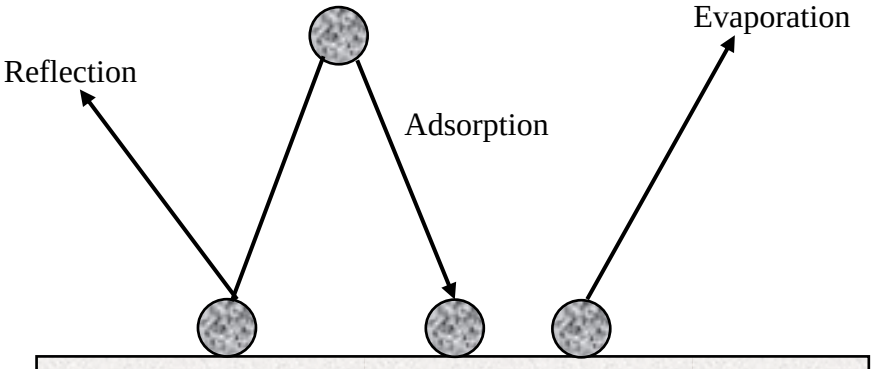


Figure 5.1 Schematic diagram of Langmuir adsorption mechanism on a flat surface (Do, 1998)

By equating the rates of adsorption and desorption, the widely used Langmuir model equation in terms of fractional loading is written as:

$$\theta = \frac{bP}{1+bP} \tag{5.1}$$

where θ is the fractional loading, P is the pressure of adsorption, and b is the parameter known as the affinity constant, which is a measure of how strong an adsorbate molecule is attracted onto a surface (Do, 1998) and is represented as:

$$b = b_{\infty}\exp\left(\frac{Q}{R_g T}\right) \tag{5.2}$$

where b_{∞} is a pre-exponential factor to b, Q is the isosteric heat of adsorption, R_g is gas constant and T is the temperature of adsorption.

Since adsorption isotherms are usually obtained in the form of amount adsorbed versus pressure. Eq. (5.1) may be rewritten as:

$$C_{\mu} = C_{\mu s}\frac{b(T)P}{1+b(T)P} \tag{5.3}$$

Where $\theta = \frac{C_{\mu}}{C_{\mu s}}$ C_{μ} is the amount of adsorbed; $C_{\mu s}$ is a saturated amount of adsorbate adsorbed, subscript μ means the adsorbed phase and b(T) is represented as:

$$b(T) = b_{\infty}\exp\left(\frac{Q}{R_g T}\right) \tag{5.4}$$

The Langmuir model is limited by its inability to fit adsorption data at high pressure and its inability to describe the heterogeneous nature of a material.

The Toth model (Toth, 1971), was developed to improve on the Langmuir model and to address the limitations associated with the model. The Toth model adequately describes adsorption at low and high pressure, in addition, the model accounts for the heterogeneous nature of the adsorbent. The expression for the Toth model is:

$$C_{\mu} = C_{\mu s}\frac{bP}{[1+(bP)^{t}]^{\frac{1}{t}}} \tag{5.5}$$

The affinity constant b is expressed as shown in Eq. (4.2)

The exponent t is expressed as:

$$t = t_0 + \alpha\left(1 - \frac{T_0}{T}\right) \tag{5.6}$$

where, t is the parameter that describes the heterogeneous nature of the adsorbate/adsorbent system and is normally less than 1 (Do, 1998), t_0 is the parameter t at some reference temperature T_o, and α is a constant parameter.

The Toth equation is equivalent to the Langmuir equation when the value of t is 1. The more the value of 't' deviates from 1, the more heterogeneous the system is said to be. Owing to its simplicity and its accurate description of the adsorption system at both high and low pressures, the Toth equation is usually recommended as the number one choice to use in fitting isotherm data of many adsorbates such as hydrocarbons, carbon oxides, hydrogen sulfide, alcohols onto activated carbon (Do, 1998).

Dubinin-Astakhov (D-A) model has been widely used to fit the physisorption of several gases on activated carbons (Rahman *et al.*, 2010, Luo *et al.*, 2011, Siemons and Busch, 2007, Himeno *et al.*, 2005). The D-A equation can provide an adequate description of the equilibrium data of carbonaceous materials with a high degree of heterogeneity and wider pore size distribution. Dubinin and Astakhov (1971) proposed the following equation:

$$W = W_o \exp\left[-\left(\frac{A}{E}\right)^{n}\right] \tag{5.7}$$

where; W represents the gas uptake in cm^3/g, W_o is the saturated volume uptake of the gas in cm^3/g, E is the characteristic energy of adsorption and n is the D-A parameter that defines the structural heterogeneity of the adsorbent. The value of n for adsorbents such as zeolites, molecular sieves is 3 (Ghosal and Smith, 1996). Depending on the heterogeneity of the material, the value of n may be within the range of 2 and 5 (Stoeckli *et al.*, 1989).

The adsorption potential A is defined as:

$$A = RT \ln\left(\frac{P_o}{P}\right) \tag{5.8}$$

Therefore, Eq. (5.7) can be represented as:

$$W = W_o\left[-\left\{\frac{RT}{E}\ln\left(\frac{P_o}{P}\right)\right\}^n\right] \tag{5.9}$$

P_o is the saturation pressure and can be expressed as:

$$P_o = P_c\left(\frac{T}{T_c}\right)^2 \tag{5.10}$$

where P_c and T_c are the critical points of the gas (methane in this study) at temperature T.

Table 5.1 Summary of isotherm models used in this study

Isotherm	Functional Form	Remarks
Langmuir	$C_\mu = C_{\mu s}\frac{b(T)P}{1+b(T)P}$	Does not provide an adequate description of equilibrium data of adsorbents at high pressure and with heterogeneous structure
Toth	$C_\mu = C_{\mu s}\frac{bP}{[1+(bP)^t]^{\frac{1}{t}}}$	Adequately describes adsorption at both low and high pressures and accounts for the heterogeneous nature of the adsorbent.
D-A	$W = W_o\left[-\left\{\frac{RT}{E}\ln\left(\frac{P_o}{P}\right)\right\}^n\right]$	It provides an adequate description of the equilibrium data of carbonaceous materials with a high degree of heterogeneity with wider pore size distribution.

5.2.2 Heat of Adsorption

Understanding of heat released during the adsorption process is essential in the kinetic study of an adsorption system. The heat of adsorption is the heat evolved during the adsorption of a mole of an adsorbate on the surface of the adsorbent (Do, 1998). The heat released during the adsorption process is partially adsorbed by the adsorbent and the remainder is released into the surrounding. The part of the heat absorbed by the adsorbent increases the temperature of the solid particle and this increase in temperature slows down the kinetics of the adsorption process (Schindler, 2008). Therefore, the understanding of the heat of adsorption is important in the study of adsorption kinetics and is a valuable criterion in the thermal management of any adsorption system (Do, 1998, Martin *et al.*, 2011).

The heat of adsorption can be calculated from the Van't Hoff thermodynamic equation (Do, 1998):

$$\frac{\Delta H}{R_g T^2} = -\left(\frac{\partial \ln P}{\partial T}\right)_{C_\mu} \tag{5.11}$$

where ΔH is the enthalpy change which is equal to the isosteric heat. All other parameters are as previously described.

To obtain the expression for calculating the heat of adsorption using the Langmuir isotherm model as expressed in Eq. (5.3), a total differentiation of Eq. (5.3) and substituting the result into Eq. (5.11) will yield the following:

$$\frac{\Delta H}{R_g T^2} = \frac{Q}{R_g T^2} + \delta(1 + bP) \tag{5.12}$$

where δ is the thermal expansion coefficient of the saturation concentration which is expressed as:

$$\frac{1}{C_{\mu s}} \frac{dC_{\mu s}}{dT} = -\delta \tag{5.13}$$

Since $(1 + bP) = \frac{1}{1-\theta}$ from Eq. (5.1)

In terms of fractional loading θ, Eq. (5.12) becomes:

$$-\Delta H = Q + \frac{\delta R_g T^2}{1-\theta} \tag{5.14}$$

The negative sign of the enthalpy change in the equation denotes that the adsorption process is exothermic (i.e. heat is released from the process). In order to obtain a measurable value of the heat of adsorption, that is, as the fractional loading tends to 1 ($\theta \rightarrow 1$), the thermal expansion coefficient of the saturation concentration (δ) must be zero (Do, 1998). This follows that the saturation capacity is independent of temperature, thus the heat of adsorption is a constant and independent of loading.

To obtain the heat of adsorption using the Toth model, the following equation is derived from the Van't Hoff equation (Do, 1998).

$$(-\Delta H) = Q - \frac{1}{t}(\propto R_g T_0)\left\{\ln(bP) - [1 + (bP)^t] \ln\left[\frac{bP}{(1+(bP)^t)^{\frac{1}{t}}}\right]\right\} \tag{5.15}$$

Eq. (5.15) is rewritten in terms of fractional loading as:

$$(-\Delta H) = Q - \frac{1}{t}(\propto R_g T_0)\left\{\ln\left[\frac{\theta}{(1-\theta^t)^{\frac{1}{t}}}\right] - \frac{\ln\theta}{(1-\theta^t)}\right\} \tag{5.16}$$

And in terms of the amount adsorbed C_μ, Eq. (5.16) is rewritten as:

$$(-\Delta H) = Q - \frac{1}{t}(\propto R_g T_0)\left\{\ln\left[\frac{C_\mu}{(C_{\mu s}^t - C_\mu^t)^{\frac{1}{t}}}\right] - \frac{\ln\left(\frac{C_\mu}{C_{\mu s}}\right)}{1-\left(\frac{C_\mu}{C_{\mu s}}\right)^t}\right\} \tag{5.17}$$

Parameter Q as defined by Do (1998) is the heat of adsorption at fractional loading (θ) of zero.

$$Q = (-\Delta H)|_{\theta=0} \tag{5.18}$$

In order to obtain the heat of adsorption using the D-A model, the Clausius-Clayperon equation is widely used to obtain the heat of adsorption of an adsorbate-adsorbent system (Do, 1998, Al-Muhtaseb and Ritter, 1999, Myers, 2002, Loh *et al.*, 2010a).

The Clausius-Clayperon equation is represented as:

$$H_{ads} = RT^2 \left[\left(\frac{\partial(\ln P)}{\partial T}\right)_c\right] \tag{5.19}$$

where H_{ads} is the heat of adsorption.

5.2.3 Adsorption Kinetics

Information such as the adsorption equilibria and adsorption kinetics are very important in understanding and design of an adsorption system such as the ANG storage system. From the perspective of system design such as the ANG storage system, it is important to provide an analysis of the adsorption rates (Özacar, 2003, Duran *et al.*, 2011, Luo *et al.*, 2011). Furthermore, it is important to understand the adsorption kinetics as most porous solids such as the activated carbon samples in this study have their adsorption rate limited by the ability of adsorbate molecules to diffuse into the porous solid interior, hence the need to understand the process of diffusion and its influence on the overall adsorption rate of the activated carbon samples. To understand the adsorption process within an adsorbent using diffusion models, it is assumed that, the movement of adsorbate molecules occurs in parallel in both the void space and also the adsorbed phase as shown in Figure 5.2 (Damköhler, 1935).

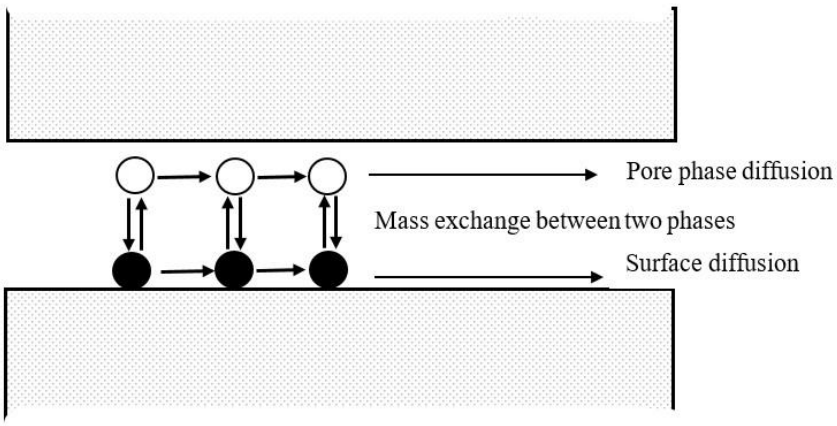


Figure 5.2 Schematic of parallel pore and surface diffusion (Do, 1998)

To describe the adsorption kinetics of an adsorbent undergoing pore and surface diffusion as illustrated in Fig. 5.2, a mass balance equation was obtained by conducting a mass balance around a tiny portion of the adsorbent (Do, 1998). The resulting equation is as shown below:

$$\varepsilon\frac{\partial C}{\partial t}+(1-\varepsilon)\frac{\partial C_{\mu}}{\partial t}=\varepsilon D_{p}\frac{1}{r^{s}}\frac{\partial}{\partial r}\left(r^{s}\frac{\partial C}{\partial r}\right)+(1-\varepsilon)D_{s}\frac{1}{r^{s}}\frac{\partial}{\partial r}\left(r^{s}\frac{\partial C_{\mu}}{\partial r}\right) \quad (5.20)$$

where ε is the voidage of the adsorbent particle, which is the accessible void space for the adsorbate and is described as the porosity of the adsorbate; C is adsorbate concentration (mole/cc of fluid); C_{μ} is the concentration of the adsorbate in the adsorbed phase; D_p is the pore diffusivity; D_s is the surface diffusivity and s is the particle shape factor and is equal to 0, l and 2 for slab, cylinder and sphere, respectively (Do, 1998).

The surface diffusivity can be obtained from the Arrhenius correlation which provides a relationship between the surface diffusivity (D_s) and the adsorption temperature (Rahman *et al.*, 2012a). This correlation is expressed mathematically as:

$$D_{s}=D_{so}\times\exp\left(-\frac{E_{a}}{RT}\right) \quad (5.21)$$

where E_a is the activation energy of the adsorbate and D_{so} is the pre-exponential constant that varies with the equilibrium pressure.

The pore diffusivity D_p is assumed to follow Knudsen mechanism and is represented as (Do and Do, 2001):

$$D_{p}=\frac{4K_{o}}{3}\sqrt{\frac{8RT}{\pi M}} \quad (5.22)$$

where K_o is the Knudsen diffusion parameter which describes the characteristics of the solid material such as pore size.

K_o is expressed as:

$K_o = \frac{r}{2}$; for cylindrical pore (5.23)

$K_o = \frac{3r}{8}$; for slit pore (5.24)

where r is the pore radius (Nicholson and Petropoulos, 1985, Do and Do, 2001).

The apparent diffusivity which is the combination of pore diffusivity and surface diffusivity describes the response of an adsorbate-adsorbent system to equilibrium. It is important to study the effect of apparent diffusivity on the system and on how it varies with temperature. The higher the value of pore and surface diffusivity, the earlier the system attains equilibrium (Do, 1998, Azimi and Mirzaei, 2012).

To describe the kinetics of adsorption in a heterogeneous adsorbent such as the activated carbon samples understudy, a non-linear adsorption system is assumed, in which the parallel diffusion mechanisms as shown in Fig. 5.2 holds and the mass balance equation (Eq. 5.20) is valid. Other assumptions include; the system is isothermal, pore diffusivity and mass transfer coefficient

are constant (Do, 1998). Adsorption isotherm such as Langmuir and Toth can be used along with the mass balance equation to describe the adsorption kinetics (Do, 1998, Do and Do, 2001, Azimi and Mirzaei, 2012).

Adsorption isotherms can be expressed as:

$$C_\mu = f(C) \tag{5.25}$$

By substituting Eq. 5.25 into Eq. 5.20, a mass balance equation for a non-linear isotherm is obtained and expressed as (Do, 1998):

$$[\varepsilon + (1-\varepsilon)f'(C)]\frac{\partial C}{\partial t} = \frac{1}{r^s}\frac{\partial}{\partial r}\left\{r^s\left[\varepsilon D_p + (1-\varepsilon)f'(C)D_s\right]\frac{\partial C}{\partial r}\right\} \tag{5.26a}$$

subject to the following boundary conditions:

$$r = 0;\ \frac{\partial C}{\partial r} = 0 \tag{5.26b}$$

$$r = R;\ [\varepsilon + (1-\varepsilon)f'(C)D_s]\frac{\partial C}{\partial r} = k_m(C_b - C) \tag{5.26c}$$

and the following initial condition

$$t = 0;\ C = C_i;\ C_\mu = C_{\mu i} = f(C_i) \tag{5.26d}$$

where C_b is the bulk concentration of adsorbate around the adsorbent; C_i is the initial concentration, and $C_{\mu i}$ is the initial adsorbed concentration which is in equilibrium with C_i.

The model equations (5.26) completely define the system kinetic behavior. Solving this set of equations will yield the concentration distribution of the adsorbate within the adsorbent. Once the solution of the concentration distribution is known, the amount adsorbed per unit volume of the adsorbent can be calculated using the following equation:

$$M(t) = V_p\left[\varepsilon C(t) + (1-\varepsilon)C_\mu(t)\right] \tag{5.27}$$

where M(t) is the amount adsorbed per unit volume as a function of time; V_p is the volume of the adsorbent, C(t) and $C_\mu(t)$ are the volumetric concentrations in the gas and adsorbed phases (Do, 1998).

5.3 Materials

5.3.1 Methane

The methane gas used was supplied by African oxygen Ltd (AFROX), Johannesburg, South Africa. The accompanying certificate of the analysis indicated a purity level of 99.95 - 100% of methane. Other components as: N_2 < 200 ppm, O_2 < 30 ppm, other hydrocarbons (OHC) < 300 ppm, and H_2 < 20 ppm.

5.3.2 Activated Carbon

The activated carbons used are ACR, ACD, and ACS. The preparation, characterization, and physical properties are as presented and discussed in chapter 4.

5.4 Experiment

5.4.1 Measurement of Adsorbents Properties

Physical properties such as BET surface area, pore size, pore volume and density of the activated carbon samples are listed in Table 4.18 in chapter 4.

5.4.2 Measurement of Adsorption Isotherms

Measurement of methane adsorption isotherms of the activated carbon samples at different temperatures of 0, 15, 25, 35 and 50 ºC and pressures up to 40 bars was carried out using Particulate Systems High Pressure Volumetric Analyser (HPVA II). The detailed experimental methods and equipment used are presented and discussed in section 3.5.

5.5 Results and Discussion

5.5.1 High Pressure Methane Adsorption

The amount of methane adsorbed on the three activated carbon samples is presented in Table 5.2. The isotherms are shown graphically in Fig. 5.3. It was observed that the plots exhibit Type I IUPAC isotherm. A sharp increase in methane uptake at lower pressures and a gradual increase as the pressure increases were observed for all the three activated carbon samples. Based on the amount of methane adsorbed per gram of the activated carbon samples, the adsorption capacity of the three activated carbon samples increases in the order of ACR > ACD > ACS. The maximum adsorbed amount of methane was attained at an average pressure of 37 bar at different temperatures. Sample ACR has the largest volume of methane adsorbed followed by ACD and ACS, respectively. This sequence agrees with the BET surface areas of the activated carbons; ACR (1925.34 m^2/g) > ACD (1826.41 m^2/g) > ACS (1484.96 m^2/g). Hence, the larger the surface area of the activated carbon, the larger the volume of methane it adsorbs. This observation is consistent with the nitrogen adsorption and it is also in agreement with previous studies (Panella *et al.*, 2005, Bénard and Chahine, 2007, Düren *et al.*, 2004).

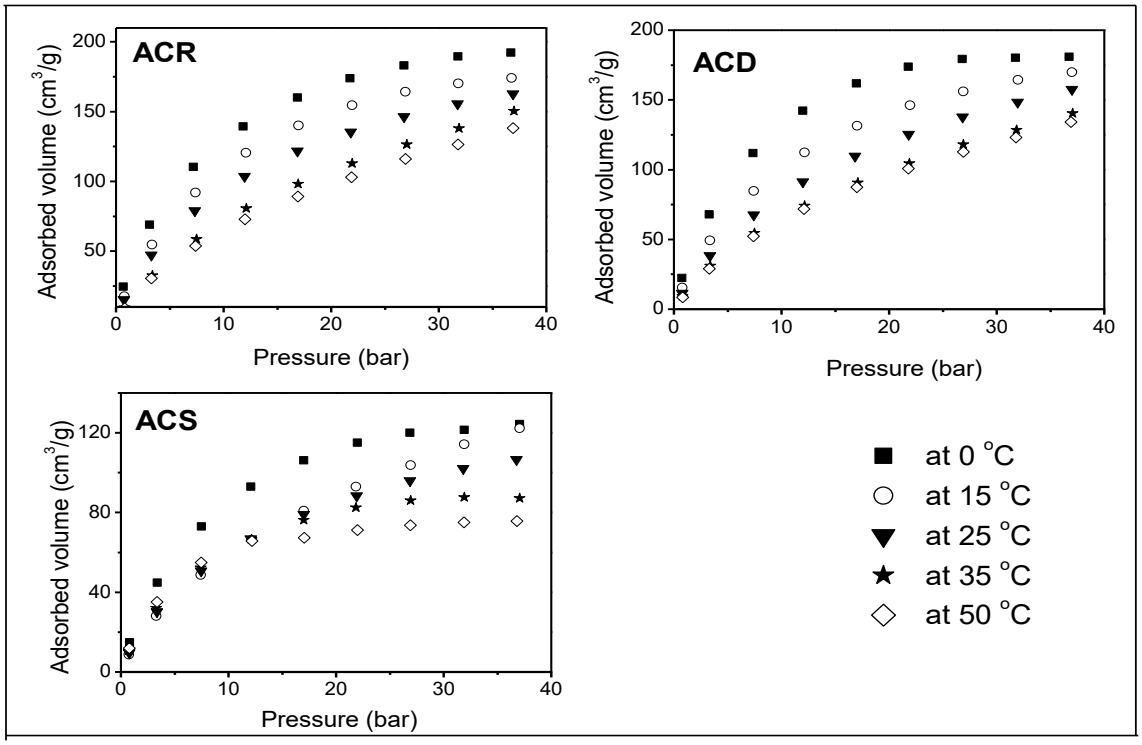


Figure 5.3 Isotherms of methane adsorption onto the activated carbon samples

Table 5.2 Experimental Data of Methane adsorption onto the activated carbon samples

Pressure (bar)	**Ads. Vol. (cm^3/g)**	**Pressure (bar)**	**Ads. Vol. (cm^3/g)**	**Pressure (bar)**	**Ads. Vol. (cm^3/g)**	**Pressure (bar)**	**Ads. Vol. (cm^3/g)**	**Pressure (bar)**	**Ads. Vol (cm^3/g)**
T = 0 ºC		T = 15 ºC		T = 25 ºC		T = 35 ºC		T = 50 ºC	
				Sample ACR					
0.8	24.49	0.8	17.65	0.8	15.36	0.8	9.50	0.8	9.01
3.1	68.95	3.4	54.63	3.3	47.32	3.4	32.61	3.3	30.55
7.2	110.38	7.4	91.92	7.3	79.11	7.5	58.47	7.4	53.70
11.8	139.35	12.1	120.44	12.0	103.62	12.1	80.56	12.0	72.94
16.9	160.06	17.0	140.12	16.9	121.81	17.0	98.09	16.9	89.22
21.8	173.89	22.0	154.61	21.8	135.46	21.9	112.96	21.9	102.87
26.9	182.98	26.9	164.19	26.8	146.43	27.0	126.45	26.9	116.10
31.8	189.57	31.8	170.24	31.8	155.64	31.9	138.07	31.8	126.47
36.7	192.17	36.8	174.08	37.0	162.71	37.0	150.33	36.9	138.18
				Sample ACD					
0.8	22.33	0.8	15.37	0.8	11.41	0.8	9.16	0.8	8.48
3.3	67.96	3.3	49.28	3.3	38.34	3.4	31.05	3.3	29.09
7.4	111.84	7.4	84.77	7.4	67.71	7.5	54.58	7.4	52.15
12.0	142.17	12.1	112.38	12.0	91.46	12.2	74.13	12.1	71.86
17.0	161.70	17.1	131.36	16.9	109.82	17.1	90.67	17.0	87.49
21.8	173.71	22.0	146.06	21.8	125.45	21.9	104.54	21.8	100.75
26.8	179.40	27.0	156.08	26.9	137.85	26.9	117.98	26.9	112.79
31.8	180.25	32.0	164.43	32.0	148.55	31.9	128.53	31.8	123.16
36.8	181.01	37.0	169.74	37.0	157.58	37.1	140.43	36.9	134.09
				Sample ACS					
0.8	14.88	0.8	8.68	0.8	9.68	0.8	10.67	0.8	11.89
3.4	44.84	3.3	28.00	3.4	30.26	3.3	32.14	3.4	35.11
7.5	72.98	7.4	48.66	7.5	50.77	7.4	52.32	7.5	54.93
12.1	92.90	12.2	66.20	12.1	66.78	12.2	66.60	12.2	65.68
17.1	106.24	17.0	80.84	17.0	79.14	17.0	76.16	17.0	67.42
22.0	115.00	21.9	93.03	21.9	88.51	21.9	82.44	22.0	71.25
26.9	120.07	26.9	103.81	26.9	95.96	26.9	86.08	26.9	73.61
31.9	121.50	31.9	114.27	31.8	102.22	31.9	87.10	31.9	75.00
37.1	124.44	37.1	122.22	36.8	106.69	37.1	87.61	36.8	75.74

Ads. Vol: Adsorbed Volume

5.5.2 Adsorption Isotherm Models

The methane adsorption data of the three activated carbon samples were fitted by Langmuir, Toth, and D-A isotherm models using non-linear regression. To show the suitability of these model equations to fit the experimental data, the adsorption data of methane onto the activated carbon samples were plotted against the data obtained from the models. The plots show the degree of a good fit between the models and the experimental data. For each temperature, the fitting between the models and experimental data is carried out using MATLAB non-linear regression method, and the parameters obtained from the fit are tabulated. A programming code written in MATLAB by Do (1998) was modified and used in fitting the experimental data to the models. The modified program, ISOFIT is presented in Appendix B1. The error of regression between the experimental data and data obtained from the models was obtained using the following equation (Loh *et al.*, 2010b):

$$\text{Error of Regression} = \frac{\sqrt{\frac{1}{N}\sum_{i=1}^{N}\left(C_{experiment}-C_{model}\right)^2}}{\frac{1}{N}\sum_{i=1}^{N} C_{experiment}} \qquad (5.28)$$

5.5.2.1 Regression of methane adsorption data with the Langmuir model

The predicted isotherms of the activated carbon samples using the Langmuir model at different temperatures were observed to be of Type I adsorption isotherm of the IUPAC classification (Thommes *et al.*, 2015), as shown in Fig. 5.4. The corresponding adsorption parameters and percentage error of the regression are presented in Table 5.3.

Table 5.3 Adsorption parameters for Langmuir model

Temperature	**ACR**			**ACD**			**ACS**		
(ºC)	$C_{\mu s}$ (cm^3/g)	b (bar^{-1})	EoR (%)	$C_{\mu s}$ (cm^3/g)	b (bar^{-1})	EoR (%)	$C_{\mu s}$ (cm^3/g)	b (bar^{-1})	EoR (%)
0	234.31	0.129	1.64	222.88	0.143	2	153.82	0.125	1.64
15	226.72	0.095	1.09	226.71	0.082	0.72	195.77	0.073	2.65
25	216.41	0.079	1.66	233.53	0.054	1.43	146.56	0.051	1.48
35	231.43	0.042	2.23	247.09	0.040	2.69	108.69	0.030	2.03
50	225.50	0.036	2.87	220.41	0.034	2.23	86.13	0.022	2.23

$C_{\mu s}$ - the maximum adsorbed volume; b – the affinity constant; EoR – Error or Regression

Parameter $C_{\mu s}$, one of the terms from the Langmuir equation is presented in Table 5.3 for all three samples at different adsorption temperatures. $C_{\mu s}$ is the maximum adsorbed volume in

cm^3/g that corresponds to a complete monolayer coverage. The values of $C_{\mu s}$ obtained for ACR and ACD were close but high compared to the values for ACS at all the temperatures evaluated.

The second parameter from the Langmuir equation is the affinity constant (b), which is an indication of how strong the methane molecule is attracted to the surface of the activated carbon samples. It is observed from Table 4.3 that, the value of b increases with a decrease in temperature for the three activated carbon samples. Do (1998) reported that, because of the greater attraction of the adsorbent molecule in the direction of the adsorbent surface, the greater the value of b, and the more the adsorbent surface is covered with adsorbent molecules. The result as presented in Table 5.3 is in agreement with this observation. As can be seen from Table 5.3, the value of b increases as temperature decreases from 50 to 0 ^oC with the largest value of b obtained at 0 ^oC for all the three activated carbon samples. The highest adsorbed volume of methane is obtained at 0 ^oC for all the three samples. This agrees with data presented in Table 5.3 that, the larger the value of b, the more methane is attracted to the surface of the sample, hence, more volume is adsorbed. Furthermore, it is observed from Table 5.3 that, for each temperature, the value of b is largest for ACR followed by ACD and then ACS. This is also true for the adsorbed volume of the three samples at each temperature as can be seen from Table 5.2 and Fig. 5.3.

As shown in Fig. 5.4, the Langmuir model is seen to provide a good fit to the experimental data obtained at different temperatures for the three activated carbon samples with an average error of regression of about 2% as shown in Table 5.3. From Fig. 5.4, the symbols represent the experimental data points (adsorbed volume) for respective pressures and temperatures, the solid lines are the predicted data from the Langmuir model. The adsorbed volume is seen to increase with pressure until a saturation volume or capacity is attained. In addition, it is observed in Fig. 5.4 that, an increase in temperature decreases the volume of methane adsorbed on all three samples. This has to do with the fact that, at a higher temperature, higher energy is gained by the adsorbed molecule to evaporate (Loh *et al.*, 2010a, Do, 1998). Because of the evaporation of the adsorbed molecule, less volume is adsorbed at higher temperatures as observed in Fig. 5.4.

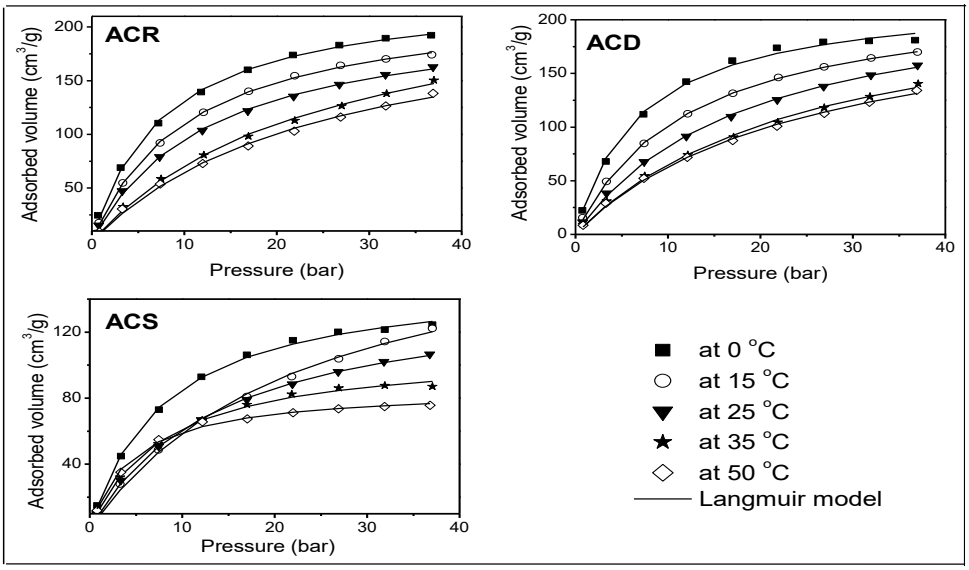


Figure 5.4 Langmuir model fitting of methane adsorption data onto activated carbon samples

5.5.2.2 Regression of methane adsorption data with Toth model

The experimental data of methane adsorption onto activated carbon samples ACR, ACD and ACS and it's fitting with the Toth isotherm model are depicted in Fig. 5.5. It can be observed from the figure that a good fit was achieved between the predicted data from the Toth model and the experimental data at different temperatures. The corresponding adsorption parameters and error of regression are presented in Table 5.4. From the adsorption parameters of the Toth equation ($C_{\mu s}$, b, and t) as listed in Table 5.4, it is observed that, the affinity constant (b), which describes the strength of attraction of methane onto the surface of the activated carbon samples, increases as temperature decreases. This is consistent with findings from the Langmuir model.

Table 5.4 Adsorption parameters for Toth model

Temp.	**ACR**				**ACD**				**ACS**			
(ºC)	$C_{\mu s}$ (cm^3/g)	b (bar^{-1})	t	EoR (%)	$C_{\mu s}$ (cm^3/g)	b (bar^{-1})	t	EoR (%)	$C_{\mu s}$ (cm^3/g)	b (bar^{-1})	t	EoR (%)
0	258.81	0.145	1.02	1.27	202.16	0.123	1.35	2.43	145.20	0.182	1.16	1.45
15	224.52	0.094	0.81	1.09	236.53	0.076	0.93	0.63	106.24	0.120	0.42	0.45
25	283.91	0.085	0.68	0.27	324.23	0.052	0.69	0.15	189.32	0.117	0.71	0.38
35	241.81	0.023	0.40	0.55	298.46	0.028	0.49	0.62	101.96	0.074	1.19	1.81
50	289.60	0.023	0.39	0.73	235.02	0.021	0.42	0.83	80.02	0.029	1.34	1.46

t – Toth equation parameter that describes system heterogeneity

Parameter t describes the level of heterogeneity of the adsorbate/adsorbent system, in this case, methane/activated carbon. The more the value of 't' deviates farther below 1, the stronger the level of heterogeneity of the system (Do, 1998). As can be observed from Table 5.4, the

parameter t for activated carbon samples ACR and ACD decreases as temperature increases, this is an indication that the system is more heterogeneous as temperature increases from 0 to 50 ^{o}C. For activated carbon sample ACS, it is observed that, the parameter t deviates more from 1 as temperature increases from 0 to 15 ^{o}C and subsequently the value inches closer to 1 as the temperature increases from 15 to 50 ^{o}C, this suggests that, the system is more heterogeneous as temperature increases from 0 to 15 ^{o}C and subsequently becomes less heterogeneous as temperature increases from 15 to 50 ^{o}C.

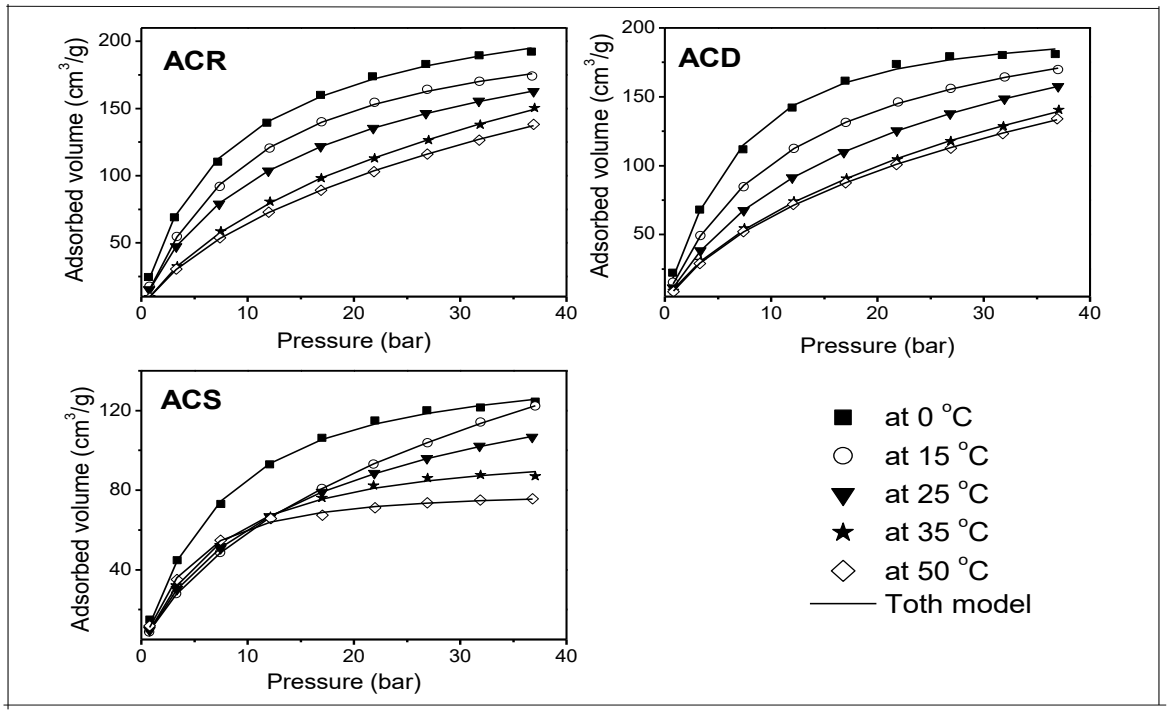


Figure 5.5 Toth model fitting of methane adsorption data onto activated carbon samples

5.5.2.3 Regression of methane adsorption data with D-A model

The Dubinin-Astakhov equation is used to fit the experimental adsorption data of methane onto the activated carbon samples. Fig. 5.6 shows the isotherms at different temperatures and shows an excellent fit between the predicted data from the D-A equation and the experimental data at different temperatures. The symbols in the figure depict the experimental data points at respective temperatures, while the solid line depicts the predicted data points from the D-A equation. The adsorption parameters (W_0, E and n) and regression error are listed in Table 5.5.

Table 5.5 Adsorption parameters for D-A model

Temp.	ACR				ACD				ACS			
(°C)	W_0 (cm^3/g)	E (J/mol)	n	EoR (%)	W_0 (cm^3/g)	E (J/mol)	n	EoR (%)	W_0 (cm^3/g)	E (J/mol)	n	EoR (%)
0	213.94	7317.8	2.00	0.94	195.49	7174.5	2.36	1.58	134.92	7329.5	2.18	1.71
15	198.43	7228.2	1.94	1.08	197.40	6989.8	1.89	0.80	176.72	7240.2	1.35	0.51
25	198.22	7129.4	1.72	0.17	205.08	6324.6	1.60	0.18	132.21	7915.2	1.91	0.36
35	216.94	5552.7	1.34	0.64	223.81	5740.8	1.42	0.83	97.05	8912.2	1.70	1.10
50	220.68	5952.1	1.35	0.84	205.45	6152.4	1.41	0.64	78.69	10837	1.36	0.93

W_o - saturated adsorbed volume; E- characteristic energy of adsorption; n - heterogeneity parameter

As seen in Table 5.5, the regression error obtained from the results of fitting the experimental data to the D-A model is very low with an average of about 0.82% for the three activated carbon samples at the different temperatures. The exponent n of the D-A equation is an indication of the heterogeneous nature of the adsorbents with the values of n obtained, varying between 1.34 and 2.91 for the three activated carbon samples. Do (1998) reported that the typical values of n for highly porous activated carbon are between 1.2 and 1.8. As depicted in Table 5.5, most of the values of n at the different temperatures of the three activated carbon samples are within this range. It is also observed from Table 5.5 that, the value of n decreases and approaches unity with increase in temperature for activated carbon samples ACR and ACD. For activated carbon sample ACS, an initial decrease was observed from 0 to 15 °C and then an increase from 15 to 25 °C for the heterogeneous nature of this adsorbent (ACS). Thereafter, subsequently decreases which approaches unity was noted from 25 to 50 °C.

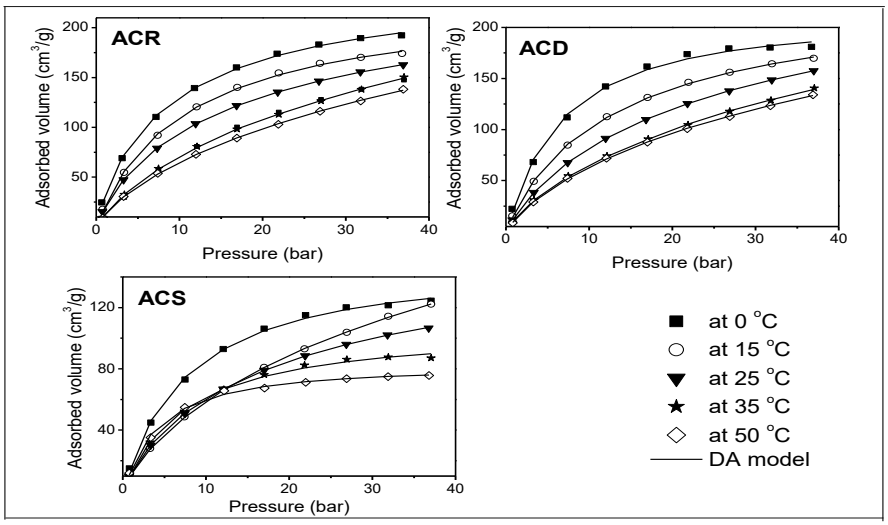


Figure 5.6 D-A model fitting of methane adsorption data onto activated carbon samples

5.5.2.4 Comparison of activated carbons from this study and other coal-based activated carbon for Methane Adsorption

The adsorbed amount of methane onto the activated carbon samples in this study is compared with methane adsorption data of activated carbon (KT) synthesized from low rank Indonesian coal and two commercial activated carbons (Martin *et al.*, 2011, Loh *et al.*, 2010b). The KT activated carbon is derived from low rank coal from the East of Indonesia, while Carbotech and Chemviron are commercial activated carbons produced from bituminous coal. The methane adsorption isotherms of these activated carbons and the activated carbon samples from this study are shown in Fig. 5.7 for methane at 25 ^{o}C and pressure up to 3.5 MPa. It is observed from Fig. 5.7 that, methane adsorbed on KT activated carbon (Martin *et al.*, 2011) is about 81.2, 80.5 and 71.4% lower than ACR, ACD, and ACS at a pressure of 3.5 MPa respectively. Methane adsorbed on commercial activated carbon, Carbotech (Martin *et al.*, 2011) is about 77.5, 76.3 and 65.7% lower than ACR, ACD and ACS at a pressure of 3.0 MPa respectively. The methane adsorbed on Chemviron is about 65.4, 63 and 47.1% lower than ACR, ACD, and ACS, respectively at a pressure of 2.5 MPa. The probable reason for the difference in adsorbed quantities can be attributed to the porous properties of the activated carbons mentioned, which are significantly lower than the porous properties of the activated carbon samples (ACR, ACD, and ACS). KT activated carbon, Carbotech and Chemviron have a surface area of 885 m^2/g, 668 m^2/g, 945 m^2/g and pore volume of 0.47 cm^3/g, 0.514 cm^3/g and 0.51 cm^3/g, respectively (Martin *et al.*, 2011, Loh *et al.*, 2010b).

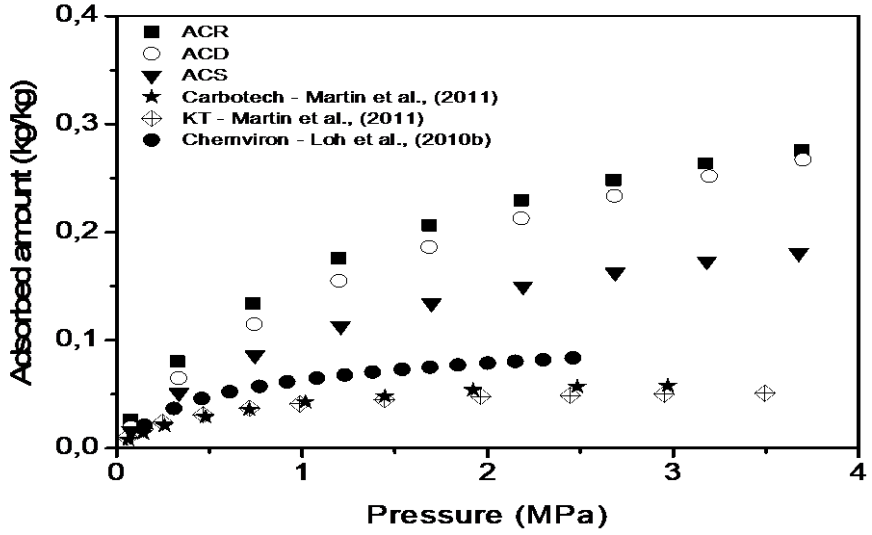


Figure 5.7 Comparison of methane adsorbed amount with coal-based activated carbons at 25 ^{o}C.

Fig. 5.8 compares the adsorbed amount of methane onto the activated carbon samples in this study with the amount of methane stored by a compressed natural gas (CNG) system at 25 ^{o}C (Wang *et al.*, 2011). It is observed that ACR provides about four times the capacity of CNG at 37 bar. ACD and ACS similarly give a significantly higher amount compared to CNG. Furthermore, the highest amount obtained for CNG at about 37 bars will require less than 10 bars to be adsorbed by the three activated carbon samples in this study. This further confirms the benefit and advantage of ANG as a natural gas storage system over CNG.

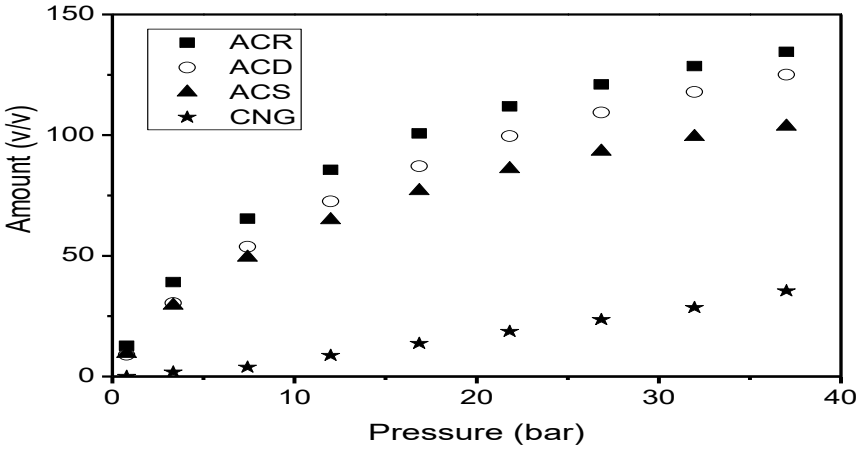


Figure 5.8 Comparison of methane adsorbed amount at 25 °C with CNG

5.5.3 Heat of Adsorption

The heat of adsorption obtained using the Langmuir model provides a constant value taking into account the homogeneous surface structure of the adsorbents (Loh *et al.*, 2010a). However, in the case of an adsorbent with heterogeneous surface structure as the case with the activated carbon samples in this study, the heat of adsorption is obtained as a function of amount adsorbed and temperature (Do, 1998, Loh *et al.*, 2010a). The activated carbon samples in this study are heterogeneous in nature as evidenced by the pore size distribution analysis discussed in section 4.5.1. The Toth and D-A isotherm models account for the heterogeneity nature of an adsorbent but since the D-A isotherm model provides the best fit to the experimental data, the D-A equation is considered most suitable in evaluating the heat of adsorption. In order to obtain the temperature and adsorbed amount dependent heat of adsorption, the Clausius-Clayperon equation (Eq. 5.19) is used along with the experimental isotherm data of the activated carbon samples.

The term $\left[\left(\frac{\partial(\ln P)}{\partial T}\right)_c\right]$ from Eq. (5.19) can be expressed further using the D-A equation (Eq.5.9 and 5.10) and substituting, Eq. 5.19 becomes:

$$H_{ads} = 2RT + E\left[\left(\ln\frac{W_o}{Cv_a}\right)^{\frac{1}{n}} + \frac{1}{n}\left(\ln\frac{W_o}{Cv_a}\right)^{\frac{1-n}{n}}\right] \tag{5.29}$$

Using Eq. 5.29 along with the D-A model parameters as listed in Table 5.5, the heat of adsorption of the three activated carbon samples at different temperatures of 0 ^{o}C, 25 ^{o}C, and 50 ^{o}C were obtained and shown in Fig. 5.9. It is observed from Fig. 5.9 that, the heat of adsorption changes with change in fractional loading of the activated carbon samples, this is by virtue of the heterogeneous nature of the samples. In addition, it is observed that the heat of adsorption of ACS is higher at the different temperatures when compared to the heat of adsorption of ACR and ACD, this is consistent with the values of the D-A model characteristic energy of adsorption as listed in Table 5.5. This means that the use of ACS as an adsorbent in the ANG storage system will increase the thermal load in temperature management of the system compared to when ACR and ACD are used as adsorbents in the ANG system.

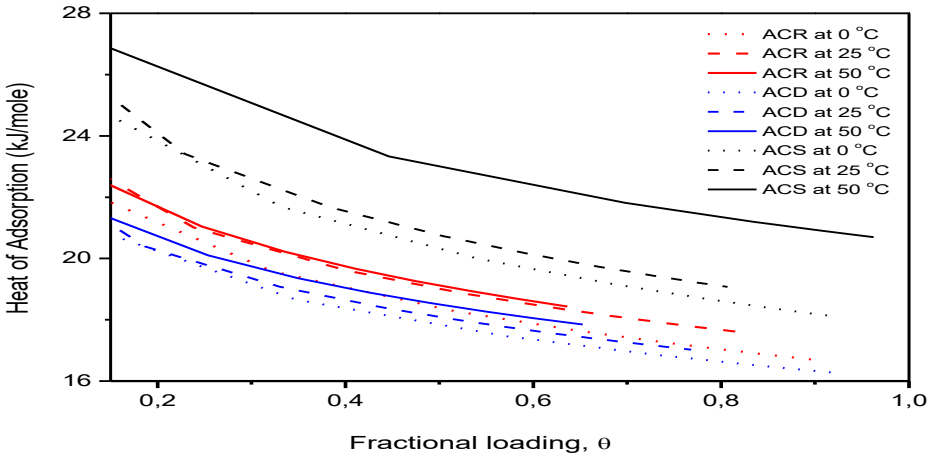


Figure 5.9 Heat of Adsorption of the Activated Carbon Samples

5.5.4 Adsorption Kinetics

The mathematical model as represented by Eq. (5.26) was simulated with the Toth isotherm model as it appropriately shows the effect of isotherm non-linearity on the kinetic behavior of the adsorption system. A programming code written in MATLAB by Do (1998) was modified and used to solve Eqs. (5.26) and (5.27). The MATLAB program, ADSORB1A.M is presented in Appendix B2. The parameters input into the modified MATLAB program to obtain kinetic

information on methane adsorption onto the activated carbon samples at temperatures of 0, 25 and 50 ^{o}C are listed in Table 5.6. The affinity constant (b) and saturation adsorption capacity ($C_{\mu s}$) from the Toth isotherm are listed in Table 5.4. The porosity (ε) of the activated carbon samples were obtained using a developed MATLAB program, used to process the SEM images of the activated carbon samples. The MATLAB program, SEMPOR.M and resulting processed images are presented in Appendices C1 – C4.

Table 5.6 Parameters used in MATLAB code ADSORB1A.M

Parameters	
Methane molecular weight	16
Pore diffusivity, D_p (cm^2/sec)	0.04
ACR radius (nm)	1.45
ACR porosity, ε	0.29
ACD radius (nm)	1.33
ACD porosity, ε	0.17
ACS radius (nm)	1.26
ACS porosity, ε	0.25
Surface diffusivity, D_s (cm^2/sec)	
0 ^{o}C	1.3×10^{-4}
25 ^{o}C	1.52×10^{-4}
50 ^{o}C	2.02×10^{-4}

The adsorption kinetics data which is the amount adsorbed per unit volume versus time for the three activated carbon samples at temperatures of 0, 25 and 50°C are plotted in Fig. 5.10.

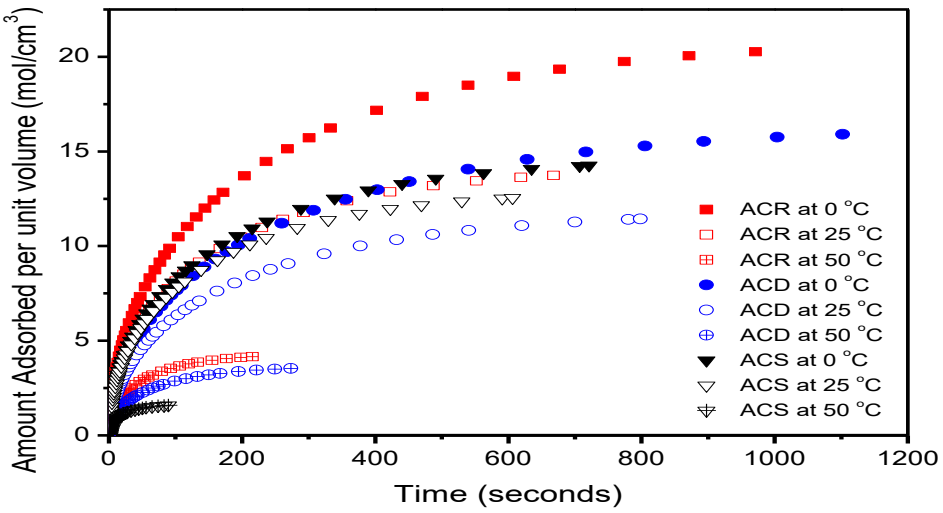


Figure 5.10 Plots of the amount adsorbed per unit volume versus time

It can be observed from Fig. 5.10 that, an increase in temperature increases the rate of adsorption, that is, the time taken to reach equilibrium. This observation is consistent with the three activated carbon samples. An increase in temperature results in the system attaining equilibrium quicker, but the adsorption capacity decreases with an increase in temperature. For sample ACR, an increase in temperature from 0 to 25 ^{o}C results in the system attaining equilibrium in a shorter time of 668 seconds compared to the 971 seconds the system took to attain equilibrium at 0 ^{o}C. On the contrary, the adsorbed amount per unit volume of the sample reduced from 20.3 mol/cm^3 to 13.7 mol/cm^3 as the temperature increased from 0 to 25 ^{o}C. Similarly, for Sample ACD, it took the system 1102 seconds to attain equilibrium at 0 ^{o}C with an adsorption capacity of 16 mol/cm^3. Whilst with an increase temperature of 25 ^{o}C, a shorter equilibrium time of 800 seconds and a reduced adsorption capacity of 11.4 mol/cm^3 was attained. In a similar way, for sample ACS, at 0 ^{o}C, the system attained equilibrium at 721 seconds with an adsorption capacity of 14.3 mol/cm^3, while at 25 ^{o}C, a shorter time of 606 seconds was achieved with a decreased adsorbed amount of 12.6 mol/cm^3. This can be attributed to the increase in diffusivity thus the reduction in adsorption capacity as reported by Do (1998).

It can be seen from Table 4.6 that, surface diffusivity increases with temperature, thus increasing the apparent diffusivity as temperature increases, noting that, apparent diffusivity is as a result of the contribution of surface diffusivity and pore diffusivity. The adsorption affinity (b) is another contributing factor to the rate of adsorption and time taken for the system to attain equilibrium. It is observed that, when the adsorption affinity is high, the apparent diffusivity is

small; as a result, the system will take longer to attain equilibrium. For sample ACR, an increase in its adsorption affinity from 0.023 to 0.085 results in the system attaining equilibrium in 668 seconds compared to the 216 seconds the system took to attain equilibrium at adsorption affinity of 0.023. This trend is consistent with the three activated carbon samples. For sample ACD, with adsorption affinity of 0.021, it took the system 273 seconds to attain an equilibrium, but with an increase adsorption affinity of 0.052, which is also as a result of a decrease in temperature, it took 800 seconds to reach equilibrium. In a similar way, for sample ACS, at an adsorption affinity of 0.029, it took 89 seconds to reach equilibrium, while at adsorption affinity of 0.117, it took 606 seconds to reach equilibrium.

The impact of the adsorption affinity on adsorption rate and time taken to attain equilibrium can be explained from the fact that adsorption affinity is a measure of how strong an adsorbate molecule is attracted to a surface of an adsorbent. Do (1998), and Azimi and Mirzaei (2012) reported that, the higher this attraction is, the higher the capacity, and consequently the penetration of the adsorbate into the adsorbent is slowed down as a result of the large uptake of the adsorbate molecule to the surface of the adsorbent. This therefore results in a longer time to attain equilibrium. It is also observed that sample ACS has the shortest time to achieve equilibrium of the three activated carbon samples, but also the lowest adsorption capacity compared to samples ACR and ACD.

5.6 Summary

The adsorption properties are the fundamental features of any adsorption system such as the ANG storage system. In this chapter, experimental adsorption isotherms using methane as the adsorbate, have been measured for three synthesized activated carbon samples. The adsorption isotherm of methane on the activated carbons revealed that the activated carbon synthesized from run-of-mine fine (ACR) has the highest adsorbed amount compared to activated carbon synthesized from coal discard (ACD) and slurry (ACS). This can be attributed to its larger surface area and pore volume. For the measured adsorbed amount, the activated carbon samples showed an improvement in adsorption capacity compared to other activated carbons derived from coal-related materials. The experimental data from methane adsorption was validated with three adsorption isotherm models, Langmuir, Toth and D-A models. The D-A model was found to provide the best fit for the three activated carbon samples with an average error of regression of 0.73, 0.81 and 0.92% for samples ACR, ACD and ACS, respectively. While the

D-A model offers a better fit than the Langmuir and Toth model, the Langmuir and Toth model adsorption data did not differ so much from the experimental data.

The heat of adsorption of the three activated carbon samples was evaluated at three different temperatures using the D-A isotherm model. The values obtained from the heat of adsorption are useful in the design of an effective thermodynamic scheme for the ANG storage system.
The adsorption kinetics was analysed by looking at the role of diffusion and its influence on the rate of adsorption. An increase in temperature was observed to cause an increase in diffusivity thereby reducing the time taken for the adsorption system to attain equilibrium. The adsorption properties obtained from this study provide the data needed in the designing of an ANG storage system. These properties are applied in the next chapter to simulate the methane adsorption onto the activated carbon samples using Aspen Adsorption (Adsim) software.

CHAPTER 6 MODELLING AND SIMULATION OF METHANE ADSORPTION ONTO ACTIVATED CARBON

6.1 Introduction

This chapter presents the modeling and simulation of a simple adsorbent system to replicate the ANG storage system. By understanding the thermal behavior in the adsorbent bed, considerable improvement is accomplished in both storage capacity and temperature management of the adsorption system.

This chapter focuses on applying the properties of the activated carbons produced in this study and considering the influence of different operating factors such as charging rate, and bed geometry (height to diameter ratios of the adsorbent bed) on designing an efficient and effective ANG storage system. The simulation is carried out by Adsim simulation software using a dynamic gas model. This model considers the real gas properties, as well as the adsorbent properties and methane adsorption uptake data. In Adsim, all the governing equations are resolved numerically. Unless otherwise stated, the simulation is conducted under the expected conditions for the ANG storage system, which is pressure of 35 bar and temperature of 25 ^{o}C.

6.2 Description of Storage System used for the Simulation

A schematic diagram used for the simulation of the ANG storage system is shown in Fig. 6.1. It consists of a storage tank with a small opening of radius (r1) at the top through which methane flows into the tank. It is filled and packed with activated carbon produced. Using a flow controller (FCV), the control of methane flow from the gas tank into the storage tank is maintained. A pressure gauge (PCV) is provided at the cylinder inlet to monitor the system pressure.

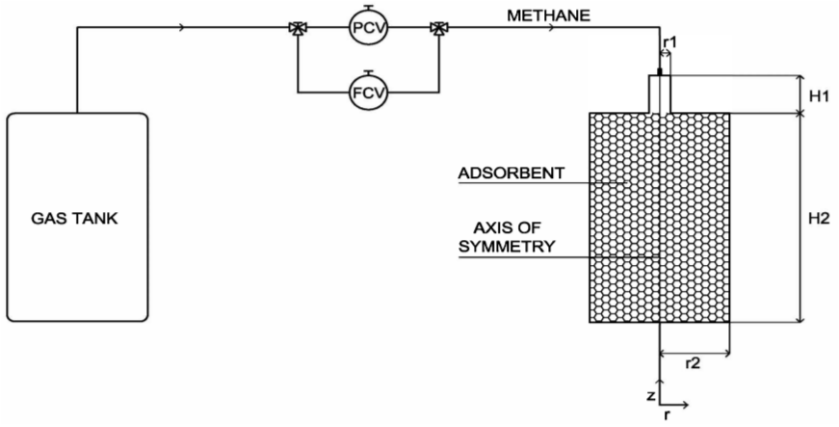


Figure 6.1 Schematic of an ANG system

6.3 Model Development

For the purpose of this simulation, a dynamic gas model of 1-D spatial dimension is used for transient heat and mass transfer analysis of the ANG system shown in Fig. 6.1. The model is analysed for various inlet and bed geometry variations. The process flow diagram of the system is shown in Fig. 6.2.

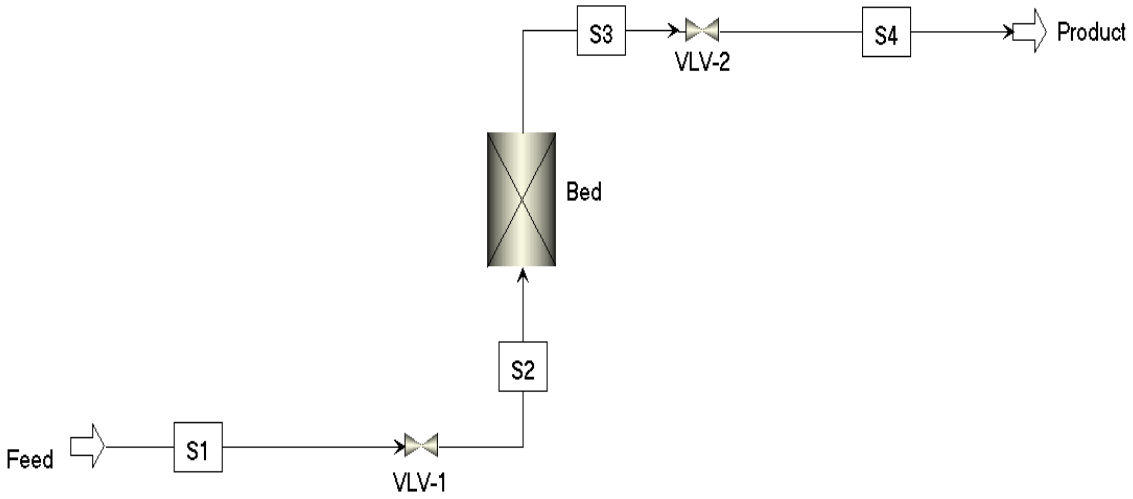


Figure 6.2 Process flow diagram (PFD) illustrating the ANG system in Adsim

6.3.1 Model Assumptions

To simplify the model the following assumptions are made:

- The gas phase is ideal;
- Gas phase pressure is constant;
- The properties of the activated carbons are assumed constant in the range of temperatures and pressures to be considered;
- Similar data to those used in other adsorbent bed simulations reported in the literature (Sahoo *et al.*, 2011) is used to facilitate comparison;
- The adsorbed gas phase and the solid adsorbent are locally in equilibrium with the gaseous phase;
- Intraparticle and film resistances to heat and mass transfer are neglected;
- The isosteric heat of adsorption is assumed to be constant;
- Enthalpy of mixing is negligible;
- Mass transfer is described using a lumped overall resistance based on the linear driving force;

- Mass transfer coefficients are constant; and
- Langmuir adsorption isotherm is used for its simplicity.

6.3.2 Governing Equations

The Langmuir model as represented by Eq. (5.3) is chosen as the adsorption isotherm for this simulation because of its simplicity.

The overall mass conservation in the porous adsorbent bed is provided by the following mass balance equation (Sahoo *et al.*, 2014, Patil and Sahoo, 2018);

$$\frac{\partial(\varepsilon_t \rho_g + \rho_b q)}{\partial t} + \nabla \cdot (\rho_g u_g) = 0 \quad (6.1)$$

where, ε_t is the total porosity, which consists of interparticle porosity (macropores), ε_b and intraparticle porosity (micropores), ε_p; ρ_b is the adsorbent bed density; ρ_g is the gas density; q is the concentration of gas adsorbed on the bed and u_g is the gas velocity.

The relationship between the total porosity, interparticle and intraparticle porosity is given as (Patil and Sahoo, 2018):

$$\varepsilon_t = \varepsilon_b + (1 - \varepsilon_b)\varepsilon_p \quad (6.2)$$

From the ideal gas law;

$$\rho_g = \frac{PM_g}{RT} \quad (6.3)$$

where, M_g is the molecular weight of gas; R is gas constant, P and T are pressure and temperature of gas respectively.

The gas velocity, u_g is evaluated using the Darcy law (Rahman *et al.*, 2011),

$$u_g = -\frac{K}{\mu_g} \nabla P \quad (6.4)$$

where, P is pressure, K is the permeability of the adsorbent bed, μ_g is gas viscosity.

The permeability, K is determined from the Ergun equation (Ergun, 1952);

$$K = \frac{4\varepsilon_b R_p^2}{180(1-\varepsilon_b)^2} \quad (6.5)$$

where, R_p is the particle radius of the adsorbent.

The energy balance for the adsorbent bed is given as (Rahman *et al.*, 2011, Patil and Sahoo, 2018);

$$C_{eff}\frac{\partial T}{\partial t} + \rho_g C_{pg} u_g \cdot \nabla T = \nabla \cdot (\lambda_{eff} \nabla T) + \rho_g \Delta H \frac{\partial q}{\partial t} \quad (6.6)$$

where, C_{eff} is the effective heat capacity; C_{pg} is gas specific heat; λ_{eff} is the effective thermal conductivity of the adsorbent bed and ΔH is the isosteric heat of adsorption.

The effective heat capacity, C_{eff} is obtained using the following equation (Sahoo *et al.*, 2011);

$$C_{eff} = (\varepsilon_t \rho_g + \rho_b q) C_{pg} + (1 - \varepsilon_t) \rho_s C_{ps} \quad (6.7)$$

where, ρ_s is the solid bed density without porosity and C_{ps} is adsorbent specific heat.

The adsorbent bed density, ρ_b is defined as (Patil and Sahoo, 2018):

$$\rho_b = (1 - \varepsilon_t) \rho_s \quad (6.8)$$

The effective thermal conductivity of the bed is obtained as (Sahoo and Ramgopal, 2016);

$$\lambda_{eff} = \varepsilon_t \lambda_g + (1 - \varepsilon_t) \lambda_s \quad (6.9)$$

where, λ_g and λ_s are the thermal conductivities of gas and adsorbent respectively.

The thermophysical parameters of the activated carbon samples (ACR, ACD, and ACS) and methane used in the simulation are listed in Table 6.1. The Adsim specifications as input in the simulation are presented in Appendix D. The Langmuir adsorption parameters used are listed in Table 5.3 at 25 ^{o}C. The gas properties for methane (density, specific heat capacity, thermal conductivity, and viscosity) are obtained from Aspen plus (V8.8) integrated NIST ThermoData Engine (TDE) database.

Table 6.1 Thermophysical parameters used in Adsim simulation

Parameter	Value
Adsorbent (ACR)	
BET surface area (m^2/g)	1925
Total pore volume (cm^3/g)	1.29
Average pore diameter (Å)	29
Density (kg/m^3)	2349
Porosity, ε_b	0.3
Darcy permeability, K (m^2)	3.2×10^{-7}
Specific heat capacity, C_{ps} (J/kg/K)	877
The average heat of adsorption, ΔH (J/mol)	19,200
Height of adsorbent bed, H_b (m)	0.2
Internal diameter of adsorbent bed, D_b (m)	0.02
Adsorbent (ACD)	
BET surface area (m^2/g)	1826
Total pore volume (cm^3/g)	1.252
Average pore diameter (Å)	26.6
Density (kg/m^3)	2242
Porosity, ε_b	0.17
Darcy permeability, K (m^2)	1.4×10^{-7}
Specific heat capacity, C_{ps} (J/kg/K)	841
The average heat of adsorption, ΔH (J/mol)	18,700
Adsorbent (ACS)	
BET surface area (m^2/g)	1485
Total pore volume (cm^3/g)	1.04
Average pore diameter (Å)	25.1
Density (kg/m^3)	2491
Porosity, ε_b	0.25
Darcy permeability, K (m^2)	2.5×10^{-7}
Specific heat capacity, C_{ps} (J/kg/K)	715
The average heat of adsorption, ΔH (J/mol)	21,200
Methane Gas	
Molecular weight	16
Density (kg/m^3)	0.656
Viscosity (Pa-s)	1.25×10^{-5}
Specific heat (J/kg/K)	2450
Thermal conductivity (W/m/K)	0.0343
Flowrate (mol/min)	0.5

6.4 Results and Discussion

Simulations were performed at fixed flow rates of 0.5mol/min and 1mol/min for an adsorbent bed filled with the activated carbons produced. The source of methane is considered to be a gas tank at a pressure of 35 bar and a temperature of 298 K. All simulations correspond to the thermophysical properties specified in Table 6.1 unless otherwise stated.

The simulation is kept constant at 298 K and information of adsorbed quantities in mol/g are obtained at different pressures to obtain the adsorption isotherm shown in Fig. 6.3. The information obtained from the simulation model of Langmuir offers a good fit to the experimental data for the three activated carbon samples.

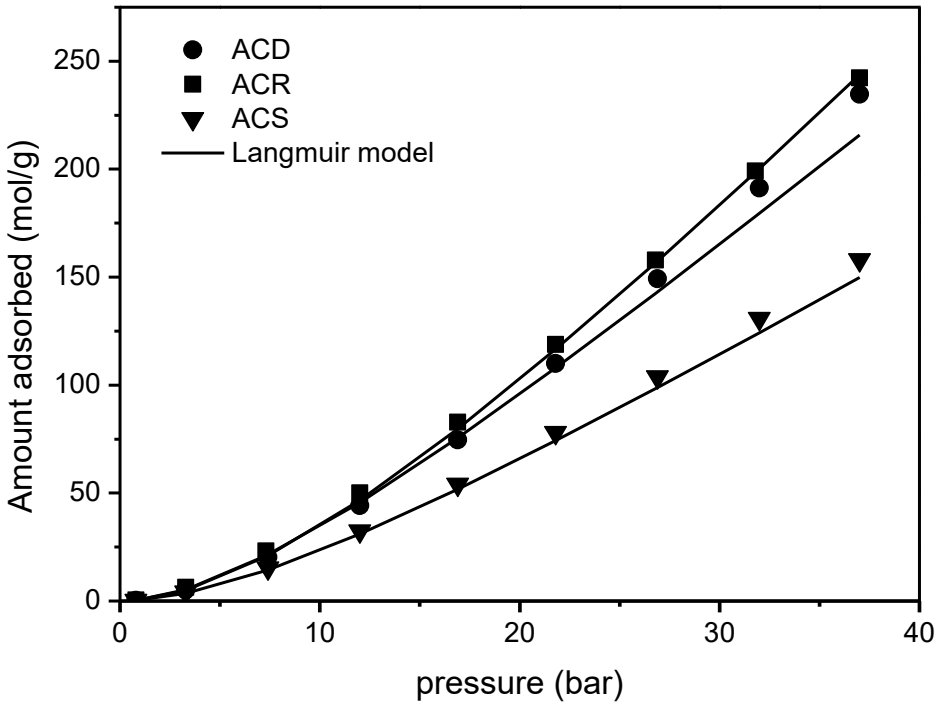


Figure 6.3 Fitting of the experimental adsorption data with the Langmuir model for methane adsorption on activated carbons produced

6.4.1 Pressure profile

Pressure distributions obtained from the simulations as shown in Fig. 6.4, reveals an almost uniform distribution of pressure in the bed for the various adsorbents. The samples quickly equilibrate to the inlet pressure (35 bar) within 2 to 3 minutes. This can be attributed to the adsorbent's high permeability. Sample ACR ($K = 3.2\times10^{-7}$) has the largest permeability, thus attain quicker pressure equilibration, then sample ACS ($K=2.5\times10^{-7}$) and sample ACD

($K=1.4\times10^{-7}$). These results are consistent with the pressure distributions reported from other simulations in highly permeable activated carbon adsorption beds (Mota *et al.*, 1997, Bastos-Neto *et al.*, 2005, Sahoo *et al.*, 2011).

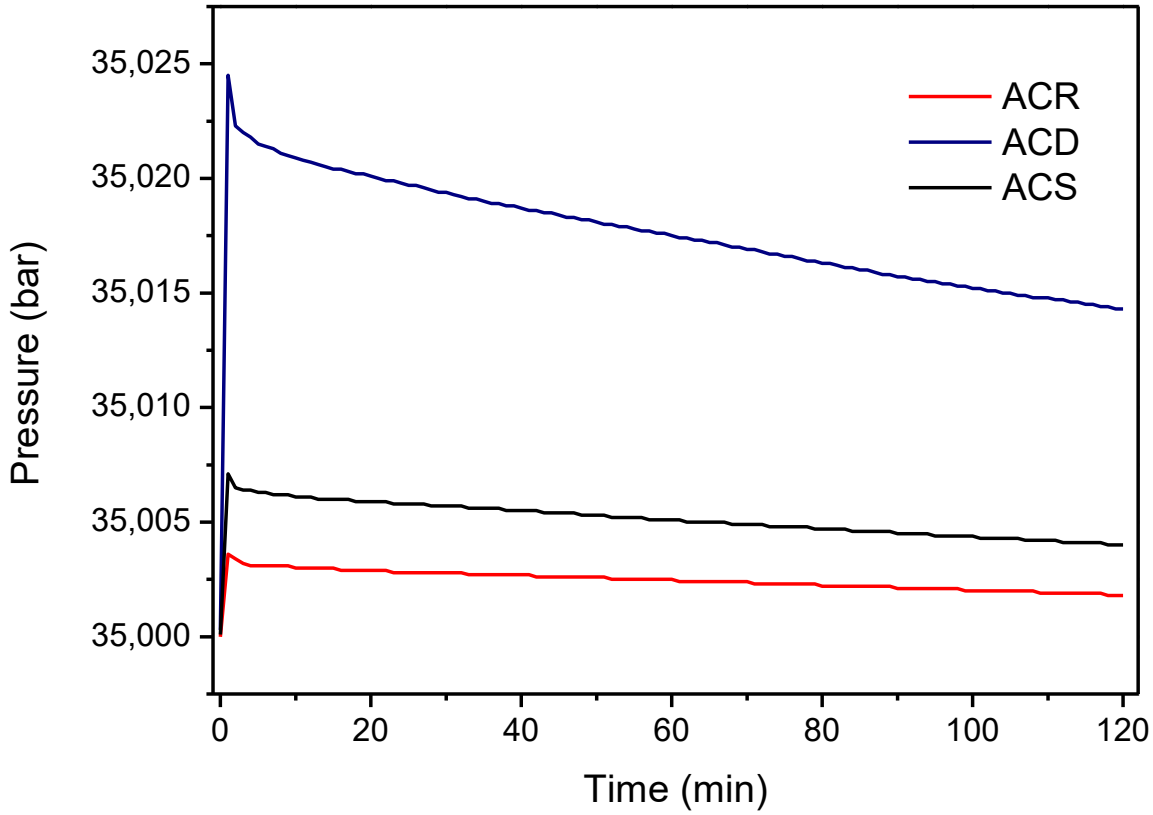


Figure 6.4 Simulated pressure profiles of the activated carbon samples as a function of time

Fig. 6.5 to 6.7 shows simulated pressure profiles along the bed height during the adsorption process. The pressure varies marginally along the height of the bed but equalizes with time. However, as the gas diffuses through the pores of Samples ACR and ACS, a small pressure gradient is observed. This is ascribed to these samples' high permeability, which allows the gas to flow rapidly through the sample pores, thus creating the noticeable gradients as time progresses beyond 60 minutes as shown in Fig. 6.5 and 6.6. The low permeability of sample ACD allows the gas to flow steadily through the pores without any gradient as shown in Fig. 6.7. A similar observation was reported by Rahman *et al.* (2011).

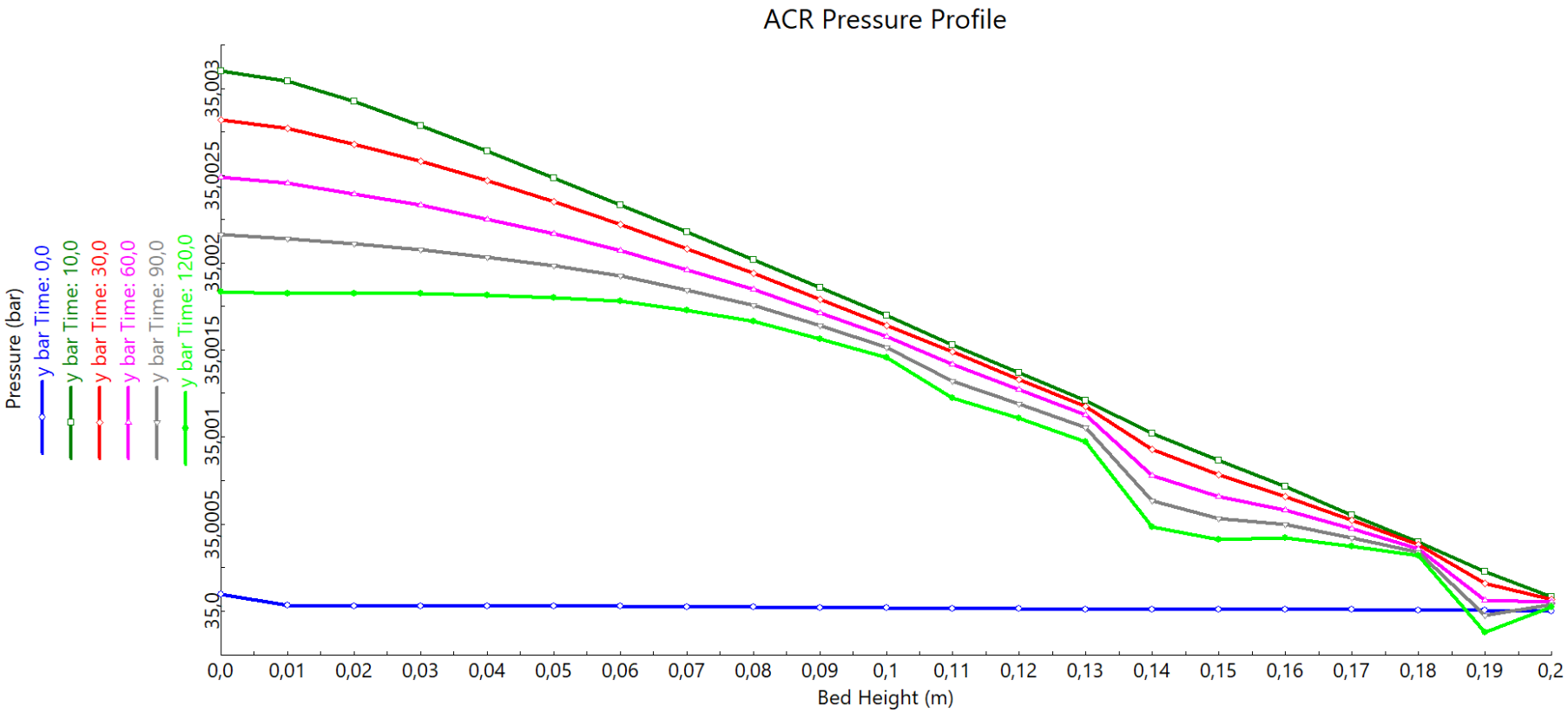


Figure 6.5 Simulated pressure profiles inside the ACR adsorbent bed along the bed height

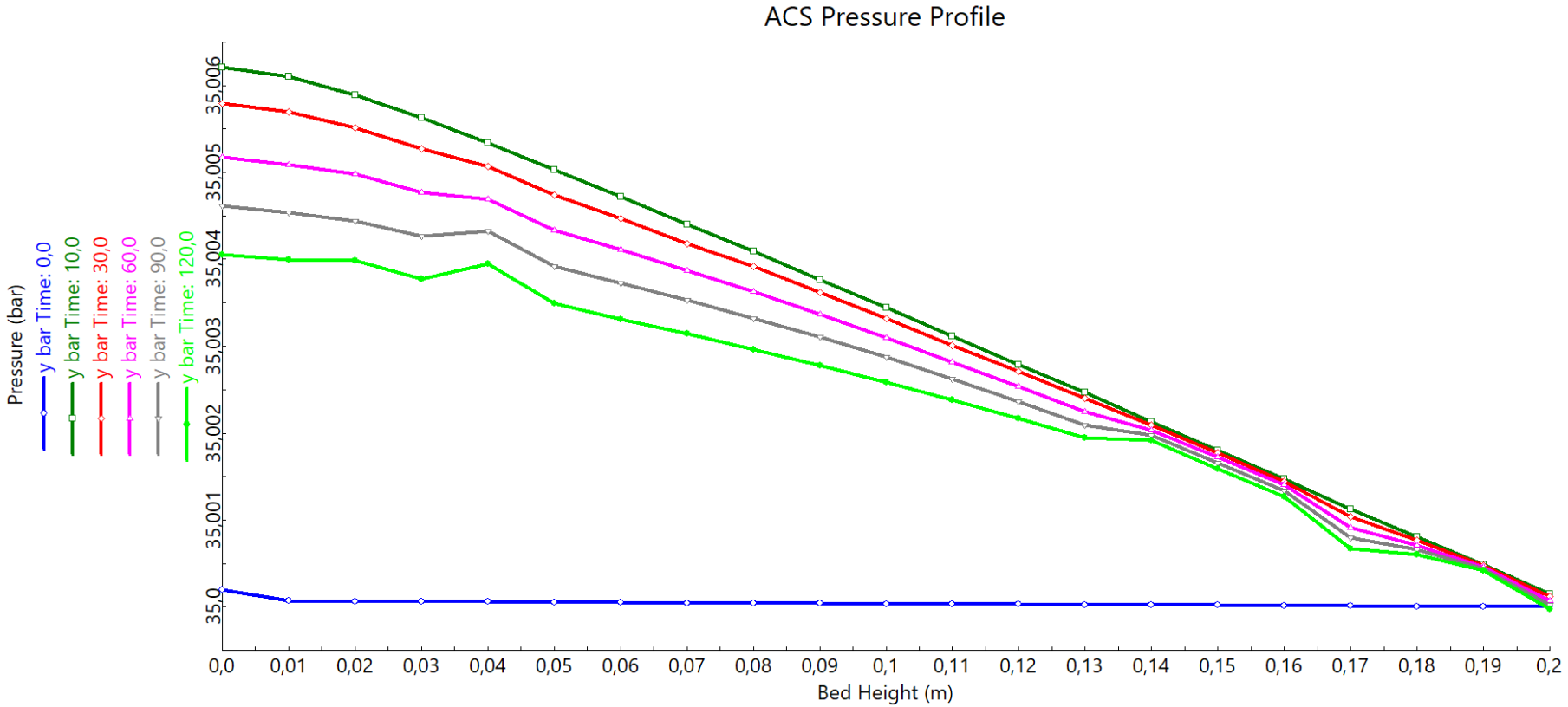


Figure 6.6 Simulated pressure profiles inside the ACS adsorbent bed along the bed height

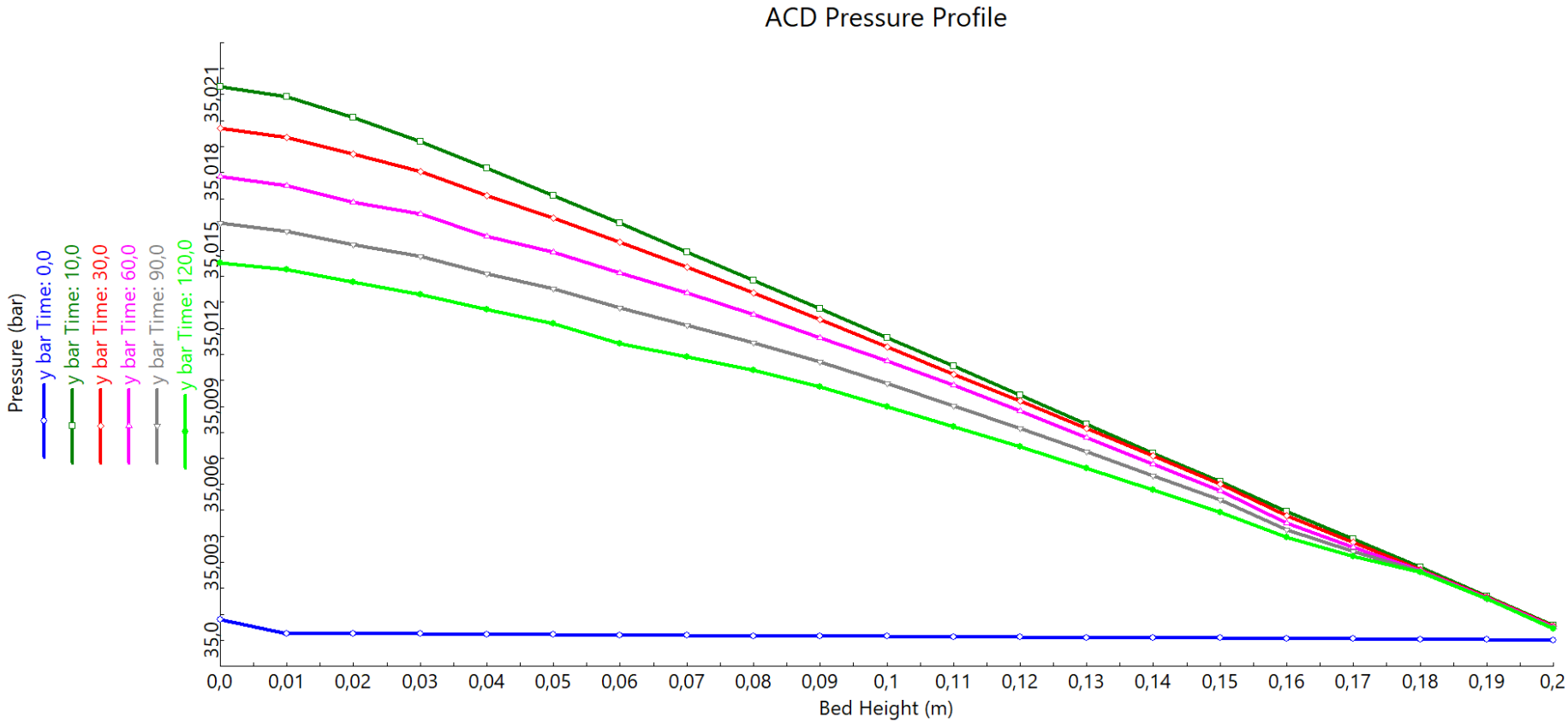


Figure 6.7 Simulated pressure profiles inside the ACD adsorbent bed along the bed height

6.4.2 Effect of Flowrate on Adsorbent Bed Temperature and Concentration

To assess the impact of different filling conditions on the adsorbent bed storage capacity, simulations are carried out at constant pressure and temperature of 35 bar and 298 K for inlet flow rates of 0.5 mol/min, 1 mol/min and 2 mol/min, respectively. From Fig. 6.8, at the early point of the charge cycle, peak temperatures are observed. The peak temperature is constant for about 24 minutes before it starts to drop for a flow rate of 0.5 mol/min. It requires about 15 minutes of steady peak temperature for the flow rate of 1 mol/min before temperature decrease is noticed, while the peak temperature was constant for the flow rate of 2 mol/min for only 4 minutes before temperature drop. From Fig. 6.8, it is evident that after the initial steady temperature period, the temperature starts to drop because the heat loss to the surrounding is much greater than the heat evolved as a result of the adsorption taking place on the bed.

Overall, the plots of Fig. 6.8 confirm the rapid decrease in adsorbent bed temperature as the gas inlet flow rate increases. This rapid drop in temperature creates thermal instability on the adsorbent bed that impacts the bed's storage capacity. This observation is in agreement with the study reported by Rios *et al.* (2011). The study reported that, due to a rapid drop in temperature as a result of an increase in flow rate, there was a significant reduction in the storage capacity of a granular activated carbon bed. To solve the problem of thermal instability, Rahman *et al.* (2011) proposed the addition of a heat exchanger to the adsorption system to provide quicker filling time from higher flow rate. In addition, Patil and Sahoo (2018) suggested that graphite powder be added to the adsorbent bed to minimize the rapid drop in temperature, which reduces thermal instability and thus enhances the storage capacity of the bed.

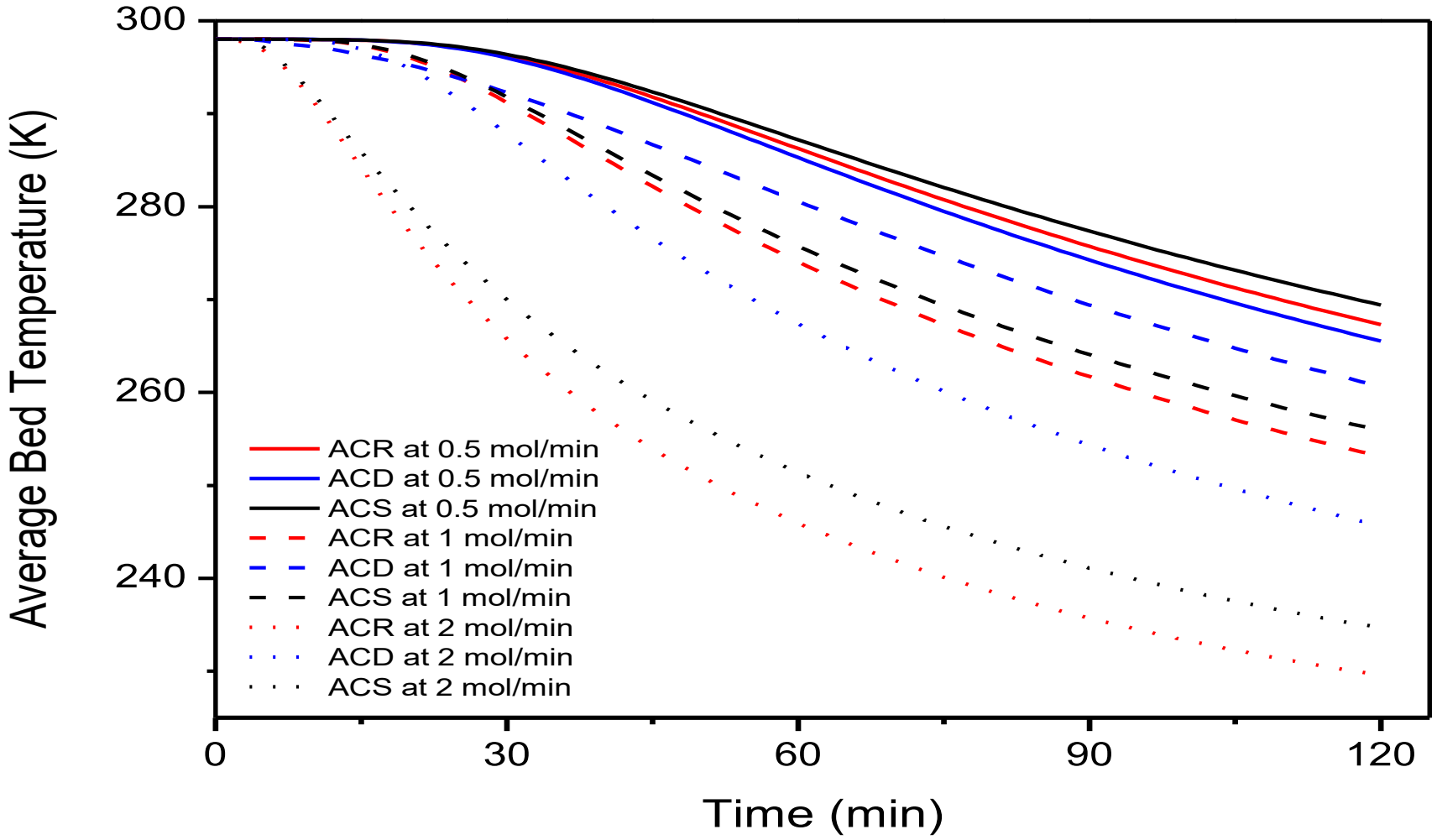


Figure 6.8 Average temperature distribution as a function of time for different adsorbent bed

Fig. 6.9 shows the average bed concentration of the different adsorbent beds at various flowrates. From the figure, it is evident that for high flow rate (2 mol/min), the bed becomes saturated with methane in 18 minutes for ACR bed, 22 minutes for ACD bed and 28 minutes for ACS bed, whereas for a low flow rate of 0.5 mol/min it takes 66 minutes for ACD bed, 72 minutes for ACS bed and 75 minutes for ACR bed to saturate. This infers that the lower the flowrate, the longer it takes for the adsorbent bed to be fully saturated with methane. This observation is consistent with a similar study which states that a low flow adsorption system operates close to the equilibrium state and takes longer to saturate (Sahoo *et al.*, 2011).

The bulk concentration of methane on the adsorbent bed is lower at high flow rates compared to a reduced flow rate. From Fig 6.9, more storage capacity for the three adsorbent beds is observed at a flow rate of 0.5 mol/min and the storage capacity is observed to decrease as the flow rate increases. This can be ascribed to the thermal instability owing to the rapid drop in temperature as shown in Fig. 6.8.

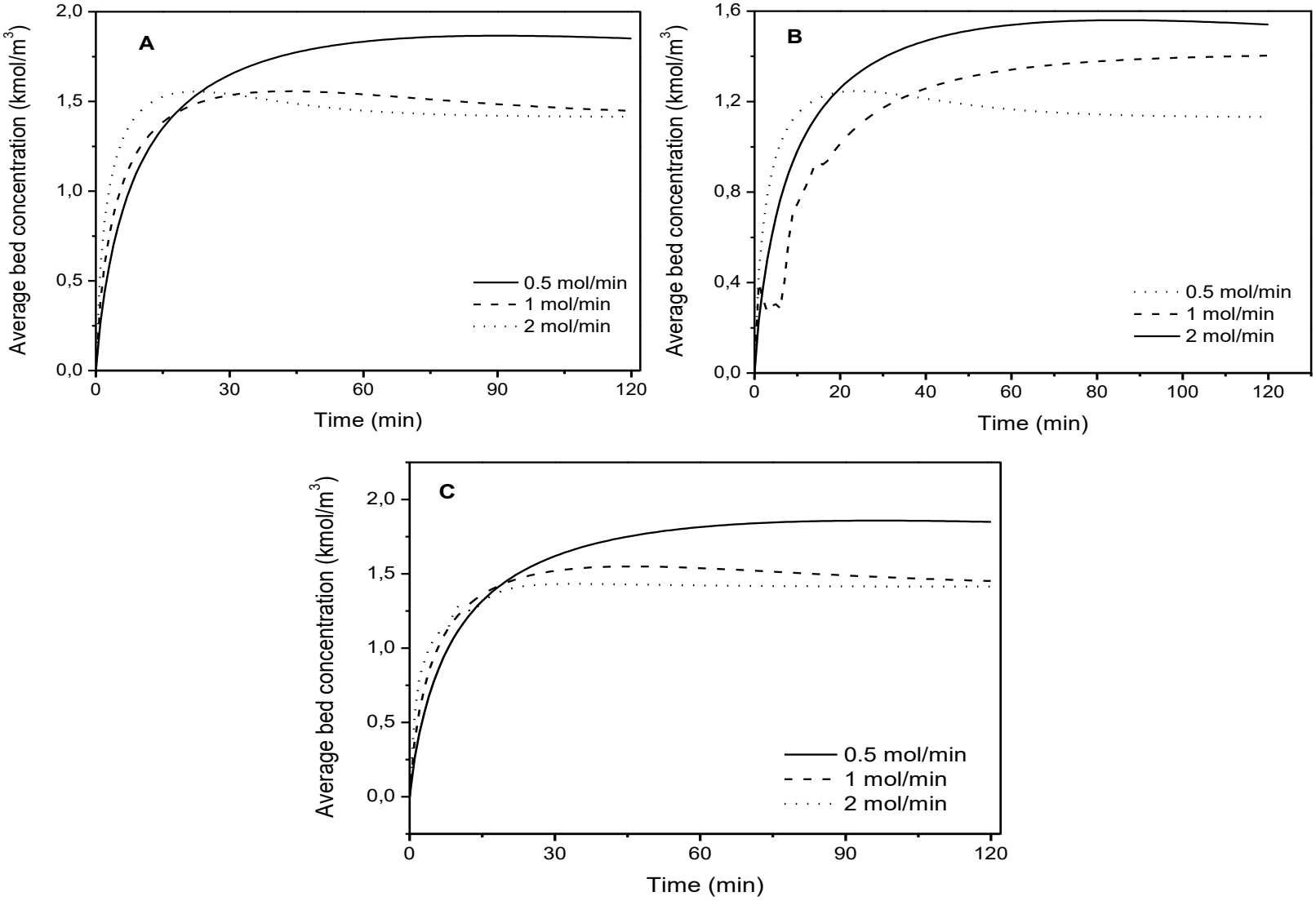


Figure 6.9 Average bed concentration as a function of time (A) ACR adsorbent bed (B) ACD adsorbent bed (C) ACS adsorbent bed

6.4.3 Effect of Adsorbent Bed Geometry on Temperature and Concentration

The adsorbent bed's thermal behavior was simulated with various bed diameter (D) to bed height (H) ratios as shown in Table 6.2. For the three adsorbents understudy, the adsorbent bed is subjected to a fixed inlet flow rate of 2 mol/min and analysed for different D/H ratios. In the simulation, as discussed in previous sections, the D/H ratio of 0.1 (bed height of 0.2 m and bed diameter of 0.02 m) is used. The bed height was increased to 0.4 m to obtain the D/H ratio of 0.05 while maintaining the bed diameter at 0.02 m. The bed diameter was increased to 0.04 m for D / H of 0.2 while retaining the bed height at 0.2 m.

Table 6.2 Physical dimension of the Adsorbent Bed for various D/H ratio

H (m)	**D (m)**	**D/H**
0.4	0.02	0.05
0.2	0.02	0.1
0.2	0.04	0.2

H – Height of adsorbent bed; D – Diameter of the adsorbent bed

Fig. 6.10 displays the temperature and concentration distributions of different adsorbent beds at various D/H ratios. With an increase in D/H ratios, the rapid drop in adsorbent bed temperature is minimized. This results in a higher average bed concentration for the three adsorbents.

Clearly increasing the adsorbent bed diameter twice over gives the adsorbent beds improvement in thermal stability as shown in Figure 6.10, as the fast drop in temperature is considerably reduced. For the three adsorbent beds, the increase in bed diameter from 0.02 m to 0.04 m shows a reduction in a temperature drop. The bed temperature for the ACR bed was observed to drop from 298 K to 246 K (ΔT = 52 K) at bed diameter of 0.02 m, but on increasing the bed diameter to 0.04 m, the temperature dropped from 298 K to 266 K (ΔT = 32 K). Similarly, the temperature drop across the ACD bed reduced from 56 K to 34 K, while the temperature drop of the ACS bed reduced from 63 K to 30 K. This can be ascribed to the bigger bed diameter that provides more exposed surface area for heat transfer, thus improving thermal stability.

As seen from the concentration distribution plot of Fig. 6.10, this improvement in bed thermal stability results in enhanced gas adsorption on the adsorbent bed. As a result of enhanced thermal stability arising from bigger bed diameter, an approximately 9% increase in maximum bed concentration is observed for the three adsorbent beds. On the other hand, while the height of the bed increased, the thermal stability of the adsorbent beds was marginally improved. However, the effect of increasing bed height for the three adsorbent beds does not have any significant impact on the average bed concentration.

Based on the different configurations examined in this study, the highest adsorption capacity with minimal thermal instability is an adsorbent bed with a D/H ratio of 0.2. Thus, storage capacity can be enhanced by selecting a suitable diameter-to-height ratio for improved thermal stability.

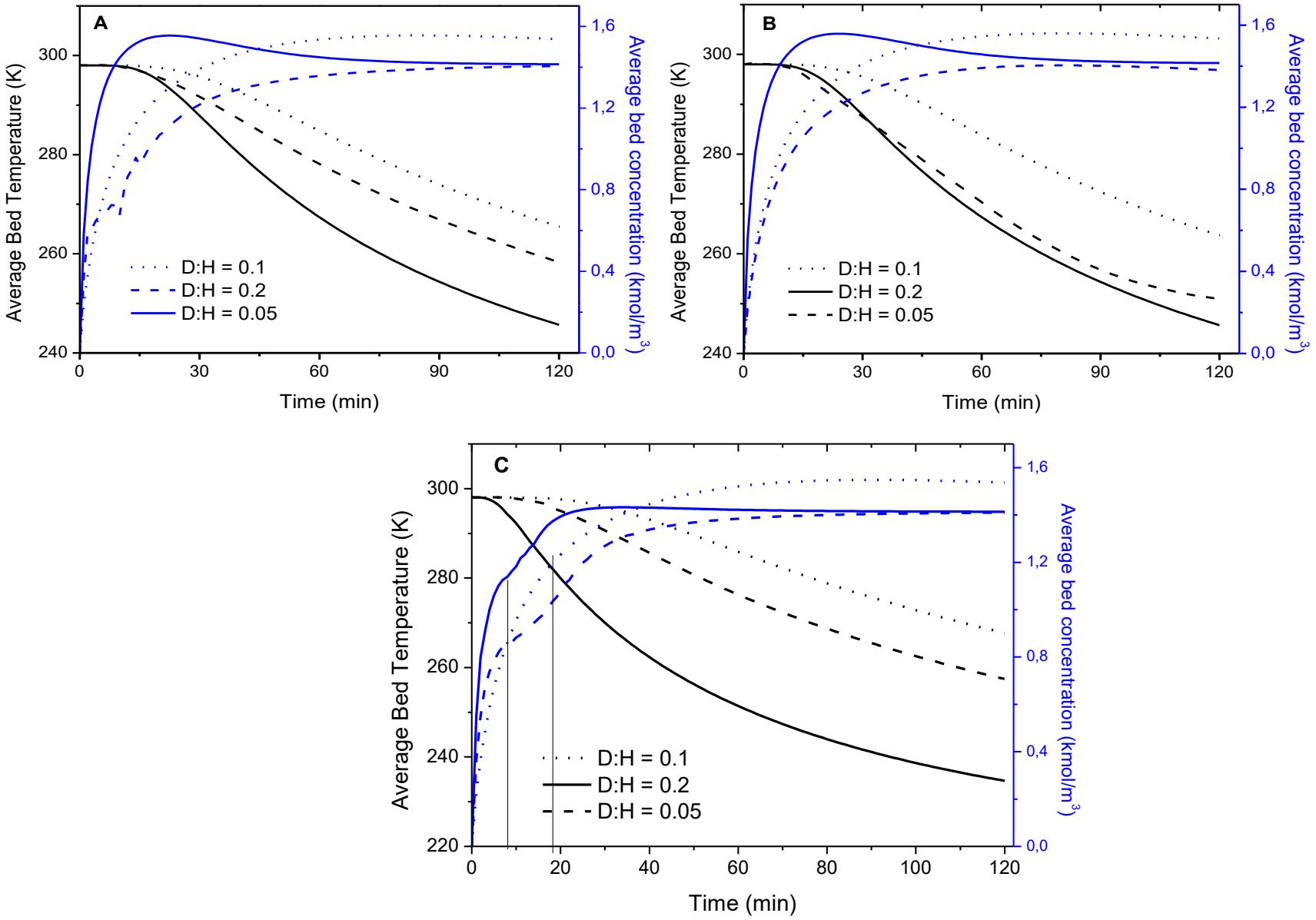


Figure 6.10 Average bed temperature and concentration as a function of time for different D/H ratio (A) ACR bed (B) ACD bed (C) ACS bed

6.5 Summary

To simulate the ANG storage system, a simple adsorption system was used to analyse the thermal behavior of an adsorbent bed using the developed activated carbons. Simulations were carried out using a dynamic gas model to simulate a variable flow rate and different bed configurations. All simulations are carried out using Aspen Adsorption (Adsim) software (V10.0).

Simulation findings show uniform pressure distribution during the charging process due to the high permeability of the adsorbent beds. The results of the simulation also revealed that the storage capacity is governed by the thermal stability of the bed. Thermal instability is observed with a high flow rate of methane into the system. A high flow rate shortens the filling time, but with lower storage capacity as a consequence of the thermal instability.

Simulations were carried out for different D/H ratios (0.05 to 0.2). The results show that the storage capacity can be improved by varying the D/H ratios. By increasing the adsorbent bed diameter, the maximum adsorbed gas concentration increased by 9%. This is because there is an improvement in bed thermal stability. Higher storage capacity and much improved thermal stability were observed at a D/H ratio of 0.2 for an inlet flow condition of 2 mol/min.

It can be concluded that the efficiency of an ANG storage system depends primarily on the appropriate choice of inlet flow conditions and storage tank configuration and also on the properties of the adsorbent.

CHAPTER 7 CONCLUSIONS AND RECOMMENDATIONS

7.1 Introduction

The dumping of coal waste is one of the problems facing the coal mining sector, in particular, its adverse environmental and public health effects. In addition to the coal waste that has already accumulated over the years, more is generated annually through coal mining and beneficiation processes. For a better understanding of the problem, this research reviewed coal waste sources, the environmental issues of coal waste and the effect on public health, and the need to beneficiate coal waste, in order to recover the misplaced carbon for reuse. Numerous studies have been conducted in the past to recover and utilize this resource for different applications, but none of these earlier researches have studied the synthesis of activated carbons from South African coal waste for application in natural gas storage.

In this study, South African coal wastes were synthesized to produce a largely porous activated carbons with high surface area for natural gas storage. In addition, the ANG storage technology proposed for the storage and transportation of natural gas as a feasible option for LNG and CNG was simulated and designed in this study. With the outcome of this research, an ANG storage system designed could be a practical option for solving and reducing some of the challenges facing the industry. The four objectives set in this study were achieved successfully and the major findings in this research outlined below.

7.2 Major Findings of this Research

1. Analysis of South African coal waste samples characteristics reveal the following:
    - The three coal waste samples contain a large proportion of fixed carbon content in excess of 40%, an indication of its suitability for producing activated carbon.
    - The three samples contain 40 to 49% inertinite maceral, and are classified as a low rank high ash South African coal
2. Findings from the synthesis and characterization of the activated carbon samples are as follows:
    - The impact of temperature (T) and KOH weight ratio (W) on the quality of the activated carbon samples was established. Increasing the temperature and KOH weight ratio was found to increase the surface area and pore volume of the activated carbon.

- The best-activated carbons from each of the coal waste samples were obtained from a temperature of 800 ^{o}C and KOH to sample ratio of 4:1. The best from sample A has a surface area of 1925.34 m^2/g and pore volume of 1.290 cm^3/g, while the best from sample B has surface area of 1826.41 m^2/g and pore volume of 1,252 cm^3/g and the best from sample C has a surface area of 1484.96 m^2/g and pore volume of 1.042 cm^3/g.
- The statistical analysis confirmed that the two factors (T and W) are significant parameters that regulate the texture of the activated carbon samples and thus their natural gas storage efficiency.
- Nitrogen adsorption at 77 K reveals a correlation between storage capacity and porous texture of the activated carbons. The storage capacity was found to be directly proportional to surface area and pore volume.
- The findings of other characterization techniques provided insight into the potential of activated carbons from coal waste for natural gas storage. SEM/EDS analysis showed the development of pores and high carbon element. The XRD assessment revealed a broad diffraction background for the three activated carbons produced, an indication of a carbon material that is mainly amorphous. The PSD showed that the activated carbon samples consist of micropores and mesopores.

3. The findings from methane/activated carbon samples adsorption isotherms measured for temperatures ranging from 0 to 50 °C and pressures up to 40 bar are as follows:
    - Activated carbon from run-of-mine fines (ACR) has the highest amount of methane adsorbed among the three activated carbon samples due to its surface area and pore volume.
    - Among the three adsorption isotherm models used to validate the methane adsorption data, the D-A model provided the best fit for the three activated carbon samples (ACR, ACD, and ACS) with an average regression error of 0.73, 0.81 and 0.92% respectively.
    - The activated carbons were observed to have improved methane adsorption capacity in the range of 47 to 81% higher than coal-related activated carbons in previous studies by Loh *et al.* (2010b) and Martin *et al.* (2011).
    - The adsorption kinetics of the methane/activated carbon system showed a strong dependence on the diffusion rate. The adsorption kinetics were evaluated taking

into account the role of diffusion and its impact on rate of adsorption. An increase in temperature was observed to cause an increase in diffusivity, thus reducing the time taken for the adsorption system to attain equilibrium.

4. Simulation study on the transient temperature and concentration profiles of the activated carbon adsorption bed was performed using Aspen Adsorption (Adsim). The findings from the simulation are as follows:
    - Uniform pressure distribution was observed throughout the bed due to the high permeability of the activated carbon samples.
    - A high flow rate causes thermal instability to the adsorbent bed, thus impacting negatively on the storage capacity.
    - By increasing the adsorbent bed diameter, high storage capacity can be achieved with a high flow rate. This provides additional surface area for effective heat transfer to minimize thermal instability and improve storage capacity by about 9%.
    - The efficiency of the system depends on the appropriate choice of flow rate and geometry of the adsorbent bed.

From the findings above, activated carbons with large surface area and pore volume can be developed from South African coal waste and used in the ANG storage system as adsorbents. This minimizes the environmental and public health impact of coal waste and also decreases the cost of adsorbents for the ANG storage system, thus making the ANG system more commercially viable.

7.3 Recommendations for Future Research

This section offers suggestions for further research. The suggestions are based on the research findings and observations. The recommendations are as follows:

- The potential for decreased use of chemical reagents by combining physical and chemical processes of activation should be studied
- Assess the potential of the hydrothermal activation method to produce activated carbon from South African coal waste for gas storage application.
- Evaluate how the integration of heat exchanger to the storage system will enhance thermal stability in order to achieve higher storage capacity.

- The adsorption isotherm information measured in this research can be evaluated at cryogenic temperatures for the methane/activated carbon pair to study the impact of low-temperature gas charge in the ANG storage system. These can be useful when considering LNG as the gas source for the ANG storage system.

REFERENCES

Aaron, D. & Tsouris, C. 2005. Separation of CO_2 from Flue Gas: A Review. *Separation Science and Technology,* 40**,** 321-348.

Abdalla, A. N., Tao, H., Bagaber, S. A., Ali, O. M., Kamil, M., Ma, X. & Awad, O. I. 2019. Prediction of emissions and performance of a gasoline engine running with fusel oil–gasoline blends using response surface methodology. *Fuel,* 253**,** 1-14.

Ahmadpour, A. & Do, D. 1996. The preparation of active carbons from coal by chemical and physical activation. *Carbon,* 34**,** 471-479.

Al-Muhtaseb, S. A. & Ritter, J. A. 1999. Roles of surface heterogeneity and lateral interactions on the isosteric heat of adsorption and adsorbed phase heat capacity. *The Journal of Physical Chemistry B,* 103**,** 2467-2479.

Alcañiz-Monge, J., Lozano-Castelló, D., Cazorla-Amorós, D. & Linares-Solano, A. 2009a. Fundamentals of methane adsorption in microporous carbons. *Microporous and mesoporous materials,* 124**,** 110-116.

Alcañiz-Monge, J., Lozano-Castelló, D., Cazorla-Amorós, D. & Linares-Solano, A. 2009b. Fundamentals of methane adsorption in microporous carbons. *Microporous and mesoporous materials,* 124**,** 110-116.

Alhasan, S., Carriveau, R. & Ting, D.-K. 2016. A review of adsorbed natural gas storage technologies. *International Journal of Environmental Studies,* 73**,** 343-356.

Amosa, M. K., Jami, M. S., Ma'an, F., Jimat, D. N. & Muyibi, S. A. 2015. A two-step optimization and statistical analysis of COD reduction from biotreated POME using empty fruit bunch-based activated carbon produced from pyrolysis. *Water Quality, Exposure and Health,* 7**,** 603-616.

Antoszczyszyn, T. & Michalska, A. 2016. The potential risk of environmental contamination by mercury contained in Polish coal mining waste. *Journal of Sustainable Mining,* 15**,** 191-196.

Arami-Niya, A., Daud, W. M. a. W. & Mjalli, F. S. 2011. Comparative study of the textural characteristics of oil palm shell activated carbon produced by chemical and physical activation for methane adsorption. *Chemical Engineering Research and Design,* 89**,** 657-664.

Aspen 2012. Aspen Adsim 2012.0: Adsorption Reference Guide. *In:* Technology, A. (ed.) version 10.0 ed.

Atoyebi, T. 2010. The preferred Natural Gas Conservation Option. *Underground Storage of Natural Gas", SPE Paper,* 136984.

Azargohar, R. & Dalai, A. 2005. Production of activated carbon from Luscar char: experimental and modeling studies. *Microporous and mesoporous materials,* 85**,** 219-225.

Azimi, A. & Mirzaei, M. 2012. Determination of effective diffusion coefficient of methane adsorption on activated carbon. *World Applied Sciences Journal,* 17**,** 1109-1114.

Badakhshan, A. & Pooladi, E. M. Gas hydrates a new means for natural gas storage and transportation. 16th World Petroleum Congress, 2000. World Petroleum Congress.

Barrett, E. P., Joyner, L. G. & Halenda, P. P. 1951. The determination of pore volume and area distributions in porous substances. I. Computations from nitrogen isotherms. *Journal of the American Chemical society,* 73**,** 373-380.

Bastos-Neto, M., Torres, A. E. B., Azevedo, D. C. & Cavalcante, C. L. 2005. A theoretical and experimental study of charge and discharge cycles in a storage vessel for adsorbed natural gas. *Adsorption,* 11**,** 147-157.

Basumatary, R., Dutta, P., Prasad, M. & Srinivasan, K. 2005. Thermal modeling of activated carbon based adsorptive natural gas storage system. *Carbon,* 43**,** 541-549.

Beckner, M. & Dailly, A. 2015. Adsorbed methane storage for vehicular applications. *Applied Energy,* 149**,** 69-74.

Belaid, M., Falcon, R., Vainikka, P. & Patsa, K. Potential and technical basis for utilising coal beneficiation discards in power generation by applying circulating fluidised bed boilers. 2nd Int. Conference on Chemical, Ecology and Environmental Sciences, June, 2013. 17-18.

Bénard, P. & Chahine, R. 2007. Storage of hydrogen by physisorption on carbon and nanostructured materials. *Scripta Materialia,* 56**,** 803-808.

Biloe, S., Goetz, V. & Mauran, S. 2001. Characterization of adsorbent composite blocks for methane storage. *Carbon,* 39**,** 1653-1662.

Birkholz, M. 2006. *Thin Film Analysis by X-Ray Scattering,* Weinheim, Germany, WILEY-VCH Verlag GmbH & Co.

Blanco, A. G., De Oliveira, J. A., López, R., Moreno-Piraján, J., Giraldo, L., Zgrablich, G. & Sapag, K. 2010. A study of the pore size distribution for activated carbon monoliths and their relationship with the storage of methane and hydrogen. *Colloids and Surfaces A: Physicochemical and Engineering Aspects,* 357**,** 74-83.

Borowski, G. & Hycnar, J. J. 2013. Utilization of fine coal waste as a fuel briquettes. *International Journal of Coal Preparation and Utilization,* 33**,** 194-204.

Bp 2016. BP Statistical Review of World Energy. 65th ed. United States.

Bp 2017. BP Energy Outlook. *BP Energy Outlook.* 2017 ed.: BP Plc.

Bp 2019. BP Statistical Review of World Energy 2019. *2019 Edition.* London, United Kingdom: BP p.l.c.

Brunauer, S., Emmett, P. H. & Teller, E. 1938. Adsorption of gases in multimolecular layers. *Journal of the American chemical society,* 60**,** 309-319.

Chakraborty, A., Saha, B. B., Ng, K. C., Koyama, S. & Srinivasan, K. 2009. Theoretical insight of physical adsorption for a single-component adsorbent+ adsorbate system: I. Thermodynamic property surfaces. *Langmuir,* 25**,** 2204-2211.

Chen, M., Zhu, L., Wu, Y., Fu, T. & Ran, Y. 2014. Enrichment of heavy metals in coal gangue by puff balls and mechanism research. *Chinese Journal of Geochemistry,* 33**,** 419-424.

Chiang, H.-L., Huang, C. & Chiang, P. 2002. The surface characteristics of activated carbon as affected by ozone and alkaline treatment. *Chemosphere,* 47**,** 257-265.

Choi, W.-J., Seo, J.-B., Jang, S.-Y., Jung, J.-H. & Oh, K.-J. 2009. Removal characteristics of CO_2 using aqueous MEA/AMP solutions in the absorption and regeneration process. *Journal of Environmental Sciences,* 21**,** 907-913.

Chong, Z. R., Yang, S. H. B., Babu, P., Linga, P. & Li, X.-S. 2016. Review of natural gas hydrates as an energy resource: Prospects and challenges. *Applied energy,* 162**,** 1633-1652.

Clarke, S. & Debruyn, J. 2012. Vehicle conversion to natural gas or biogas. *Ontario Ministry of Agriculture and Food***,** 12-043.

Cohen, E. R. 2007. *Quantities, units and symbols in physical chemistry,* Royal Society of Chemistry.

Cuhadaroglu, D. & Uygun, O. A. 2008. Production and characterization of activated carbon from a bituminous coal by chemical activation. *African journal of Biotechnology,* 7.

Dağdelen, S., Acemioğlu, B., Baran, E. & Koçer, O. 2014. Removal of remazol brilliant blue R from aqueous solution by pirina pretreated with nitric acid and commercial activated carbon. *Water, Air, & Soil Pollution,* 225**,** 1899.

Dai, X.-D., Liu, X.-M., Qian, L., Yan, Z.-F. & Zhang, J. 2006. A novel method to synthesize super-activated carbon for natural gas adsorptive storage. *Journal of Porous Materials,* 13**,** 399-405.

Damköhler, G. 1935. Über die Adsorptionsgeschwindigkeit von Gasen an porösen Adsorbentien. *Zeitschrift für Physikalische Chemie,* 174**,** 222-238.

Davies, G. & Seaton, N. 1998. The effect of the choice of pore model on the characterization of the internal structure of microporous carbons using pore size distributions. *Carbon,* 36**,** 1473-1490.

Davies, G., Seaton, N. & Vassiliadis, V. 1999. Calculation of pore size distributions of activated carbons from adsorption isotherms. *Langmuir,* 15**,** 8235-8245.

Dawe, R. A. & Lucas, A. G. 2000. *Modern petroleum technology,* John Wiley & Sons Inc.

Delavar, M., Ghoreyshi, A. A., Jahanshahi, M., Khalili, S. & Nabian, N. 2012. Equilibria and kinetics of natural gas adsorption on multi-walled carbon nanotube material. *RSC Advances,* 2**,** 4490-4497.

Deppe, G., Tam, S., Currier, R., Young, J., Anderson, G., Le, L. & Spencer, D. 2006. Developments in the SIMTECHE Process-Separation of CO_2 From Coal Syngas by Formation of Hydrates. NEXANT. INC.

Do, D. & Do, H. 2001. Surface diffusion of hydrocarbons in activated carbon: Comparison between constant molar flow, differential permeation and differential adsorption bed methods. *Adsorption,* 7**,** 189-209.

Do, D. D. 1998. *Adsorption analysis: equilibria and kinetics,* Imperial college press London.

Dubinin, M. & Astakhov, V. 1971. Description of adsorption equilibria of vapors on zeolites over wide ranges of temperature and pressure. ACS Publications.

Duran, C., Ozdes, D., Gundogdu, A. & Senturk, H. B. 2011. Kinetics and isotherm analysis of basic dyes adsorption onto almond shell (Prunus dulcis) as a low cost adsorbent. *Journal of Chemical & Engineering Data,* 56**,** 2136-2147.

Düren, T., Sarkisov, L., Yaghi, O. M. & Snurr, R. Q. 2004. Design of new materials for methane storage. *Langmuir,* 20**,** 2683-2689.

El Qada, E. N., Allen, S. J. & Walker, G. M. 2006. Adsorption of methylene blue onto activated carbon produced from steam activated bituminous coal: a study of equilibrium adsorption isotherm. *Chemical Engineering Journal,* 124**,** 103-110.

Eliseev, O. 2009. Gas-to-liquid technologies. *Russian Journal of General Chemistry,* 79**,** 2509-2519.

Energy, B. 2018. BP Energy Outlook 2018 Edition.

Enersea. 2017. *Cost Effective Technology* [Online]. EnerSea Transport Inc. Available: http://enersea.com/cng-technology/ [Accessed 13/03/2019 2019].

Ergun, S. 1952. Fluid flow through packed columns. *Chem. Eng. Prog.*, 48**,** 89-94.

Esteves, I. A., Lopes, M. S., Nunes, P. M. & Mota, J. P. 2008. Adsorption of natural gas and biogas components on activated carbon. *Separation and Purification Technology,* 62**,** 281-296.

Falcon, L. M. & Falcon, R. 1985. Fundamental Factors affecting the efficicnecy of fine coal beneficiation. *In:* MINTEK (ed.). South Africa.

Falcon, R. & Ham, A. 1988. The characteristics of South African coals. *Journal of the Southern African Institute of Mining and Metallurgy,* 88**,** 145-161.

Figueiredo, J., Pereira, M., Freitas, M. & Orfao, J. 1999. Modification of the surface chemistry of activated carbons. *Carbon,* 37**,** 1379-1389.

Frère, M. G. & De Weireld, G. F. 2002. High-pressure and high-temperature excess adsorption isotherms of N_2, CH_4, and C_3H_8 on activated carbon. *Journal of Chemical & Engineering Data,* 47**,** 823-829.

Gao, S., Ge, L., Rufford, T. E. & Zhu, Z. 2017. The preparation of activated carbon discs from tar pitch and coal powder for adsorption of CO_2, CH_4 and N_2. *Microporous and Mesoporous Materials,* 238**,** 19-26.

Ghosal, R. & Smith, D. M. 1996. Micropore characterization using the Dubinin-Astakhov equation to analyze high pressure CO_2 (273 K) adsorption data. *Journal of Porous Materials,* 3**,** 247-255.

Gong, G.-Z., Qiang, X., Zheng, Y.-F., Ye, S.-F. & Chen, Y.-F. 2009. Regulation of pore size distribution in coal-based activated carbon. *New Carbon Materials,* 24**,** 141-146.

Gopalakannan, S. & Senthilvelan, T. 2013. Application of response surface method on machining of Al–SiC nano-composites. *Measurement,* 46**,** 2705-2715.

Gregg, S. J., Sing, K. S. W. & Salzberg, H. 1967. Adsorption surface area and porosity. *Journal of the Electrochemical Society,* 114**,** 279C-279C.

Group, I. R. 2014. JSC Severstal. Company business profile. Available: http://www.infomine.ru/files/catalog/356/file_356_eng.pdf [Accessed Oct 2014].

Gudmundsson, J., Andersson, V., Levik, O. & Parlaktuna, M. Hydrate concept for capturing associated gas. European Petroleum Conference, 1998. Society of Petroleum Engineers.

Gupta, A. K. & Paul, B. 2015. Ecorestoration of Coal Mine Overburden Dump to Prevent Environmental Degradation: A Review. *Research Journal of Environmental Sciences,* 9**,** 307.

Hamedi, M., Farahani, R. Z., Husseini, M. M. & Esmaeilian, G. R. 2009. A distribution planning model for natural gas supply chain: A case study. *Energy Policy,* 37**,** 799-812.

Hattingh, D., Blignault, C., Van Niekerk, T. & James, M. 2008. Characterization of the influences of FSW tool geometry on welding forces and weld tensile strength using an instrumented tool. *Journal of Materials Processing Technology,* 203**,** 46-57.

Henmi, T. 1987. Synthesis of hydroxy-sodalite ("zeolite") from coal waste ash. *Soil science and plant nutrition,* 33**,** 517-521.

Hesas, R. H., Arami-Niya, A., Daud, W. M. a. W. & Sahu, J. 2013. Preparation of granular activated carbon from oil palm shell by microwave-induced chemical activation: Optimisation using surface response methodology. *Chemical Engineering Research and Design,* 91**,** 2447-2456.

Himeno, S., Komatsu, T. & Fujita, S. 2005. High-pressure adsorption equilibria of methane and carbon dioxide on several activated carbons. *Journal of Chemical & Engineering Data,* 50**,** 369-376.

Hou, P., Cannon, F. S., Nieto-Delgado, C., Brown, N. R. & Gu, X. 2013. Effect of preparation protocol on anchoring quaternary ammonium/epoxide-forming compound into granular activated carbon for perchlorate adsorption: Enhancement by Response Surface Methodology. *Chemical engineering journal,* 223**,** 309-317.

Hsu, L.-Y. & Teng, H. 2000. Influence of different chemical reagents on the preparation of activated carbons from bituminous coal. *Fuel Processing Technology,* 64**,** 155-166.

Hu, Z. & Srinivasan, M. 1999. Preparation of high-surface-area activated carbons from coconut shell. *Microporous and Mesoporous Materials,* 27**,** 11-18.

Hu, Z., Srinivasan, M. P. & Ni, Y. 2000. Preparation of mesoporous high-surface-area activated carbon. *Advanced materials,* 12**,** 62-65.

Iccp 2001. The new inertinite classification (ICCP System 1994). *Fuel,* 80**,** 459-471.

Isah, U., Abdulraheem, G., Bala, S., Muhammad, S. & Abdullahi, M. 2015. Kinetics, equilibrium and thermodynamics studies of CI Reactive Blue 19 dye adsorption on coconut shell based activated carbon. *International Biodeterioration & Biodegradation,* 102**,** 265-273.

Judd, R., Gladding, D., Hodrien, R., Bates, D., Ingram, J. & Allen, M. The use of adsorbed natural gas technology for large scale storage. Preprint Symposium Am Chem Soc. Div Fuel Chem, ACS, 1998. 575-579.

Karger, J. & Ruthven, D. 1992. Diffusion in zeolites and other microporous materials. *John New York: Wiley and Sons*.

Khan, M. I., Yasmeen, T., Khan, M. I., Farooq, M. & Wakeel, M. 2016. Research progress in the development of natural gas as fuel for road vehicles: A bibliographic review (1991–2016). *Renewable and Sustainable Energy Reviews,* 66**,** 702-741.

Kim, N.-J., Lee, J. H., Cho, Y. S. & Chun, W. 2010. Formation enhancement of methane hydrate for natural gas transport and storage. *Energy,* 35**,** 2717-2722.

Koh, C. A. & Sloan, E. D. 2007. Natural gas hydrates: Recent advances and challenges in energy and environmental applications. *AIChE journal,* 53**,** 1636-1643.

Kondo, M., Okubo, T., Asami, A., Noro, S. I., Yoshitomi, T., Kitagawa, S., Ishii, T., Matsuzaka, H. & Seki, K. 1999. Rational Synthesis of Stable Channel-Like Cavities with Methane Gas Adsorption Properties:[{Cu2 (pzdc) 2 (L)} n](pzdc= pyrazine-2, 3-dicarboxylate; L= a Pillar Ligand). *Angewandte Chemie International Edition,* 38**,** 140-143.

Köseoğlu, E. & Akmil-Başar, C. 2015. Preparation, structural evaluation and adsorptive properties of activated carbon from agricultural waste biomass. *Advanced Powder Technology,* 26**,** 811-818.

Kraber, S. 2013. How to get started with Design Expert Software. Stat-Ease, Inc.

Largitte, L. & Pasquier, R. 2016. A review of the kinetics adsorption models and their application to the adsorption of lead by an activated carbon. *Chemical Engineering Research and Design,* 109**,** 495-504.

Le Roux, A. 2014. *Opportunity for electricity generation from discard coal at the Witbank Coalfields.* Stellenbosch: Stellenbosch University.

Li, H., Eddaoudi, M., O'keeffe, M. & Yaghi, O. M. 1999. Design and synthesis of an exceptionally stable and highly porous metal-organic framework. *Nature,* 402**,** 276-279.

Lillo-Ródenas, M., Cazorla-Amorós, D. & Linares-Solano, A. 2003. Understanding chemical reactions between carbons and NaOH and KOH: an insight into the chemical activation mechanism. *Carbon,* 41**,** 267-275.

Lillo-Ródenas, M., Marco-Lozar, J., Cazorla-Amorós, D. & Linares-Solano, A. 2007. Activated carbons prepared by pyrolysis of mixtures of carbon precursor/alkaline hydroxide. *Journal of Analytical and Applied Pyrolysis,* 80**,** 166-174.

Lin, H.-Y., Chen, Y.-W. & Li, C. 2003. The mechanism of reduction of iron oxide by hydrogen. *Thermochimica Acta,* 400**,** 61-67.

Linares-Solano, A., Lillo-Ródenas, M., Marco-Lozar, J. P., Kunowsky, M. & Romero-Anaya, A. J. 2012. NaOH and KOH for preparing activated carbons used in energy and environmental applications. *International Journal of Energy, Environment and Economics,* 20**,** 355.

Linares-Solano, A., Lozano-Castelló, D., Lillo-Ródenas, M. & Cazorla-Amorós, D. 2007. Carbon activation by alkaline hydroxides: preparation and reactions, porosity and performance. *Chemistry & Physics of Carbon.* CRC Press.

Linares-Solano, A., Lozano-Castelló, D., Lillo-Ródenas, M. & Cazorla-Amorós, D. 2008. Controlling porosity to improve activated carbon applications. *Recent Advances in Adsorption Processes for Environmental Protection and Security.* Springer.

Lloyd, P. 2000. The potential of coal wastes in South Africa. *Journal of the Southern African Institute of Mining and Metallurgy,* 100**,** 69-72.

Loh, W. S., Kumja, M., Rahman, K. A., Ng, K. C., Saha, B. B., Koyama, S. & El-Sharkawy, I. I. 2010a. Adsorption parameter and heat of adsorption of activated carbon/HFC-134a pair. *Heat Transfer Engineering,* 31**,** 910-916.

Loh, W. S., Rahman, K. A., Chakraborty, A., Saha, B. B., Choo, Y. S., Khoo, B. C. & Ng, K. C. 2010b. Improved isotherm data for adsorption of methane on activated carbons. *Journal of Chemical & Engineering Data,* 55**,** 2840-2847.

Lowell, S., Shields, J. E., Thomas, M. A. & Thommes, M. 2012. *Characterization of porous solids and powders: surface area, pore size and density*, Springer Science & Business Media.

Lozano-Castello, D., Alcaniz-Monge, J., De La Casa-Lillo, M., Cazorla-Amoros, D. & Linares-Solano, A. 2002a. Advances in the study of methane storage in porous carbonaceous materials. *Fuel,* 81**,** 1777-1803.

Lozano-Castello, D., Cazorla-Amoros, D. & Linares-Solano, A. 2002b. Powdered activated carbons and activated carbon fibers for methane storage: a comparative study. *Energy & fuels,* 16**,** 1321-1328.

Lozano-Castello, D., Lillo-Rodenas, M., Cazorla-Amoros, D. & Linares-Solano, A. 2001. Preparation of activated carbons from Spanish anthracite: I. Activation by KOH. *Carbon,* 39**,** 741-749.

Lua, A. C. & Yang, T. 2004. Effect of activation temperature on the textural and chemical properties of potassium hydroxide activated carbon prepared from pistachio-nut shell. *Journal of colloid and interface science,* 274**,** 594-601.

Luo, J., Liu, Y., Jiang, C., Chu, W., Jie, W. & Xie, H. 2011. Experimental and modeling study of methane adsorption on activated carbon derived from anthracite. *Journal of Chemical & Engineering Data,* 56**,** 4919-4926.

Maiti, S. K. 2012. *Ecorestoration of the coalmine degraded lands*, Springer Science & Business Media.

Makal, T. A., Li, J.-R., Lu, W. & Zhou, H.-C. 2012. Methane storage in advanced porous materials. *Chemical Society Reviews,* 41**,** 7761-7779.

Marsh, H. & Reinoso, F. R. 2006. *Activated carbon*, Elsevier.

Marston, E. & Gray, S. 2018. OGA: Gas-to-Wire Concept Boosts Offshore Power Output. *Offshore Wind* [Online]. Available: https://www.offshorewind.biz/2018/09/19/oga-gas-to-wire-concept-boosts-offshore-power-output/ [Accessed 14/03/2019].

Martin, A., Idrus Alhamid, M., Nasruddin, Suryawan, B., Soong Loh, W., Bin Ismail, A., Chun, W. & Choon Ng, K. 2017. High-Pressure Adsorption Isotherms of Carbon Dioxide and Methane on Activated Carbon From Low-Grade Coal of Indonesia. *Heat Transfer Engineering,* 38**,** 396-402.

Martin, A., Loh, W. S., Rahman, K. A., Thu, K., Surayawan, B., Alhamid, M. I. & Ng, K. C. 2011. Adsorption isotherms of CH4 on activated carbon from Indonesian low grade coal. *Journal of Chemical & Engineering Data,* 56**,** 361-367.

Martins, A. C., Pezoti, O., Cazetta, A. L., Bedin, K. C., Yamazaki, D. A., Bandoch, G. F., Asefa, T., Visentainer, J. V. & Almeida, V. C. 2015. Removal of tetracycline by NaOH-activated carbon produced from macadamia nut shells: kinetic and equilibrium studies. *Chemical Engineering Journal,* 260**,** 291-299.

Matranga, K. R., Myers, A. L. & Glandt, E. D. 1992. Storage of natural gas by adsorption on activated carbon. *Chemical engineering science,* 47**,** 1569-1579.

Meisen, A. & Shuai, X. 1997. Research and development issues in CO_2 capture. *Energy Conversion and Management,* 38**,** S37-S42.

Menon, V. & Komarneni, S. 1998. Porous adsorbents for vehicular natural gas storage: a review. *Journal of Porous Materials,* 5**,** 43-58.

Mills, S. 2018. The use of coal-derived wastes as a source of enevrgy. London, United KIngdom: IEA Clean Coal Center.

Molina-Sabio, M. & Rodrıguez-Reinoso, F. 2004. Role of chemical activation in the development of carbon porosity. *Colloids and Surfaces A: Physicochemical and Engineering Aspects,* 241**,** 15-25.

Mondal, M. K., Balsora, H. K. & Varshney, P. 2012. Progress and trends in CO_2 capture/separation technologies: a review. *Energy,* 46**,** 431-441.

Mondal, S., Sinha, K., Aikat, K. & Halder, G. 2015. Adsorption thermodynamics and kinetics of ranitidine hydrochloride onto superheated steam activated carbon derived from mung bean husk. *Journal of Environmental Chemical Engineering,* 3**,** 187-195.

Mota, J. B., Rodrigues, A., Saatdjian, E. & Tondeur, D. 1997. Dynamics of natural gas adsorption storage systems employing activated carbon. *Carbon,* 35**,** 1259-1270.

Moyo, A., Filho, J. A., Harrison, S. & Broadhurst, J. 2018. Characterising the environmental risks of coal preparation wastes: A study of fine coal slurry waste and discards from South African collieries. *IMWA 2018 Annual Conference.* Pretoria, South Africa.

Mueller, U., Schubert, M., Teich, F., Puetter, H., Schierle-Arndt, K. & Pastre, J. 2006. Metal–organic frameworks—prospective industrial applications. *Journal of Materials Chemistry,* 16**,** 626-636.

Myers, A. 2002. Thermodynamics of adsorption in porous materials. *AIChE Journal,* 48**,** 145-160.

Nasri, N. S., Hamza, U. D., Ismail, S. N., Ahmed, M. M. & Mohsin, R. 2014. Assessment of porous carbons derived from sustainable palm solid waste for carbon dioxide capture. *Journal of Cleaner Production,* 71**,** 148-157.

Nicholson, D. & Petropoulos, J. H. 1985. Calculation of the Surface Flow of a Dilute Gas in Model Pores From First Principles. Part III. *Journal of Colloid Interface Science,* 106**,** 538-546.

North, B., Engelbrecht, A. & Oboirien, B. 2015. Feasibility study of electricity generation from discard coal. *Journal of the Southern African Institute of Mining and Metallurgy,* 115**,** 573-580.

Okhovat, A., Ahmadpour, A., Ahmadpour, F. & Khaki Yadegar, Z. 2012. Pore size distribution analysis of coal-based activated carbons: investigating the effects of activating agent and chemical ratio. *ISRN Chemical Engineering,* 2012.

Omri, A. & Benzina, M. 2012. Characterization of activated carbon prepared from a new raw lignocellulosic material: Ziziphus spina-christi seeds. *Journal de la Société Chimique de Tunisie,* 14**,** 175-183.

Onifade, M. & Genc, B. 2018. A review of spontaneous combustion studies–South African context. *International Journal of Mining, Reclamation and Environment***,** 1-21.

Ottiger, S., Pini, R., Storti, G., Mazzotti, M., Bencini, R., Quattrocchi, F., Sardu, G. & Deriu, G. 2006. Adsorption of pure carbon dioxide and methane on dry coal from the Sulcis Coal Province (SW Sardinia, Italy). *Environmental progress & sustainable energy,* 25**,** 355-364.

Özacar, M. 2003. Equilibrium and kinetic modelling of adsorption of phosphorus on calcined alunite. *Adsorption,* 9**,** 125-132.

Panella, B., Hirscher, M. & Roth, S. 2005. Hydrogen adsorption in different carbon nanostructures. *Carbon,* 43**,** 2209-2214.

Papin, A., Ignatova, A. Y., Nevedrov, A. & Cherkasova, T. 2015. Fuel briquetting using finely disperse waste of coal mining and processing. *Journal of Mining Science,* 51**,** 895-900.

Parkyns, N., Quinn, D. & Patrick, J. 1995. Porosity in carbons. *Edward Arnold, London,* 293-325.

Particulate & Systems 2011. HPVA Series Operator's Manual. *In:* Micromeritics (ed.) *HPVA Series.* Georgia, U.S.A: Micromeritics.

Patil, K. H. & Sahoo, S. 2018. Charge characteristics of adsorbed natural gas storage system based on MAXSORB III. *Journal of Natural Gas Science and Engineering,* 52**,** 267-282.

Piechura, H. 2014. Application of Doosan Lentjes' CFB technology to discard coals. *South African Journal of Chemical Engineering,* 19**,** 99-111.

Policicchio, A., Filosa, R., Abate, S., Desiderio, G. & Colavita, E. 2017. Activated carbon and metal organic framework as adsorbent for low-pressure methane storage applications: an overview. *Journal of Porous Materials,* 24**,** 905-922.

Policicchio, A., Maccallini, E., Agostino, R. G., Ciuchi, F., Aloise, A. & Giordano, G. 2013. Higher methane storage at low pressure and room temperature in new easily scalable large-scale production activated carbon for static and vehicular applications. *Fuel,* 104**,** 813-821.

Prauchner, M. J. & Rodriguez-Reinoso, F. 2008. Preparation of granular activated carbons for adsorption of natural gas. *Microporous and Mesoporous Materials,* 109**,** 581-584.

Princewill, I. & Ikiensikimama, S. Virtual Pipeline Technology in Nigeria: Technical and Economic Analysis. SPE Nigeria Annual International Conference and Exhibition, 2016. Society of Petroleum Engineers.

Pupier, O., Goetz, V. & Fiscal, R. 2005. Effect of cycling operations on an adsorbed natural gas storage. *Chemical Engineering and Processing: Process Intensification,* 44**,** 71-79.

Quinn, D. F. & Macdonald, J. A. 1992. Natural Gas Storage. *Carbon,* 30**,** 1097 - 1103.

Radich, J., Rogers, R., French, W. & Zhang, G. 2009. Biochemical reaction and diffusion in seafloor gas hydrate capillaries: Implications for gas hydrate stability. *Chemical Engineering Science,* 64**,** 4278-4285.

Rahman, K. A., Chakraborty, A., Saha, B. B. & Ng, K. C. 2012a. On thermodynamics of methane+ carbonaceous materials adsorption. *International Journal of Heat and Mass Transfer,* 55**,** 565-573.

Rahman, K. A., Loh, W. S., Chakraborty, A., Saha, B. B., Chun, W. G. & Ng, K. C. 2011. Thermal enhancement of charge and discharge cycles for adsorbed natural gas storage. *Applied Thermal Engineering,* 31**,** 1630-1639.

Rahman, K. A., Loh, W. S., Ng, K. C. & Chun, W. Experimental Investigations of Adsorbed Natural Gas Storage System with Enhanced Thermal Management. International Journal of Modern Physics: Conference Series, 2012b. World Scientific, 190-195.

Rahman, K. A., Loh, W. S., Yanagi, H., Chakraborty, A., Saha, B. B., Chun, W. G. & Ng, K. C. 2010. Experimental adsorption isotherm of methane onto activated carbon at sub-and supercritical temperatures. *Journal of Chemical & Engineering Data,* 55**,** 4961-4967.

Rights, C. F. E. 2015. *In pictures: What coal is doing to the Mpumalanga Highveld* [Online]. Center for Environmental Rights. Available: https://cer.org.za/news/in-pictures-what-coal-is-doing-to-the-mpumalanga-highveld [Accessed 16/11/2017 2017].

Rios, R. B., Bastos-Neto, M., Amora, M. R., Torres, A. E. B., Azevedo, D. C. S. & Cavalcante, C. L. 2011. Experimental analysis of the efficiency on charge/discharge cycles in natural gas storage by adsorption. *Fuel,* 90**,** 113-119.

Rodrigues, L. A. & Da Silva, M. L. C. P. 2010. Thermodynamic and kinetic investigations of phosphate adsorption onto hydrous niobium oxide prepared by homogeneous solution method. *Desalination,* 263**,** 29-35.

Rodriguez-Reinoso, F. & Molina-Sabio, M. 1992. Activated carbons from lignocellulosic materials by chemical and/or physical activation: an overview. *Carbon,* 30**,** 1111-1118.

Rodríguez-Reinoso, F., Nakagawa, Y., Silvestre-Albero, J., Juárez-Galán, J. & Molina-Sabio, M. 2008. Correlation of methane uptake with microporosity and surface area of chemically activated carbons. *Microporous and mesoporous Materials,* 115**,** 603-608.

Rouquerol, J., Rouquerol, F., Llewellyn, P., Maurin, G. & Sing, K. S. 2013. *Adsorption by powders and porous solids: principles, methodology and applications,* Academic press.

Ruthven, D. M. 1984. *Principles of adsorption and adsorption processes,* John Wiley & Sons.

Sáez, A. & Toledo, M. 2009. Thermal effect of the adsorption heat on an adsorbed natural gas storage and transportation systems. *Applied Thermal Engineering,* 29**,** 2617-2623.

Sahoo, P., Prajwal, B., Dasetty, S. K., John, M., Newalkar, B., Choudary, N. & Ayappa, K. 2014. Influence of exhaust gas heating and L/D ratios on the discharge efficiencies for an activated carbon natural gas storage system. *Applied energy,* 119**,** 190-203.

Sahoo, P. K., John, M., Newalkar, B. L., Choudhary, N. V. & Ayappa, K. G. 2011. Filling Characteristics for an Activated Carbon Based Adsorbed Natural Gas Storage System. *Industrial & Engineering Chemistry Research,* 50**,** 13000-13011.

Sahoo, S. & Ramgopal, M. 2016. Theoretical performance of an adsorbed natural gas storage system subjected to variable charge–discharge conditions. *International Journal of Ambient Energy,* 37**,** 372-383.

Schindler, B. J. 2008. *Henry's Law Behavior and Density Functional Theory Analysis of Adsorption Equilibrium.*

Sekhohola, L. M. & Cowan, A. K. 2017. Biological conversion of low-grade coal discard to a humic substance-enriched soil-like material. *International Journal of Coal Science & Technology,* 4**,** 183-190.

Şenel, İ. G., Gürüz, A. G., Yücel, H., Kandas, A. W. & Sarofim, A. F. 2001. Characterization of pore structure of Turkish coals. *Energy & fuels,* 15**,** 331-338.

Shamsuddin, M., Yusoff, N. & Sulaiman, M. 2016. Synthesis and characterization of activated carbon produced from kenaf core fiber using H3PO4 activation. *Procedia Chemistry,* 19**,** 558-565.

Siemons, N. & Busch, A. 2007. Measurement and interpretation of supercritical CO_2 sorption on various coals. *International Journal of Coal Geology,* 69**,** 229-242.

Sing, K., Everett, D., Haul, R., Moscou, L., Pierotti, R., Rouquerol, J. & Siemieniewska, T. 1985. International union of pure and applied chemistry, IUPAC. *Pure Appl. Chem,* 57**,** 603.

Skinner, J. & Brown, M. 2011. The Inefficiencies and Deficiencies of Coal waste. *Vt. J. Envtl. L.,* 13**,** 229.

Sohn, S. & Kim, D. 2005. Modification of Langmuir isotherm in solution systems—definition and utilization of concentration dependent factor. *Chemosphere,* 58**,** 115-123.

Sreńscek-Nazzal, J., Kamińska, W., Michalkiewicz, B. & Koren, Z. C. 2013. Production, characterization and methane storage potential of KOH-activated carbon from sugarcane molasses. *Industrial Crops and Products,* 47**,** 153-159.

Stat-Ease 2018. *Handbook for Experimenters,* Minneapolis, United States, Stat-Ease, Inc.

Stenning, D. & Cran, J. A. The Coselle CNG carrier the shipment of natural gas by sea in compressed form. 16th World Petroleum Congress, 2000. World Petroleum Congress.

Stoeckli, H., Kraehenbuehl, F., Ballerini, L. & De Bernardini, S. 1989. Recent developments in the Dubinin equation. *Carbon,* 27**,** 125-128.

Stolboushkin, A. Y., Ivanov, A. & Fomina, O. 2016. Use of Coal-Mining and Processing Wastes in Production of Bricks and Fuel for Their Burning. *Procedia Engineering,* 150**,** 1496-1502.

Sun, J., Hippo, E., Marsh, H., O'brien, W. & Crelling, J. 1997. Activated carbon produced from an Illinois basin coal. *Carbon,* 35**,** 341-352.

Sun, Y., Liu, C., Su, W., Zhou, Y. & Zhou, L. 2009. Principles of methane adsorption and natural gas storage. *Adsorption,* 15**,** 133-137.

Suzuki, M. 1990. *Adsorption engineering,* Kodansha.

Swanepoel, E. 2008. Fully explore coal discard use to improve security. *Mining Weekly* [Online]. Available: http://www.miningweekly.com/article/fully-explore-coal-discard-use-to-improve-security-urges-government-2008-06-27/rep_id:3650 [Accessed 24/02/2017].

Taheri, Z., Shabani, M. R., Nazari, K. & Mehdizaheh, A. 2014. Natural gas transportation and storage by hydrate technology: Iran case study. *Journal of Natural Gas Science and Engineering,* 21**,** 846-849.

Tanner, P. 2007. Guidelines for the rehabilitation of mined land. *Chamber of Mines of South Africa, Johannesburg,* 4.

Taylor, M., Dawe, R. A. & Thomas, S. Fire and Ice: Gas hydrate transportation-A possibility for the Caribbean region. SPE Latin American and Caribbean Petroleum Engineering Conference, 2003. Society of Petroleum Engineers.

Teng, H. & Lin, H. C. 1998. Activated carbon production from low ash subbituminous coal with CO_2 activation. *AIChE journal,* 44**,** 1170-1177.

Thomas, S. & Dawe, R. A. 2003. Review of ways to transport natural gas energy from countries which do not need the gas for domestic use. *Energy,* 28**,** 1461-1477.

Thommes, M. 2010. Physical adsorption characterization of nanoporous materials. *Chemie Ingenieur Technik,* 82**,** 1059-1073.

Thommes, M., Kaneko, K., Neimark, A. V., Olivier, J. P., Rodriguez-Reinoso, F., Rouquerol, J. & Sing, K. S. 2015. Physisorption of gases, with special reference to the evaluation of surface area and pore size distribution (IUPAC Technical Report). *Pure and Applied Chemistry,* 87**,** 1051-1069.

Thu, K., Kim, Y.-D., Ismil, A. B., Saha, B. B. & Ng, K. C. 2014. Adsorption characteristics of methane on Maxsorb III by gravimetric method. *Applied Thermal Engineering,* 72**,** 200-205.

Toth, J. 1971. State equation of the solid-gas interface layers. *Acta chim. hung.,* 69**,** 311-328.

Tudor, T. 2019. Arq Technology - Energy Unbound. *Clean Coal Technologies Conference.* Houston, United States.

Üner, O., Geçgel, Ü. & Bayrak, Y. 2015. Preparation and characterization of mesoporous activated carbons from waste watermelon rind by using the chemical activation method with zinc chloride. *Arabian Journal of Chemistry*.

Vasiliev, L., Kanonchik, L., Mishkinis, D. & Rabetsky, M. A new method of methane storage and transportation. IV Minsk International Seminar, Heat Pipes, Heat Pumps, Refrigerators, Minsk, Belarus, 2000.

Wang, G., Tian, Y., Jiang, J. & Wu, J. 2018. Multimodels computation for adsorption capacity of activated carbon. *Adsorption Science & Technology,* 36**,** 508-520.

Wang, J. & Kaskel, S. 2012. KOH activation of carbon-based materials for energy storage. *Journal of Materials Chemistry,* 22**,** 23710-23725.

Wang, S. & Lu, G. 1997. Effects of Oxide Promoters on Metal Dispersion and Metal− Support Interactions in Ni Catalysts Supported on Activated Carbon. *Industrial & engineering chemistry research,* 36**,** 5103-5109.

Wang, Y., Hashim, M., Ercan, C., Khawajah, A. & Othman, R. High pressure methane adsorption on granular activated carbons. 21st Annual Saudi-Japan Symposium, November, 2011.

Wegrzyn, J. & Gurevich, M. 1996. Adsorbent storage of natural gas. *Applied energy,* 55**,** 71-83.

Wood, D. A., Nwaoha, C. & Towler, B. F. 2012. Gas-to-liquids (GTL): A review of an industry offering several routes for monetizing natural gas. *Journal of Natural Gas Science and Engineering,* 9**,** 196-208.

Wu, F.-C., Tseng, R.-L. & Juang, R.-S. 2005. Preparation of highly microporous carbons from fir wood by KOH activation for adsorption of dyes and phenols from water. *Separation and Purification technology,* 47**,** 10-19.

Wu, H., Simmons, J. M., Liu, Y., Brown, C. M., Wang, X. S., Ma, S., Peterson, V. K., Southon, P. D., Kepert, C. J. & Zhou, H. C. 2010. Metal–organic frameworks with exceptionally high methane uptake: where and how is methane stored? *Chemistry–A European Journal,* 16**,** 5205-5214.

Yamamoto, K. 2015. Overview and introduction: pressure core-sampling and analysis in the 2012–2013 MH21 offshore test of gas production from methane hydrate in teh eastern Nankai Trough. *Mar Petrol Geol,* 14.

Yang, G., Song, S., Li, J., Tang, Z., Ye, J. & Yang, J. 2019. Preparation and CO_2 adsorption properties of porous carbon by hydrothermal carbonization of tree leaves. *Journal of Materials Science & Technology,* 35**,** 875-884.

Yang, R. T. 2013. *Gas separation by adsorption processes,* Butterworth-Heinemann.

Yang, X., Zheng, Q., Gu, A. & Lu, X. 2005. Experimental studies of the performance of adsorbed natural gas storage system during discharge. *Applied Thermal Engineering,* 25**,** 591-601.

Yorgun, S. & Yıldız, D. 2015. Preparation and characterization of activated carbons from Paulownia wood by chemical activation with H_3PO_4. *Journal of the Taiwan Institute of Chemical Engineers,* 53**,** 122-131.

Zakaria, Z. & George, T. 2011. The performance of commercial activated carbon absorbent for adsorbed natural gas storage. *International Journal of Research and Reviews in Applied Sciences,* 9.

Zhang, H., Chen, J. & Guo, S. 2008. Preparation of natural gas adsorbents from high-sulfur petroleum coke. *Fuel,* 87**,** 304-311.

Zhao, W., Fierro, V., Zlotea, C., Aylon, E., Izquierdo, M., Latroche, M. & Celzard, A. 2011. Optimization of activated carbons for hydrogen storage. *international journal of hydrogen energy,* 36**,** 11746-11751.

Zhou, L., Liu, J., Su, W., Sun, Y. & Zhou, Y. 2010. Progress in studies of natural gas storage with wet adsorbents. *Energy & Fuels,* 24**,** 3789-3795.

Zhou, L., Zhou, Y. & Sun, Y. 2004. A comparative study of hydrogen adsorption on superactivated carbon versus carbon nanotubes. *International Journal of Hydrogen Energy,* 29**,** 475-479.

APPENDICES

APPENDIX A: Abstract of Journal Publications and Conference Proceedings

Appendix A1: Paper 1

Parts of this thesis were compiled and published as a Journal paper titled 'Experimental Evaluation of Activated Carbon Derived from South Africa Discard Coal for Natural Gas Storage' Published by International Journal of Coal Science & Technology. https://doi.org/10.1007/s40789-019-0262-5

Abstract

Lacking in literature is the use of discard coal to produce activated carbon and in its subsequent use in the storage of natural gas. In this study, the characterization and gas storage evaluation of a largely porous activated carbon with large surface area synthesized from discard coal were investigated. Discard coals are waste material generated from the coal beneficiation process. In developing the activated carbon, chemical activation route with the use of KOH reagent was applied. The effects of KOH/discard coal weight ratio (1:1, 2.5:1, 4:1), temperature (400 – 800 ^oC) and particle size (0.15 – 0.25 µm, 250 – 500 µm, 500 - 1000 µm) on the adsorptive properties of the activated carbon were methodically evaluated and optimized using Response Surface Methodology (RSM). The synthesized activated carbon was characterized using BET, SEM/EDS, and XRD. The results showed that for each activation process, the surface area and pore volume of the resulting activated carbon increased with increased temperature and KOH/discard coal weight ratio. The maximum surface area of 1826.41 m^2/g, the pore volume of 1.252 cm^3/g and pore size of 2.77nm were obtained at a carbonization temperature of 800 ^oC and KOH/discard coal weight ratio of 4:1. Methane and nitrogen adsorption data at high pressure were fitted to Toth isotherm model with a predictive accuracy of about 99%. Adsorption parameters using the Toth model provides useful information in the design of adsorbed natural gas storage system. According to the requirements of adsorbent desired for natural gas storage, it could be stated that the synthesized activated carbon could well be applied for natural gas storage.

Appendix A2: Paper 2

A review paper on natural gas purification in addition to some parts of this thesis literature review was compiled and published as a Journal paper titled 'Towards a Cleaner Natural Gas Production: Recent Developments on Purification Technologies', Journal of Separation Science and Technology, 2019, Vol. 54, No. 15, pp. 2461–2497, 2019. https://doi.org/10.1080/01496395.2018.1547761

Abstract

The development of new, efficient and cost-effective technologies for acid gases (CO2 and H2S) removal from natural gas is pertinent for cleaner energy productions. The removal of acid gases from natural gas can be carried out using different techniques (chemical, physical or hybrid). Although the widely employed techniques are generally effective, they have some ascribed drawbacks such as process efficiency and high energy cost. Emerging techniques are being considered to reduce or eliminate these limitations but their deployment on an industrial scale may require that certain scientific and technological criteria, such as higher selectivity and gas separation kinetics, be met. Unprecedented and lacking in previous appraisals, this review has focused on the emerging and sustainable developments on acid gases removal from natural gas, but not without a critical evaluation of the existing technologies to provide a better background on the subject, ascertain the status-quo and identify gaps for further improvements. The efficiency of these emerging technologies are analysed with a focus on ionic liquids and their blends, binding organic liquids, enzyme-based separation technologies, and others. This review also features a brief contribution of the authors towards the development of low-cost materials for CO_2/natural gas separation. This article is expected to serve as an in-depth requisite background for further research on carbon capture processes with respect to natural gas purification.

Appendix A3: Paper 3

The third publication was published as a book chapter titled ‘Energy Storage Properties of Graphene Nanofillers’ in the book titled ‘Graphene-Based Nanotechnologies for Energy and Environmental Applications’ published in Elsevier. https://doi.org/10.1016/B978-0-12-815811-1.00009-0

Abstract

Increasing demand in global energy resources has necessitated the need for a breakthrough in energy storage system development. The unique features of graphene make it appealing in energy storage applications. Outstanding performance in energy storage devices has been attributed to the remarkable properties of graphene such as large specific surface area, outstanding chemical stability, great mechanical adaptability, and exceptional electrical and thermal conductivity. These unique properties have made graphene a material of choice for electrodes in energy storage devices. The electrode of supercapacitors made from graphene-based materials has shown huge potential in storage applications. In this chapter, we discuss these unique characteristics of graphene when used as active material or as a component and its application in energy storage devices.

Appendix A4: Paper 4

Parts of this thesis were compiled and submitted to Fuel Journal for publication. The paper is currently under peer review. The paper is titled 'Natural Gas Storage Properties of Adsorbents Synthesized from three different Coal Waste in South Africa'

Abstract

Adsorbed natural gas (ANG) storage has been identified as the most promising low-pressure alternative to storing natural gas. However, the successful implementation of this technology is largely constrained by the cost of adsorbents besides the thermal management of the system. The utility and cost of an appropriate adsorbent such as activated carbon are fundamental to the productivity of the ANG technology. In this study, activated carbons were prepared from three South Africa coal waste samples (run-of-mine fines, discard and flotation slurry) by KOH activation. The adsorption isotherm of methane on the synthesized activated carbons revealed that the activated carbon synthesized from run-of-mine fines (ACR) has the highest adsorbed amount compared to activated carbons synthesized from coal discard (ACD) and slurry (ACS). The maximum adsorbed amount of methane was attained at an average pressure of 37 bar with ACR having the largest volume of methane adsorbed at 162.71 cm^3/g followed by ACD (157.58 cm^3/g) and ACS (106.69 cm^3/g) respectively. This sequence agrees with the BET surface areas of the activated carbons; ACR (1925.34 m^2/g) > ACD (1826.41 m^2/g) > ACS (1484.96 m^2/g). Hence, the larger the surface area of the synthesized activated carbon, the more amount of methane it adsorbs. The methane adsorption data for the three activated carbons were validated with Langmuir, Toth, and D-A isotherm models. It was found that the D-A model was the best fit for all the three activated carbons. Based on the requirements of suitable porous materials for ANG application, the study indicated that the produced activated carbons from South Africa coal wastes could well be applied for natural gas storage.

Appendix A5: Conference Proceeding 1

Parts of this thesis compiled and presented as a paper titled ‘Porous Carbon Materials from South Africa Coal waste for Gas Storage Applications: synthesis, characterization and high pressure methane adsorption’ at the 9th International Conference on Clean Coal Technologies, Houston, Texas, USA, June 3 - 7, 2019.

Abstract

Availability, tuneable microstructure and large specific surface area of porous carbon materials have made it suitable for gas storage applications. In this study, activated carbons were prepared from three distinct South Africa coal wastes (run-of-mine fines, discard and flotation slurry) by KOH activation. Preliminary analysis (proximate and ultimate analysis) of the coal waste samples showed a high percentage of carbon and low ash content, a good indication of good material for preparing porous carbon. The synthesized activated carbons were characterized by nitrogen at 77 K adsorption– desorption isotherms, SEM/EDS, FTIR, and XRD. The largest surface area of 1925.34 m2/g, 1893.41 m2/g, 1484.96 m2/g, pore volume of 1.26 cm3/g, 1.21 cm3/g, 1.03 cm3/g and pore size of 2.51 nm, 2.66 nm and 2.90 nm were obtained for activated carbons _om ROM fines, discard and slurry respectively. SEM/EDS analysis showed the development of pores and the presence of high carbon element, FTIR analysis confirmed the presence of carbonyls, alkenes, and hydroxyls. XRD analysis reveals a broad diffraction background which is an indication of a largely amorphous structure. Based on the requirements of suitable porous materials for gas storage applications, it could be stated that the produced activated carbons from South Africa coal wastes could well be applied for gas storage.

Appendix A6: Conference Proceeding 2

Another paper titled 'Low-Cost Microporous Material for Natural Gas Storage: Preparation and Characterization' was presented at the 12th European Conference on Fuel and Energy Research and its Applications (ECCRIA), University of Cardiff, Cardiff, United Kingdom, September 5 – 7, 2018.

Abstract

Adsorbed natural gas (ANG) technology has been proposed as a viable alternative to liquefied natural gas and compressed natural gas for the storage and transportation of natural gas. However, the extensive usage and commercialization of the adsorbed natural gas (ANG) storage system is largely constrained by adsorbent cost besides the thermal management of the system. The utility of an appropriate adsorbent such as activated carbon is fundamental to the productivity of this technology. Activated carbon (AC) is a suitable porous material for storing natural gas due to its high specific surface area and porosity which can easily be controlled and optimized. In this study, we address the problem of adsorbent cost for natural gas storage through the preparation of a largely porous AC with the high surface area from coal discard; waste material from coal beneficiation process. In developing the AC, chemical activation route with the use of KOH reagent was applied. The effects of KOH/coal discard weight ratio (1:1, 2.5:1, 4:1), carbonization temperature (400 – 800 ^oC) and particle size (0.15 – 0.25nm) on the adsorptive properties of the AC were methodically evaluated and optimized using Response Surface Methodology (RSM). The results presented herein are the summary of the synthesis and FTIR, SEM, TGA, XRD characterization of the developed activated carbon from coal discard. The results showed that for each activation process, the surface area, pore volume and pore size of the resulting AC increased with increased carbonization temperature and KOH/coal discard weight ratio. The maximum surface area of 1766.84m^2/g, pore volume of 1.02cm^3/g and pore size of 2.77nm were obtained at a carbonization temperature of 800^oC and KOH/coal discard weight ratio 4:1. Increasing the particle size of the coal discard resulted in a decreased yield and porosity of the resulting AC. According to the requirements of adsorbent desired for ANG application, it could be stated that the produced low-cost AC could well be applied for natural gas storage.

APPENDIX B: MATLAB Programming Codes

Appendix B1: ISOFIT Code

```
% matlab script isofit .m
% optimal parameters from adsorption isotherm models
% ISOTHERM EXPRESSIONS:
%
%     1. Langmuir:        cmu    = cmus * b*P/(1+b*P)
%                         The parameter array:
%                         a(1)   = cmus
%                         a(2)   = b
%
%     2. Toth:            cmu    = cmus*b*P/[1+(b*P)^t] ^(1/t)
%                         The parameter array:
%                         a(1)   = cmus
%                         a(2)   = b
%                         a(3)   = t
%
%     3. DA:                     cmu    = cmus*exp[-(A/E)^n]
%                         where
%                         A      = RT*log(P0/P)
%                         The parameter array:
%                         a(1)   = cmus
%                         a(2)   = E
%                         a(3)   = n
%
%+++++++++++++++++++++++++++++++++++++++++++++++++++++++++++++++++++++++++++++
% NOMENCLATURE:
%     a                   =     Array for the isotherm parameter
%     a_optimal           =     Array for the optimal isotherm parameter
%     b                   =     Affinity
%     c                   =     Energy of adsorbate-adsorbate interaction
%     cmus                =     Maximum adsorbed amount
%     E                   =     Characteristic energy used in DA equation
%     f                   =     Variable for the string of the isotherm expression
%     fdata               =     Cell array containing strings as elements
%     fname               =     variable for the filename containing data
%     n                   =     Exponent in DA equation
%     p                   =     Pathname variable used to append the new path
%     vapor_pressure       =    vapor pressure of sub-critical gases
%     Residual            =     Residual
```

```
%      t                    =      Toth heterogeneity parameter
%      temp           =     Temperature
%      x                    =      Array containing pressure data
%      y                    =      Array containing the amount adsorbed data
%      y1                   =      Array containing the calculated adsorbed amount
%++++++++++++++++++++++++++++++++++++++++++++++++++++++++++++++++++++++++++++++
%
%++++++++++++++++++++++++++++++++++++++++++++++++++++++++++++++++++++++++++++++
%      clear all
%      clc
% DECLARE GLOBAL STATEMENTS
       global T P0
       Rg            = 8.3142;           % Gas constant
  fdata = {'Langmuir', 'Toth', 'DA'};
%-------------------------------------------------------------------------------
--------
% USER SUPPLY section
k_selection                = 1;
%Selection indicator (1 for Langmuir, 2 for Toth and 3 for DA)
newpath                = 'C:\matlabR12\work\Adsorption modeling\Equilibria\Fitting
             one adsorbate & one temperature';% Put the path here where your data
             file is stored
fname                      = 'iso1.dat';% Your data file name including the
             extension
T                          = 273.15;     % Adsorption temperature
P0                         = 94.42              % Vapor pressure.
max                        = 10000;      % Maximum number of iterations
tol                        = 1e-6;              % Tolerance on parameter and
residual
%-------------------------------------------------------------------------------
----------
% DATA MANIPULATION
f      = fdata{k_selection};      % Isotherm function string
path(path,newpath);        % Append your new path to the existing path
eval(['load ' fname]);             % Load the file
% IF THE FILENAME CONTAINS AN EXTENSION, REMOVE IT
n1                   = find(fname=='.');
if ~isempty(n1);
  n2          = length(fname);
  fname(n1:n2)       = [];
end;
% ASSIGN THE DATA INTO PRESSURE (X) CONCENTRATION (Y) ARRAYS
p                    = eval([fname '(:,1)']);   p             = p';
cmu                  = eval([fname '(:,2)']);   cmu    = cmu';
```

```
% REMOVE ZERO PRESSURE FROM THE DATA; OTHERWISE INFINITY IS ENCOUNTERED IN POLYFIT
if p(1)==0;
  p                 = p(2:length(p));
  cmu               = cmu(2:length(cmu));
end

% INITIAL GUESS FOR THE ISOTHERM PARAMETERS
if k_selection < 10
       coeff        = polyfit(1./p, 1./cmu, 1);
       b_guess      = coeff(2)/coeff(1);
       cmus_guess   = 1/coeff(2);
end

switch f
       case 'Langmuir'
              a(1)   = cmus_guess;
              a(2)   = b_guess;
              disp(['The Computer chooses the following initial guesses for the ',
f, ' isotherm']);
              disp(['cmus = ', num2str(a(1)),', b = ',num2str(a(2))]);
       case 'Toth'
              a(1)   = cmus_guess;
              a(2)   = b_guess;
              a(3)   = 1;
              disp(['The Computer chooses the following initial guesses for the ',
f, ' isotherm']);
              disp(['cmus = ', num2str(a(1)),', b = ',num2str(a(2)),', t = ',
num2str(a(3))]);
       case 'DA'
              coeff   = polyfit((Rg*T*log(P0./p)).^2, log(cmu), 1);
              E_guess       = 1/sqrt(-coeff(1));
              cmus_guess    = exp(coeff(2));
              a(1)          = cmus_guess;
              a(2)          = E_guess;
              a(3)          = 2;
              disp(['The Computer chooses the following initial guesses for the ',
f, ' isotherm']);
              disp(['cmus = ', num2str(a(1)),', E = ',num2str(a(2)),', n = ',
num2str(a(3))]);
       end;
% THIS LOOP WILL ENSURE THAT THE USER PROVIDE REASONABLY GOOD INITIAL GUESS
%      BEFORE THE OPTIMIZATION IS STARTED
k      = 1;
```

```
       while k
       guess (f,a,p,cmu); % THIS ROUTINE PLOTS THE DATA AND THE GUESSED CURVE
       iyes   = input('Do you wish to further change the guessing parameters? =
','s');
       if iyes=='y' | iyes=='yes' | iyes=='Y' | iyes=='Yes'
        switch f
              case 'Langmuir'
                    a = input('Enter new guess [cmus b] = ');
              case 'Toth'
                    a = input('Enter the initial guess [cmus b t] = ');
              case 'DA'
                     a     = input('Enter the initial guess [cmus E n] = ');
              end;
              else
               k     = 0; % THIS WILL INTERRUPT THE LOOP
              end
              end

% OPTIMIZATION & KEEP CHECK ON THE CPUTIME
       start_time    = cputime;
              options(2)    = tol;        % TERMINATION TOLERANCE FOR A
              options(3)    = tol;        % TERMINAL TOLERANCE FOR THE FUNCTION
RESIDUAL
              options(14)   = max;        % MAXIMUM NUMBER OF ITERATIONS
       [a_optimal,options] = fmins('residual',a,options,[],f,p,cmu);
%-------------------------------------
% PLOTTING THE RESULTS
%-------------------------------------
       cmu1          = feval(f,a_optimal,p)'
       plot(p,cmu,'o',p,cmu1);
       xlabel('Pressure');
       ylabel('Amount adsorbed');
       title([f ' isotherm']);grid;

%-----------------------------------------------------
% DISPLAY THE RESULTS ON COMMAND WINDOWS
%-----------------------------------------------------
disp(' RESULTS');
switch f
case 'Langmuir'
disp(['cmus = ',num2str(a_optimal(1)),'; b = ',num2str(a_optimal(2))]);
case 'Toth'
```

```
disp(['cmus = ',num2str(a_optimal(1)),'; b = ',num2str(a_optimal(2)),'; t =
',num2str(a_optimal(3))]);

case 'DA'

disp(['cmus = ',num2str(a_optimal(1)),'; E = ',num2str(a_optimal(2)),'; n =
',num2str(a_optimal(3))]);


end;


Residual     = sqrt(residual(a_optimal,f,p,cmu));    % THIS IS THE RESIDUAL

cpu          = cputime - start_time;                 % THIS IS THE CPU TIME

disp(['Residual = ',num2str(Residual),'; Number of Iteration =
',num2str(options(10)),'; CPU time = ',num2str(cpu)]);


%--------------------------------

% THIS IS THE END OF THE PROGRAM

%--------------------------------
```

Appendix B2: ADSORB1A.M Code

```
% matlab script isofit .m

% single component adsorption kinetics in a single particle with Toth Isotherm

%

% NOMENCLATURE:

% Variable Units Description

% A     :      : First derivative collocation matrix

% al          :      : Parameter alpha for Jacobi polynomial

% amount      : mole/cc : Adsorbate amount per unit particle volume

% amounti : mole/cc : Adsorbate amount per unit particle volume at t = 0

% amount : mole/cc : Adsorbate amount per unit particle volume at t = infinity

% b           : cc/mole    : Affinity constant in the isotherm equation

% B           :                   : Second derivative collocation matrix

% be          :                   : Parameter beta for Jacobi polynomial

% biot  :             : Biot number for mass transfer through film

% C     :             : Matrix defined as: 4*u(i)*b(i,j)+2*(s+1)*a(i,j)

% c     : mole/cc    : Concentration of the free species

% c0    : mole/cc    : Reference concentration

% cb    : mole/cc    : Bulk concentration

% ci    : mole/cc    : Initial concentration

% cmu   : mole/cc    : Concentration of the adsorbed species

% cmu0  : mole/cc : Reference concentration of the adsorbed species

% cmui  : mole/cc    : Initial adsorbed concentration

% cmub : mole/cc : Final adsorbed concentration in equilibrium with cb

% cmus  : mole/cc    : Saturation adsorbed concentration
```

```
% delta : (-) : Parameter, the ratio of the surface diffusion flux to the pore
diffusion flux
% Dp    : cm^2/sec   : Pore diffusivity
% Ds    : cm^2/sec   : Surface diffusivity
% fractional_uptake :(-) : Fractional uptake
% half_time   :(-) : Nondimensional half time for slab, cylinder and sphere
% n     :            : Number of interior collocation points
% n0    :     : = 1 if the point x=0 is counted; otherwise =0
% n1    : : = 1 if the point x=1 is counted; otherwise =0
% nt    : : n + n0 + n1
% omega       : (-)              : Nondimensional integration vector
% omega0      : (-)       : Nondimensional initial integration vector
% porosity : (-) : particle porosity
% u     :             : Interpolation points = x^2
% R : cm : Particle radius for cylinder and sphere, half length for slab
% s : (-) : Particle shape factor (0 for slab, 1 for cylinder, 2 for sphere)
% t, tout :          : nondimensional time
% time  : sec : real time
% t_initial          : (-) : Initial time (usually = 0)
% t_final     : (-) : Final nondimensional time
% x     : (-) : Nondimensional distance (=r/R)
% y     : (-)  : Nondimensional concentration
% ynp1  : (-) : Nondimensional concentration at surface (x=1)
% yout  :             : Integration vector for ODE15s
% y0    :     : Initial condition for the integration vector
% w     : : Radau quadrature weight
%
%+++++++++++++++++++++++++++++++++++++++++++++++++++++++++++++++++++++
% USAGE:
% Type ADSORB1A
%+++++++++++++++++++++++++++++++++++++++++++++++++++++++++++++++++++++
       clear all
       clc

% DECLARE SOME GLOBAL VARIABLES
  global n u A B C               % Collocation vectors and matrices
       global porosity R                % Particle characteristics
       global b cmus              % Isotherm characteristics
       global c0 cb ci                  % Concentrations of free species
       global cmu0 cmub cmui      % Concentrations of adsorbed species
       global Dp Ds                     % Diffusion characteristics
```

```
        global biot delta

        half_time     = [0.19674 0.0631 0.03055];

%-------------------------------------------------------------------------
% USER SUPPLY section
        s                   = 2;                % particle shape factor
        R                   = 1.26;             % particle radius (cm)
        porosity            = 0.25;             % particle porosity (-)
        ci                  = 0;          % initial gas concentration (mole/cc)
        cb            = 0.84;             % bulk gas concentration (mole/cc)
        c0            = 0.84;             % reference concentration (mole/cc)
        b             = 0.029;            % adsorption affinity (cc/mole)
        cmus          = 80.02;            % maximum adsorption capacity (mole/cc)
        biot          = 100;        % biot number (-)
        Dp            = 0.041;            % pore diffusivity (cm^2/sec)
        Ds            = 2.02e-4;          % surface diffusivity (cm^2/sec)

        cmu0                = cmus*b*c0/(1+b*c0);
        delta               = (1 - porosity)*Ds*cmu0/porosity/Dp/c0;
        t_initial     = 0;                % initial time for integration
        t_final = 10*half_time(s+1)*( porosity + (1-porosity)*b*cmus/(1+b*c0) )/(1 +
delta);
%-------------------------------------------------------------------------

% COLLOCATION section
        n                           = 5;
        n0                          = 0;
        n1                          = 1;
        al                          = 1;
        be                          = (s-1)/2;

        nt                          = n + n0 + n1;
        A                           = zeros(nt);
        B                           = zeros(nt);
        C                           = zeros(nt);

        [dif,u]             = JCRoot(n,n0,n1,al,be);
        A                           = AB(n,n0,n1,1,dif,u);
        B                           = AB(n,n0,n1,2,dif,u);
        w                           = RDW(n,n0,n1,al-1,be,u,dif);
```

```
        for i=1:nt;
                C(i,:) = 4.*u(i).*B(i,:)+2.*(s+1).*A(i,:);
        end

% CHECK FOR THE SYSTEM PARAMETERS
        lambda        = b*c0;
        if lambda>50
                disp(['The adsorption affinity is too high' ...
        'You might have problem with the convergence'])
        end

% CALCULATIONS OF NECESSARY PARAMETERS
        cmu0                = cmus*b*c0/(1+b*c0);
        cmui                = cmus*b*ci/(1+b*ci);
        cmub                = cmus*b*cb/(1+b*cb);
        delta               = (1 - porosity)*Ds*cmu0/porosity/Dp/c0;
        amounti             = porosity*ci + (1 - porosity)*cmui;
        amountb             = porosity*cb + (1 - porosity)*cmub;

% CALL ODE SOLVER
        omega0              = (ci/c0)*ones(n,1);
        options             = odeset('Reltol',1e-2,'Abstol',1e-5,'bdf','off');
        [tout,omega]= ode15s('fadsorb1',[t_initial t_final], omega0, options);

%-----------------------------------------------------------
% SOLUTIONS: CONCENTRATION PROFILES & FRACTIONAL UPTAKE
%-----------------------------------------------------------
for i=1:length(tout)
        ynp1(i) =(cb/c0 -
2*sum(A(n+1,1:n).*omega(i,1:n))/biot)/(1+2*A(n+1,n+1)/biot);
        end

        omega               = [omega ynp1'];

% CALCULATE THE CONCENTRATIONS OF THE FREE SPECIES AND THE ADSORBED SPECIES
% AND THE FRACTIONAL UPTAKE
        time                = tout.*R.^2./porosity/Dp; % real time (sec)

for i=1:length(tout)
c(i,:)        = c0.*omega(i,:);
cmu(i,:)             = cmus.*b.*c(i,:)./(1 + b.*c(i,:) );
amount(i) = porosity*dot( w, c(i,:) ) + (1 - porosity)*dot( w, cmu(i,:) );
```

```
fractional_uptake(i)       = (amount(i) - amounti) ./ (amountb - amounti);
       end
  [amount]'
  time
[fractional_uptake]'

%-----------
% PLOTTING
% %-----------
%      figure(1)
%      subplot(2,2,1)
%      plot(time,omega,'r-');
%      xlabel('time (sec)');
%      ylabel('y');
%      grid;
%      title('Dimensionless Conc. versus time')
       subplot(2,1,1)
       plot(time,fractional_uptake,'r-');
       xlabel('time (sec)');
       ylabel('uptake');
       grid;
       title('Fractional Uptake versus time');

       subplot(2,1,2)
       plot(time,amount,'r-');
       xlabel('time (sec)');
       ylabel('Amount adsorbed per unit volume (mole/cc)');
       grid;
       title('Amount adsorbed (mole/cc) versus time');

%      subplot(2,2,4)
%      dt = floor(length(tout)/10);
%      for i=1:dt:length(tout)
%             plot(sqrt(u),omega(i,:),'r-',sqrt(u),omega(i,:),'ro');
%             hold on
%      end
%      title('Concentration profiles');
%
%
% THIS IS THE END OF THIS PROGRAM
```

APPENDIX C: SEM IMAGES Analysis in MATLAB

Appendix C1: SEMPOR.M MATLAB Code

```
% Extraction of porosity and pore size distribution from SEM images

% We assume that the input SEM images are gray-scale and darker parts of the image
% shows deeper surfaces which are considered as pore spaces

%
clear; close all; clc;
%File_Name='jibrildiscardA.jpg'; % I have put 2 sample images in the folder SEM1.jpg
and SEM2.jpg
File_Name='ACD Jibril 1.jpg'; % I have put 2 sample images in the folder SEM1.jpg
and SEM2.jpg
Resolution=0.459; % micron/pixel % this is the spatial resolution of the input
N=4; % Number of intensity levels in the image,
% if you think that the result porosity is overestimated, just increase this number
and vice versa, it accepts integers
A=imread(File_Name);
if ndims(A)==3; B=rgb2gray(A); end

level = multithresh(B,N);
C= imquantize(B,level);
RGB1 = label2rgb(B);
imwrite(RGB1,[File_Name(1:end-4) '_Depth Map.png']);

P=zeros(size(C));
for I=1:size(C,1)
  for J=1:size(C,2)
  if C(I,J)==1
  P(I,J)=1;
  end
  end
end
P=1-P;
P=bwmorph(P,'majority',1);

imwrite(P,[File_Name(1:end-4) '_Binary Segmentation.png']);

Conn=8;
[s1,s2]=size(P);
D=-bwdist(P,'cityblock');
B=medfilt2(D,[3 3]);
B=watershed(B,Conn);
Pr=zeros(s1,s2);

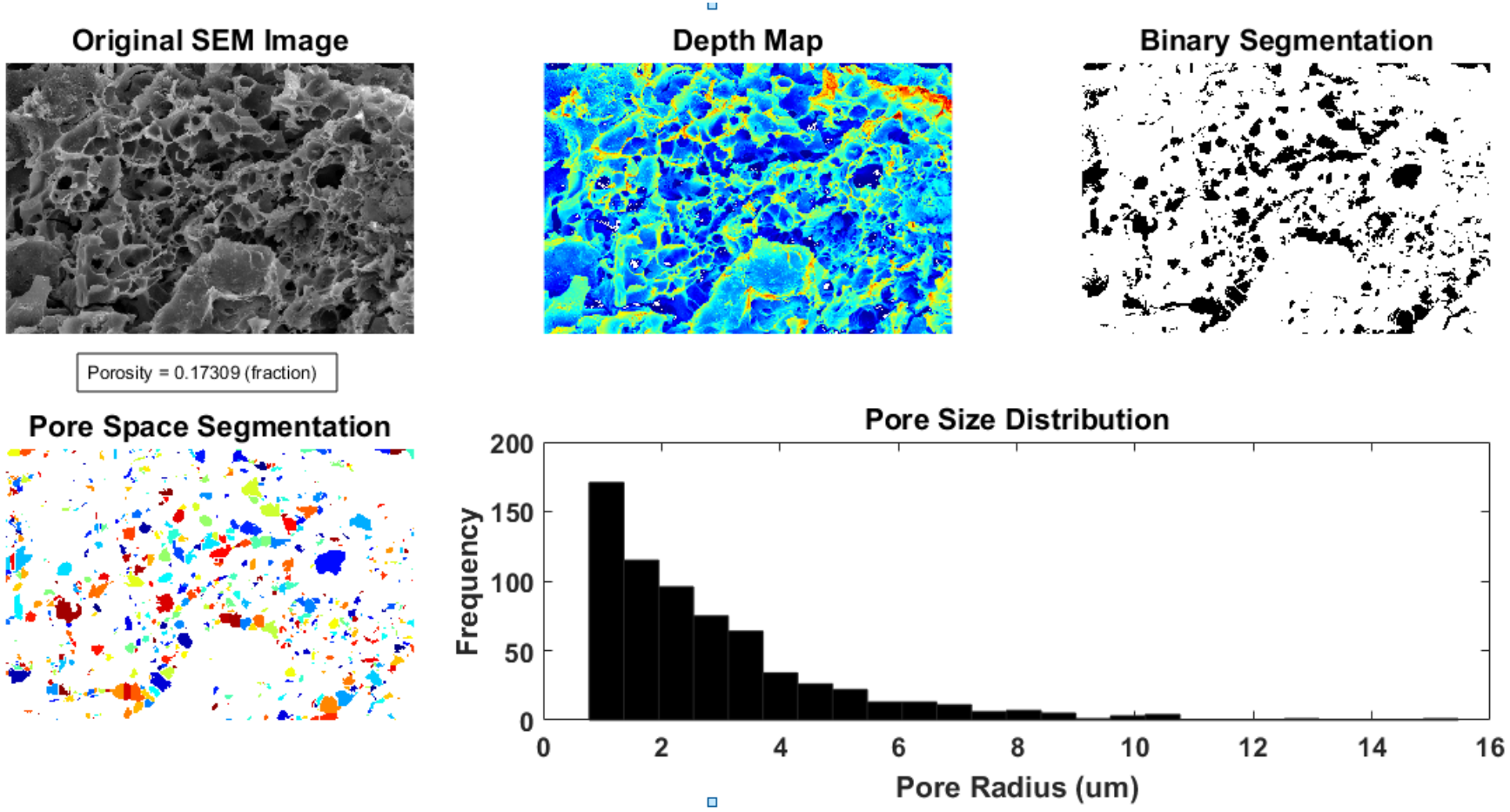
for I=1:s1
  for J=1:s2
  if P(I,J)==0 && B(I,J)~=0
  Pr(I,J)=1;
```

```
  end
  end
end
Pr=bwareaopen(Pr,9,Conn);

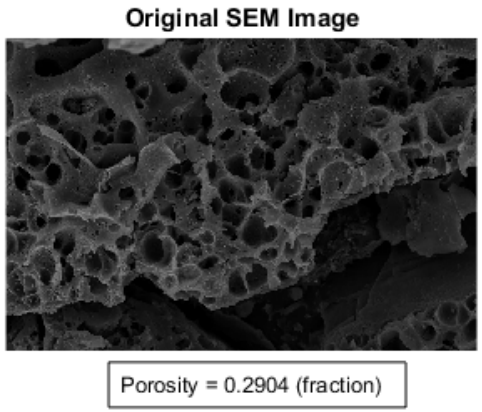
[Pr_L,Pr_n]=bwlabel(Pr,Conn);
RGB2 = label2rgb(Pr_L,'jet','white','shuffle');
imwrite(RGB2,[File_Name(1:end-4) '_Pore Space Segmentation.png']);
V=zeros(Pr_n,1);
for I=1:s1
  for J=1:s2
  if Pr_L(I,J)~=0
  V(Pr_L(I,J))=V(Pr_L(I,J))+1;
  end
  end
end
SP=4*pi*sum(sum(Pr))/(sum(sum(bwperim(Pr,4))))^2;
X=Resolution.*(V./pi).^.5; % Pore radius
Porosity=1-mean(P(:))
Average_Pore_radius=mean(X) % micron
Standard_Deviation_of_Pore_radius=std(X) % micron

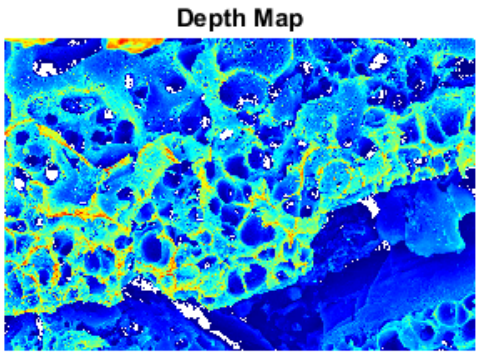
figure;
subplot(2,3,1); imshow(A); title('Original SEM Image');
subplot(2,3,2); imshow(RGB1); title('Depth Map');
subplot(2,3,3); imshow(P); title('Binary Segmentation');
subplot(2,3,4); imshow(RGB2); title('Pore Space Segmentation');
annotation('textbox',[0 .9 .1 .1], 'String', [ 'Porosity = ' num2str(Porosity) '
(fraction)']);
subplot(2,3,5:6);  hist(X,25);  xlabel('Pore  Radius  (um)');  ylabel('Frequency');
title('Pore Size Distribution');
set(gcf, 'Position' , get(0, 'Screensize' ));
```

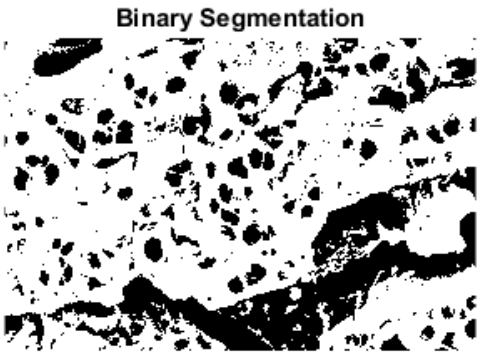
Appendix C2: Sample ACD processed images in MATLAB

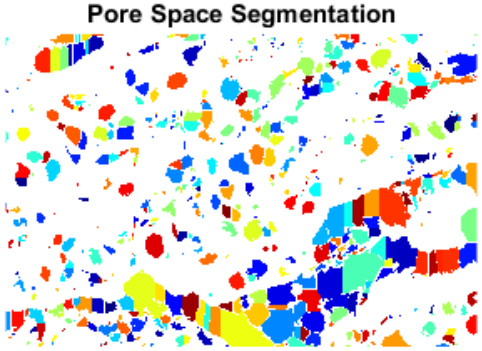


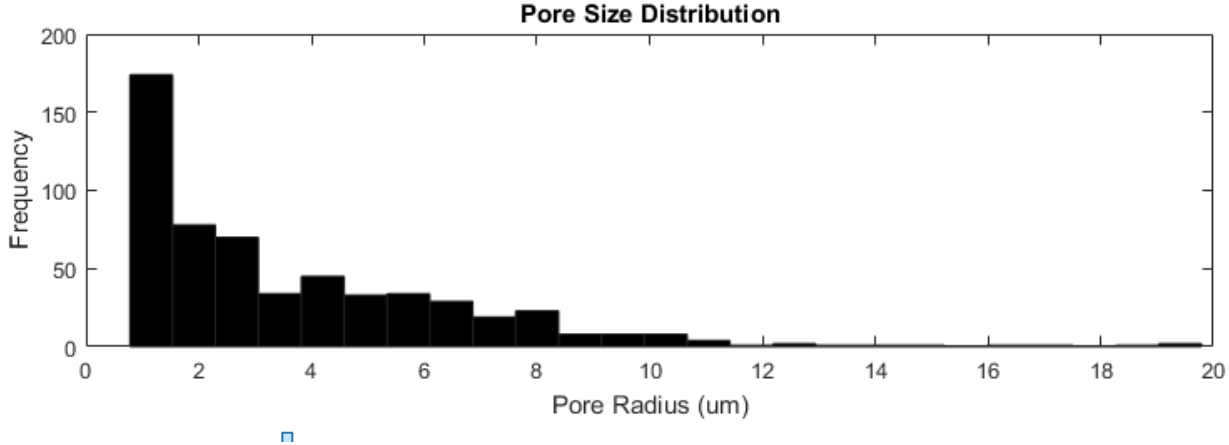
Appendix C3: Sample ACR processed images in MATLAB



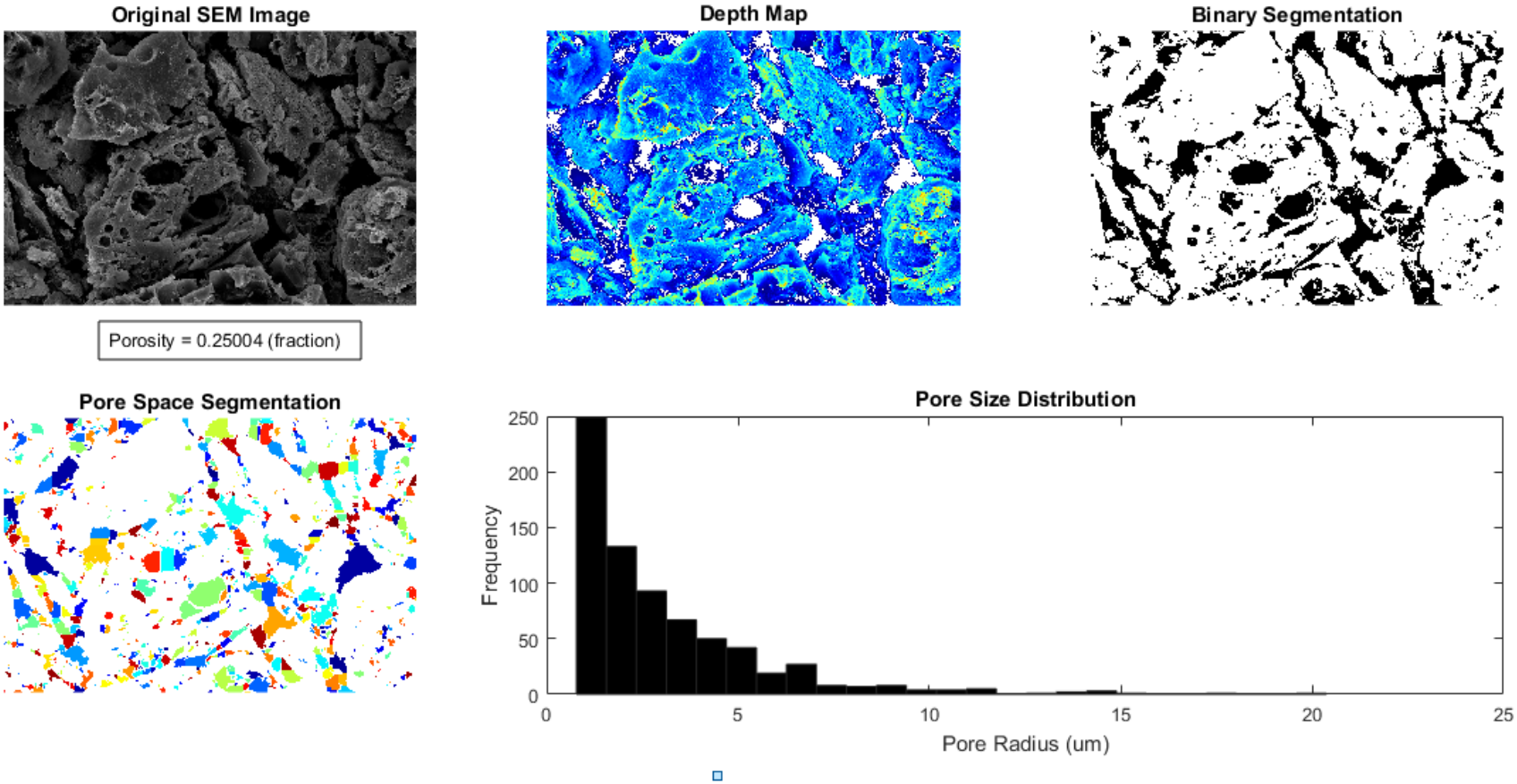








Appendix C4: Sample ACS processed images in MATLAB



APPENDIX D: Adsim Specifications

Number of Layers	**1**
Bed Type	Vertical
Spatial dimensions	1-D
Internal heat exchanger	None
Discretization method	UDS1
Number of nodes	20
Material balance assumption	Convection with estimated dispersion
Momentum balance	Ergun equation
Film model	Solid
Kinetic model assumption	Lumped resistance
Form of lumped resistance model	Linear
Form of mass transfer coefficient	Constant
Molecular diffusivities	Fixed
Initial bed temperature	298 K
Gas source temperature	298 K
Ambient temperature	298 K
Energy balance assumption	Non-isothermal with gas and solid conduction
Consider heat adsorption phase	None
Form of heat transfer coefficient	Estimated
Form of gas thermal conductivity	Constant
Heat transfer to the Environment	Adiabatic
Solid phase heat capacity	Constant
Valve model type	Reversible flow setter
Valve characteristics	Linear
Apply Stop action	No
Specifications made available	Flow/CV
Temperature calculation	Calculate from energy balance